Stem Cells International

Bone Microenvironment, Stem Cells, and Bone Tissue Regeneration

Guest Editors: ZuFu Lu, Jenneke Kleine-Nulend, and Bin Li

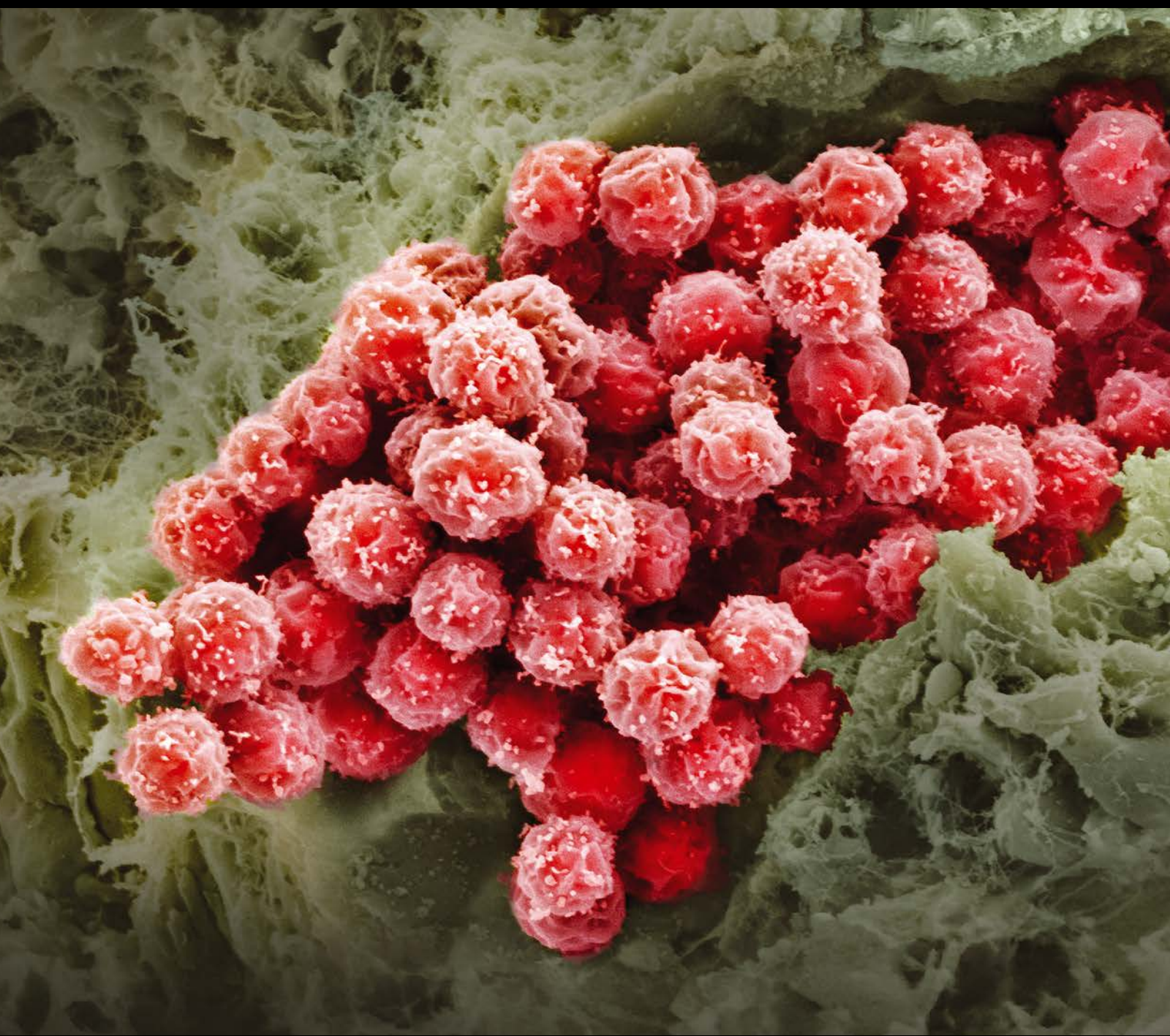

Bone Microenvironment, Stem Cells, and Bone Tissue Regeneration

Stem Cells International

Bone Microenvironment, Stem Cells, and Bone Tissue Regeneration

Guest Editors: ZuFu Lu, Jenneke Kleine-Nulend, and Bin Li

Editorial Board

Contents

Hindawi Publishing Corporation
Stem Cells International
Volume 2017, Article ID 1315243, 2 pages
http://dx.doi.org/10.1155/2017/1315243

Editorial

Bone Microenvironment, Stem Cells, and Bone Tissue Regeneration

ZuFu Lu,[1] Jenneke Kleine-Nulend,[2] and Bin Li[3]

[1]*Biomaterials and Tissue Engineering Research Unit, School of AMME, University of Sydney, Sydney, NSW 2006, Australia*
[2]*Department of Oral Cell Biology, ACTA, University of Amsterdam and VU Amsterdam, MOVE Research Institute Amsterdam, Amsterdam, Netherlands*
[3]*Department of Orthopaedics, The First Affiliated Hospital, Orthopaedic Institute, Soochow University, 188 Shizi St., Suzhou, Jiangsu 215006, China*

Correspondence should be addressed to ZuFu Lu; zufu.lu@sydney.edu.au

Received 26 December 2016; Accepted 26 December 2016; Published 17 January 2017

Despite the remarkable regenerative capacity of bone, the regeneration of large bone defects and the repair of nonunion bone fractures remain a major challenge in orthopaedic surgeries. Bone is the second most commonly transplanted tissue with over 1.5 million bone graft surgeries being performed annually in the United States [1]. However, the major limitations confronted with conventional bone grafts include limited availability and donor site morbidity for autografts and the risk of pathogen transmission for allografts [2, 3]. Given these limitations, there is a great need for developing novel and effective approaches for the regeneration of large bone defects and the repair of nonunion bone fracture.

Stem cell-based bone tissue engineering offers a promising approach for regenerating critical sized bone defects or repairing nonunion bone fracture. Understanding and recreating a signalling environment to control the differentiation of stem cells into the bone lineage would be of great importance. The components in bone microenvironment, which include a mineral phase (hydroxyapatite nanocrystals), an organic phase (composed of 90% collagen type I), a cellular phase (osteoblasts, osteoclasts, and osteocytes), and a soluble factor phase (growth factors and/or cytokines), provide a specific and balanced signalling network, which contribute to the innate bone metabolic and anabolic activities and maintain the structure and functions of the bone. Substantial efforts, therefore, have been made to mimic the bone tissue microenvironmental components for controlling the commitment of stem cells into osteogenic lineage cells for bone tissue regeneration. For example, by mimicking the bone nanostructure to engineering bone-related biomaterials, researchers have incorporated nanocrystals into biomaterials and demonstrated that they are effective in regulating various cellular functions including cell adhesion, proliferation, and differentiation [4, 5]; in addition, mimicking the signals provided by bone cellular phase (e.g., osteoblasts) has also been shown as a feasible approach to control stem cell fate into osteogenic lineage [5, 6]. Moreover, the cytokines and/or growth factors within bone microenvironment play a key role as well in the bone remodeling process, and mimicking their signals has been proven to be very successful in steering MSCs into bone lineage. Recently, inflammatory factors, transiently expressed by macrophages upon tissue injury, have increasingly been appreciated for their role in tissue repair and regeneration [7–9].

In this special issue, some cutting-edge original researches as well as review articles related to priming stem cell fate into the osteogenic lineage via mimicking the bone components (e.g., bone extracellular matrix, cells, and growth factors) were introduced and provided the readers with the updated knowledge and progression in the topic of bone microenvironment, stem cells, and bone tissue regeneration.

ZuFu Lu
Jenneke Kleine-Nulend
Bin Li

References

[1] D. Marsh, "Concepts of fracture union, delayed union, and nonunion," *Clinical Orthopaedics and Related Research*, vol. 355, pp. S22–S30, 1998.

[2] J. A. Goulet, L. E. Senunas, G. L. DeSilva, and M. L. V. H. Greenfield, "Autogenous iliac crest bone graft: complications and functional assessment," *Clinical Orthopaedics and Related Research*, no. 339, pp. 76–81, 1997.

[3] C. F. Lord, M. C. Gebhardt, W. W. Tomford, and H. J. Mankin, "Infection in bone allografts. Incidence, nature, and treatment," *The Journal of Bone & Joint Surgery—American Volume*, vol. 70, no. 3, pp. 369–376, 1988.

[4] G. Wang, Z. Lu, X. Zhao, A. Kondyurin, and H. Zreiqat, "Ordered HAp nanoarchitecture formed on HAp-TCP bioceramics by 'nanocarving' and mineralization deposition and its potential use for guiding cell behaviors," *Journal of Materials Chemistry B*, vol. 1, no. 19, pp. 2455–2462, 2013.

[5] Z. Lu, S.-I. Roohani-Esfahani, G. Wang, and H. Zreiqat, "Bone biomimetic microenvironment induces osteogenic differentiation of adipose tissue-derived mesenchymal stem cells," *Nanomedicine: Nanotechnology, Biology, and Medicine*, vol. 8, no. 4, pp. 507–515, 2012.

[6] Z. Lu, S.-I. Roohani-Esfahani, P. C. L. Kwok, and H. Zreiqat, "Osteoblasts on rod shaped hydroxyapatite nanoparticles incorporated pcl film provide an optimal osteogenic niche for stem cell differentiation," *Tissue Engineering - Part A*, vol. 17, no. 11-12, pp. 1651–1661, 2011.

[7] Z. Lu, G. Wang, C. R. Dunstan et al., "Activation and promotion of adipose stem cells by tumour necrosis factor-α preconditioning for bone regeneration," *Journal of Cellular Physiology*, vol. 228, no. 8, pp. 1737–1744, 2013.

[8] G. E. Glass, J. K. Chan, A. Freidin, M. Feldmann, N. J. Horwood, and J. Nanchahal, "TNF-α promotes fracture repair by augmenting the recruitment and differentiation of muscle-derived stromal cells," *Proceedings of the National Academy of Sciences of the United States of America*, vol. 108, no. 4, pp. 1585–1590, 2011.

[9] P. M. Mountziaris, P. P. Spicer, F. K. Kasper, and A. G. Mikos, "Harnessing and modulating inflammation in strategies for bone regeneration," *Tissue Engineering—Part B: Reviews*, vol. 17, no. 6, pp. 393–402, 2011.

Hindawi Publishing Corporation
Stem Cells International
Volume 2017, Article ID 4045238, 6 pages
http://dx.doi.org/10.1155/2017/4045238

Review Article

Osteopontin: Relation between Adipose Tissue and Bone Homeostasis

Carolina De Fusco,[1] Antonietta Messina,[1] Vincenzo Monda,[1] Emanuela Viggiano,[1,2] Fiorenzo Moscatelli,[3] Anna Valenzano,[3] Teresa Esposito,[1] Chieffi Sergio,[1] Giuseppe Cibelli,[3] Marcellino Monda,[1] and Giovanni Messina[1,3]

[1]*Department of Experimental Medicine, Section of Human Physiology and Unit of Dietetic and Sport Medicine, Second University of Naples, 16 Costantinopoli Str., 80138 Naples, Italy*
[2]*Department of Medicine, University of Padua, Padua, Italy*
[3]*Department of Clinical and Experimental Medicine, University of Foggia, Foggia, Italy*

Correspondence should be addressed to Giovanni Messina; gianni.messina@unina2.it

Received 29 April 2016; Revised 19 November 2016; Accepted 18 December 2016; Published 17 January 2017

Academic Editor: Armand Keating

Osteopontin (OPN) is a multifunctional protein mainly associated with bone metabolism and remodeling. Besides its physiological functions, OPN is implicated in the pathogenesis of a variety of disease states, such as obesity and osteoporosis. Importantly, during the last decades obesity and osteoporosis have become among the main threats to health worldwide. Because OPN is a protein principally expressed in cells with multifaceted effects on bone morphogenesis and remodeling and because it seems to be one of the most overexpressed genes in the adipose tissue of the obese contributing to osteoporosis, this mini review will highlight recent insights about relation between adipose tissue and bone homeostasis.

1. Introduction

Osteopontin (OPN), also defined as secreted phosphoprotein-1 [1] (SPP1), sialoprotein-1 [1, 2], or early T lymphocyte activation 1 (Eta-1) [3] belongs to the small integrin-binding ligand N-linked glycoprotein (SIBLING) family [4]. SIBLING family consists of noncollagenous proteins (NCPs), primarily involved in bone metabolism and mainly located within the mineralized tissue such as bone and dentin, which also includes bone sialoprotein (BSP (IBSP)), dentin matrix protein 1 (DMP1), dentin sialophosphoprotein (DSPP), and matrix extracellular phosphoglycoprotein (MEPE) [5, 6]. These soluble secreted glycoproteins undergo posttranslational modifications. They are extensively and heterogeneously spliced, translated, phosphorylated, glycosylated, and proteolysed. These modifications give them bioactive properties [7]. SIBLING proteins exert biological roles in both paracrine and autocrine manner and through multiple functional domains may bind to cell surface integrins [7]. Originally described by Senger in 1979 as a secreted, 60-kDa transformation-specific phosphoprotein [8], human OPN is the most studied component of SIBLING family. It is a Arg-Gly-Asp (RGD) containing multifunctional soluble extracellular matrix-associated glycoprotein of 34 kDa [8] (apparent MW up to 75 kDa) [5, 6]. OPN has a gly-arg-gly-asp-ser (GRGDS) [9] cell binding domain with ~314 amino acid residues that can regulate cell activities through integrin receptors.

It is encoded by the *SPP1* gene, which maps to the long arm of chromosome 4 [6] as a tandem array and generates three splice variants of mRNA, including the isoforms OPN-A, OPN-B, and OPN-C. OPN-A constitutes the full-length variant [2], whereas isoforms B (missing exon 5) and C (missing exon 4) are the splice variants [1, 2]. These different forms can display specific expression and have distinct biological roles in different cell contexts. The name "osteopontin" was chosen by Heinegard's group that cloned the protein from the rat osteosarcoma. OPN is produced by cells located in the osteoid matrix, and its name "osteopontin" denotes the property of acting as a bridge ("pons" in Latin) between cells

and hydroxyapatite of bone [2, 6]. OPN exists as a secreted (sOPN) and intracellular form (iOPN) [2], being translated from different start codon in the single OPN mRNA.

Intracellular OPN was initially described by Sodek's group in rat calvarial cells [2, 3].

Although OPN exists intracellularly as a regulator of cytoskeleton dynamics and gene expression, most studies have focused on the secreted form.

2. Osteopontin Functions

OPN is a multifunctional protein widely distributed in many tissues and body fluids, such as plasma, urine, milk, and bile [10, 11]. It is produced by several cell types, including immune cells like activated macrophages and T cells, cells of brain and kidney, vascular smooth muscle cells, bone marrow myoblasts, dendritic cells, hepatocytes, and neural cells [2, 6, 9]. Furthermore, OPN is produced by cells involved in bone morphogenesis such as osteoblasts and osteoclasts. OPN regulates various biological activities including matrix remodeling and tissue calcification, monocytes/macrophages migration and chemiotaxis, production of a variety of proinflammatory cytokines and chemokines, and inhibition of apoptosis activities [6]. Furthermore, it is involved in pathophysiological processes as malignancy, insulin resistance and type 2 diabetes, autoimmune disorders, atherosclerosis, steatotic hepatitis, end-stage kidney failure, response to stress, obesity-induced inflammation, and osteoporosis [3, 8]. Recently, numerous researches have examined whether there is a relationship between obesity and osteoporosis. Obesity and osteoporosis are two related polygenic disorders of body composition and represent a major health threat worldwide, with high impact on both morbidity and mortality [12, 13]. Interestingly, an increase of OPN levels in serum and cerebrospinal fluid was found in Alzheimer's disease (AD) patients [14]. AD is a chronic neurodegenerative disease and is the cause of 60% to 70% of cases of dementia [15–18]. Conversely, a decrease of OPN levels was associated with the improvement of cognitive functions [19, 20].

At bone level, OPN has multifaceted effects on morphogenesis and remodeling [3, 6, 13, 14], being associated with bone turnover and bone mineral density (BMD). Experimental evidence suggests that the gene of OPN is one of the most overexpressed genes in the adipose tissue of obese patients [1, 8].

3. Fat-Bone Relation

The relationship between obesity and skeleton is complex and not yet fully understood. Body mass index (BMI) is generally recognized to have a good positive correlation with bone mineral density (BMD) as measured by central Dual-Energy X-Ray Absorptiometry (DXA) [21]. For a long time it has been thought that obesity was apparently beneficial for bone metabolism [22, 23], particularly in women after menopause, playing a protective effect against the development of bone loss and osteoporosis. Adiposity might ensure bone health probably for the relative hyperestrogenism produced by adipocytes from androgen precursor in postmenopausal women [24–26]. Also the well-established positive effect of mechanical loading (muscle contraction and gravitational loading) related to body weight might positively influence BMD, by decreasing apoptosis and facilitating osteogenic differentiation through the activation of Wnt/b-catenin signaling pathway [27–31]. However, in last decades the view that obesity has an protective effect against osteoporosis has been questioned [32, 33]. Some reports have shown that excessive visceral fat and fat mass have negative effects on bone health, being associated with low total bone mineral density and content [34–36]. According to these results, another study conducted in healthy premenopausal women demonstrated that central adiposity was associated with low bone quality [37]. Furthermore, it has been suggested that in men and pre- and postmenopausal women fat mass plays a key role in bone health, representing the significant determinant of BMD at the lumbar spine and proximal femur [19, 22]. Similarly, Greco et al. [38], in a cross-sectional study, evaluated 340 obese women and showed that trunk fat negatively correlated with BMD playing a detrimental role in skeletal metabolism in terms of low BMD, bone markers, and systemic factors influencing bone tissue.

Interestingly, Papakitsou et al. [39] found in obese women a lower rate of bone formation as measured by the serum concentration of type I collagen propeptide, suggesting that obesity can inhibit the production of new collagen. Finally, recent in vitro data supported the hypothesis of decreased osteoblast activity in subjects with increase of trunk mass because of alterations of the Wnt/β-catenin pathway [40]. Therefore, obesity and fat accumulation might be detrimental to bone health. However, further investigations are required to better understand the complex pathophysiological relationship between body weight and BMD. Different theories have been proposed to explain the complex interplay between adipose tissue and bone [16, 17]. It has been proposed that the pathophysiological relevance of adipose tissue in bone turnover resides in the participation of three possible mechanisms. (1) There is an intimate link between adipocytes and osteoblasts related to their common origin from a progenitor cell, the pluripotential mesenchymal stem cell (MSCs) that resides in a specialized bone niche [41–43]. As a common precursor, the controlled lineage commitment of MSCs plays an important role in the maintenance of skeleton homeostasis. Osteoblast/adipocyte differentiation, although not mutually exclusive, is intertwined and highly regulated by several cell-derived transcription factors [44] and has been implicated in modification of bone remodeling. For example, recently Yeung et al. [45] have demonstrated that postmenopausal women have more than twice bone marrow fat compared with premenopausal women. (2) Adipose tissue is not only a passive energy reservoir but also an active, complex endocrine organ [16, 17] that plays an important role in regulating whole body homeostasis. Adipose tissue secretes various signaling molecules and bioactive compounds, named adipokines (leptin, resistin, IL6, osteopontin, etc.). Adipokines influence bone remodeling (obesity of bone) through upregulated proinflammatory cytokine production and exert an indirect effect on the sympathetic tone via hypothalamic nuclei. Expression

array studies on human adipose tissue have pointed out an activation of several inflammatory pathways in obesity [46]. In fact, chronic low-grade inflammation is associated with adipose tissue expansion in obesity and it is determined by increased systemic concentrations of proinflammatory endocrine cytokines, such as TNF-alfa [47], and osteopontin [1, 33] in patients and animal models of obesity. These cytokines may uncouple bone remodeling by stimulating osteoclast activity or inhibiting bone formation modifying the receptor activator [16]. Thus, all these mechanisms may represent a crosstalk between adipose tissue and skeleton, detrimental for bone health. The exact nature of factor that triggers this mechanisms is unknown.

Osteocalcin is a 49-amino acid bone matrix noncollagen protein produced by osteoblasts, which is involved in bone deposition and calcium homeostasis. Studies show that osteocalcin also has an important role in energy homeostasis and glucose metabolism: in cross-sectional and prospective epidemiological studies, circulating osteocalcin levels are inversely associated with the risk of type 2 diabetes [48, 49], metabolic syndrome [50, 51], overall/abdominal adiposity and insulin resistance [52], and reduced BMD [38].

Furthermore, OC levels were positively associated with cognitive performance in older nondemented women [53–56]. Genetic osteocalcin deletion induced glucose intolerance, increased fat mass, insulin resistance, decreased expression of insulin target genes in liver and muscle, and decreased adiponectin gene expression in adipose tissue. In contrast, recombinant osteocalcin administration improved insulin secretion and sensitivity and prevented high-fat-induced obesity and diabetes.

In addition to improving pancreatic insulin secretion, experimental models show that osteocalcin can protect against high-fat-induced obesity, insulin resistance, and nonalcoholic fatty liver disease (NAFLD) [57, 58]. Epidemiological studies are sometimes conflicting and require further validation [59]. Currently the osteocalcin is emerging as an important modulator of energy homeostasis and the metabolism of glucose in various tissues, raising the possibility that this bone-derived hormone may become a new treatment for obesity-related disorders, a hypothesis currently being tested.

4. Dysregulation of Osteopontin

In mouse models and obese humans, OPN is one of many inflammatory molecules overexpressed in adipose tissue [60, 61]. Besides, its levels showed a great difference in adipose tissue between monozygotic twins discordant for obesity condition [62]. Its overexpression in obese adipose tissue is mainly attributable to accumulation of the macrophages [1] and other inflammatory cells, stromal vascular cells, and adipocytes. Nomiyama et al. [63] suggested that OPN might be involved in linking obesity-induced inflammatory processes and metabolic changes in adipose tissue. Similarly, it has described a high level of OPN RNA expression in adipose tissue of obese insulin resistant rats and humans [8]. Kiefer and colleagues [1] showed that obesity is associated with a striking increase of OPN expression selectively within adipose tissue. Adipose tissues are the major source of OPN and also of its obesity-induced upregulation. These data point toward a specific pathophysiological role of OPN in obesity. Therefore, OPN could be a key regulator of inflammatory processes linked to obesity-induced adipose tissue inflammation and become a major target for treatment of adipose tissue inflammation-related disorders. Recently, it has been shown that genetic OPN deficiency and antibody-mediated neutralisation in mice improve inflammation and protect from obesity and insulin resistance induced by a high-fat diet [46]. OPN would act as proinflammatory cytokine and have pleiotropic function in inflammation. The primary role of OPN seems to facilitate recovery of the organism after injury or infection [38]. However, several studies have highlighted the critical role of OPN in regulating not only adipose tissue inflammation, but also insulin resistance and diabetes mellitus [64, 65].

Recently, an alteration of adipose tissue function has been related to various human metabolism disorders such as osteoporosis [66]. It has been suggested that OPN influences adipogenic process, in bone marrow of obese women, contributing to the development of osteoporosis. An imbalance has been described between normal adipogenesis and osteogenesis of MSCs, prevailing adipocyte differentiation on osteoblast differentiation [67]. MSCs isolated from bone marrow in postmenopausal patients with osteoporosis express more adipocytic differentiation markers than those in women with normal bone mass [68]. Meunier et al. [69] analyzed 81 iliac crest biopsies from elderly women and observed a considerable amount of fat in bone marrow of women with osteoporosis, relative to levels of fat in healthy young women. This observation was confirmed in subsequent studies [70–72]. An increment of marrow adipocytes was observed also by Schellinger et al. [73]. After oophorectomy, rats showed an increase in the amount of fat in the bone marrow [17]. Fat infiltration might considerate a typical example of lipotoxicity. Triggiani and colleagues [30], too, have observed similar results.

Many researchers considered osteoporosis as a faultiness of bone marrow MSCs [74] in differentiating into other cell lineages, with adipogenesis being enhanced compared to osteoblastogenesis. Molecular mechanisms of adipocyte differentiation have been studied using both in vitro and in vivo models but the cellular and molecular mechanisms mediating the pathological switch in fat remain to be determined [39]. What is the player of the fat-bone axis in the bone marrow? Because OPN−/− mice could be due to changes in the balance between osteogenic and adipogenic differentiation by MSCs [3], we want to know the role of OPN in MSCs differentiation. Further studies are needed to define the precise relationship between obesity and osteoporosis. Previous studies have shown that, in overweight and obese humans, the dysregulation of circulating signaling factors, such as inflammatory cytokines, might play an important role in changes of MSC differentiation [75–78]. Among cytokines, OPN may represent a multifaceted regulator between fat and bone on bone remodeling and contribute to the development of osteoporosis [3]. In the study conducted by Inoue and Shinohara [3] on the effects of secreted OPN in regulating MSC

differentiation, the authors revealed an important role of OPN-integrin $\alpha v/\beta 1$ in regulating adipogenic and osteogenic differentiation. Di Bernardo et al. [78] in their study in vitro observed that the incubation of MSCs with the sera of overweight individuals promoted a bias in differentiating MSCs in adipogenic line, probably for a modification of circulating cytokines. OPN by itself induces expression of a variety of proinflammatory cytokines and chemokines being an important regulator for initiating adipose tissue macrophage and macrophage-like cells infiltration, triggering a vicious circle in which inflammatory cytokines play important roles in MSC differentiation. Moreover, other studies are required to elucidate the precise role of OPN in the pathophysiology of osteoporosis and as a possible crucial link of bone-adipose axis.

5. Conclusion

OPN was identified in 1980; it is a key regulator of many metabolic and inflammatory diseases, such as diabetes, cardiovascular disease, and obesity. Some studies have shown that OPN is causally involved in the pathogenesis of insulin resistance and type 2 diabetes, while other studies have shown that OPN is a protective islet protein preserving insulin secretion. In addition, experimental and epidemiological evidence emerging disclosed complex cytokine and hormonal crosstalk between bone cells, liver, and adipose tissue, which adjusts coordinated bone remodeling, energy metabolism, and glucose homeostasis; changes in this network may contribute to the pathogenesis of obesity and related disorders [58], but some key questions have not yet been resolved. Therefore, further research will clarify the clinical significance of these changes that cause metabolic and inflammatory diseases, and they will identify individuals at higher risk for developing such complications and for therapeutic purposes.

Disclosure

Carolina De Fusco and Antonietta Messina are first authors.

Competing Interests

The authors declare that they have no competing interests.

References

[1] F. W. Kiefer, M. Zeyda, J. Todoric et al., "Osteopontin expression in human and murine obesity: extensive local up-regulation in adipose tissue but minimal systemic alterations," *Endocrinology*, vol. 149, no. 3, pp. 1350–1357, 2008.

[2] Y. Wen, S. Jeong, Q. Xia, and X. Kong, "Role of osteopontin in liver diseases," *International Journal of Biological Sciences*, vol. 12, no. 9, pp. 1121–1128, 2016.

[3] M. Inoue and M. L. Shinohara, "Intracellular osteopontin (iOPN) and immunity," *Immunologic Research*, vol. 49, no. 1–3, pp. 160–172, 2011.

[4] Q. Chen, P. Shou, L. Zhang et al., "An osteopontin-integrin interaction plays a critical role in directing adipogenesis and osteogenesis by mesenchymal stem cells," *Stem Cells*, vol. 32, no. 2, pp. 327–337, 2014.

[5] K. A. Staines, V. E. MacRae, and C. Farquharson, "The importance of the SIBLING family of proteins on skeletal mineralisation and bone remodelling," *Journal of Endocrinology*, vol. 214, no. 3, pp. 241–255, 2012.

[6] A. N. Kothari, M. L. Arffa, V. Chang et al., "Osteopontin—a master regulator of epithelial-mesenchymal transition," *Journal of Clinical Medicine*, vol. 5, no. 4, p. 39, 2016.

[7] T. E. Kruger, A. H. Miller, A. K. Godwin, and J. Wang, "Bone sialoprotein and osteopontin in bone metastasis of osteotropic cancers," *Critical Reviews in Oncology/Hematology*, vol. 89, no. 2, pp. 330–341, 2014.

[8] A. Oldberg, A. Franzen, and D. Heinegard, "Cloning and sequence analysis of rat bone sialoprotein (osteopontin) cDNA reveals an Arg-Gly-Asp cell-binding sequence," *Proceedings of the National Academy of Sciences of the United States of America*, vol. 83, no. 23, pp. 8819–8823, 1986.

[9] J. Sodek, B. Ganss, and M. McKee, "Osteopontin," *Critical Reviews in Oral Biology & Medicine*, vol. 11, no. 3, pp. 279–303, 2000.

[10] J. Chapman, P. D. Miles, J. M. Ofrecio et al., "Osteopontin is required for the early onset of high fat diet-induced insulin resistance in mice," *PLoS ONE*, vol. 5, no. 11, Article ID e13959, 2010.

[11] F. W. Kiefer, S. Neschen, B. Pfau et al., "Osteopontin deficiency protects against obesity-induced hepatic steatosis and attenuates glucose production in mice," *Diabetologia*, vol. 54, no. 8, pp. 2132–2142, 2011.

[12] C. J. Rosen and M. L. Bouxsein, "Mechanisms of disease: is osteoporosis the obesity of bone?" *Nature Clinical Practice Rheumatology*, vol. 2, no. 1, pp. 35–43, 2006.

[13] S. Rössner, "Obesity: the disease of the twenty-first century," *International Journal of Obesity*, vol. 26, no. S4, pp. S2–S4, 2002.

[14] C. Comi, M. Carecchio, A. Chiocchetti et al., "Osteopontin is increased in the cerebrospinal fluid of patients with Alzheimer's disease and its levels correlate with cognitive decline," *Journal of Alzheimer's Disease*, vol. 19, no. 4, pp. 1143–1148, 2010.

[15] C. Aurilio, M. C. Pace, M. B. Passavanti et al., "Chronic pain pharmacological treatment in patients with depressive disorders," *African Journal of Psychiatry*, vol. 18, article 307, 2015.

[16] A. Burns and S. Iliffe, "Alzheimer's disease," *BMJ*, vol. 338, p. b158, 2009.

[17] S. Chieffi, C. Secchi, and M. Gentilucci, "Deictic word and gesture production: their interaction," *Behavioural Brain Research*, vol. 203, no. 2, pp. 200–206, 2009.

[18] A. Iavarone, M. Patruno, F. Galeone, S. Chieffi, and S. Carlomagno, "Brief report: error pattern in an autistic savant calendar calculator," *Journal of Autism and Developmental Disorders*, vol. 37, no. 4, pp. 775–779, 2007.

[19] P. Iaffaldano, M. Ruggieri, R. G. Viterbo, M. Mastrapasqua, and M. Trojano, "The improvement of cognitive functions is associated with a decrease of plasma Osteopontin levels in Natalizumab treated relapsing multiple sclerosis," *Brain, Behavior, and Immunity*, vol. 35, pp. 96–101, 2014.

[20] S. Chieffi, M. Conson, and S. Carlomagno, "Movement velocity effects on kinaesthetic localisation of spatial positions," *Experimental Brain Research*, vol. 158, no. 4, pp. 421–426, 2004.

[21] C. Poiana, M. Carsote, V. Radoi, A. Mihai, and C. Capatina, "Prevalent osteoporotic fractures in 622 obese and non- obese menopausal women," *Journal of medicine and life*, vol. 8, no. 4, pp. 462–466, 2015.

[22] M. Monda, G. Messina, I. Scognamiglio et al., "Short-term diet and moderate exercise in young overweight men modulate cardiocyte and hepatocarcinoma survival by oxidative stress," *Oxidative Medicine and Cellular Longevity*, vol. 2014, Article ID 131024, 7 pages, 2014.

[23] E. A. Greco, A. Lenzi, and S. Migliaccio, "The obesity of bone," *Therapeutic Advances in Endocrinology and Metabolism*, vol. 6, no. 6, pp. 273–286, 2015.

[24] L. Guo, X. Yang, H. Zhu et al., "Sertoli-Leydig cell tumor presenting hyperestrogenism in a postmenopausal woman: a case report and review of the literature," *Taiwanese Journal of Obstetrics and Gynecology*, vol. 51, no. 4, pp. 620–624, 2012.

[25] V. Monda, A. Valenzano, F. Moscatelli et al., "Modifications of activity of autonomic nervous system, and resting energy expenditure in women using hormone-replacement therapy," *Biology and Medicine*, vol. 8, no. 5, article no. 306, 2016.

[26] G. Messina, V. Monda, F. Moscatelli et al., "Role of orexin system in obesity," *Biology and Medicine*, vol. 7, Article ID 1000248, 2015.

[27] K. Hayashida, Y. Takeda, H. Yatake et al., "Relationship between bone mineral density and body composition estimated by dual-energy x-ray absorptiometry: comparison between groups aged 20–39 and 40–59 years," *Kobe Journal of Medical Sciences*, vol. 61, no. 4, pp. E97–E101, 2015.

[28] J. Menzel, R. di Giuseppe, A. Wientzek, A. Kroke, H. Boeing, and C. Weikert, "Physical activity, bone health, and obesity in Peri-/Pre- and postmenopausal women: results from the EPIC-potsdam study," *Calcified Tissue International*, vol. 97, no. 4, pp. 376–384, 2015.

[29] D. Gatti, O. Viapiana, L. Idolazzi et al., "Distinct effect of zoledronate and clodronate on circulating levels of DKK1 and sclerostin in women with postmenopausal osteoporosis," *Bone*, vol. 67, pp. 189–192, 2014.

[30] A. I. Triggiani, A. Valenzano, M. A. P. Ciliberti et al., "Heart rate variability is reduced in underweight and overweight healthy adult women," *Clinical Physiology and Functional Imaging*, 2015.

[31] F. Moscatelli, G. Messina, A. Valenzano et al., "Differences in corticospinal system activity and reaction response between karate athletes and non-athletes," *Neurological Sciences*, vol. 37, no. 12, pp. 1947–1953, 2016.

[32] S. Migliaccio, E. A. Greco, R. Fornari, L. M. Donini, and A. Lenzi, "Is obesity in women protective against osteoporosis?" *Diabetes, Metabolic Syndrome and Obesity: Targets and Therapy*, vol. 4, pp. 273–282, 2011.

[33] K. Zhu, M. Hunter, A. James, E. M. Lim, and J. P. Walsh, "Associations between body mass index, lean and fat body mass and bone mineral density in middle-aged Australians: the Busselton Healthy Ageing Study," *Bone*, vol. 74, pp. 146–152, 2015.

[34] M. Monda, G. Messina, C. Mangoni, and B. De Luca, "Resting energy expenditure and fat-free mass do not decline during aging in severely obese women," *Clinical Nutrition*, vol. 27, no. 4, pp. 657–659, 2008.

[35] G. Messina, A. Viggiano, D. Tafuri et al., "Role of orexin in obese patients in the intensive care unit," *Journal of Anesthesia and Clinical Research*, vol. 5, no. 3, Article ID 1000395, 2014.

[36] K.-C. Kim, D.-H. Shin, S.-Y. Lee, J.-A. Im, and D.-C. Lee, "Relation between obesity and bone mineral density and vertebral fractures in Korean postmenopausal women," *Yonsei Medical Journal*, vol. 51, no. 6, pp. 857–863, 2010.

[37] A. Cohen, D. W. Dempster, R. R. Recker et al., "Abdominal fat is associated with lower bone formation and inferior bone quality in healthy premenopausal women: a transiliac bone biopsy study," *Journal of Clinical Endocrinology and Metabolism*, vol. 98, no. 6, pp. 2562–2572, 2013.

[38] E. A. Greco, D. Francomano, R. Fornari et al., "Negative association between trunk fat, insulin resistance and skeleton in obese women," *World Journal of Diabetes*, vol. 4, no. 2, pp. 31–39, 2013.

[39] E. F. Papakitsou, A. N. Margioris, K. E. Dretakis et al., "Body mass index (BMI) and parameters of bone formation and resorption in postmenopausal women," *Maturitas*, vol. 47, no. 3, pp. 185–193, 2004.

[40] F. Wannenes, V. Papa, E. A. Greco et al., "Abdominal fat and sarcopenia in women significantly alter osteoblasts homeostasis in vitro by a WNT/β-catenin dependent mechanism," *International Journal of Endocrinology*, vol. 2014, Article ID 278316, 10 pages, 2014.

[41] L. da Silva Meirelles, P. C. Chagastelles, and N. B. Nardi, "Mesenchymal stem cells reside in virtually all post-natal organs and tissues," *Journal of Cell Science*, vol. 119, no. 11, pp. 2204–2213, 2006.

[42] T. Akune, S. Ohba, S. Kamekura et al., "PPARγ insufficiency enhances osteogenesis through osteoblast formation from bone marrow progenitors," *Journal of Clinical Investigation*, vol. 113, no. 6, pp. 846–855, 2004.

[43] C. M. Digirolamo, D. Stokes, D. Colter, D. G. Phinney, R. Class, and D. J. Prockop, "Propagation and senescence of human marrow stromal cells in culture: a simple colony-forming assay identifies samples with the greatest potential to propagate and differentiate," *British Journal of Haematology*, vol. 107, no. 2, pp. 275–281, 1999.

[44] T. Takahashi, "Overexpression of Runx2 and MKP-1 stimulates transdifferentiation of 3T3-L1 preadipocytes into bone-forming osteoblasts in vitro," *Calcified Tissue International*, vol. 88, no. 4, pp. 336–347, 2011.

[45] D. K. W. Yeung, J. F. Griffith, G. E. Antonio, F. K. H. Lee, J. Woo, and P. C. Leung, "Osteoporosis is associated with increased marrow fat content and decreased marrow fat unsaturation: a proton MR spectroscopy study," *Journal of Magnetic Resonance Imaging*, vol. 22, no. 2, pp. 279–285, 2005.

[46] S. Nair, Y. H. Lee, E. Rousseau et al., "Increased expression of inflammation-related genes in cultured preadipocytes/stromal vascular cells from obese compared with non-obese Pima Indians," *Diabetologia*, vol. 48, no. 9, pp. 1784–1788, 2005.

[47] G. S. Hotamisligil, N. S. Shargill, and B. M. Spiegelman, "Adipose expression of tumor necrosis factor-α: direct role in obesity-linked insulin resistance," *Science*, vol. 259, no. 5091, pp. 87–91, 1993.

[48] A. Movahed, B. Larijani, I. Nabipour et al., "Reduced serum osteocalcin concentrations are associated with type 2 diabetes mellitus and the metabolic syndrome components in post-menopausal women: the crosstalk between bone and energy metabolism," *Journal of Bone and Mineral Metabolism*, vol. 30, no. 6, pp. 683–691, 2012.

[49] C. Ngarmukos, L.-O. Chailurkit, S. Chanprasertyothin, B. Hengprasith, P. Sritara, and B. Ongphiphadhanakul, "A reduced serum level of total osteocalcin in men predicts the development of diabetes in a long-term follow-up cohort," *Clinical Endocrinology*, vol. 77, no. 1, pp. 42–46, 2012.

[50] M. M. Oosterwerff, N. M. Van Schoor, P. Lips, and E. M. W. Eekhoff, "Osteocalcin as a predictor of the metabolic syndrome in older persons: a population-based study," *Clinical Endocrinology*, vol. 78, no. 2, pp. 242–247, 2013.

[51] K. B. D. S. Magalhães, M. M. Magalhães, E. T. Diniz, C. S. Lucena, L. Griz, and F. Bandeira, "Metabolic syndrome and central fat distribution are related to lower serum osteocalcin concentrations," *Annals of Nutrition and Metabolism*, vol. 62, no. 3, pp. 183–188, 2013.

[52] Y. Bao, M. Xiaojing, R. Yang et al., "Inverse relationship between serum osteocalcin levels and visceral fat area in Chinese men," *Journal of Clinical Endocrinology and Metabolism*, vol. 98, no. 1, pp. 345–351, 2013.

[53] S. Bradburn, J. S. McPhee, L. Bagley et al., "Association between osteocalcin and cognitive performance in healthy older adults," *Age and Ageing*, vol. 45, no. 6, pp. 844–849, 2016.

[54] S. Chieffi, A. Iavarone, A. Viggiano, M. Monda, and S. Carlomagno, "Effect of a visual distractor on line bisection," *Experimental Brain Research*, vol. 219, no. 4, pp. 489–498, 2012.

[55] S. Chieffi, T. Iachini, A. Iavarone, G. Messina, A. Viggiano, and M. Monda, "Flanker interference effects in a line bisection task," *Experimental Brain Research*, vol. 232, no. 4, pp. 1327–1334, 2014.

[56] A. Viggiano, S. Chieffi, D. Tafuri, G. Messina, M. Monda, and B. De Luca, "Laterality of a second player position affects lateral deviation of basketball shooting," *Journal of Sports Sciences*, vol. 32, no. 1, pp. 46–52, 2014.

[57] A. Kode, I. Mosialou, B. C. Silva et al., "FoxO1 protein cooperates with ATF4 protein in osteoblasts to control glucose homeostasis," *The Journal of Biological Chemistry*, vol. 287, no. 12, pp. 8757–8768, 2012.

[58] G. Musso, E. Paschetta, R. Gambino, M. Cassader, and F. Molinaro, "Interactions among bone, liver, and adipose tissue predisposing to diabesity and fatty liver," *Trends in Molecular Medicine*, vol. 19, no. 9, pp. 522–535, 2013.

[59] N. Abseyi, Z. Şiklar, M. Berberoğlu, B. Hacihamdioğlu, Ş. S. Erdeve, and G. Öçal, "Relationships between osteocalcin, glucose metabolism, and adiponectin in obese children: is there crosstalk between bone tissue and glucose metabolism?" *JCRPE Journal of Clinical Research in Pediatric Endocrinology*, vol. 4, no. 4, pp. 182–188, 2012.

[60] D. D. Sears, G. Hsiao, A. Hsiao et al., "Mechanisms of human insulin resistance and thiazolidinedione-mediated insulin sensitization," *Proceedings of the National Academy of Sciences of the United States of America*, vol. 106, no. 44, pp. 18745–18750, 2009.

[61] H. Xu, G. T. Barnes, Q. Yang et al., "Chronic inflammation in fat plays a crucial role in the development of obesity-related insulin resistance," *The Journal of Clinical Investigation*, vol. 112, no. 12, pp. 1821–1830, 2003.

[62] K. H. Pietiläinen, J. Naukkarinen, A. Rissanen et al., "Global transcript profiles of fat in monozygotic twins discordant for BMI: pathways behind acquired obesity," *PLoS Medicine*, vol. 5, no. 3, pp. 472–483, 2008.

[63] T. Nomiyama, D. Perez-Tilve, D. Ogawa et al., "Osteopontin mediates obesity-induced adipose tissue macrophage infiltration and insulin resistance in mice," *The Journal of Clinical Investigation*, vol. 117, no. 10, pp. 2877–2888, 2007.

[64] F. J. A. de Paula, M. C. Horowitz, and C. J. Rosen, "Novel insights into the relationship between diabetes and osteoporosis," *Diabetes/Metabolism Research and Reviews*, vol. 26, no. 8, pp. 622–630, 2010.

[65] F. W. Kiefer, M. Zeyda, K. Gollinger et al., "Neutralization of osteopontin inhibits obesity-induced inflammation and insulin resistance," *Diabetes*, vol. 59, no. 4, pp. 935–946, 2010.

[66] M. Kawai, F. J. A. de Paula, and C. J. Rosen, "New insights into osteoporosis: the bone-fat connection," *Journal of Internal Medicine*, vol. 272, no. 4, pp. 317–329, 2012.

[67] J. P. Rodrguez, L. Montecinos, S. Ros, P. Reyes, and J. Martnez, "Mesenchymal stem cells from osteoporotic patients produce a type I collagen-deficient extracellular matrix favoring adipogenic differentiation," *Journal of Cellular Biochemistry*, vol. 79, no. 4, pp. 557–565, 2000.

[68] I. Sekiya, B. L. Larson, J. T. Vuoristo, J.-G. Cui, and D. J. Prockop, "Adipogenic differentiation of human adult stem cells from bone marrow stroma (MSCs)," *Journal of Bone and Mineral Research*, vol. 19, no. 2, pp. 256–264, 2004.

[69] P. Meunier, J. Aaron, C. Edouard, and G. Vignon, "Osteoporosis and the replacement of cell populations of the marrow by adipose tissue. A quantitative study of 84 iliac bone biopsies," *Clinical Orthopaedics and Related Research*, vol. 80, pp. 147–154, 1971.

[70] C. Rozman, E. Feliu, L. Berga, J.-C. Reverter, C. Climent, and M.-J. Ferrán, "Age-related variations of fat tissue fraction in normal human bone marrow depend both on size and number of adipocytes: a stereological study," *Experimental Hematology*, vol. 17, no. 1, pp. 34–37, 1989.

[71] G. Messina, C. Vicidomini, A. Viggiano et al., "Enhanced parasympathetic activity of sportive women is paradoxically associated to enhanced resting energy expenditure," *Autonomic Neuroscience: Basic and Clinical*, vol. 169, no. 2, pp. 102–106, 2012.

[72] S. Verma, J. H. Rajaratnam, J. Denton, J. A. Hoyland, and R. J. Byers, "Adipocytic proportion of bone marrow is inversely related to bone formation in osteoporosis," *Journal of Clinical Pathology*, vol. 55, no. 9, pp. 693–698, 2002.

[73] D. Schellinger, Chin Shoou Lin, H. G. Hatipoglu, and D. Fertikh, "Potential value of vertebral proton MR spectroscopy in determining bone weakness," *American Journal of Neuroradiology*, vol. 22, no. 8, pp. 1620–1627, 2001.

[74] B. Gao, L. Yang, and Z.-J. Luo, "Transdifferentiation between bone and fat on bone metabolism," *International Journal of Clinical and Experimental Pathology*, vol. 7, no. 5, pp. 1834–1841, 2014.

[75] M. Esposito, F. P. Serpe, G. Diletti et al., "Serum levels of polychlorinated dibenzo-p-dioxins, polychlorinated dibenzofurans and polychlorinated biphenyls in a population living in the Naples area, southern Italy," *Chemosphere*, vol. 94, pp. 62–69, 2014.

[76] A. Viggiano, U. Nicodemo, E. Viggiano et al., "Mastication overload causes an increase in O2- production into the subnucleus oralis of the spinal trigeminal nucleus," *Neuroscience*, vol. 166, no. 2, pp. 416–421, 2010.

[77] B. Rinaldi, F. Guida, A. Furiano et al., "Effect of prolonged moderate exercise on the changes of nonneuronal cells in early myocardial infarction," *Neural Plasticity*, vol. 2015, Article ID 265967, 8 pages, 2015.

[78] G. Di Bernardo, G. Messina, S. Capasso et al., "Sera of overweight people promote in vitro adipocyte differentiation of bone marrow stromal cells," *Stem Cell Research and Therapy*, vol. 5, no. 1, article 4, 2014.

Hindawi Publishing Corporation
Stem Cells International
Volume 2016, Article ID 7403890, 12 pages
http://dx.doi.org/10.1155/2016/7403890

Research Article

Implant Composed of Demineralized Bone and Mesenchymal Stem Cells Genetically Modified with AdBMP2/AdBMP7 for the Regeneration of Bone Fractures in *Ovis aries*

Adelina A. Hernandez-Hurtado,[1,2] Gissela Borrego-Soto,[1,2] Ivan A. Marino-Martinez,[2] Jorge Lara-Arias,[3] Viktor J. Romero-Diaz,[4] Adalberto Abrego-Guerra,[5] Jose F. Vilchez-Cavazos,[3,6] Guillermo Elizondo-Riojas,[7] Herminia G. Martinez-Rodriguez,[1] Marcela A. Espinoza-Juarez,[1,2] Gloria C. Lopez-Romero,[1,2] Alejandro Robles-Zamora,[1] Oscar F. Mendoza Lemus,[3,6] Rocio Ortiz-Lopez,[1,2] and Augusto Rojas-Martinez[1,2]

[1]*Departmento de Bioquímica y Medicina Molecular, Facultad de Medicina, Universidad Autónoma de Nuevo León, Monterrey, Mexico*
[2]*Centro de Investigación y Desarrollo en Ciencias de la Salud, Universidad Autónoma de Nuevo León, Monterrey, Mexico*
[3]*Banco de Huesos y Tejidos, Hospital Universitario, Universidad Autónoma de Nuevo León, Monterrey, Mexico*
[4]*Departmento de Morfología, Facultad de Medicina, Universidad Autónoma de Nuevo León, Monterrey, Mexico*
[5]*Facultad de Medicina Veterinaria y Zootecnia, Universidad Autónoma de Nuevo León, Monterrey, Mexico*
[6]*Servicio de Ortopedia y Traumatología, Hospital Universitario, Universidad Autónoma de Nuevo León, Monterrey, Mexico*
[7]*Servicio de Radiología e Imagen, Hospital Universitario, Universidad Autónoma de Nuevo León, Monterrey, Mexico*

Correspondence should be addressed to Augusto Rojas-Martinez; arojasmtz@gmail.com

Received 30 April 2016; Accepted 29 June 2016

Academic Editor: Bin Li

Adipose-derived mesenchymal stem cells (ADMSCs) are inducible to an osteogenic phenotype by the bone morphogenetic proteins (BMPs). This facilitates the generation of implants for bone tissue regeneration. This study evaluated the *in vitro* osteogenic differentiation of ADMSCs transduced individually and in combination with adenoviral vectors expressing BMP2 and BMP7. Moreover, the effectiveness of the implant containing ADMSCs transduced with the adenoviral vectors AdBMP2/AdBMP7 and embedded in demineralized bone matrix (DBM) was tested in a model of tibial fracture in sheep. This graft was compared to ewes implanted with untransduced ADMSCs embedded in the same matrix and with injured but untreated animals. *In vivo* results showed accelerated osteogenesis in the group treated with the AdBMP2/AdBMP7 transduced ADMSC graft, which also showed improved restoration of the normal bone morphology.

1. Introduction

Mesenchymal stem cells (MSCs) are adult cells with fibroblastoid morphology and ability to differentiate into multiple tissues including bone, fat, muscle, and cartilage [1]. MSCs are identified by the positive expression of *CD13*, *CD73*, *CD90,* and *CD105* genes, whereas they are negative for expression of hematopoietic markers such as CD34 and CD45 [2–4].

MSCs from adipose tissue are easily accessible and yield up to 5,000 fibroblast forming units (CFU-F) per gram of adipose tissue, in comparison to around 100–1000 CFU-F per milliliter from bone marrow [5, 6]. Its high proliferation rate facilitates expanding ADMSCs in the laboratory for therapeutic purposes. Furthermore, it has been shown that these cells have four properties that could be useful in cell therapy: angiogenicity, osteogenicity, immunomodulation, and promotion of tissue remodeling [7].

ADMSCs of different species can be induced to osteogenic differentiation by stimulation with some members of the bone morphogenetic protein family (BMPs) [8–10].

Although the mechanism is still unclear, multiple BMPs promote osteogenic differentiation of ADMSCs, mostly through the SMAD and the noncanonical Wnt mediated Wnt5a signaling pathways [11]. This osteogenic differentiation can be achieved by stimulation with homodimeric or heterodimeric combinations of BMP ligands. Some reports suggest that BMP2/BMP7 or BMP2/BMP9 combinations are more effective in inducing osteogenesis in MSCs [12–14].

Most preclinical trials for osteogenic induction using MSCs and BMPs have been tested in rodents and other small animals [15–18]. Preclinical trials in large animals are necessary to obtain morphological and biomechanical information of implants based on MSCs that try to repair bone defects in large mammals, particularly in bones supporting body weight such as leg bones [19–21]. In addition, some reports reveal differences in osteogenic potential between species [22]. Although preclinical data of implants for bone regeneration employing MSCs are increasing, data generated from large mammals, such as sheep, are needed for scaling and translating technologies for clinical trials.

Our team previously generated an implant for bone regeneration in a canine mandibular distraction model. The implant was constituted by bone marrow MSCs transduced with BMP2 and embedded in DBM [23]. For the present report, the challenge was to repair a major lesion in the tibia of a sheep model. This bone is involved in supporting body weight at rest and during the movement of this large mammal. To assess the quality of newly formed bone, physical and histological evaluations were performed to test this implant, by studying the speed of the osteogenic regeneration, the quality of the healed tissues, and the morphology of the regenerated bones. The study group treated with BMP2/BMP7 transduced ADMSCs was compared with controls including a group treated with an implant of nontransduced ADMSCs and with a group of injured but untreated sheep.

2. Materials and Methods

This study was approved by the Ethics Committee of the University Hospital of the Universidad Autonoma de Nuevo Leon (UANL) with approval number BI12-003. Care of the animal used during experimental protocols was conducted according to the Mexican Official Standard for the handling of laboratory animals (NOM-062-ZOO-1999) within the premises of the School of Veterinary Medicine of the UANL.

2.1. Generation of Adenoviral Vectors. Adenoviral vectors AdBMP7 and AdBMP9 were constructed using the AdEasy vector system (Agilent Technologies, Santa Clara, CA) according to the methodology by Luo et al. [24]. AdBMP7 and AdBMP9 are first generation serotype 5 adenoviruses (ΔE1, ΔE3) that are transgene carriers of the human BMP7 and BMP9 proteins, respectively, directed by the cytomegalovirus (CMV) early promoter. AdBMP2 is a previously described [25] adenoviral vector carrying the BMP2 protein, kindly donated by Dr. Cristopher Evans. Recombinant adenoviruses were amplified in HEK293 cells, purified with cesium chloride gradients and dialyzed in buffer consisting of 10 mM Tris-HCl (pH 8.0), 140 mM NaCl, 1 mM $MgCl_2$, and 10% glycerol. Viral titration was performed by determining the optical density at 260 nm and by lytic plaques forming units according to the AdEasy vector system manual (Agilent Technologies).

2.2. Isolation and Characterization of Adipose Tissue ADMSCs. ADMSCs were isolated from biopsies of approximately 4 grams of sternal adipose tissue from sheep with a weight of 20 kg. Biopsies were transported at 4°C in phosphate buffer (PBS) supplemented with antibiotic/antimycotic and processed within the first 2 hours after lipectomy. Adipose tissue was excised and digested with type I collagenase 0.1% for 30 minutes at 37°C under constant stirring. After enzymatic digestion, it was centrifuged at 1,000 ×g for 5 minutes to form a cell pellet. The supernatant was discarded and 3 washes with PBS were performed to remove the fat phase and tissue debris. The cell pellet was resuspended in Dulbecco's Modified Eagle's medium (DMEM) (Invitrogen) supplemented with 1x glutamine (Invitrogen), 10% fetal bovine serum (FBS) (Invitrogen), and 1x antibiotic/antimycotic (GIBCO). Cells were incubated at 37°C with 5% CO_2 for 3 days. Nonadherent cells were removed with the spent medium and medium changes were performed periodically until an 80% confluence.

For immunophenotyping 10^6 cells per animal were used using anti-CD271-PE (Miltenyi Biotec), anti-MSCA-1 (W8B2)-APC (Miltenyi Biotec), and anti-CD45-FITC (Beckman Coulter) antibodies. CyAn ADP Analyzer (Beckman Coulter) cytometry was used for measurements. In addition to immunophenotyping, expression of the markers CD34, CD45, CD116, CD73, and GAPDH was determined by qPCR (quantitative real-time PCR) as an internal control using the primers listed in Supplementary Table S1 in Supplementary Material available online at http://dx.doi.org/10.1155/2016/7403890. For this, RNA extraction of total ADMSCs third passage with TRIzol® (Invitrogen) was performed following the manufacturer's instructions and cDNA was synthesized using SuperScript™ III First-Strand Synthesis SuperMix (Invitrogen), SYBR® GreenER™ qPCR SuperMix (Invitrogen), and they were analyzed by the $2^{-\Delta\Delta Ct}$ method. cDNA, 100 ng, was used for each reaction.

2.3. Differentiation of ADMSCs In Vitro. We seeded 90,000 cells/well in 6-well plaques and incubated these overnight at 37°C with 5% CO_2. Afterwards, ADMSCs were transduced with AdBMP2, AdBMP7, AdBMP9 (MOI = 100) and AdBMP2/AdBMP7 and AdBMP2/AdBMP9 (MOI = 50/50) combinations for 3 hours; subsequently 3 washes with PBS were performed. A positive control in which cells were stimulated with osteogenic medium (Advanced DMEM 10% FBS, 50 μM ascorbic acid, 10 mM β-glycerophosphate, and 100 mM dexamethasone) and a negative control of unstimulated cells were included. All experiments were performed in triplicate.

2.4. qPCR to Assess Osteogenic Differentiation. Osteogenic differentiation was assessed by osteocalcin (OC) and collagen type I (Col I) expression on days 8, 16, and 32 after induction using qPCR with the primers listed in Supplementary Table S1. Expression of the GAPDH gene was measured as a

gene normalizer. The reactions were performed as described above. The values registered for the unstimulated cells group (negative control) were considered baseline levels of expression and these were subtracted from the values of the other two groups.

2.5. Histological Staining. Histological analyses were performed on days 1 and 32 after induction of ADMSCs transduced with individual and combined adenoviral vectors and positive and negative controls as mentioned above. Masson's trichrome stain was used to observe cell morphology and collagen deposits, and von Kossa staining was used to observe calcium deposits. The production of type I and type II collagen was evaluated by immunohistochemistry (IHC). Slides were observed under a Nikon Model E600 microscope.

2.6. ELISA. Production of BMP2 and BMP7 proteins was verified by ELISA in ADMSCs transduced with AdBMP2, AdBMP7, the combination AdBMP2/AdBMP7, and the positive and negative controls on days 8, 16, and 32 after induction, using the commercial kits Quantikine-ELISA Human BMP2 and Quantikine-ELISA Human BMP7 (R&D Systems).

2.7. Obtaining Demineralized Bone Matrix (DBM). The DBM was obtained from sheep cancellous bone. The bones were ground in a special mill for bone. Traces of blood and fat were completely eliminated with a solution of 3% H_2O_2 and distilled, hot, sterile water. Subsequently, demineralization of the bone was conducted with 0.6 N HCl solution for 24 hours. Washes with distilled and sterile water were performed and the solution neutralized with a phosphate buffer at pH 7.0. The ground and demineralized bone was lyophilized to −0.070 mbar at −45°C for 24 hours and subsequently sterilized with gamma radiation.

2.8. Bone Regeneration Assays In Vivo. Twenty-one Pelibuey ewes of approximately 6 months of age and approximately 20 kg were used. Sheep were randomly assigned to three experimental groups made up of seven sheep each: Group I, control without an implant; Group II, implant with a DBM seeded with ADMSCs without transduction; Group III, implant with a DBM and ADMSCs transduced with AdBMP2/AdBMP7. The sheep were subjected to a first surgery to obtain adipose tissue, which was processed for the isolation of ADMSCs by enzymatic digestion with collagenase I, as described above. ADMSCs were grown to 10^6 cells per animal.

2.8.1. Generation and Grafting of Implants. Ten million ADMSCs obtained from adipose tissue for the generation of the implants were used; these were embedded in 1 cm^3 of DBM in 24-well plates. For Group III, ADMSCs were previously transduced with the vectors AdBMP2/AdBMP7 for 3 hours and then 3 washes with PBS were performed as described for the differentiation *in vitro*. The implants were transported on ice under sterile conditions immediately to the School of Veterinary Medicine and Animal Husbandry where the surgical procedure was performed. Surgery consisted of a distraction of the tibia under general anesthesia with a first step of sedation with ketamine (1 mL/10 kg of weight) and xylazine (0.5 mL/kg of weight). Later, the anesthetic 5% isoflurane was administered via an intratracheal tube and administration of the anesthetic was continued at 1-2% throughout the surgery with oxygen. Aseptically and with the animal in lateral decubitus, the medial side of the posterior tibial shaft was approached. The periosteum in the same area was removed, the center of the tibial shaft was identified, and a block of bone of 1 cm^3 was removed with the aid of a hand saw. One 3.5 mm dynamic compression plate (DCP) was placed, and a bone distraction of 10 mm was verified. The 3.5 mm DCP was fixed with 4 proximal and 4 distal osteotomy screws. Closure was performed with continuous 2-0 vicryl suture. Postoperative recovery was carried out in individual metabolic cages. During the next 7 days postsurgically, 1-2 mL/40 kg/24 h of Ceftiofur sodium (40 mg/mL) and 1-2 mL/50 kg/24 h of Flunixin (50 mg/mL) were administered intramuscularly; also, daily cleaning of the wound was carried out until healing with an antiseptic povidone-iodine solution and 10% Aluspray® (Vetoquinol, France).

2.8.2. Radiographic Analysis and 3D Tomography. Immediately postoperative, anteroposterior, and lateral X-rays were performed to confirm the space between the proximal and distal ends of the tibia. Each experimental group was given radiographic followup at weeks 4, 7, and 10. Five radiographic images of each animal at different observation times were obtained. 3D computerized tomography (CT) scan was performed in postmortem specimens of the injured bones from each animal. The bone segments were arrayed in the experimental groups abs immobilized in vertical position on a cardboard surface and were analyzed with a General Electric Light Speed VCT™ system using the following protocol: 100.0 kV, 100 mA, and 0.6 mm. This study was performed to study bone shapes, transversal structure and density, and bone regeneration.

2.8.3. Specimen Collection and Evaluation of Osteogenesis. Ten weeks after surgery, the sheep were euthanized with an intravenous overdose of phenobarbital-KCl and implants were retrieved for a postmortem neoformed bone assessment with histological staining of the fragment of the injured area of the sheep from each group. Before fixation, bone specimens were analyzed by CT scan as described before. For histological staining, implant areas were removed and fixed with formalin and glutaraldehyde for 7 days and decalcified with formic acid 10% for two weeks and 2 N HCl for 24 h. They were then dehydrated in alcohol and included in paraffin. Five-micron thick sections were made for staining with H&E and Masson's trichrome to observe morphology/cell repopulation and bone matrix synthesis, respectively. IHC was also performed for detection of collagen type I, collagen type II, and collagen type X, for which a pretreatment in buffer citrate pH = 6.0 was done, which consisted of preheating at 65°C and then incubation at 85°C for 20 minutes. Anti-collagen type I (rabbit polyclonal, dilution 1 : 300, cat. # ab34710), anti-collagen type II (rabbit polyclonal, dilution 1 : 500, cat. # ab34712), and anti-collagen type X (rabbit polyclonal, dilution 1 : 500, cat. # ab58632) antibodies from Abcam™ were

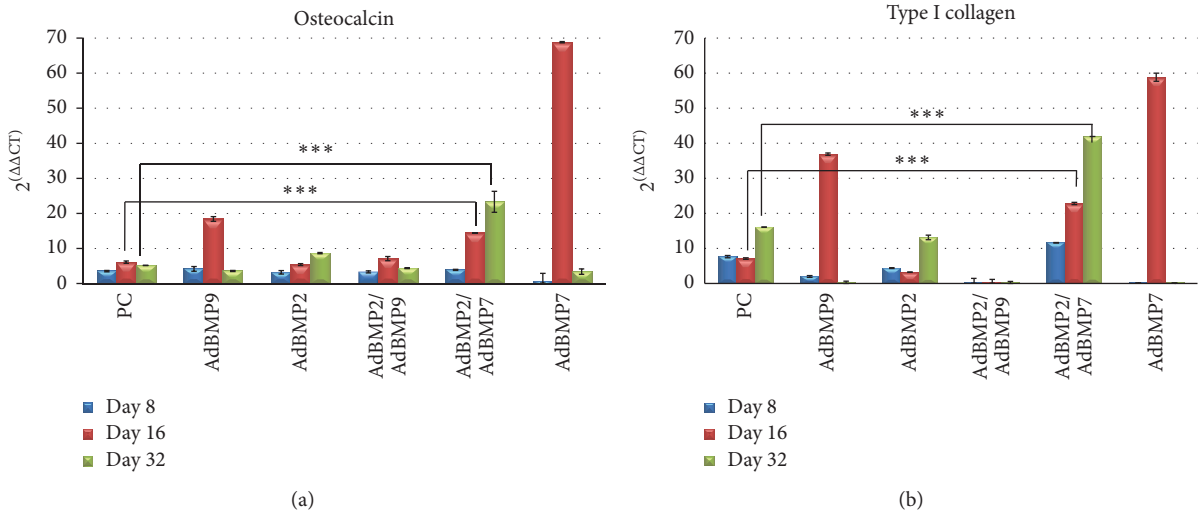

Figure 1: Relative expression analysis of (a) osteocalcin and (b) type I collagen by qPCR of MSCs transduced with AdBMP-2, AdBMP7, AdBMP9, and the combinations AdBMP2/AdBMP7 and AdBMP2/AdBMP9 on days 8, 16, and 32 after induction. The combination AdBMP2/AdBMP7 shows higher levels of osteocalcin and osteopontin and these were maintained for 32 days. *** significance level $P < 0.05$.

used. Sections were incubated with antibodies for 15 mins at room temperature and detected using the Mouse & Rabbit Specific HRP/DAB Detection IHC Kit, also from Abcam. Sections were counterstained with hematoxylin.

2.8.4. Biosafety and Toxicity Studies. Biosafety tests were conducted to evaluate the possible effect of adenoviral vectors on animals (particularly, inflammatory liver injury). Liver function tests and a blood count of each animal was performed one day before taking adipose tissue and 20 days after implant surgery. For each of the sheep, two blood samples from the jugular vein before and after the procedure were drawn.

2.9. Statistical Analysis. Expression data were analyzed to find statistically significant differences between the values of each experimental group using Student's t-test. SigmaPlot v11 (Systat Software) was used. The data are presented as mean ± standard deviation. The data obtained from ELISA tests were analyzed by the ANOVA test. A P value < 0.05 was considered significant.

3. Results

3.1. Characterization of ADMSCs. The cells isolated from adipose tissue showed fibroblastoid morphology and the mesenchymal phenotype was confirmed by positivity for the surface markers CD271 and MSCA-1 (85% of the cell population for both markers) and negative for CD45. qPCR demonstrated expression of CD166 and CD73 characteristic of ADMSCs and absence of CD45 and CD34, characteristic markers of hematopoietic cell lines.

3.2. In Vitro Differentiation Assays. Relative expression analysis of osteocalcin I and type I collagen mRNA was measured at different days of observation (days 8, 16, and 32) in the following groups: a positive control of ADMSCs cultured in osteogenic medium, ADMSCs singled transduced with AdBMP2, AdBMP7, AdBMP9, and combined transductions with AdBMP2/AdBMP7 and AdBMP2/AdBMP9. This study showed significantly increased levels of tested messengers in the group treated with the AdBMP2/AdBMP7 combination (Figures 1(a) and 1(b)). The effect in the group treated with AdBMP2 also showed a sustained, but less intense effect, similar to that observed in the control group for osteocalcin, and low levels of transcripts for collagen I. Although ADMSCs transduced with AdBMP7 had the highest expression levels of osteocalcin I and collagen type I, these were not sustained until day 32, as what also occurred with AdBMP9 and the AdBMP2/AdBMP9 combination. Additionally, cell death was observed in the cultures treated with AdBMP9 alone and in combination at day 32 of incubation. For this reason it was not possible to determine the production of proteins in subsequent assays.

Special stains, Masson's trichrome and von Kossa, were used to identify collagen and calcium deposits, respectively, in the experimental groups. Masson's trichrome showed the presence of collagen matrix on day 32 in ADMSCs transduced with the AdBMP2/AdBMP7 combination with a discrete blue staining of collagen mesh. However, the AdBMP2/AdBMP9 combination showed a higher proportion of collagen, resembling the staining of the positive control group (Figure 2(a)). The von Kossa stain identified scattered calcium deposits on the slides at day 1 after induction. The deposits at day 32 were mostly concentrated in a colocalization with the cell population; more deposits were observed with the combinations AdBMP2/AdBMP7 and AdBMP2/AdBMP9, with the combination AdBMP2/AdBMP7 being most similar to the positive control in cell organization and intensity of staining (Figure 2(b)). The presence of type I collagen by IHC was well established in the AdBMP2, AdBMP9 groups and with the combination AdBMP2/AdBMP7, with the latter group presenting a more uniform distribution of collagen type I fibers

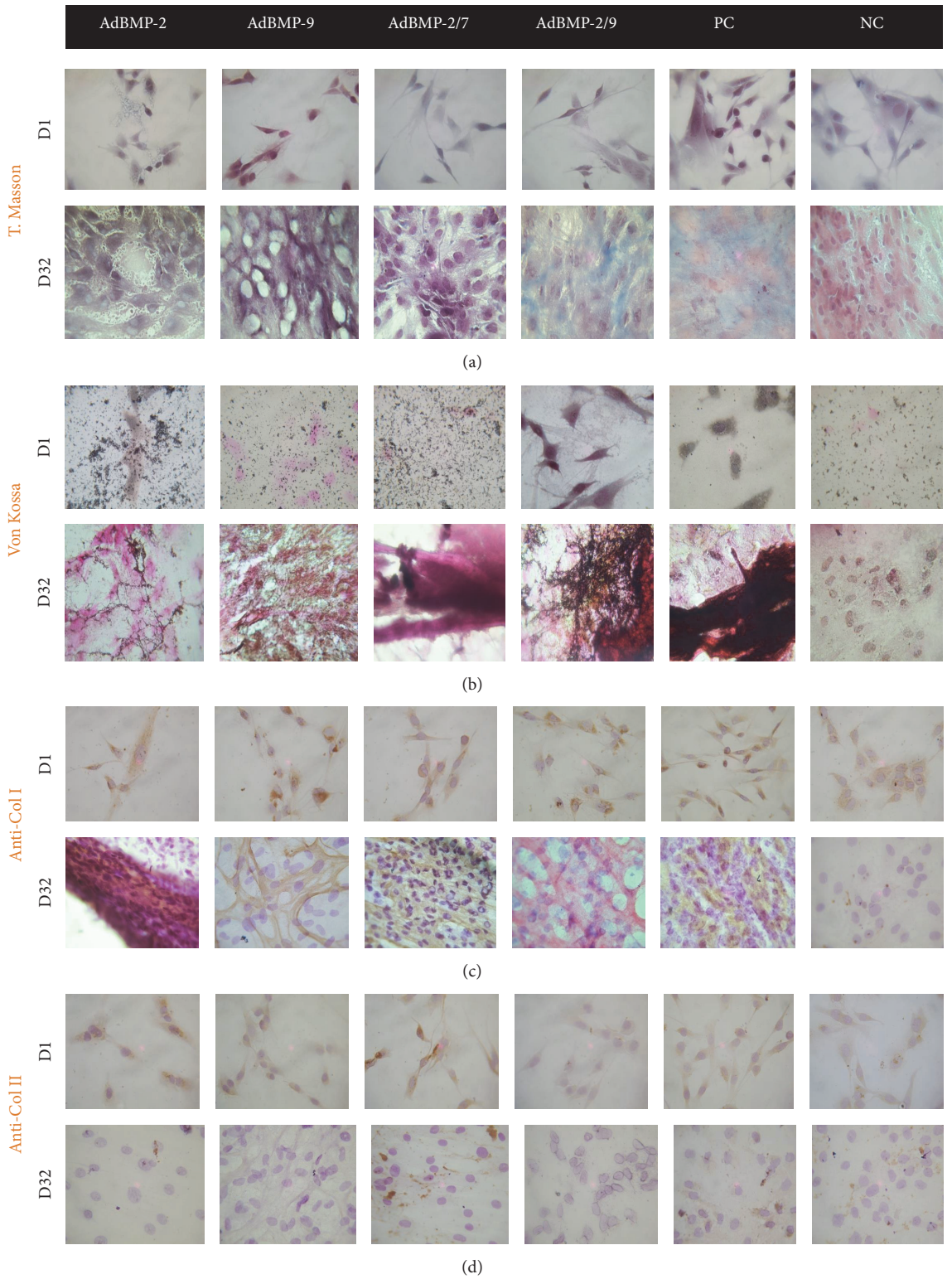

Figure 2: Histological staining at days 1 and 32 of culture. Masson's trichrome for the identification of collagen and amorphous material; (b) von Kossa for the identification of calcifications; (c) IHC for collagen I; (d) IHC for collagen II. PC: positive control; NC: negative control. Micrographs with 10x amplification.

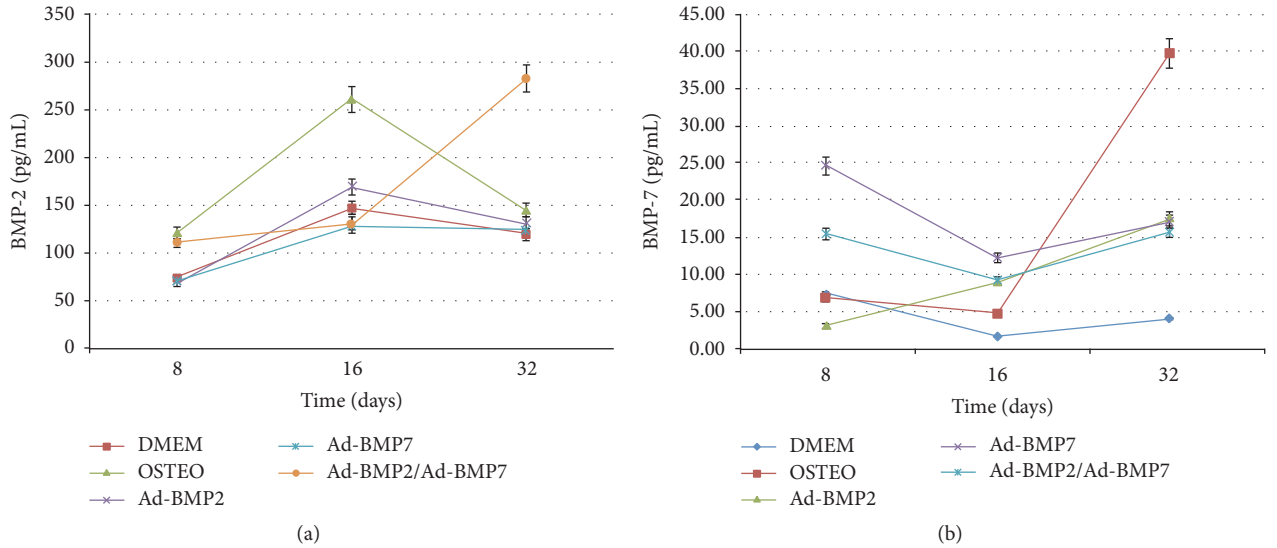

Figure 3: ELISA. (a) Analysis of the protein BMP2 and (b) BMP7 by ELISA of MSCs transduced with the vectors AdBMP2, AdBMP7, the combination AdBMP2/AdBMP7, and the positive (OSTEO) and negative (DMEM) controls on days 8, 16, and 32 after induction.

between cells (Figure 2(c)). Collagen type II was detected slightly in most cells at day 1 of culture and was absent in all groups at day 32, except for the combination AdBMP2/AdBMP7 (Figure 2(d)).

Levels of BMP2 and BMP7 proteins measured by ELISA showed that expression of BMP2 was sustained up to day 32 in the group transduced with the combination AdBMP2/AdBMP7, with this expression being different from the rest of the groups in the same observation period ($P < 0.05$) (Figure 3(a)). Conversely, expression of BMP7 at day 32 was higher in the positive control; however, at days 8 and 16, the expression of BMP7 in the ADMSCs groups transduced with AdBMP7 and the AdBMP2/AdBMP7 combination showed greater expression with their levels being maintained up to day 32 (Figure 3(b)). Different statistical differences were established for the BMP2 and BMP7 expression levels between groups in each of the observation points (ANOVA $P < 0.05$).

3.3. Bone Regeneration Assays In Vivo. Radiographic followup at 10 weeks showed a faster closure of the lesions in Group III (Figure 4). The lesion in this group was completely filled at week 7 after implant. In contrast, bone distractions in the Groups I and II were not fully filled at week 10 of followup. Radiographic images also showed that bone formation in control groups was altered, causing a bone deformation in the area of the lesion, while in Group III, the X-ray showed that the lesion was uniformly filled, resulting in a bone appearance and consistency similar to that of a healthy bone.

Postmortem H&E histological comparisons among the groups, including healthy tibia as a positive control (PC), showed that bones in Group III have preserved periosteum and the cortex showed a compact and uniform bone matrix, consisting of osteocollagen, with immersed gaps of bone cells (osteocytes) and blood vessels in the lamellar bone architecture. In Group I, periosteal thickening was seen, and areas of dense fibrous tissue were observed in cortical and trabecular bone. In the medullary cavity, extended fibrosis with scarce cancellous bone, lack of hyaline cartilage, and abundant amorphous and fibrillar material was observed. Furthermore, lymphocyte, plasma cells, and macrophages infiltrates were also observed. Group II showed thickening of periosteum, while the bone cortex showed formation of highly vascularized fibrocollagenous zones. Small areas of hypertrophic hyaline cartilage were present in the medullary cavity of the lesion with large areas of fibrous tissue. In Group III, the periosteum appeared thin and slightly fibrous, with abundant stellate and fusiform differentiating cells. Bone cortex showed abundant cancellous tissue constituted by a uniform and compact matrix without cartilaginous tissue. The proportion of compact bone tissue was greater than in groups I and II (Figure 5(a)).

The blue coloring of the collagen matrix by Masson's trichrome demonstrated that production of collagen matrix in Group III was higher when compared to the other groups, which showed fibrous tissue and amorphous material. The compact and uniform collagen matrix of Group III resembled the matrix of healthy tibia (Figure 5(b)). IHC studies showed type I collagen in all three groups (Figure 6(a)). Focal areas of hyaline cartilage showed weak staining for type II collagen in Group I (Figure 6(b)). Type X collagen was present in trabecular bone in all groups (Figure 6(c)).

3.4. 3D CT-Scan Analysis. Sagittal sections of the treated tibia from each sheep per group were performed and non-injured tibias were used as healthy controls (Figure 7). In Groups I and II, bones were totally deformed by the formation of calluses in the area of the lesion without defining the cortex and medulla, while in Group III images that more closely resembled a healthy tibia they were seen. In Figure 8 the lesion area of each sheep is shown and it can be seen that,

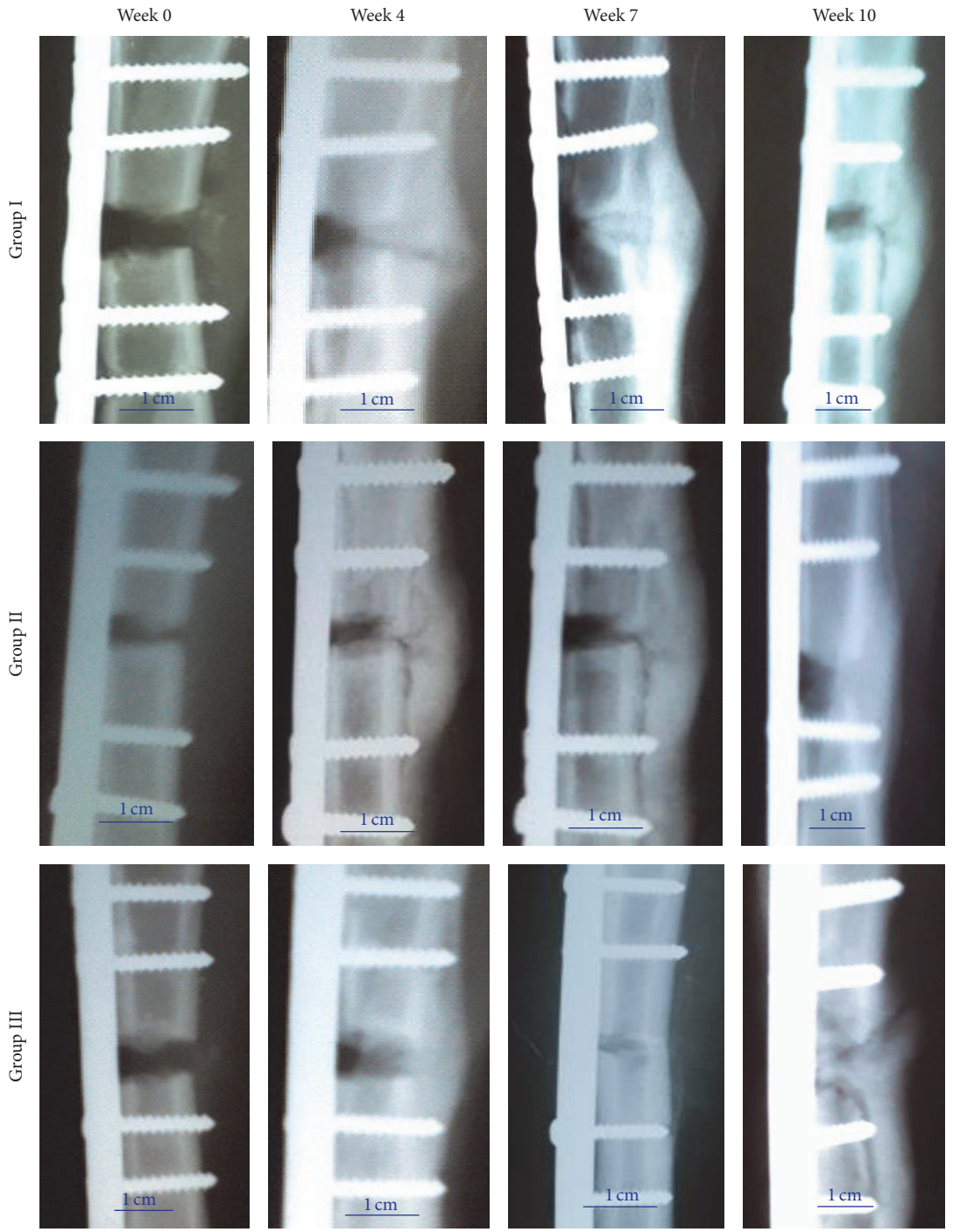

Figure 4: Radiographic followup at 0 to 10 weeks of treatment groups: Group I, control without an implant; Group II, implant with a DBM seeded with MSCs without transduction; and Group III, implant with a DBM and MSCs transduced with AdBMP2/AdBMP7. Scale bar: 1 cm.

in Group III, bones are more uniform in appearance, size, and cortical density, similar to the control tibias.

3.5. Biosafety and Toxicity Studies. Table 1 shows the laboratory tests that were performed before and 20 days after surgery to assess the overall toxicity of adenoviral vectors used in Group III. It can be seen that the results were within normal values reported for this species, showing that no inflammatory processes or alterations in liver function tests demonstrate any adverse effects.

4. Discussion

This study analyzed the *in vitro* osteogenic potential of ovine ADMSCs transduced with AdBMP2, AdBMP7, and AdBMP9 alone and in the combinations AdBMP2/AdBMP7

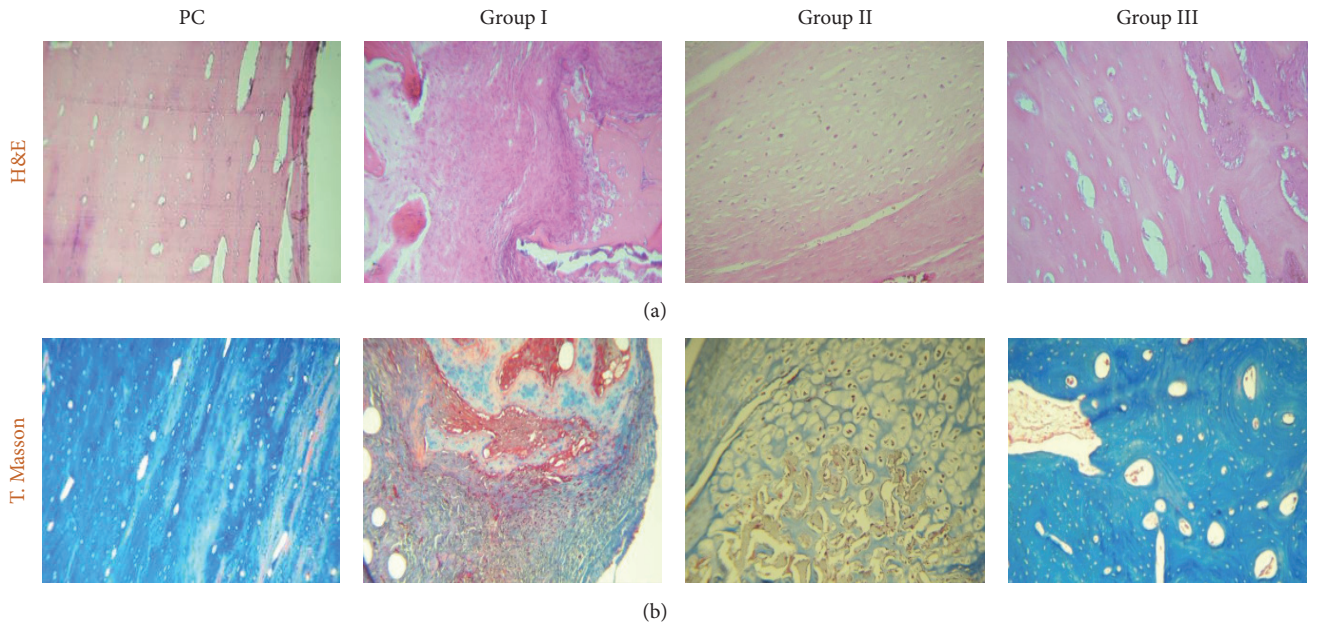

Figure 5: Postmortem histological staining. (a) H&E; (b) Masson's trichrome. PC: positive control. Micrographs with 10x amplification.

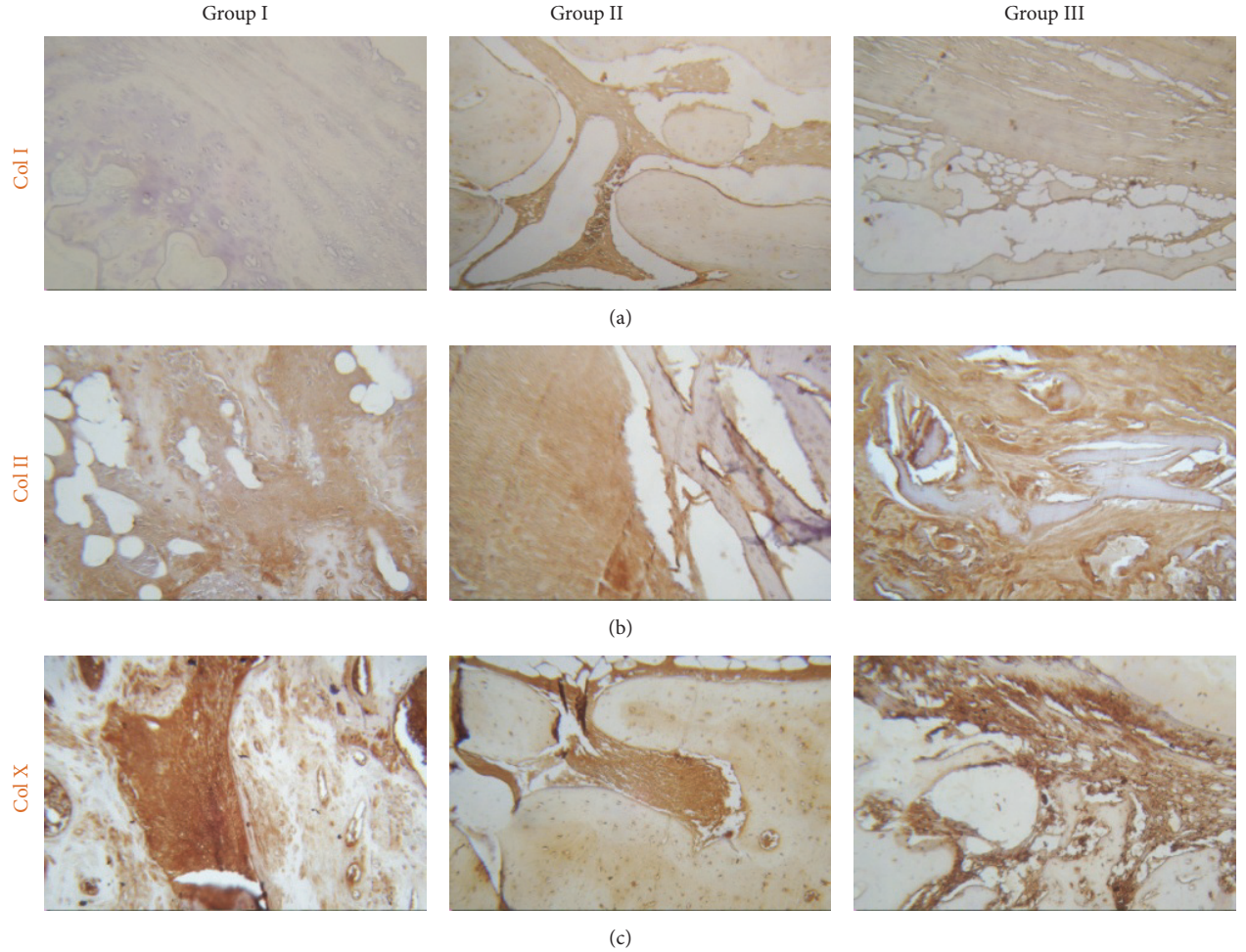

Figure 6: Postmortem IHC. (a) IHC for collagen I; (b) IHC for collagen II and (c) IHC for collagen X. Micrographs with 10x amplification.

Table 1: Toxicity studies related to the use of adenoviral vectors.

Analytical parameter	Reference range	Group I		Group II		Group III	
		Pre S	Post S	Pre S	Post S	Pre S	Post S
Leukocytes (μL)	4000–12000	5507.5 ± 0.3	11086 ± 0.3	9748.3 ± 0.3	8375 ± 0.2	11251.7 ± 0.5	8758.3 ± 0.3
Hemoglobin (g/dL)	9–15	11.9 ± 0.2	9.72 ± 0.1	10.2 ± 0.2	10.3 ± 0.1	10.7 ± 0.1	10.1 ± 0.1
Platelets (thousands/μL)	220–680	376.2 ± 0.5	832.2 ± 0.3	470.3 ± 0.2	779.3 ± 0.4	684.1 ± 0.4	720.8 ± 0.5
PT (g/dL)	6.0–7.9	6.36 ± 0.1	6.68 ± 0.1	6.1 ± 0.0	7.1 ± 0.1	6.8 ± 0.1	6.8 ± 0.1
Albumin (g/dL)	2.4–3.0	3.46 ± 0.1	2.9 ± 0.1	3.1 ± 0.1	3.1 ± 0.1	3.1 ± 0.1	3.2 ± 0.1
Globulin (g/dL)	3.5–5.7	2.86 ± 0.1	3.76 ± 0.2	3.05 ± 0.1	4.2 ± 0.3	3.7 ± 0.2	3.5 ± 0.2
AST (IU/L)	66–194	146.4 ± 0.4	174.6 ± 0.3	131.5 ± 0.3	140.3 ± 0.6	112.1 ± 0.1	104.3 ± 0.2
ALT (IU/L)	12–37	17.8 ± 0.3	27 ± 0.9	19 ± 0.5	16.7 ± 0.3	15 ± 0.6	16.5 ± 0.4
Total bilirubin (mg/dL)	0.0–1.0	0.108 ± 0.4	0.032 ± 0.4	0.1 ± 0.6	0.04 ± 1.1	0.06 ± 0.6	0.04 ± 0.8
Total bilirubin (mg/dL)	0.0–0.2	0.03 ± 0.2	0.03 ± 0.4	0.1 ± 0.8	0.1 ± 1.2	0.04 ± 1.0	0.1 ± 0.7
Indirect bilirubin (mg/dL)	0.0–1.0	0.076 ± 0.6	0.03 ± 0.4	0.1 ± 0.8	0.1 ± 1.2	0.04 ± 1.0	0.1 ± 0.7
Alkaline phosphatase (IU/L)	68–387	305.8 ± 0.5	134.4 ± 0.2	167.5 ± 0.6	188.5 ± 0.3	198 ± 0.4	211.3 ± 0.3
GGT (IU/L)	36–102	53.8 ± 0.2	51.8 ± 0.1	68.2 ± 0.3	73.7 ± 0.3	49.07 ± 0.2	58.0 ± 0.4

Pre S: presurgery; Post S: postsurgery.

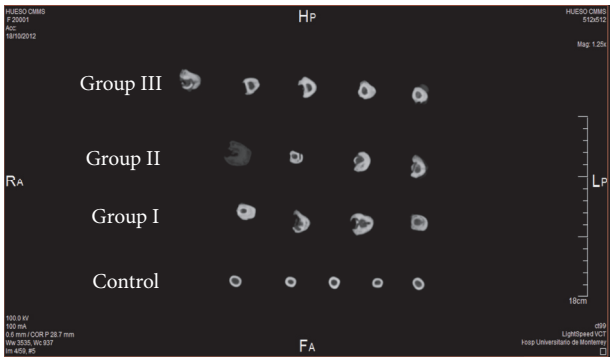

Figure 7: 3D computerized tomography of a sagittal slice of sheep bones 10 weeks after surgery (postmortem) represented by group.

and AdBMP2/AdBMP9. The aim was to determine the optimum components for the design of an implant for bone regeneration preclinical trials in a mammal model for a major bone lesion that allows thinking about future translation of this therapy into clinical trials.

In vitro gene expression studies demonstrated that the combination AdBMP2/AdBMP7 stimulates sustained expression of osteogenic markers until day 32 of observation. Histology of this group shows a production of a collagen matrix and suitable mineralization. IHC showed that collagen type I is the predominant protein in the collagen matrix formed by the ADMSCs stimulated with AdBMP2/AdBMP7. Although AdBMP7 alone stimulates increased expression of both osteogenic markers by day 16, these levels fall at day 32 in *in vitro* assays. Nonsustained expression of osteogenic markers in this group and the loss of adherence to the culture dish may suggest an altered osteogenic differentiation.

Zhu et al. evaluated the expression of osteogenic markers in cells A549, C2C12, and MC3T3-E1 transduced with the adenoviral vectors carrying BMP7, BMP2, and an adenovirus without transgene, alone and in combination. They found that, after 12 days of transduction, the combination BMP2 and BMP7 overexpressed alkaline phosphatase and osteocalcin 6 to 40 times more than treatment with BMP2 and BMP7 alone [26]. In addition, this combination significantly increased the rate of bone formation and spinal fusions in a mouse model [26, 27].

This study also demonstrates that BMP2 and BMP7 proteins are produced at high concentrations. BMP2 was expressed higher and more consistently, particularly in cells transduced with the combination Ad-BMP2/AdBMP7 at day 32 of incubation. Koh and colleagues, who used transduced fibroblasts with adenovirus carrying the genes of the BMP2 and BMP7 to regenerate craniofacial bone, reported similar results. These researchers also observed high alkaline phosphatase production with this combination [28]. Qing et al. studied bone regeneration using stem cells derived from rat adipose tissue transduced with lentivirus carriers of the BMP2 and BMP7 genes. They observed high alkaline phosphatase activity, calcium deposits, and high expression of the osteogenic markers osteocalcin and osteopontin after 14 days of incubation [29]. Currently, the recombinant proteins rhBMP2 and rhBMP7 have already been approved by the Food and Drug Administration (FDA) to be used in clinical trials [30]. Some reports of the use of rhBMP2 and rhBMP7

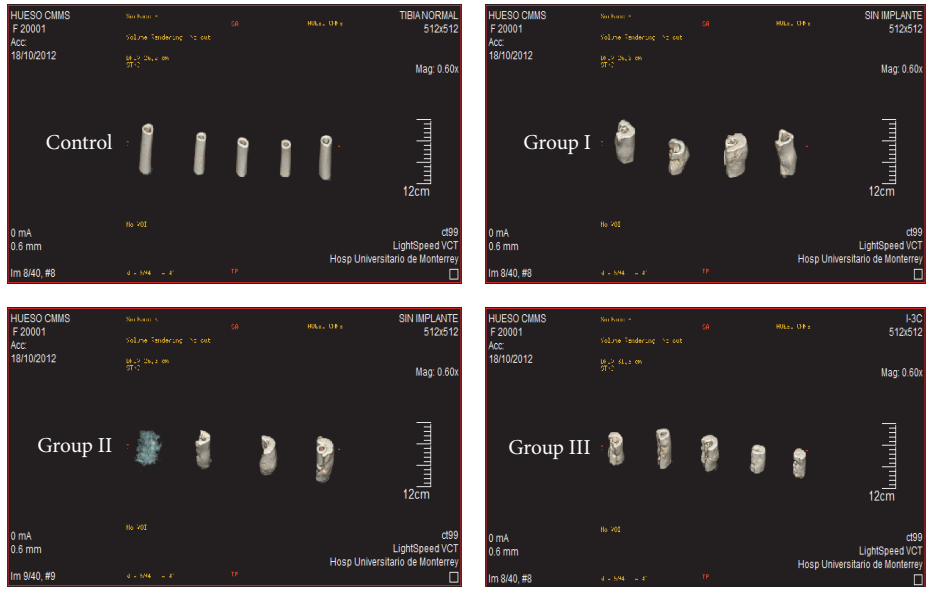

Figure 8: 3D computerized tomography of the area of a lesion in each sheep by group 10 weeks after surgery (postmortem).

in bone regeneration trials in rodents show promising results that demonstrate ossification between weeks 6 and 8 after treatment [26, 27, 31–33].

In an ovine model of bone distraction, the osteogenic potential of rhBMP2 at a dose of 4 mg/day on days 3, 10, and 17 after distraction of the tibia was evaluated and it was observed that 3 days of treatment were sufficient to regenerate normal trabecular microarchitecture [34]. However, the production of recombinant proteins is still a costly process and treatment requires repeated applications, which increases the cost of therapy. Recently, a slow release method for rhBMP2 and rhBMP7 was tested in a fibrin hydrogel of hyaluronic acid for regeneration of spinal disc in goats in a period of 12 weeks; but no disc regeneration was observed in any of the study groups. The authors postulate that this could occur due to the low doses of BMPs, a short followup time, and/or insufficient release of the heterodimers rhBMP2/rhBMP7 [20].

Alternative techniques based on gene transduction using naked DNA or viral vectors for the expression of BMPs can be option for the development of self-stimulated implants that steadily express growth factors at the site of the lesion, in large and small mammals [29, 35–37]. However, the injection of AdBMP2 and Ad-BMP7 in the site of an osteotomy in 450 kg equines to induce osteogenesis after a 16-week evaluation did not show differences between the control and the transduced groups [38].

In vivo analysis of this study showed a satisfactory recovery of sheep in Group III. Radiologic studies showed that complete bone healing in this group was achieved in less time (7–10 weeks) unlike other experimental groups where consolidation was not achieved and bone deformation was observed. In the 3D CT scan, it was observed that, in Group III, shape, size, structure, and cortical density were more similar to the control group than to Groups I and II. Also, no liver or inflammatory disorders due to the use of adenoviral vectors were found. Dong and colleagues reported that complete bone healing was achieved using MSCs transduced with a recombinant adenovirus AdCbfa1a at 12 weeks after a lesion to the right radius in the front leg in rabbits [39]. In the canine model where the implant with MSCs transduced with AdBMP2/AdBMP7 was previously tested, radiographic followup showed complete healing in the treated jaw at week 6 after distraction [23]. These data indicate a marked reduction in bone healing time when genetically modified MSCs are used.

In summary, the discussed reports illustrate the technical difficulties that persist for the development of a promising implant, but the results of the present study support the generation of an optimal implant for bone regeneration in sheep.

4.1. Conclusions. The present study demonstrates the enhanced and sustained effect of the transduction of ovine ADMSCs with a combination of BMP2 and BMP7 that is suitable for the development of a bone regeneration implant to be tested in a sheep model with the purpose of advancing preclinical analyses for future clinical trials of bone regeneration.

Disclosure

All authors are responsible for the content and writing of this research paper.

Competing Interests

The authors declare that they have no competing interests.

Authors' Contributions

Adelina A. Hernandez-Hurtado and Gissela Borrego-Soto contributed equally to this work.

Acknowledgments

This work was supported by CONACYT through the approved grant: SSA/IMSS/ISSSTE-CONACYT-2008-01-87362. The authors thank Sergio Lozano-Rodriguez, M.D., for his help in translating the manuscript.

References

[1] H. Salehi, N. Amirpour, A. Niapour, and S. Razavi, "An overview of neural differentiation potential of human adipose derived stem cells," *Stem Cell Reviews and Reports*, vol. 12, no. 1, pp. 26–41, 2016.

[2] P. Kasten, I. Beyen, M. Egermann et al., "Instant stem cell therapy: characterization and concentration of human mesenchymal stem cells in vitro," *European Cells and Materials*, vol. 16, pp. 47–55, 2008.

[3] C. Muñiz, C. Teodosio, A. Mayado et al., "Ex vivo identification and characterization of a population of CD13high CD105$^+$ CD45$^-$ mesenchymal stem cells in human bone marrow," *Stem Cell Research & Therapy*, vol. 6, no. 1, p. 169, 2015.

[4] J. Kobolak, A. Dinnyes, A. Memic, A. Khademhosseini, and A. Mobasheri, "Mesenchymal stem cells: identification, phenotypic characterization, biological properties and potential for regenerative medicine through biomaterial micro-engineering of their niche," *Methods*, vol. 99, pp. 62–68, 2016.

[5] C. Romagnoli and M. L. Brandi, "Adipose mesenchymal stem cells in the field of bone tissue engineering," *World Journal of Stem Cells*, vol. 6, no. 2, pp. 144–152, 2014.

[6] X. Zhang, M. Hirai, S. Cantero et al., "Isolation and characterization of mesenchymal stem cells from human umbilical cord blood: reevaluation of critical factors for successful isolation and high ability to proliferate and differentiate to chondrocytes as compared to mesenchymal stem cells from bone marrow and adipose tissue," *Journal of Cellular Biochemistry*, vol. 112, no. 4, pp. 1206–1218, 2011.

[7] K. Pill, S. Hofmann, H. Redl, and W. Holnthoner, "Vascularization mediated by mesenchymal stem cells from bone marrow and adipose tissue: a comparison," *Cell Regeneration*, vol. 4, no. 1, pp. 1–10, 2015.

[8] H. L. Fu, Z. Y. Diao, L. Shao, and D. P. Yang, "BMP-2 promotes chondrogenesis of rat adipose-derived stem cells by using a lentiviral system," *Genetics and Molecular Research*, vol. 13, no. 4, pp. 8620–8631, 2014.

[9] Z. Lin, J.-S. Wang, L. Lin et al., "Effects of BMP2 and VEGF165 on the osteogenic differentiation of rat bone marrow-derived mesenchymal stem cells," *Experimental and Therapeutic Medicine*, vol. 7, no. 3, pp. 625–629, 2014.

[10] P. N. Taşli, S. Aydin, M. E. Yalvaç, and F. Şahin, "Bmp 2 and Bmp 7 induce odonto-and osteogenesis of human tooth germ stem cells," *Applied Biochemistry and Biotechnology*, vol. 172, pp. 1–10, 2014.

[11] X. Zhang, J. Guo, Y. Zhou, and G. Wu, "The roles of bone morphogenetic proteins and their signaling in the osteogenesis of adipose-derived stem cells," *Tissue Engineering Part B: Reviews*, vol. 20, no. 1, pp. 84–92, 2014.

[12] O. Drevelle, A. Daviau, M.-A. Lauzon, and N. Faucheux, "Effect of BMP-2 and/or BMP-9 on preosteoblasts attached to polycaprolactone functionalized by adhesive peptides derived from bone sialoprotein," *Biomaterials*, vol. 34, no. 4, pp. 1051–1062, 2013.

[13] K. D. Hankenson, K. Gagne, and M. Shaughnessy, "Extracellular signaling molecules to promote fracture healing and bone regeneration," *Advanced Drug Delivery Reviews*, vol. 94, pp. 3–12, 2015.

[14] S. Khosla, J. J. Westendorf, and M. J. Oursler, "Building bone to reverse osteoporosis and repair fractures," *The Journal of Clinical Investigation*, vol. 118, no. 2, pp. 421–428, 2008.

[15] Y. S. Jang, C. H. Choi, Y. B. Cho, M.-K. Kang, and C. H. Jang, "Recombinant human BMP-2 enhances osteogenesis of demineralized bone matrix in experimental mastoid obliteration," *Acta Oto-Laryngologica*, vol. 134, no. 8, pp. 785–790, 2014.

[16] R. Visser, K. Bodnarova, P. M. Arrabal, M. Cifuentes, and J. Becerra, "Combining bone morphogenetic proteins-2 and -6 has additive effects on osteoblastic differentiation in vitro and accelerates bone formation in vivo," *Journal of Biomedical Materials Research. Part A*, vol. 104, no. 1, pp. 178–185, 2016.

[17] X. He, Y. Liu, X. Yuan, and L. Lu, "Enhanced healing of rat calvarial defects with MSCs loaded on BMP-2 releasing chitosan/alginate/hydroxyapatite scaffolds," *PLoS ONE*, vol. 9, no. 8, Article ID e104061, 2014.

[18] G. X. Wang, L. Hu, H. X. Hu, Z. Zhang, and D. P. Liu, "In vivo osteogenic activity of bone marrow stromal stem cells transfected with Ad-GFP-HBMP-2," *Genetics and Molecular Research*, vol. 13, no. 2, pp. 4456–4465, 2014.

[19] F. Liu, E. Ferreira, R. M. Porter et al., "Rapid and reliable healing of critical size bone defects with genetically modified sheep muscle," *European Cells and Materials*, vol. 30, pp. 118–131, 2015.

[20] M. Peeters, S. E. Detiger, L. S. Karfeld-Sulzer et al., "BMP-2 and BMP-2/7 heterodimers conjugated to a fibrin-hyaluronic acid hydrogel in a large animal model of mild intervertebral disc degeneration," *BioResearch Open Access*, vol. 4, no. 1, pp. 398–406, 2015.

[21] R. E. Geuze, L. F. H. Theyse, D. H. R. Kempen et al., "A differential effect of bone morphogenetic protein-2 and vascular endothelial growth factor release timing on osteogenesis at ectopic and orthotopic sites in a large-animal model," *Tissue Engineering—Part A*, vol. 18, no. 19-20, pp. 2052–2062, 2012.

[22] T. J. Heino, J. J. Alm, N. Moritz, and H. T. Aro, "Comparison of the osteogenic capacity of minipig and human bone marrow-derived mesenchymal stem cells," *Journal of Orthopaedic Research*, vol. 30, no. 7, pp. 1019–1025, 2012.

[23] Y. Castro-Govea, V. H. Cervantes-Kardasch, G. Borrego-Soto et al., "Human bone morphogenetic protein 2-transduced mesenchymal stem cells improve bone regeneration in a model of mandible distraction surgery," *The Journal of Craniofacial Surgery*, vol. 23, no. 2, pp. 392–396, 2012.

[24] J. Luo, Z.-L. Deng, X. Luo et al., "A protocol for rapid generation of recombinant adenoviruses using the AdEasy system," *Nature Protocols*, vol. 2, no. 5, pp. 1236–1247, 2007.

[25] O. B. Betz, V. M. Betz, A. Nazarian et al., "Direct percutaneous gene delivery to enhance healing of segmental bone defects," *The Journal of Bone & Joint Surgery—American Volume*, vol. 88, no. 2, pp. 355–365, 2006.

[26] W. Zhu, B. A. Rawlins, O. Boachie-Adjei et al., "Combined bone morphogenetic protein-2 and -7 gene transfer enhances osteoblastic differentiation and spine fusion in a rodent model," *Journal of Bone and Mineral Research*, vol. 19, no. 12, pp. 2021–2032, 2004.

[27] T. Morimoto, T. Kaito, Y. Matsuo et al., "The bone morphogenetic protein-2/7 heterodimer is a stronger inducer of bone regeneration than the individual homodimers in a rat spinal fusion model," *Spine Journal*, vol. 15, no. 6, pp. 1379–1390, 2015.

[28] J. T. Koh, Z. Zhao, Z. Wang, I. S. Lewis, P. H. Krebsbach, and R. T. Franceschi, "Combinatorial gene therapy with BMP2/7 enhances cranial bone regeneration," *Journal of Dental Research*, vol. 87, no. 9, pp. 845–849, 2008.

[29] W. Qing, C. Guang-Xing, G. Lin, and Y. Liu, "The osteogenic study of tissue engineering bone with BMP2 and BMP7 gene-modified rat adipose-derived stem cell," *Journal of Biomedicine & Biotechnology*, vol. 2012, Article ID 410879, 7 pages, 2012.

[30] K. R. K. Garrison, I. Shemilt, S. Donell et al., "Bone morphogenetic protein (BMP) for fracture healing in adults," *The Cochrane Database of Systematic Reviews*, no. 6, pp. 1–51, 2010.

[31] T. Barr, A. J. A. McNamara, G. K. B. Sándor, C. M. L. Clokie, and S. A. F. Peel, "Comparison of the osteoinductivity of bioimplants containing recombinant human bone morphogenetic proteins 2 (Infuse) and 7 (OP-1)," *Oral Surgery, Oral Medicine, Oral Pathology, Oral Radiology and Endodontology*, vol. 109, no. 4, pp. 531–540, 2010.

[32] J. Su, H. Xu, J. Sun, X. Gong, and H. Zhao, "Dual delivery of BMP-2 and bFGF from a new nano-composite scaffold, loaded with vascular stents for large-size mandibular defect regeneration," *International Journal of Molecular Sciences*, vol. 14, no. 6, pp. 12714–12728, 2013.

[33] S.-H. Jun, E.-J. Lee, T.-S. Jang, H.-E. Kim, J.-H. Jang, and Y.-H. Koh, "Bone morphogenic protein-2 (BMP-2) loaded hybrid coating on porous hydroxyapatite scaffolds for bone tissue engineering," *Journal of Materials Science: Materials in Medicine*, vol. 24, no. 3, pp. 773–782, 2013.

[34] T. Floerkemeier, F. Witte, J. Nellesen, F. Thorey, H. Windhagen, and M. Wellmann, "Repetitive recombinant human bone morphogenetic protein 2 injections improve the callus microarchitecture and mechanical stiffness in a sheep model of distraction osteogenesis," *Orthopedic Reviews (Pavia)*, vol. 4, no. 1, article e13, 2012.

[35] J. Z. Li, H. Li, T. Sasaki et al., "Osteogenic potential of five different recombinant human bone morphogenetic protein adenoviral vectors in the rat," *Gene Therapy*, vol. 10, no. 20, pp. 1735–1743, 2003.

[36] M. Zhao, Z. Zhao, J.-T. Koh, T. Jin, and R. T. Franceschi, "Combinatorial gene therapy for bone regeneration: cooperative interactions between adenovirus vectors expressing bone morphogenetic proteins 2, 4, and 7," *Journal of Cellular Biochemistry*, vol. 95, no. 1, pp. 1–16, 2005.

[37] A. C. O. Carreira, W. F. Zambuzzi, M. C. Rossi, R. A. Filho, M. C. Sogayar, and J. M. Granjeiro, "Bone Morphogenetic Proteins: promising molecules for bone healing, bioengineering, and regenerative medicine," *Vitamins and Hormones*, vol. 99, pp. 293–322, 2015.

[38] L. L. Southwood, C. E. Kawcak, C. Hidaka et al., "Evaluation of direct in vivo gene transfer in an equine metacarpal IV ostectomy model using an adenoviral vector encoding the bone morphogenetic protein-2 and protein-7 gene," *Veterinary Surgery*, vol. 41, no. 3, pp. 345–354, 2012.

[39] S.-W. Dong, D.-J. Ying, X.-J. Duan et al., "Bone regeneration using an acellular extracellular matrix and bone marrow mesenchymal stem cells expressing Cbfa1," *Bioscience, Biotechnology and Biochemistry*, vol. 73, no. 10, pp. 2226–2233, 2009.

Hindawi Publishing Corporation
Stem Cells International
Volume 2016, Article ID 3187491, 9 pages
http://dx.doi.org/10.1155/2016/3187491

Review Article

Mesenchymal Stem Cells Subpopulations: Application for Orthopedic Regenerative Medicine

Vanessa Pérez-Silos,[1,2] Alberto Camacho-Morales,[1,3] and Lizeth Fuentes-Mera[1,2]

[1]*Departamento de Bioquímica y Medicina Molecular, Universidad Autónoma de Nuevo León (UANL), Monterrey, NL, Mexico*
[2]*Unidad de Terapias Experimentales, Centro de Investigación y Desarrollo en Ciencias de la Salud, Universidad Autónoma de Nuevo León (UANL), Monterrey, NL, Mexico*
[3]*Unidad de Neurociencias, Centro de Investigación y Desarrollo en Ciencias de la Salud, Universidad Autónoma de Nuevo León (UANL), Monterrey, NL, Mexico*

Correspondence should be addressed to Lizeth Fuentes-Mera; lizeth46@hotmail.com

Received 27 April 2016; Revised 10 July 2016; Accepted 7 August 2016

Academic Editor: Bin Li

Research on mesenchymal stem cells (MSCs) continues to progress rapidly. Nevertheless, the field faces several challenges, such as inherent cell heterogeneity and the absence of unique MSCs markers. Due to MSCs' ability to differentiate into multiple tissues, these cells represent a promising tool for new cell-based therapies. However, for tissue engineering applications, it is critical to start with a well-defined cell population. Additionally, evidence that MSCs subpopulations may also feature distinct characteristics and regeneration potential has arisen. In this report, we present an overview of the identification of MSCs based on the expression of several surface markers and their current tissue sources. We review the use of MSCs subpopulations in recent years and the main methodologies that have addressed their isolation, and we emphasize the most-used surface markers for selection, isolation, and characterization. Next, we discuss the osteogenic and chondrogenic differentiation from MSCs subpopulations. We conclude that MSCs subpopulation selection is not a minor concern because each subpopulation has particular potential for promoting the differentiation into osteoblasts and chondrocytes. The accurate selection of the subpopulation advances possibilities suitable for preclinical and clinical studies and determines the safest and most efficacious regeneration process.

1. Introduction

Stem cells are well defined by their ability to self-renew and to differentiate into a range of cell types. In the adult organism, these cells are responsible for maintaining the homeostasis of their respective tissues. The maintenance of stemness and pluripotency of stem cells proceeds in the stem cell niche, where stem cells receive adequate signals from the stroma and other cell types either via receptors or by secreted soluble factors within this microenvironmental niche [1].

Mesenchymal stem cells (MSCs) were generally defined based on their capacity to self-renew and on their phenotype. The International Society for Cellular Therapy (ISCT) has proposed the following minimum criteria for the definition of the MSCs: (I) adherence to plastic surfaces under standard cell culture conditions; (II) the expression of cell surface markers, such as CD90, CD73, and CD105, and the lack of expression of CD14, CD34, CD45, CD79, or CD19 and HLA-DR, and (III) the capability to differentiate into chondrocytes, osteoblasts, and adipocytes [2].

Considerable effort has been expended to identify specific surface markers that characterize MSCs, yet disagreement in the literature has prevented the creation of definitive standards. In this regard, additional studies have also associated other markers with MSCs, such as CD271, Stro-1, vascular cell adhesion molecule-1 (VCAM-1), and CD146 [3–5].

The current review highlights recent findings in the identification and isolation of MSCs subpopulations, which could improve expansion strategies in the near future and the clinical use of MSCs differentiated into osteogenic and chondrogenic lineages.

MSCs subpopulations from several sources in conjunction with specific growth factors and/or scaffold are potentially useful for a variety of clinical orthopedic conditions involving bone and cartilage. There are several clinical trials using MSCs subpopulations to repair critical-sized injuries caused by trauma or infection, aside from replacing chronically degenerated tissue, such as articular cartilage. We recognize that variability in MSC-based clinical trial outcomes is likely due not only to differences amongst various MSCs sources but also to cell heterogeneity and inadequate selection of the subpopulation.

2. Sources of Mesenchymal Stem Cells

MSCs were first depicted by Friedenstein et al. in 1968 as adherent fibroblast-like cells with multipotent differentiation abilities. This study indicated that clonal populations belonging to the colony forming unit-fibroblastoids (CFU-Fs) result in osteoblasts, chondrocytes, and hematopoietic supportive cells *in vivo* [6]. MSCs were initially isolated from bone marrow (BM), and, in recent years, the isolation of adult mesenchymal stem cells from different sources has been reported. The comparative quality, character, and differentiation potential of MSCs from each of these sources differ and are still debated. MSCs have been isolated from multiple adult human tissues, such as adipose tissue [7, 8], articular cartilage [9], brain [10], endometrium [11], menstrual blood [12], peripheral blood [13], skin and foreskin [14, 15], and synovial fluid [16]. Additionally, perinatal organs and tissues that are normally discarded after delivery, namely, amniotic fluid [17], amniotic membrane [18, 19], full placenta and fetal membrane [20], subamniotic umbilical cord lining membrane [21, 22], and Wharton's jelly [23], have been shown to be rich sources of proliferative MSCs. Other sources include dental tissue, such as the pulp tissue of permanent human dental pulp stem cells (DPSCs) [24], stem cells from human exfoliated deciduous teeth (SHED) [25], periodontal ligament progenitor cells (PDLPs), and PDL stem cells (PDLSCs) [26]. Satellite cells in muscle and pericytes around blood vessels also share multipotent characteristics to differentiate into connective tissue phenotypes under specific conditions [27, 28].

Interestingly, in recent years, the use of bone marrow as a source of MSCs has decreased. A strong trend is observed in the use of various postfetal tissues besides adipose tissue as a major source for isolation.

3. Mesenchymal Stem Cell Subpopulations

MSCs were first identified in the bone marrow as an adherent population of nonhematopoietic stem cells with the capability of differentiating into different cell types of predominantly mesodermal origin. Cultures of MSCs show high heterogeneity, and the application of MSCs cultures in tissue regeneration depends mainly on their differentiation potential. Consequently, researchers are actively attempting to preselect cell subpopulations with higher osteochondrogenic potential in order to achieve a thorough translation of MSC-based therapies for orthopedic applications. Research over the last years has demonstrated that the use of a specific MSCs subpopulation ensures successful differentiation into a particular cell line.

MSCs are classically selected on the basis of their adherence to plastic, which however results in a heterogeneous population of cells. Prospective identification of the antigenic profile of the MSCs population (subpopulations) by FACS-based (fluorescence-activated cell sorting) approaches gives rise to cells with MSCs activity *in vitro* and would allow for the isolation of very pure populations of MSCs for research or clinical use [29, 30].

Several markers have been proposed to enrich these subpopulations, but the majority of these markers are defined for BM. In addition to a phenotypic variation depending on the MSCs source, the surface markers of freshly isolated MSCs may also differ from those of cultured MSCs. Although there have been attempts to increase MSCs purity by physical means, positive selection based on a specific MSCs marker offers a better alternative. Amongst a number of positive markers proposed in the past, CD271, CD105, CD44, CD90, and CD117 seem to offer adequate selectivity. Moreover, the isolation of homogeneous MSCs is best achieved by cell sorting with a combination of positive and negative markers.

Blood vessels within skeletal muscle anchor several precursor populations. It is reported that pericytes, which surround endothelial cells of capillaries and venules, possess multipotent differentiation potential [28, 31]. In 2012, Corselli et al. reported that, in addition to MSCs being derived from pericytes, adventitial cells could also give rise to MSCs [32]. In a recent article by Zhao et al., it was demonstrated that, during incisor trauma, pericytes and adventitial cells (perivascular stem cells, PSC) are recruited to modulate hemostasis and repair. Further, *in vitro*, these PSC were shown to exhibit typical MSCs features. Sorting pericytes ($CD45^-/CD146^+/CD34^-$) and adventitial cells ($CD45^-/CD146^-/CD34^+$) by FACS is a process that requires a few hours [33–35] (Figure 1). This isolation method allows simultaneous purification of three multipotent cell populations, from three structural layers of blood vessels: pericytes from media, adventitial cells from adventitia, and myogenic endothelial cells from intima [36]. More recently, König et al. enriched a $CD146^+$ subpopulation ($CD146^+/NG2^+/CD45^-$) of pericytes from an isolated stromal vascular fraction of mouse fat tissue and demonstrated its efficient osteoblasts differentiation *in vitro* and ability to colonize cancellous bone scaffolds and regenerate large bone defects *in vivo* [37].

In a study conducted by Busser et al. (2015), immunomagnetic selections with 5 single surface markers were performed to isolate MSCs subpopulations from BM and adipose tissue (AT): CD271, SUSD2, MSCA-1, CD44, and CD34. Compared to the whole population of unselected ADSCs, the authors observed that CD271 selection can define AT cell population with higher multipotency and a higher proliferative capability [38].

Cuthbert et al. used FACS for the isolation of the subpopulation $CD45^{low}/CD73^+/CD271^+$ from BM phenotype in order to enrich MSCs fractions. $CD271^+$ immunomagnetic selection resulted in a substantial increase in MSCs purity and high expression of bone-related transcripts and

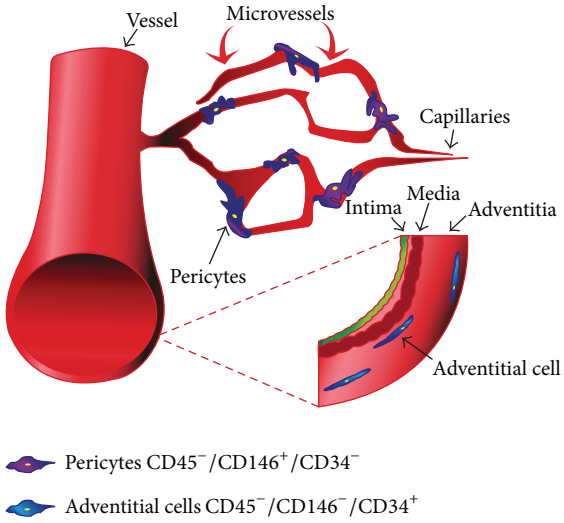

FIGURE 1: Pericytes and adventitial cells associated with skeletal muscle microvessels. A scheme showing the MSC subpopulations present in the three structural layers of blood vessels: pericytes (green) from media, adventitial cells (yellow) from adventitia, and myogenic endothelial cells from intima. Illustration of the phenotype of the corresponding cells: pericytes ($CD45^-/CD146^+/CD34^-$) and adventitial cells ($CD45^-/CD146^-/CD34^+$).

vascularization, such as BMP-2, COL1A2, VEGFC, and SPARC transcripts [39].

Clearly, the use of strategies based on the coexpression of more than one surface marker improves the purity of the isolated MSCs population.

Mabuchi et al. (2013) reported in fresh human BM an improved clonal isolation technique and demonstrated that the combination of three cell surface markers (LNGFR, THY-1, and VCAM-1) allows the selection of highly enriched clonogenic cells. The marker combination $LNGFR^+/THY\text{-}1^+/VCAM\text{-}1^+$ (LTV) represents a valuable strategy for the isolation of MSCs with broad potentiality features that are genetically more stable [40].

Likewise, based on the simultaneous use of three stem cell markers, Leyva-Leyva et al. (2013) selected and sorted by FACS two homogeneous subpopulations of hMSCs which coexpress the $CD73^+/CD44^+/CD105^+$ (6%–12%) or $CD73^+/CD44^+/CD105^-$ (80%–88%) antigens. This systematic method for the isolation of hMSCs generated homogeneous cultures for osteoblast differentiation with an enhanced ability to mineralize [18].

3.1. Osteogenic Differentiation from Mesenchymal Stem Cell Subpopulations. Unlike many other tissues, bone is an exceptional tissue that regenerates completely in the absence of scar tissue [41]. The bone healing process has three stages: inflammation, bone generation, and bone remodeling. When the bones fracture, bleeding occurs in the area resulting in inflammation and blood clotting at the fracture site. These events provide the primary structural stability and support for the production of new bone. Following an inflammatory stage, there is mesenchymal and angiogenic activation. Blood vessels and MSCs are recruited to the injury site and proliferate. Afterward, MSCs differentiate into either chondrocytes or osteoblasts. Mesenchymal cells differentiate into osteoprogenitors and then proliferate and differentiate into osteoblasts beginning the production and also secretion of osteoid, followed by mineralization, a process termed intramembranous ossification. On the other hand, chondrocytes proliferate and mineralize, and next bone tissue is deposited on the cartilage matrix through a process termed endochondral ossification. Both processes are completed by remodeling the bone to restore normal shape and function.

Most of the approaches of bone tissue engineering use bone marrow-derived cells that are easily accessible, can differentiate into chondrocytes and osteoblasts *in vitro*, and seem to be an ideal autologous cell type [41–44]. Other autologous cell types such as adipose-derived cells, which are also very accessible and possess osteogenic and chondrogenic potential *in vitro*, represent lately a very attractive source.

Adipose-derived stromal cells (ADSCs) are a very useful stem cell population, as they are abundant and can be easily acquired and isolated. However, at the clonal level, only 21% of the population of plastic-adherent ADSCs clones are determined to be tripotent with an additional 31% and 29% exhibiting bipotent and unipotent features, respectively [45]. Interestingly, only 48% of the clones are osteogenic, which means that the surface marker prognostic for osteogenic potency would improve the efficacy of these cells for bone tissue engineering.

Stem cell-based bone tissue engineering with ADSCs has shown great promise for the treatment of large bone deficits. By FACS, a $CD105^{low}$ cells subpopulation with enhanced osteogenic differentiation has been identified. Using single-cell transcriptional analysis, it was found that expression patterns of the cell surface receptor endoglin (CD105) were closely associated with the osteogenic potential of ADSCs (Table 1). By combining microfluidic analysis with FACS, compared with $CD105^{high}$ and unsorted cells, $CD105^{low}$ ADSCs were found to be capable of enhanced osteogenic differentiation [46]. The isolation of ADSCs negative for CD105 was required to form an osteogenic population. This approach was based on previous studies which demonstrated that $CD105^-$ ADSCs possess enhanced adipogenic and osteogenic potential, probably due to the reduced TGF-β/SMAD2 signaling [46, 47].

Additionally, Leyva-Leyva et al. (2013) positively selected the surface markers CD73, CD44, and CD105 from human amniotic membrane by FACS [18]. Two subpopulations with dissimilar osteoblastic differentiation potential were isolated: $CD44^+/CD73^+/CD105^+$ ($CD105^+$) and $CD44^+/CD73^+/CD105^-$ ($CD105^-$). Using *in vitro* analysis, it was found that the $CD105^-$ MSCs subpopulation was associated with more effective calcium deposition. Furthermore, through *in vivo* trials, it was demonstrated that grafts containing $CD105^-$ promoted adequate graft integration, improved host vascular infiltration, and showed efficient repair through intramembranous ossification (Table 1). By contrast, grafts containing $CD105^+$ showed abundant fibrocartilaginous tissue and deficient endochondral ossification [48].

Table 1: MSC subpopulations with enhanced osteogenic differentiation.

Subpopulation markers	Isolation method	Source	Reference
$CD105^{low}$	FACS	hADSCs	Levi et al. 2011 [46]
$CD44^{+}/CD73^{+}/CD105^{-}$	FACS	AM-hMSCs	Leyva-Leyva et al. 2015 [48]
$CD105^{-}$	Microbeads	mADSCs	Anderson et al. 2013 [49]
$CD105^{+}$	Microbeads	BM hMSCs	Aslan et al. 2006 [52] Dennis et al. 2007 [54] Jarocha et al. 2008 [53]
$CD90^{high}$	FACS	Rat dental pulp cells	Hosoya et al. 2012 [56]
$CD90^{+}$	FACS	hADSCs	Chung et al. 2013 [58]
	FACS	mADSCs	Yamamoto et al. 2014 [50]
$SSEA\text{-}4^{+}$	Magnetic beads	hADSCs	Mihaila et al. 2013 [59]

$CD105^{+}$ and $CD105^{-}$ represent independent subpopulations that maintain their properties upon several passages. In addition to the enhanced osteogenic differentiation potential of the $CD105^{-}$ subpopulation, Anderson et al. reported advantageous immunomodulatory properties. Interestingly, compared to $CD105^{+}$, $CD105^{-}$ murine-derived MSCs suppress the proliferation of $CD4^{+}$ T cells more efficiently [49]. Meanwhile, in humans, the analysis for HLA system profile revealed that the $CD105^{-}$ subpopulation lacked HLA-ABC and HLA-DR (61.65%), which classifies them as nonimmunogenically active [18].

It seems that the surface marker CD105 might predict weak osteogenesis when the source of the isolation is adipose tissue or amniotic membrane [46, 48, 50]; however, when the source is bone marrow, conflicting data have been reported [51].

Aslan et al. found that, in bone marrow, $CD105^{+}$ cells displayed enhanced *in vitro* osteogenic differentiation [52]. Likewise, Jarocha et al. reported that expanded $CD105^{+}$ populations possess higher expression levels for RUNX2 and OCN (early and late osteogenic molecular markers, resp.) [53].

Dennis et al. found that there was good correlation between *in vitro* mineralization and *in vivo* osteogenesis of $CD105^{+}$ cells [54]. Interestingly, these authors also observed a correlation between *in vivo* bone scores with the presence of $CD105^{+}$ cell, suggesting that specific subpopulation seems to be a key aspect in predicting the osteogenic potential of cells

A second cell surface receptor was also found to correlate with the expression of osteogenic markers independent of CD105. CD90 (Thy-1) was originally discovered as a thymocyte antigen, which could be useful to identify and isolate ADSCs subpopulations. $CD90^{high}$ ADSCs had greater reprogramming capacity than $CD90^{low}$ ADSCs, suggesting that ADSCs have heterogeneous subpopulations [55]. Moreover, Hosoya et al. evaluated the capacity of rat $CD90^{high}$ and $CD90^{low}$ subodontoblastic dental pulp stem cells to differentiate into hard tissue-forming cells in response to bone morphogenetic protein-2 stimulation and observed that $CD90^{high}$ had accelerated ability to mineralize *in vitro* and *in vivo* (Table 1) [56].

CD90 and CD105 have been identified as early MSCs markers present on both BM-MSCs and ADSCs. Chung et al. demonstrated that, compared with $CD90^{-}$ or unsorted cells, $CD90^{+}$ subpopulation isolated from human adipose tissue has enhanced osteogenic potential *in vitro* and *in vivo*; in fact, the authors proposed CD90 as a better surface marker to isolate cells with osteogenic potential [57, 58]. Murine-derived ADSCs were sorted for the expression of the surface markers CD90 and CD105 using flow cytometry. ADSCs were sorted into four groups: $CD90^{+}/CD105^{-}$, $CD90^{+}/CD105^{+}$, $CD90^{-}/CD105^{+}$, and $CD90^{-}/CD105^{-}$, in which $CD90^{+}/CD105^{-}$ and $CD90^{+}/CD105^{+}$ cells had robust osteogenic potential and displayed mineralized nodules, whereas strong expression of CD105 might predict weak osteogenesis [50].

Consistent findings indicate that the absence of CD105 and the expression of CD90 surface markers characterize subpopulations with increased efficiency of differentiation into osteogenic lineage.

It has been advised not to discard the possibility of including other markers as part of an osteogenic profile analysis. Recently, the expression of the human embryonic stem cells marker SSEA-4 in a subpopulation of human adipose tissue ($SSEA\text{-}4^{+}$ hASCs) has been reported. The subpopulation has the ability to differentiate into osteogenic lineages but also into endothelial lineages, which represents a useful approach to obtain these two cell types from the source and consequently is relevant for bone tissue engineering applications (Table 1) [59, 60].

3.2. Chondrogenic Differentiation from Mesenchymal Stem Cell Subpopulations. For clinical success, MSCs must be held in the area of injury and produce extracellular matrix in a physiological context, where low nutrient conditions produced by avascularity, nutrition, and waste production are prevalent. Certain MSCs subpopulations are more resilient to metabolic challenge than others.

Chondrogenic differentiation of BM-MSCs has been extensively studied *in vitro* in micromass pellet, which promotes cell condensation, aside from cell-cell and cell-extracellular matrix (ECM) connections [61, 62]. Consequently, cells progress into a highly proliferative stage to

Table 2: MSC subpopulations with enhanced chondrogenic differentiation.

Subpopulation markers	Isolation method	Source	Reference
$CD9^+/CD90^+/CD166^+$	FACS	SM	Fickert et al. 2003 [74]
$CD271^+$	FACS	SM	Arufe et al. 2010 [76]
	Magnetic beads	SM	Hermida-Gómez et al. 2010 [78]
$CD73^+CD39^+$	FACS	SM	Gullo and De Bari 2013 [77]
$CD105^+$	Magnetic beads	SM	Arufe et al. 2009 [79]
$CD105^-$	FACS	mTPCs	Asai et al. 2014 [80]
$CD146^+$	FACS	BM	Hagmann et al. 2013 [84]
	Magnetic beads	HU-MSCs	Wu et al. 2016 [86]

produce typical components of the cartilaginous matrix (collagen type 2, collagen type 9, aggrecan, and cartilage oligomeric matrix protein). Lastly, cells become round and then go through hypertrophy expressing collagen type X and MMP13 [63–67].

Cartilage is susceptible to damage and has a reduced capacity for regeneration. Procedures committed to recruit stem cells from BM by penetration to the subchondral bone have been commonly used to treat localized cartilage defects [68]. More recently, autologous chondrocyte implantation has been introduced [69]. Research on cartilage tissue engineering in recent years has focused on the use of adult MSCs as an alternative source of autologous chondrocytes [70].

MSCs can differentiate into chondrocytes and fibrochondrocytes, resulting in a combination of cartilaginous fibrous and hypertrophic tissues, whereby the clinical success lasted for a short time because these cells do not possess functional mechanical properties [71]. Conversely, compared to MSCs derived from BM, MSCs from synovial tissue have been revealed to enhance chondrogenic potential and diminish the hypertrophic differentiation [72, 73].

Fickert et al. sorted a triplicate positive subpopulation from the synovial membrane (SM) of patients with osteoarthritis ($CD9^+/CD90^+/CD166^+$). In the micromass of sorted cell cultures, Col2 was located predominantly in the inner areas, indicating that the subpopulation of SM-derived cells has the capacity to differentiate efficiently towards the chondrogenic lineage (Table 2). However, no major differences between sorted and unsorted SM cells were evidenced [74, 75].

In 2010, Arufe et al. analyzed the chondrogenic potential of subpopulations of human synovial membrane MSCs sorted for CD73, CD106, and CD271 markers. Compared with $CD106^+$ and $CD271^+$ subpopulations, $CD73^+$ cells evidenced the highest expression of *SOX9* (a key transcription factor that is necessary for early chondrogenesis), aggrecan, and COL2A1 at day 46 of chondrogenic induction. However, the $CD73^+$ cells also showed the expression of COL10A1, indicating the presence of hypertrophy during differentiation [76].

More recently, in 2013, it was reported that the isolation of a different SM subpopulation based on surface markers CD73 and CD39 displayed consistent dynamics over passaging. The $CD73^+CD39^+$ cell subpopulation displayed higher expression levels of *SOX9* and a significantly greater chondrogenic potency than the $CD73^+CD39^-$ cell subpopulation (Table 2) [77].

Regarding the CD271 surface marker, compared to the other subpopulations, the $CD271^+$ subpopulation expressed the highest levels of COL2 staining. Spheroids formed from $CD271^+$ and $CD73^+$ subpopulations from normal human synovial membranes that imitate the native cartilage extracellular matrix more closely than $CD106^+$ MSCs, with the result that both are excellent candidates to use in cartilage tissue engineering [76].

Hermida-Gómez et al. strengthened this finding, showing that, during spontaneous cartilage repair, $CD271^+$ provides higher quality chondral repair than the $CD271^-$ subpopulation. The implantation of MSCs $CD271^+$ provided such benefits as greater filling of the chondral defect and improved integration between the repair tissue and native cartilage (Table 2) [78].

Meanwhile, Arufe et al. reported the isolation by a magnetic separator of a $CD105^+$ subpopulation from human synovial membrane. These researchers evidenced a homogeneous cellular culture, which expressed Sox9 and had the ability to develop spheroids after 7 days in the presence of chondrogenic medium (Table 2). Interestingly, the extracellular matrix produced is rich in Col2 and showed no evidence of fibrocartilage tissue. The analysis of the $CD105^-$ subpopulation was not reported [79].

Tendon-derived progenitor cells (TPCs) from mice contained two subpopulations: one positive and one negative for CD105. Compared to the *in vitro* case with $CD105^+$, the $CD105^-$ negative cells showed superior chondrogenic potential, and it was proposed that differences in the capability of chondrogenic differentiation are due to different modes of smad1/5 and smad2/3 signaling activation as a result of TGFβs (Table 2) [80].

Various parameters have been considered in hMSCs' chondrogenic differentiation. In particular, it has been evidenced that hMSCs' expansion *in vitro* required FGF-2 and IGF-1 to enhance the proliferative and chondrogenic potential [81–83]. A highly efficient strategy is based on the preselection during the expansion phase of the MSCs by adding growth factors. In 2013, Hagmann et al. reported that FGF-2 suppressed CD146 expression and significantly improved chondrogenic differentiation [84]. Despite the observations

from the preselection with FGF-2 and resulting suppression of CD146, in 2014, these researchers demonstrated that, compared to control MSCs, $CD146^+$ FACS-sorted cells showed significantly increased GAG/DNA content after chondrogenic differentiation [85]. It should be noted that subpopulations, such as $CD146^+$ from human umbilical cords, not only provide more efficient cartilage regeneration process but also provide an anti-inflammatory protective microenvironment resulting from decreased expression of IL-6 (Table 2) [86].

4. Conclusions

The current review highlights recent findings in the isolation and characterization of MSCs subpopulations and the potential applications for osteogenic or chondrogenic differentiation.

It was evident that the source of the MSCs subpopulation had an effect on the differentiation potential, and certainly the use of strategies based on the coexpression of more than one surface marker improves the purity of the isolated MSCs population.

These findings indicate that the absence of the CD105 surface marker characterizes subpopulations with improved osteogenesis when the source of isolation is adipose tissue or amniotic membrane. Furthermore, subpopulations expressing CD271 or CD146 markers appear to provide higher quality for chondral repair.

An accurate selection of the subpopulation puts forward possibilities suitable for preclinical and clinical studies and determines the safest and most efficacious regeneration process.

Abbreviations

ACPC:	Articular cartilage progenitor cells
ADSCs:	Adipose-derived stromal cells
ALP:	Alkaline phosphatase
AM:	Amniotic membrane
AT:	Adipose tissue
BM:	Bone marrow
BM-MSCs:	Bone marrow mesenchymal stem cells
CD:	Cluster of differentiation
CFU-Fs:	Colony forming unit-fibroblastoids
DPSCs:	Dental pulp stem cells
ECM:	Extracellular matrix
FACS:	Fluorescence-activated cell sorting
ISCT:	International Society for Cellular Therapy
HU-MSCs:	Human umbilical mesenchymal stem cells
MSCs:	Mesenchymal stem cells
PDLPs:	Periodontal ligament progenitor cells
PDLSCs:	PDL stem cells
PSC:	Perivascular stem cells
OA:	Osteoarthritis
SHED:	Stem cells from human exfoliated deciduous teeth
SM:	Synovial membrane
TPCs:	Tendon-derived progenitor cells
VCAM:	Vascular cell adhesion molecule.

Competing Interests

The authors declare that there are no competing interests regarding the publication of this paper.

Authors' Contributions

All authors were involved in drafting the paper, and all authors approved the final version to be published.

References

[1] D. L. Jones and A. J. Wagers, "No place like home: anatomy and function of the stem cell niche," *Nature Reviews Molecular Cell Biology*, vol. 9, no. 1, pp. 11–21, 2008.

[2] M. Dominici, K. Le Blanc, I. Mueller et al., "Minimal criteria for defining multipotent mesenchymal stromal cells. The International Society for Cellular Therapy position statement," *Cytotherapy*, vol. 8, no. 4, pp. 315–317, 2006.

[3] S. A. Boxall and E. Jones, "Markers for characterization of bone marrow multipotential stromal cells," *Stem Cells International*, vol. 2012, Article ID 975871, 12 pages, 2012.

[4] V. Rasini, M. Dominici, T. Kluba et al., "Mesenchymal stromal/stem cells markers in the human bone marrow," *Cytotherapy*, vol. 15, no. 3, pp. 292–306, 2013.

[5] L. da Silva Meirelles, P. C. Chagastelles, and N. B. Nardi, "Mesenchymal stem cells reside in virtually all post-natal organs and tissues," *Journal of Cell Science*, vol. 119, no. 11, pp. 2204–2213, 2006.

[6] A. J. Friedenstein, K. V. Petrakova, A. I. Kurolesova, and G. P. Frolova, "Heterotopic of bone marrow. Analysis of precursor cells for osteogenic and hematopoietic tissues," *Transplantation*, vol. 6, no. 2, pp. 230–247, 1968.

[7] W. Wagner, F. Wein, A. Seckinger et al., "Comparative characteristics of mesenchymal stem cells from human bone marrow, adipose tissue, and umbilical cord blood," *Experimental Hematology*, vol. 33, no. 11, pp. 1402–1416, 2005.

[8] X. Zhang, M. Yang, L. Lin et al., "Runx2 overexpression enhances osteoblastic differentiation and mineralization in adipose—derived stem cells in vitro and in vivo," *Calcified Tissue International*, vol. 79, no. 3, pp. 169–178, 2006.

[9] S. Alsalameh, R. Amin, T. Gemba, and M. Lotz, "Identification of mesenchymal progenitor cells in normal and osteoarthritic human articular cartilage," *Arthritis & Rheumatism*, vol. 50, no. 5, pp. 1522–1532, 2004.

[10] F. Appaix, M. F. Nissou, B. van der Sanden et al., "Brain mesenchymal stem cells: the other stem cells of the brain?" *World Journal of Stem Cells*, vol. 6, no. 2, pp. 134–143, 2014.

[11] A. N. Schüring, N. Schulte, R. Kelsch, A. Röpke, L. Kiesel, and M. Götte, "Characterization of endometrial mesenchymal stem-like cells obtained by endometrial biopsy during routine diagnostics," *Fertility and Sterility*, vol. 95, no. 1, pp. 423–426, 2011.

[12] J. G. Allickson, A. Sanchez, N. Yefimenko, C. V. Borlongan, and P. R. Sanberg, "Recent studies assessing the proliferative capability of a novel adult stem cell identified in menstrual blood," *The Open Stem Cell Journal*, vol. 3, pp. 4–10, 2011.

[13] R. Ab Kadir, S. H. Zainal Ariffin, R. Megat Abdul Wahab, S. Kermani, and S. Senafi, "Characterization of mononucleated human peripheral blood cells," *The Scientific World Journal*, vol. 2012, Article ID 843843, 8 pages, 2012.

[14] G. Bartsch Jr., J. J. Yoo, P. De Coppi et al., "Propagation, expansion, and multilineage differentiation of human somatic stem cells from dermal progenitors," *Stem Cells and Development*, vol. 14, no. 3, pp. 337–348, 2005.

[15] U. Riekstina, R. Muceniece, I. Cakstina, I. Muiznieks, and J. Ancans, "Characterization of human skin-derived mesenchymal stem cell proliferation rate in different growth conditions," *Cytotechnology*, vol. 58, no. 3, pp. 153–162, 2008.

[16] T. Morito, T. Muneta, K. Hara et al., "Synovial fluid-derived mesenchymal stem cells increase after intra-articular ligament injury in humans," *Rheumatology*, vol. 47, no. 8, pp. 1137–1143, 2008.

[17] M.-S. Tsai, J.-L. Lee, Y.-J. Chang, and S.-M. Hwang, "Isolation of human multipotent mesenchymal stem cells from second-trimester amniotic fluid using a novel two-stage culture protocol," *Human Reproduction*, vol. 19, no. 6, pp. 1450–1456, 2004.

[18] M. Leyva-Leyva, L. Barrera, C. López-Camarillo et al., "Characterization of mesenchymal stem cell subpopulations from human amniotic membrane with dissimilar osteoblastic potential," *Stem Cells and Development*, vol. 22, no. 8, pp. 1275–1287, 2013.

[19] J. Cai, W. Li, H. Su et al., "Generation of human induced pluripotent stem cells from umbilical cord matrix and amniotic membrane mesenchymal cells," *The Journal of Biological Chemistry*, vol. 285, no. 15, pp. 11227–11234, 2010.

[20] C. M. Raynaud, M. Maleki, R. Lis et al., "Comprehensive characterization of mesenchymal stem cells from human placenta and fetal membrane and their response to osteoactivin stimulation," *Stem Cells International*, vol. 2012, Article ID 658356, 13 pages, 2012.

[21] K. Kita, G. G. Gauglitz, T. T. Phan, D. N. Herndon, and M. G. Jeschke, "Isolation and characterization of mesenchymal stem cells from the sub-amniotic human umbilical cord lining membrane," *Stem Cells and Development*, vol. 19, no. 4, pp. 491–502, 2010.

[22] H. Ali and F. Al-Mulla, "Defining umbilical cord blood stem cells," *Stem Cell Discovery*, vol. 2, no. 1, pp. 15–23, 2012.

[23] H.-S. Wang, S.-C. Hung, S.-T. Peng et al., "Mesenchymal stem cells in the Wharton's jelly of the human umbilical cord," *STEM CELLS*, vol. 22, no. 7, pp. 1330–1337, 2004.

[24] M. Seifrtová, R. Havelek, J. Ćmielová et al., "The response of human ectomesenchymal dental pulp stem cells to cisplatin treatment," *International Endodontic Journal*, vol. 45, no. 5, pp. 401–412, 2012.

[25] M. Miura, S. Gronthos, M. Zhao et al., "SHED: stem cells from human exfoliated deciduous teeth," *Proceedings of the National Academy of Sciences of the United States of America*, vol. 100, no. 10, pp. 5807–5812, 2003.

[26] E. Prateeptongkum, C. Klingelhöffer, S. Müller, T. Ettl, and C. Morsczeck, "Characterization of progenitor cells and stem cells from the periodontal ligament tissue derived from a single person," *Journal of Periodontal Research*, vol. 51, no. 2, pp. 265–272, 2016.

[27] S.-I. Fukada, A. Uezumi, M. Ikemoto et al., "Molecular signature of quiescent satellite cells in adult skeletal muscle," *Stem Cells*, vol. 25, no. 10, pp. 2448–2459, 2007.

[28] M. Crisan, S. Yap, L. Casteilla et al., "A perivascular origin for mesenchymal stem cells in multiple human organs," *Cell Stem Cell*, vol. 3, no. 3, pp. 301–313, 2008.

[29] D. C. Colter, I. Sekiya, and D. J. Prockop, "Identification of a subpopulation of rapidly self-renewing and multipotential adult stem cells in colonies of human marrow stromal cells," *Proceedings of the National Academy of Sciences of the United States of America*, vol. 98, no. 14, pp. 7841–7845, 2001.

[30] R. R. Pochampally, J. R. Smith, J. Ylostalo, and D. J. Prockop, "Serum deprivation of human marrow stromal cells (hMSCs) selects for a subpopulation of early progenitor cells with enhanced expression of OCT-4 and other embryonic genes," *Blood*, vol. 103, no. 5, pp. 1647–1652, 2004.

[31] D. O. Traktuev, S. Merfeld-Clauss, J. Li et al., "A population of multipotent CD34-positive adipose stromal cells share pericyte and mesenchymal surface markers, reside in a periendothelial location, and stabilize endothelial networks," *Circulation Research*, vol. 102, no. 1, pp. 77–85, 2008.

[32] M. Corselli, C.-W. Chen, B. Sun, S. Yap, J. P. Rubin, and B. Péault, "The tunica adventitia of human arteries and veins as a source of mesenchymal stem cells," *Stem Cells and Development*, vol. 21, no. 8, pp. 1299–1308, 2012.

[33] H. Zhao, J. Feng, K. Seidel et al., "Secretion of shh by a neurovascular bundle niche supports mesenchymal stem cell homeostasis in the adult mouse incisor," *Cell Stem Cell*, vol. 14, no. 2, pp. 160–173, 2014.

[34] M. Corselli, M. Crisan, I. R. Murray et al., "Identification of perivascular mesenchymal stromal/stem cells by flow cytometry," *Cytometry Part A*, vol. 83, no. 8, pp. 714–720, 2013.

[35] A. Askarinam, A. W. James, J. N. Zara et al., "Human perivascular stem cells show enhanced osteogenesis and vasculogenesis with nel-like molecule I protein," *Tissue Engineering—Part A*, vol. 19, no. 11-12, pp. 1386–1397, 2013.

[36] W. C. W. Chen, A. Saparov, M. Corselli et al., "Isolation of blood-vessel-derived multipotent precursors from human skeletal muscle," *Journal of Visualized Experiments*, no. 90, Article ID e51195, 2014.

[37] M. A. König, D. D. Canepa, D. Cadosch et al., "Direct transplantation of native pericytes from adipose tissue: a new perspective to stimulate healing in critical size bone defects," *Cytotherapy*, vol. 18, no. 1, pp. 41–52, 2016.

[38] H. Busser, M. Najar, G. Raicevic et al., "Isolation and characterization of human mesenchymal stromal cell subpopulations: comparison of bone marrow and adipose tissue," *Stem Cells and Development*, vol. 24, no. 18, pp. 2142–2157, 2015.

[39] R. J. Cuthbert, P. V. Giannoudis, X. N. Wang et al., "Examining the feasibility of clinical grade $CD271^+$ enrichment of mesenchymal stromal cells for bone regeneration," *PLoS ONE*, vol. 10, no. 3, Article ID e0117855, 2015.

[40] Y. Mabuchi, S. Morikawa, S. Harada et al., "$LNGFR^+THY\text{-}1^+VCAM\text{-}1^{hi+}$ cells reveal functionally distinct subpopulations in mesenchymal stem cells," *Stem Cell Reports*, vol. 1, no. 2, pp. 152–165, 2013.

[41] L. Marzona and B. Pavolini, "Play and players in bone fracture healing match," *Clinical Cases in Mineral and Bone Metabolism*, vol. 6, no. 2, pp. 159–162, 2009.

[42] M. F. Pittenger, A. M. Mackay, S. C. Beck et al., "Multilineage potential of adult human mesenchymal stem cells," *Science*, vol. 284, no. 5411, pp. 143–147, 1999.

[43] P. Bianco and P. G. Robey, "Stem cells in tissue engineering," *Nature*, vol. 414, no. 6859, pp. 118–121, 2001.

[44] V. Viateau, G. Guillemin, V. Bousson et al., "Long-bone critical-size defects treated with tissue-engineered grafts: a study on sheep," *Journal of Orthopaedic Research*, vol. 25, no. 6, pp. 741–749, 2007.

[45] F. Guilak, K. E. Lott, H. A. Awad et al., "Clonal analysis of the differentiation potential of human adipose-derived adult stem cells," *Journal of Cellular Physiology*, vol. 206, no. 1, pp. 229–237, 2006.

[46] B. Levi, D. C. Wan, J. P. Glotzbach et al., "CD105 protein depletion enhances human adipose-derived stromal cell osteogenesis through reduction of transforming growth factor β1 (TGF-β1) signaling," *The Journal of Biological Chemistry*, vol. 286, no. 45, pp. 39497–39509, 2011.

[47] L. Choy, J. Skillington, and R. Derynck, "Roles of autocrine TGF-β receptor and Smad signaling in adipocyte differentiation," *The Journal of Cell Biology*, vol. 149, no. 3, pp. 667–682, 2000.

[48] M. Leyva-Leyva, A. López-Diáz, L. Barrera et al., "Differential expression of adhesion-related proteins and MAPK pathways lead to suitable osteoblast differentiation of human mesenchymal stem cells subpopulations," *Stem Cells and Development*, vol. 24, no. 21, pp. 2577–2590, 2015.

[49] P. Anderson, A. B. Carrillo-Gálvez, A. García-Pérez, M. Cobo, and F. Martín, "CD105 (Endoglin)-negative murine mesenchymal stromal cells define a new multipotent subpopulation with distinct differentiation and immunomodulatory capacities," *PLoS ONE*, vol. 8, no. 10, Article ID e76979, 2013.

[50] M. Yamamoto, H. Nakata, J. Hao, J. Chou, S. Kasugai, and S. Kuroda, "Osteogenic potential of mouse adipose-derived stem cells sorted for CD90 and CD105 in vitro," *Stem Cells International*, vol. 2014, Article ID 576358, 17 pages, 2014.

[51] T. Rada, R. L. Reis, and M. E. Gomes, "Distinct stem cells subpopulations isolated from human adipose tissue exhibit different chondrogenic and osteogenic differentiation potential," *Stem Cell Reviews and Reports*, vol. 7, no. 1, pp. 64–76, 2011.

[52] H. Aslan, Y. Zilberman, L. Kandel et al., "Osteogenic differentiation of noncultured immunoisolated bone marrow-derived CD105+ cells," *Stem Cells*, vol. 24, no. 7, pp. 1728–1737, 2006.

[53] D. Jarocha, E. Lukasiewicz, and M. Majka, "Adventage of Mesenchymal Stem Cells (MSC) expansion directly from purified bone marrow $CD105^+$ and $CD271^+$ cells," *Folia Histochemica et Cytobiologica*, vol. 46, no. 3, pp. 307–314, 2008.

[54] J. E. Dennis, K. Esterly, A. Awadallah, C. R. Parrish, G. M. Poynter, and K. L. Goltry, "Clinical-scale expansion of a mixed population of bone marrow-derived stem and progenitor cells for potential use in bone tissue regeneration," *Stem Cells*, vol. 25, no. 10, pp. 2575–2582, 2007.

[55] K. Kawamoto, K. Konno, H. Nagano et al., "CD90- (Thy-1-) high selection enhances reprogramming capacity of murine adipose-derived mesenchymal stem cells," *Disease Markers*, vol. 35, no. 5, pp. 573–579, 2013.

[56] A. Hosoya, T. Hiraga, T. Ninomiya et al., "Thy-1-positive cells in the subodontoblastic layer possess high potential to differentiate into hard tissue-forming cells," *Histochemistry and Cell Biology*, vol. 137, no. 6, pp. 733–742, 2012.

[57] J. B. Mitchell, K. McIntosh, S. Zvonic et al., "Immunophenotype of human adipose-derived cells: temporal changes in stromal-associated and stem cell-associated markers," *Stem Cells*, vol. 24, no. 2, pp. 376–385, 2006.

[58] M. T. Chung, C. Liu, J. S. Hyun et al., "CD90 (Thy-1)-positive selection enhances osteogenic capacity of human adipose-derived stromal cells," *Tissue Engineering—Part A*, vol. 19, no. 7-8, pp. 989–997, 2013.

[59] S. M. Mihaila, A. M. Frias, R. P. Pirraco et al., "Human adipose tissue-derived ssea-4 subpopulation multi-differentiation potential towards the endothelial and osteogenic lineages," *Tissue Engineering—Part A*, vol. 19, no. 1-2, pp. 235–246, 2013.

[60] S. M. Mihaila, A. K. Gaharwar, R. L. Reis, A. Khademhosseini, A. P. Marques, and M. E. Gomes, "The osteogenic differentiation of SSEA-4 sub-population of human adipose derived stem cells using silicate nanoplatelets," *Biomaterials*, vol. 35, no. 33, pp. 9087–9099, 2014.

[61] J. J. Auletta, L. A. Solchaga, E. A. Zale, and J. F. Welter, "Fibroblast growth factor-2 enhances expansion of human bone marrow-derived mesenchymal stromal cells without diminishing their immunosuppressive potential," *Stem Cells International*, vol. 2011, Article ID 235176, 10 pages, 2011.

[62] T. Felka, R. Schfer, P. De Zwart, and W. K. Aicher, "Animal serum-free expansion and differentiation of human mesenchymal stromal cells," *Cytotherapy*, vol. 12, no. 2, pp. 143–153, 2010.

[63] R. Williams, I. M. Khan, K. Richardson et al., "Identification and clonal characterisation of a progenitor cell sub-population in normal human articular cartilage," *PLoS ONE*, vol. 5, no. 10, Article ID e13246, 2010.

[64] B. Grigolo, L. Roseti, M. Fiorini et al., "Transplantation of chondrocytes seeded on a hyaluronan derivative (Hyaff®-11) into cartilage defects in rabbits," *Biomaterials*, vol. 22, no. 17, pp. 2417–2424, 2001.

[65] K. W. Kavalkovich, R. E. Boynton, J. M. Murphy, and F. Barry, "Chondrogenic differentiation of human mesenchymal stem cells within an alginate layer culture system," *In Vitro Cellular & Developmental Biology—Animal*, vol. 38, no. 8, pp. 457–466, 2002.

[66] R. Tuli, W.-J. Li, and R. S. Tuan, "Current state of cartilage tissue engineering," *Arthritis Research and Therapy*, vol. 5, no. 5, pp. 235–238, 2003.

[67] C. Karlsson, C. Brantsing, T. Svensson et al., "Differentiation of human mesenchymal stem cells and articular chondrocytes: analysis of chondrogenic potential and expression pattern of differentiation-related transcription factors," *Journal of Orthopaedic Research*, vol. 25, no. 2, pp. 152–163, 2007.

[68] A. Schmitt, M. Van Griensven, A. B. Imhoff, and S. Buchmann, "Application of stem cells in orthopedics," *Stem Cells International*, vol. 2012, Article ID 394962, 11 pages, 2012.

[69] E. H. Lee and J. H. P. Hui, "The potential of stem cells in orthopaedic surgery," *Journal of Bone and Joint Surgery—Series B*, vol. 88, no. 7, pp. 841–851, 2006.

[70] M. C. Ronzière, E. Perrier, F. Mallein-Gerin, and A.-M. Freyria, "Chondrogenic potential of bone marrow- and adipose tissue-derived adult human mesenchymal stem cells," *Bio-Medical Materials and Engineering*, vol. 20, no. 3-4, pp. 145–158, 2010.

[71] D. J. Huey, J. C. Hu, and K. A. Athanasiou, "Unlike bone, cartilage regeneration remains elusive," *Science*, vol. 338, no. 6109, pp. 917–921, 2012.

[72] M. Pei, D. Chen, J. Li, and L. Wei, "Histone deacetylase 4 promotes TGF-β1-induced synovium-derived stem cell chondrogenesis but inhibits chondrogenically differentiated stem cell hypertrophy," *Differentiation*, vol. 78, no. 5, pp. 260–268, 2009.

[73] D. Studer, C. Millan, E. Öztürk, K. Maniura-Weber, and M. Zenobi-Wong, "Molecular and biophysical mechanisms regulating hypertrophic differentiation in chondrocytes and mesenchymal stem cells," *European Cells and Materials*, vol. 24, pp. 118–135, 2012.

[74] S. Fickert, J. Fiedler, and R. E. Brenner, "Identification, quantification and isolation of mesenchymal progenitor cell from

osteoarthritic synovium by fluorescence automated cell sorting," *Osteoarthritis and Cartilage*, vol. 11, no. 11, pp. 790–800, 2003.

[75] S. Fickert, J. Fiedler, and R. E. Brenner, "Identification of subpopulations with characteristics of mesenchymal progenitor cells from human osteoarthritic cartilage using triple staining for cell surface markers," *Arthritis Research & Therapy*, vol. 6, no. 5, pp. R422–R432, 2004.

[76] M. C. Arufe, A. De La Fuente, I. Fuentes, F. J. De Toro, and F. J. Blanco, "Chondrogenic potential of subpopulations of cells expressing mesenchymal stem cell markers derived from human synovial membranes," *Journal of Cellular Biochemistry*, vol. 111, no. 4, pp. 834–845, 2010.

[77] F. Gullo and C. De Bari, "Prospective purification of a subpopulation of human synovial mesenchymal stem cells with enhanced chondro-osteogenic potency," *Rheumatology*, vol. 52, no. 10, pp. 1758–1768, 2013.

[78] T. Hermida-Gómez, I. Fuentes-Boquete, M. J. Gimeno-Longas et al., "Bone marrow cells immunomagnetically selected for CD271+ antigen promote *in vitro* the repair of articular cartilage defects," *Tissue Engineering Part A*, vol. 17, no. 7-8, pp. 1169–1179, 2011.

[79] M. C. Arufe, M. C. De La Fuente, I. Fuentes-Boquete, F. J. De Toro, and F. J. Blanco, "Differentiation of synovial CD-105$^+$ human mesenchymal stem cells into chondrocyte-like cells through spheroid formation," *Journal of Cellular Biochemistry*, vol. 108, no. 1, pp. 145–155, 2009.

[80] T. Felka, R. Schäfer, P. De Zwart, and W. K. Aicher, "Animal serum-free expansion and differentiation of human mesenchymal stromal cells," *Cytotherapy*, vol. 12, no. 2, pp. 143–153, 2012.

[81] C. Millan, E. Öztürk, K. Maniura-Weber, and M. Zenobi-Wong, "Molecular and biophysical mechanisms regulating hypertrophic differentiation in chondrocytes and mesenchymal stem cells," *European Cells and Materials*, vol. 24, pp. 118–135, 2012.

[82] L. A. Solchaga, K. Penick, J. D. Porter, V. M. Goldberg, A. I. Caplan, and J. F. Welter, "FGF-2 enhances the mitotic and chondrogenic potentials of human adult bone marrow-derived mesenchymal stem cells," *Journal of Cellular Physiology*, vol. 203, no. 2, pp. 398–409, 2005.

[83] I. Garza-Veloz, V. J. Romero-Diaz, M. L. Martinez-Fierro et al., "Analyses of chondrogenic induction of adipose mesenchymal stem cells by combined co-stimulation mediated by adenoviral gene transfer," *Arthritis Research & Therapy*, vol. 15, no. 4, article R80, 2013.

[84] S. Hagmann, B. Moradi, S. Frank et al., "FGF-2 addition during expansion of human bone marrow-derived stromal cells alters MSC surface marker distribution and chondrogenic differentiation potential," *Cell Proliferation*, vol. 46, no. 4, pp. 396–407, 2013.

[85] S. Hagmann, S. Frank, T. Gotterbarm, T. Dreher, V. Eckstein, and B. Moradi, "Fluorescence activated enrichment of CD146+ cells during expansion of human bone-marrow derived mesenchymal stromal cells augments proliferation and GAG/DNA content in chondrogenic media," *BMC Musculoskeletal Disorders*, vol. 15, no. 1, article 322, 2014.

[86] C.-C. Wu, F.-L. Liu, H.-K. Sytwu, C.-Y. Tsai, and D.-M. Chang, "CD146$^+$ mesenchymal stem cells display greater therapeutic potential than CD146$^-$ cells for treating collagen-induced arthritis in mice," *Stem Cell Research & Therapy*, vol. 7, article 23, 2016.

Hindawi Publishing Corporation
Stem Cells International
Volume 2016, Article ID 1416047, 13 pages
http://dx.doi.org/10.1155/2016/1416047

Research Article

Slowly Delivered Icariin/Allogeneic Bone Marrow-Derived Mesenchymal Stem Cells to Promote the Healing of Calvarial Critical-Size Bone Defects

Tianlin Liu,[1,2] Xin Zhang,[3] Yuan Luo,[1,4] Yuanliang Huang,[1,2] and Gang Wu[5]

[1] *Laboratory of Oral Biomedical Science and Translational Medicine, Department of Oral and Maxillofacial Surgery, School of Stomatology, Tongji University, Shanghai, China*
[2] *Department of Stomatology, Shanghai East Hospital Affiliated with Tongji University, Jimo Road No. 150, Shanghai 200120, China*
[3] *Stomatology Hospital Affiliated with Zhejiang University College of Medicine, Hangzhou, China*
[4] *Shanghai Stomatosis Prevention and Treatment Center, Shanghai, China*
[5] *Department of Oral Implantology and Prosthetic Dentistry, Academic Center for Dentistry Amsterdam (ACTA), MOVE Research Institute, University of Amsterdam and VU University Amsterdam, Gustav Mahlerlaan 3004, 1081 LA Amsterdam, Netherlands*

Correspondence should be addressed to Yuanliang Huang; huangyuanliang_hyl@163.com and Gang Wu; g.wu@acta.nl

Received 6 April 2016; Revised 4 August 2016; Accepted 11 August 2016

Academic Editor: Heinrich Sauer

Bone tissue engineering technique is a promising strategy to repair large-volume bone defects. In this study, we developed a 3-dimensional construct by combining icariin (a small-molecule Chinese medicine), allogeneic bone marrow-derived mesenchymal stem cells (BMSCs), and a siliceous mesostructured cellular foams-poly(3-hydroxybutyrate-co-3-hydroxyhexanoate) (SMC-PHBHHx) composite scaffold. We hypothesized that the slowly released icariin could significantly promote the efficacy of SMC-PHBHHx/allogeneic BMSCs for repairing critical-size bone defects in rats. In in vitro cellular experiments, icariin at optimal concentration (10^{-6} mol/L) could significantly upregulate the osteogenesis- and angiogenesis-related genes and proteins, such as Runx2, ALP, osteocalcin, vascular endothelial growth factors, and fibroblast growth factors, as well as the mineralization of BMSCs. Icariin that was adsorbed onto the SMC-PHBHHx scaffold showed a slow release profile within a 2-week monitoring span. Eight weeks after implantation in calvarial critical-size bone defects, the constructs with icariin were associated with significantly higher bone volume density, trabecular thickness, trabecular number, and significantly lower trabecular separation than the constructs without icariin. Histomorphometric analysis showed that icariin was also associated with a significantly higher density of newly formed blood vessels. These data suggested a promising application potential of the icariin/SMC-PHBHHx/allogeneic BMSCs constructs for repairing large-volume bone defects in clinic.

1. Introduction

Large-volume bone defects may result from congenital non-union, trauma, inflammation, and clinical treatments such as osteosarcoma-resection. The osseous repair of large-volume bone defects is still a challenge in the fields of orthopedics, maxillofacial surgery, and dental implantology. Although autologous bone grafts are routinely adopted to treat large-volume bone defects, the disadvantages of these grafts (e.g., limited quantity, donor site morbidity) have engendered tremendous efforts to develop alternatives [1], among which bone tissue engineering technique is highly promising [2, 3]. Bone tissue engineering technique is an interdisciplinary science that applies the principles of biology and engineering to develop viable substitutes for restoring, maintaining, or improving the function of bone tissue. A good combination of osteogenic cells, osteopromotive drugs, and osteoconductive biomaterials is critical for the success of this technique.

The accumulation, proliferation, and osteogenic differentiation of multipotent mesenchymal stem cells (MSCs) are indispensable for a proper fracture healing [4]. Thereby, bone marrow-derived MSCs- (BMSCs-) based strategies are

introduced to promote the healing of bone fractures and other bone metabolic diseases in clinics [5]. Their ability to modulate immune responses enables the application of allogeneic BMSCs without a substantial risk of immune rejection [5]. Continuous attempts have already been performed in preclinical models to apply allogeneic BMSCs in promoting the repair of bone defects [6]. In segmental critical-size bone defects, allogeneic BMSCs could significantly promote bone regeneration in a comparable level with autologous BMSCs [7]. The application of allogeneic BMSCs is also advantageous over autologous BMSCs due to their timeliness and sufficient availability [8].

Growth factors can be frequently adopted to further enhance and accelerate bone healing process. In the field of bone regeneration, bone morphogenetic proteins (BMPs) are the most important growth factors. Recombinant human BMP-2 and BMP-7 have been proved to significantly promote bone formation both in animal models and in clinical trials [9–11]. However, the effective doses of BMPs for current clinical use are always too high [12, 13], which results in a substantial economic burden to patients and healthcare system. Furthermore, the transiently high dosage may also lead to a series of potential side effects, such as the overstimulation of osteoclastic bone resorption [14], which may compromise its therapeutic effect. For promoting bone repair, one of the viable alternatives can be Chinese medicine, such as icariin. Icariin, a small-molecule drug extracted from a Chinese traditional medicine Herba Epimedii [15], shows a very promising potential. Icariin has been shown to enhance in vitro osteoblastogenesis [16, 17] through the induction of endogenous BMP-2 and nitric oxide (NO) [18, 19]. On the other hand, icariin is also able to reduce osteoclastogenesis through suppressing the signaling of MAPKs/NF-κB (mitogen-activated protein kinase/nuclear factor kappa-light-chain-enhancer of activated B cells) [20] and enhancing the ratio of OPG/RANKL [21]. In addition, icariin can promote angiogenesis, which may further facilitate the repair of large-volume bone defects. In comparison with BMPs, icariin, as a small-molecule drug, can also be easily synthesized, presenting an inexpensive drug to promote bone regeneration.

In the field of bone tissue engineering, an ideal scaffold should have a proper biodegradability and a good biocompatibility to accommodate osteogenic cells. Furthermore, a good slow-delivery capacity is also critical for prolonging the release profile of bioactive agents, thereby maximizing their biological effects. In this study, we adopted a novel composite SMC-PHBHHx (20 : 80) that incorporates biocompatible siliceous mesostructured cellular foams (SMC) [22] into high-toughness and easily moldable poly(3-hydroxybutyrate-co-3-hydroxyhexanoate) (PHBHHx) [23] using a solvent casting and salt-leaching method [24]. The highly porous and well-interconnected structure conferred excellent physicochemical, biological, and drug-release properties on this novel composite scaffold.

Hitherto, it remains unclear whether icariin can promote the efficacy of allogeneic BMSCs-based tissue engineering technique in repairing large-volume bone defects. In this study, we first selected the best concentration of icariin by assessing its effect on promoting the proliferation and early differentiation of allogenic BMSCs. Thereafter, we evaluated the promoting effect of icariin on the osteogenesis- and angiogenesis-related genes and proteins. Finally, we evaluated the efficacy of slowly delivered icariin from the novel SMC-PHBHHx scaffold to treat in vivo calvarial critical-size bone defects in rats through radiographic and histomorphometric analysis. We hypothesized that the slowly released icariin could significantly promote the efficacy of SMC-PHBHHx/allogeneic BMSCs for repairing critical-size bone defects.

2. Materials and Methods

2.1. In Vitro Cellular Evaluation

2.1.1. Culture of BMSCs. BMSCs in passage 1 were purchased from ATCC and cultured with DMEM (Dulbecco's Modified Eagle Medium, Cyagen, Guangzhou, China) supplemented with 10% fetal bovine serum (FBS), 100 U/mL penicillin, and 100 mg/mL streptomycin at 37°C under the atmosphere of 5% CO_2 and 100% relative humidity. The passage was carried out when the cells were confluent to 80%. The cells of passage 4 were used in the following studies.

2.1.2. Multiple Differentiation. To identify the multipotency, the allogeneic BMSCs were induced to osteogenic, chondrogenic, and adipogenic differentiation using osteogenic medium, adipogenic medium, and chondrogenic medium (Cyagen, Guangzhou, China), respectively. The medium was replaced every 3 days. The osteogenic, chondrogenic, and adipogenic differentiation were examined at 14 days, 21 days, and 22 days, respectively. The staining was done using an alizarin red staining solution and oil red staining solution (Cyagen, Guangzhou, China) to check osteogenesis and adipogenesis, respectively. In order to check chondrogenesis, the chondrogenic cell pellets were fixed, embedded in paraffin, sectioned, and stained with alcian blue staining solution (Cyagen, Guangzhou, China) to detect the glycosaminoglycans. The images of various differentiations were captured using light microscope (Eclipse Ti-U, Nikon, Tokyo, Japan).

2.1.3. Concentration Selection Test. To identify the optimal concentration of icariin, cell proliferation assay and alkaline phosphatase (ALP) activities were performed with a time-course and dose-dependent setup. Cell proliferation was assessed using the cell counting kit-8 (CCK-8) (Yeasen, Shanghai, China). 2000 BMSCs per well were seeded in 96-well plates. After refreshing the medium 24 h after seeding, 100 μL of culture medium with different concentrations (0, 10^{-9}, 10^{-8}, 10^{-7}, 10^{-6}, 10^{-5}, and 10^{-4} Mol/L) of icariin (Tauto Biotech, Shanghai, China) was added to each well. Six wells per group were measured. The treatment medium was refreshed every 3 days. After 1-, 3-, 5-, and 7-day incubation, the treatment medium was replaced with 100 μL CCK-8 working solution according to the manufacture's instruction. After a 40 min incubation, the OD (optical density) values were measured at 450 nm. ALP activity and total protein content were measured after the treatment for 1 day, 3 days, 5 days, and 7 days. ALP activity was determined using LabAssay ALP

Table 1: Primer sequences for real-time quantitative polymerase chain reaction analysis of the expression of osteogenic genes (Runx2, alkaline phosphatase (ALP), and osteocalcin (OCN)) and angiogenic genes (vascular endothelial growth factor (VEGF) and fibroblast growth factors (FGF)).

Gene	Primers (F = forward; R = reverse)
ALP	F: 5′-GTC CCA CAA GAG CCC ACA AT-3′; R: 5′-CAA CGG CAG AGC CAG GAA T-3′
OCN	F: 5′-CAG TAA GGT GGT GAA TAG ACT CCG-3′; R: 5′-GGT GCC ATA GAT GCG CTT G-3′
Runx2	F: 5′-TCT TCC CAA AGC CAG AGC G-3′; R: 5′-TGC CAT TCG AGG TGG TCG-3′
VEGF	F: 5′-CTT GAG TTG GGA GGA GGA TG-3′; R: 5′-TGG CAG GCA AAC AGA CTT C-3′
FGF	F: 5′-CTC TGT CTC CCG CAC CCT AT-3′; R: 5′-CCT TCC ACC CAA AGC AGT AG-3′
GAPDH	F: 5′-GGC AAG TTC AAC GGC ACA GT-3′; R: 5′-GCC AGT AGA CTC CAC GAC AT-3′

colorimetric assay kit (Wako Pure Chemicals, Osaka, Japan). The total protein content was measured at 570 nm using a commercial BCA Protein Assay kit (Beyotime, Shanghai, China) to normalize the ALP activity.

2.1.4. The Expression of Osteogenesis and Angiogenesis-Related Genes and Proteins. To identify the effect of icariin on osteogenesis-related genes and proteins, BMSCs were cultured in an osteogenic medium as described above. For the angiogenesis-related genes and proteins, BMSCs were cultured in full culture medium without extra inductive agents. The effects of icariin on stimulating the expression of osteogenic and angiogenic genes were examined by quantitative RT-PCR 3 days, 5 days, 7 days, and 14 days after treatment. Total RNA was extracted from the cells using a Trizol Kit (Invitrogen, USA). The cDNA was synthesized from total RNA with a Primescrip™ RT Reagent Kit (Takara Biotechnology, Dalian, China). Real-time polymerase chain reaction (PCR) was performed using 1 μL of cDNA product in a 25 μL reaction volume with Mastercycler® ep realplex Real-Time PCR System (Eppendorf, Germany). In each PCR reaction, SYBR® Premix Ex Taq™ II (Takara Biotechnology), specific primers (Table 1), and 1 μL of cDNA were used according to the manufacturer's instructions. GAPDH was used as housekeeping gene. We calculated the folds of upregulation for each gene of interest using the following formula:

$$2^{-[(\text{CT gene of interest} - \text{CT internal control}) \text{ sample} - (\text{CT gene of interest} - \text{CT internal control}) \text{ control}]}. \quad (1)$$

Western blot analysis was used to assess the expression level of osteogenesis- and angiogenesis-related proteins such as ALP, osteocalcin (OCN), runt-related transcription factor 2 (Runx2), vascular endothelial growth factor (VEGF), and fibroblast growth factors (FGF). After 3 days, 5 days, 7 days, and 14 days, cells lysis was made using M-PER Mammalian Protein Extraction Reagent (ThermoFisher, USA) with a protease and phosphatase inhibitor cocktail (Sigma, USA). Anti-rat primary antibodies were used to detect osteogenesis- and angiogenesis-related proteins ALP, OCN, Runx2, FGF, and VEGF. Horseradish peroxidase-labeled secondary antibodies were then used to label detect the primary antibodies. Images were acquired using darkroom development techniques for chemiluminescence. Image-Pro Plus 6.0 software was adopted to analyze the Integral Optical Density (IOD).

2.1.5. Cell Matrix Mineralization. The effect of 10^{-6} mol/L icariin on the matrix mineralization of BMSCs was examined in osteogenic medium as described in Multilineage Differentiation of Allogeneic BMSCs with DMSO as control. After 14- and 21-day treatments, mineralized nodules were determined by alizarin red staining. Culture plates were photographed using NISElementsF2.20 (Eclipse 80i, Nikon, Tokyo, Japan), and the calcified area was quantified using Image-Pro Plus 6.0 software.

2.2. In Vivo Study

2.2.1. Preparation of SMC-PHBHHx Composite. The SMC-PHBHHx composite was fabricated as previously reported [24]. Briefly, to prepare SMC, 1.6 M HCl solution containing 0.53 mM Pluronic P123 (BASF, Frankfurt, Germany) and 0.23 M 1,3,5-triethylbenzene was stirred and kept in 40°C for 60 minutes. Thereafter, tetraethyl orthosilicate was added to reach the final concentration of 0.28 M and reacted for 20 hours at 40°C. The mixture was then subjected to an autoclave at 100°C for 24 hours under static conditions. After cooling at room temperature, the white precipitate was collected, dried, and calcined at 550°C for 6 hours to produce the SMC materials. To prepare SMC/PHBHHx composite, SMC was added to the chloroform containing PHBHHx (20 wt%) to a final concentration of 5 wt% with stirring for 24 hours. After adding NaCl particles with diameters ranging from 300 to 500 μm, the mixture was cast into cylindrical PTFE molds. The samples were then air-dried under flowing air for 24 hours and subsequently vacuum-dried at 40°C for 48 hours. The NaCl particles were then removed by immersing in deionized water for 72 hours with the water replaced every 6 hours. Thereafter, the samples were air-dried for 24 hours and vacuum-dried overnight to obtain the sponge-like scaffolds.

2.2.2. Preparing the Constructs of Icariin/SMC-PHBHHx/Allogeneic BMSCs. To prepare icariin/SMC-PHBHHx composite, we adopted SMC-PHBHHx (20 : 80) discs (5 mm in diameter and 1.5 mm in thickness) and 10^{-6} mol/L icariin suspension in DMEM. 200 μL of either icariin-containing or non-icariin-containing suspension was then adsorbed onto each SMC-PHBHHx disc with a mild shaking for 72 hours.

The icariin/SMC-PHBHHx discs were then freeze-dried under sterile condition for 48 hours. The discs were thereafter stored in 4°C for later use. Allogeneic BMSCs were seeded onto either icariin-containing or non-icariin-containing SMC-PHBHHx discs with a mild shaking for 72 hours at 37°C under 5% CO_2 before implantation.

2.2.3. Characterization of Icariin/SMC-PHBHHx Constructs

(1) Scanning Electronic Microscope. Scanning electron microscope (Phenom™ Pro, Eindhoven, The Netherlands) was adopted to reveal the influence of icariin adsorption on the surface morphologies of SMC-PHBHHx composite and BMSCs. For this purpose, either icariin-containing or non-icariin-containing SMC-PHBHHx discs with or without allogeneic BMSCs were mounted on aluminium stubs and sputtered with gold particles.

(2) Release Kinetics of BSA In Vitro. The release kinetics of icariin was monitored over a 15-day period in vitro using a high-performance liquid chromatography (BAS PM-80, West Lafayette, IN). Each sample ($n = 6$) was introduced into a 1.5 mL Eppendorf tube containing 1 mL of DMEM. The tubes were incubated for up to 14 days in a shaking water bath (60 agitations/minute), which was maintained at 37°C. Triplicate 200 μL aliquots of the medium (containing released FITC-BSA) were withdrawn for analysis after 12 hours, 1 day, 2 days, 3 days, 4 days, 5 days, 6 days, 8 days, 10 days, 12 days, and 14 days. The temporal release of icariin was expressed as a percentage of the total amount of adsorbed icariin.

2.2.4. Surgery. The calvarial critical-size bone defects in rats were established as previously described [25]. Briefly, 6 male Sprague-Dawley rats (5-week-old and weighing 180–220 g) were randomly assigned into 2 groups: either icariin-containing or non-icariin-containing SMC-PHBHHx/allogeneic BMSCs constructs. The animal care was performed in accordance with the guidelines of the Ethical Committee of Shanghai East Hospital Affiliated with Tongji University, Shanghai, China. All animal experiments were carried out according to the ethic laws and regulations of China. Critical-sized cranial defects (5 mm in diameter) were created in these rats. Briefly, the rats were anaesthetized with an intraperitoneal injection of pentobarbital (Nembutal 3.5 mg/100 g). A subcutaneous injection of 0.5 mL of 1% lidocaine as a local anesthetic was given along the sagittal midline of the skull. A sagittal incision was made over the scalp from the nasal bone to the middle sagittal crest and the periosteum was dissected. The 5 mm defects were created using a dental surgical drill with a trephine with a constant cooling rinse. Subsequently, the calvarial disk was carefully removed to avoid tearing the dura. After rinsing with physiological saline to wash out any bone fragments, samples from various groups were implanted randomly into these defects. Afterwards, the periosteum and the scalp were closed in layers with interrupted 4-0 Vicryl resorbable sutures.

2.2.5. Radiographic Evaluation. Eight weeks after operation, the rats were sacrificed by intramuscular injection of overdose of Sumianxin II. All the 6 calvarial blocks of the sacrificed animals were harvested and immediately immersed into the 10% neutrally buffered formalin for fixation. Radiographic analysis of bone regeneration within the defects was performed using an X-ray unit (Vario^{DG}, Sirona), with the exposure time set at 0.03 seconds. After a 2-day fixation, the specimens were scanned along the sagittal direction though by micro-CT (Inveon, Siemens) with a resolution of 18 μm followed by an off-line reconstruction. After scanning, the selection of the area of interest was performed manually. Our preliminary study showed that the grey value of SMC-PHBHHx material was around −217, which was lower than water. The thresholding of mineralized bone was set at 500.

The following morphometric parameters obtained in direct mode were adopted to estimate the bone regeneration within the defects using software Siemens Inveon:

(1) Relative bone volume (bone volume/tissue volume, BV/TV: %)

(2) Trabecular number (Tb.N: 1/mm)

(3) Trabecular separation (Tb.Sp: mm)

(4) Trabecular thickness (Tb.Th: mm).

2.2.6. Histomorphometric Analysis. The samples were then decalcified in 4.18% EDTA + 0.8% formalin at pH 7.2 for four weeks at 4°C, rinsed with phosphate buffer, and embedded in paraffin. Serial 6 μm thickness sections were stained with hematoxylin-eosin (HE). The numbers of blood vessels were evaluated under light microscopy. The final magnification was ×50.

2.3. Statistical Analysis. We first used both Kolmogorov-Smirnov test and D'Agostino and Pearson omnibus normality test to comprehensively check the normality of the data of each group. According to the results, we selected either parametric tests or nonparametric tests to analyze the data. The data in concentration selection test were statically analyzed using two-way ANOVA. For the other data, we used either unpaired t-test or Man–Whitney test to compare the effect of icariin with the corresponding control (no icariin). The level of significance was set at $p < 0.05$. SPSS software (version 20) for a Windows computer system was employed for the statistical analysis.

3. Results

3.1. Multilineage Differentiation of Allogeneic BMSCs. Multilineage differentiation assay showed that the allogeneic BMSCs could differentiate into osteogenesis, chondrogenesis, and adipogenesis (Figure 1). For the osteogenic differentiation, the mineralized nodules in cell matrix—the final osteogenic differentiation marker—were stained red (indicated by black arrows in Figure 1(a)). The chondrogenic differentiation was approved by the abundant presence of glycosaminoglycans that were a typical chondrogenic differentiation marker and were stained blue in the cell pellet by alcian blue (indicated by black arrows in Figure 1(b)). The adipogenic differentiation was characterized by the oil droplets within the cells that were stained red (indicated by black arrows in Figure 1(c)).

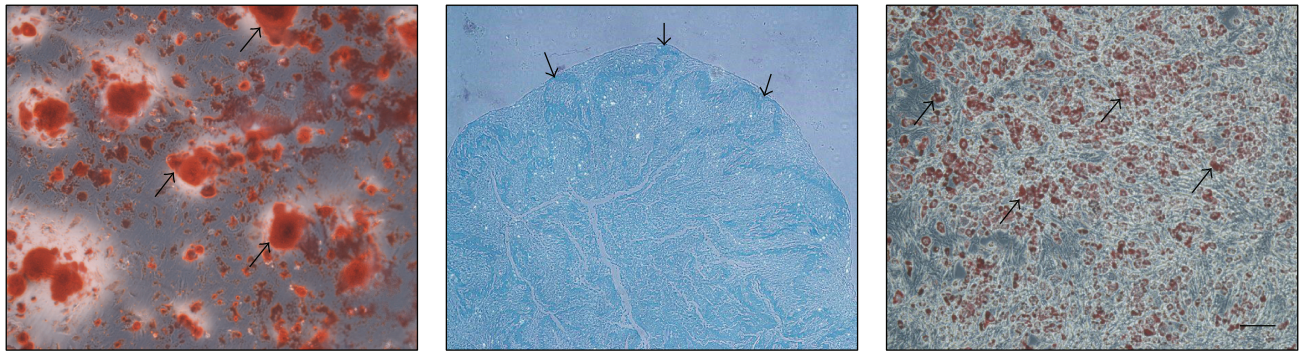

(a) (b) (c)

Figure 1: Light micrographs depicting the (a) osteogenic, (b) chondrogenic, and (c) adipogenic differentiation of multipotent BMSCs. The black arrows indicated the red-stained mineralized nodules in (a), blue-stained chondrogenic cell pellet in (b), and red-stained lipid droplets in cells in (c). Bar = 100 μm.

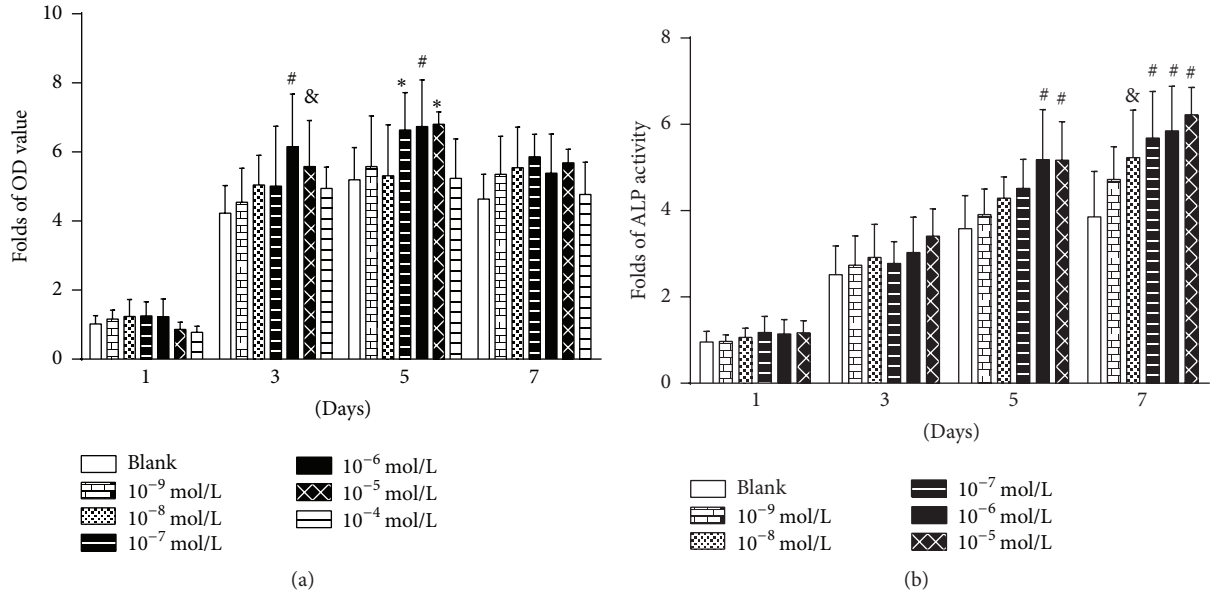

Figure 2: Time-course and dose-dependent tests to select the optimal concentration of icariin for inducing the osteogenic differentiation of BMSCs. Icariin of 0, 10^{-9}, 10^{-8}, 10^{-7}, 10^{-6}, 10^{-5}, or 10^{-4} mol/L was used to treat preosteoblasts for 1 day, 3 days, 5 days, and 7 days. (a) Cell proliferation assays; (b) alkaline phosphatase (ALP) activity assays. All data are presented as mean values together with the standard deviation (SD). $^{*}p < 0.05$; $^{\&}p < 0.01$; $^{\#}p < 0.001$ indicating the statistical difference between the indicated group and the control group (blank) at the same time point.

3.2. Concentration Selection through Cell Proliferation and ALP Activity Assays. Icariin at only 10^{-5} mol/L and 10^{-6} mol/L resulted in significantly higher OD value (indicator for cell proliferation) than the blank control after a 3-day treatment. On the 5th day, icariin at 10^{-5} mol/L, 10^{-6} mol/L, and 10^{-7} mol/L was associated with significantly higher OD value than the blank control. The average OD value under the induction of 10^{-6} mol/L icariin was the highest on all the selected time points (Figure 2(a)). Icariin at 10^{-5} mol/L and 10^{-6} mol/L resulted in a significantly higher ALP activity than the control after a 5-day treatment. Icariin ranging from 10^{-8} mol/L to 10^{-4} mol/L was associated with significantly higher OD value than the blank control on the 7th day. The value of ALP activity induced by 10^{-6} mol/L was the highest and second highest on the 5th day and 7th day, respectively (Figure 2(b)). Consequently, we selected 10^{-6} mol/L as the optimal concentration for icariin in the following tests.

3.3. Expression of Osteogenesis- and Angiogenesis-Related Genes. In comparison with the control (no icariin), 10^{-6} mol/L icariin could induce significantly higher expression of osteogenesis-related genes, such as Runx2 mRNA (at 3 days, 7 days, and 14 days) (Figure 3(a)), ALP mRNA (at 7 days and 14 days) (Figure 3(b)), and OCN mRNA (at 14 days) (Figure 3(c)), as well as angiogenesis-related genes,

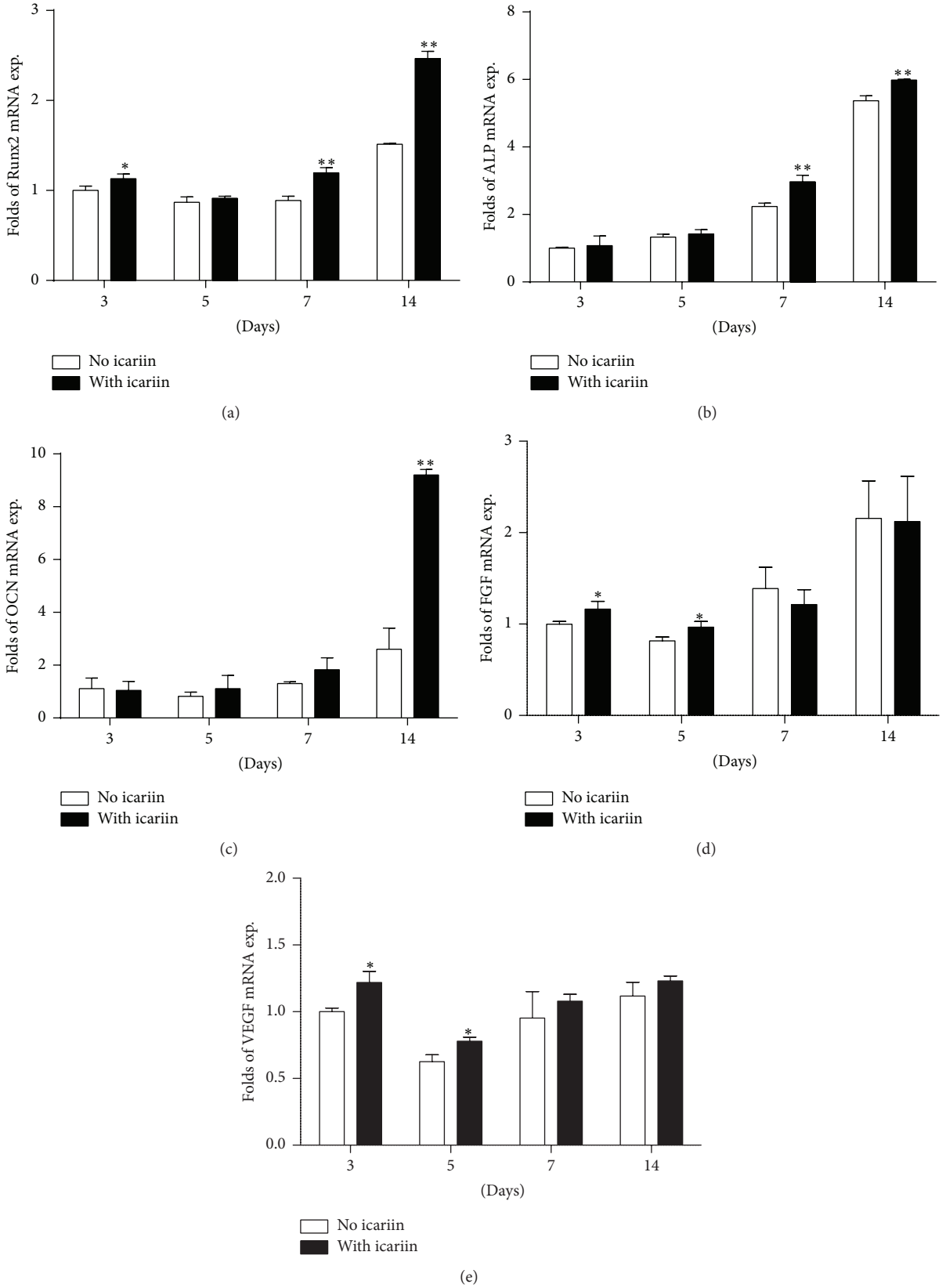

Figure 3: Graphs depicting the fold changes of the expression of osteogenesis-related and angiogenesis-related mRNA in BMSCs under the stimulation of icariin for 3 days, 5 days, 7 days, and 14 days. (a) Runx2, (b) alkaline phosphatase (ALP), (c) osteocalcin (OCN), (d) fibroblast growth factors (FGF), and (e) vascular endothelial growth factor (VEGF). All data are presented as mean values together with the standard deviation (SD). $^{*}p < 0.05$; $^{**}p < 0.01$ indicating the statistical difference between the experimental group (with icariin) and the control group (no icariin) at the same time point.

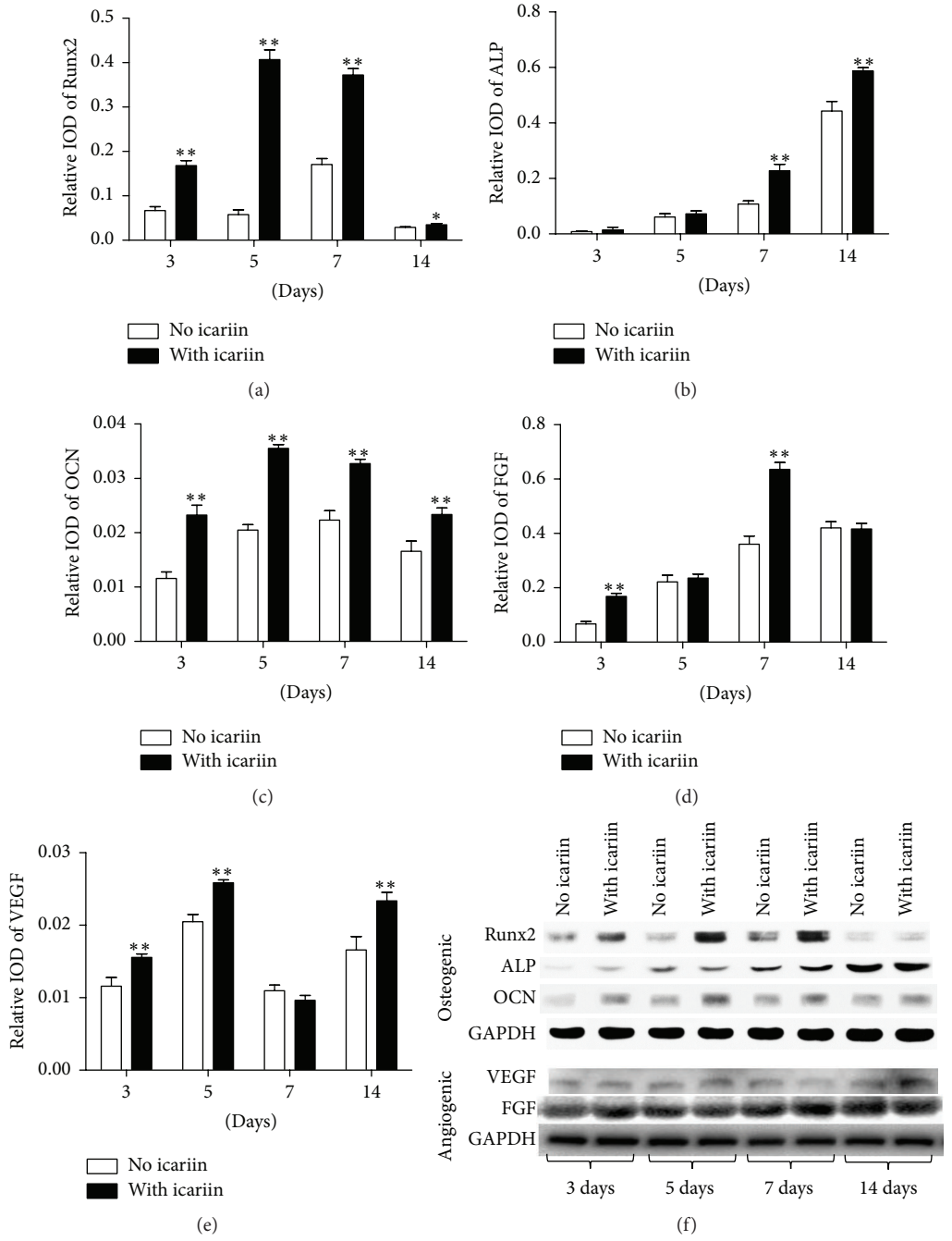

Figure 4: Graphs depicting the fold changes of the expression of osteogenesis-related and angiogenesis-related proteins in BMSCs under the stimulation of 10^{-6} mol/L icariin for 3 days, 5 days, 7 days, and 14 days. (a) Runx2, (b) alkaline phosphatase (ALP), (c) osteocalcin (OCN), (d) fibroblast growth factors (FGF), (e) vascular endothelial growth factor (VEGF), and (f) photographs of western blot analysis from a representative experiment. All data are presented as mean values together with the standard deviation (SD). $^{*}p < 0.05$; $^{**}p < 0.01$ indicating the statistical difference between the experimental group (with icariin) and the control group (no icariin) at the same time point.

such as FGF mRNA (at 3 days and 5 days) (Figure 3(d)) and VEGF mRNA (at 3 days and 5 days) (Figure 3(e)), than the corresponding no-icariin treatments.

3.4. Expression of Osteogenesis- and Angiogenesis-Related Proteins. Western blot analysis showed that 10^{-6} mol/L icariin could induce significantly higher expression of osteogenesis-related proteins, such as Runx2 (at all the time points) (Figure 4(a)), ALP (at 7 days and 14 days) (Figure 4(b)), and OCN (at all the time points) (Figure 4(c)), as well as angiogenesis-related genes, such as FGF (at 3 days, 5 days, and 14 days) (Figure 4(d)) and VEGF (at 3 days and 7 days) (Figure 4(e)), than the corresponding no-icariin treatments.

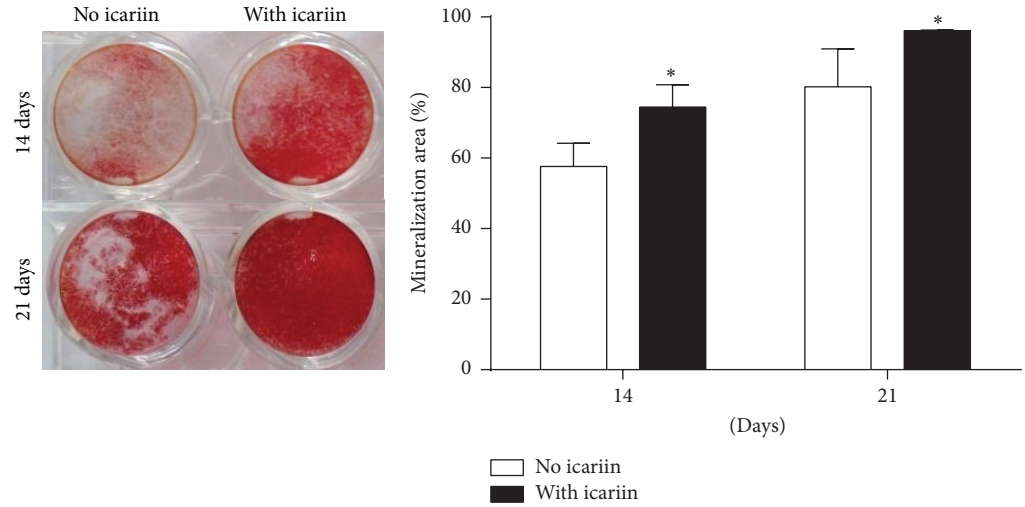

Figure 5: Mineralization assay of BMSCs with or without the stimulation of 10^{-6} mol/L icariin for 14 days and 21 days. All data are presented as mean values together with the standard deviation (SD). $^{*}p < 0.05$ indicating the statistical difference between the experimental group (with icariin) and the control group (no icariin) at the same time point.

3.5. In Vitro Mineralization of Allogeneic BMSCs Induced by Icariin. The mineralization area in the group either with or without 10^{-6} mol/L icariin increased with time. On both the 14th day and the 21st day, 10^{-6} mol/L icariin resulted in significantly higher mineralization area than the control (no icariin) (Figure 5).

3.6. SEM Characterization of Icariin Adsorption and Cell Adhesion. The SMC-PHBHHx composite scaffolds showed an interconnected porous structure (Figures 6(a) and 6(b)). The adsorption of icariin onto the scaffolds did not significantly change the structure and topography of the scaffold (Figures 6(c) and 6(d)). Qualitative observation showed that more BMSCs could be found on icariin-containing SMC-PHBHHx composite scaffolds than on non-icariin-containing ones (Figures 6(c) and 6(f)).

3.7. Release Kinetics of Icariin. The release kinetics of the adsorbed icariin from the SMC-PHBHHx composite followed a biphasic course: an initial (5 days) rapid phase and a subsequent slower phase (Figure 7). The adsorbed icariin showed a slow release profile with nearly 10% per day within the first 5 days. During the subsequent slower phase (days 5–14), the adsorbed icariin was released 2.2% per day with 70% depleted by the end of 14 days.

3.8. Micro-CT Analysis and Histological Observation of Newly Formed Bone Tissue. Micro-CT analysis showed that the constructs with icariin resulted in significantly higher BV/TV (Figure 8(a)), Tb.Th (Figure 8(b)), and Tb.N (Figure 8(c)) and significantly lower Tb.Sp (Figure 8(d)) than the constructs with no icariin. Histological observations showed significantly less new bone formation within the defects treated with SMC-PHBHHx/allogeneic BMSCs with no icariin (Figure 9(a)) than that with icariin (Figure 9(b)).

3.9. Histomorphometric Analysis of Blood Vessels. Histomorphometric analysis indicated that the numbers of blood vessels within the defects treated with SMC-PHBHHx with icariin were significantly higher than those within the defects treated with SMC-PHBHHx without icariin (Figure 9(c)).

4. Discussion

Critical-size bone defects, a standard experimental model for large-volume bone defects, are commonly used to evaluate the treatment efficacy of novel biomaterials. The lack of osteogenic cells, osteoinductive growth factors, and osteoconductive scaffolds always leads to a nonosseous repair in a critical-size bone defect. Bone tissue engineering is a technique to integrate various knowledge in osteogenic stem cells, osteoconductive scaffolds, and osteoinductive growth factors with an aim of significantly accelerating and promoting bone regeneration. In this study, we, for the first time, showed that the slowly released icariin could significantly promote the efficacy of SMC-PHBHHx/allogeneic BMSCs for repairing critical-size bone defects.

The selection of bioactive agents is critical for the effect of a tissue engineering technique. BMPs are still the most potent growth factors for bone tissue engineering. BMPs can bind their transmembrane serine/threonine kinase receptors [26] and trigger two main downstream signaling pathways: Smad-dependent and Smad-independent signaling pathways [27]. Activated BMP receptors phosphorylate Smad1/5/8, which assembles into a complex with Smad4 and translocates to the nucleus, regulating the transcription of target genes, such as Runx2 [26]. In addition to Smad-dependent signaling, a series of Smad-independent downstream signaling pathways, including MAPK pathways, such as p38, c-Jun N-terminal kinase (JNK), and extracellular signal-related kinase (ERK), are also activated [28]. Stimulating the expression of endogenous BMPs is the pathway to exert osteoinductive effects of many drugs, such as icariin [29]. Icariin could enhance the

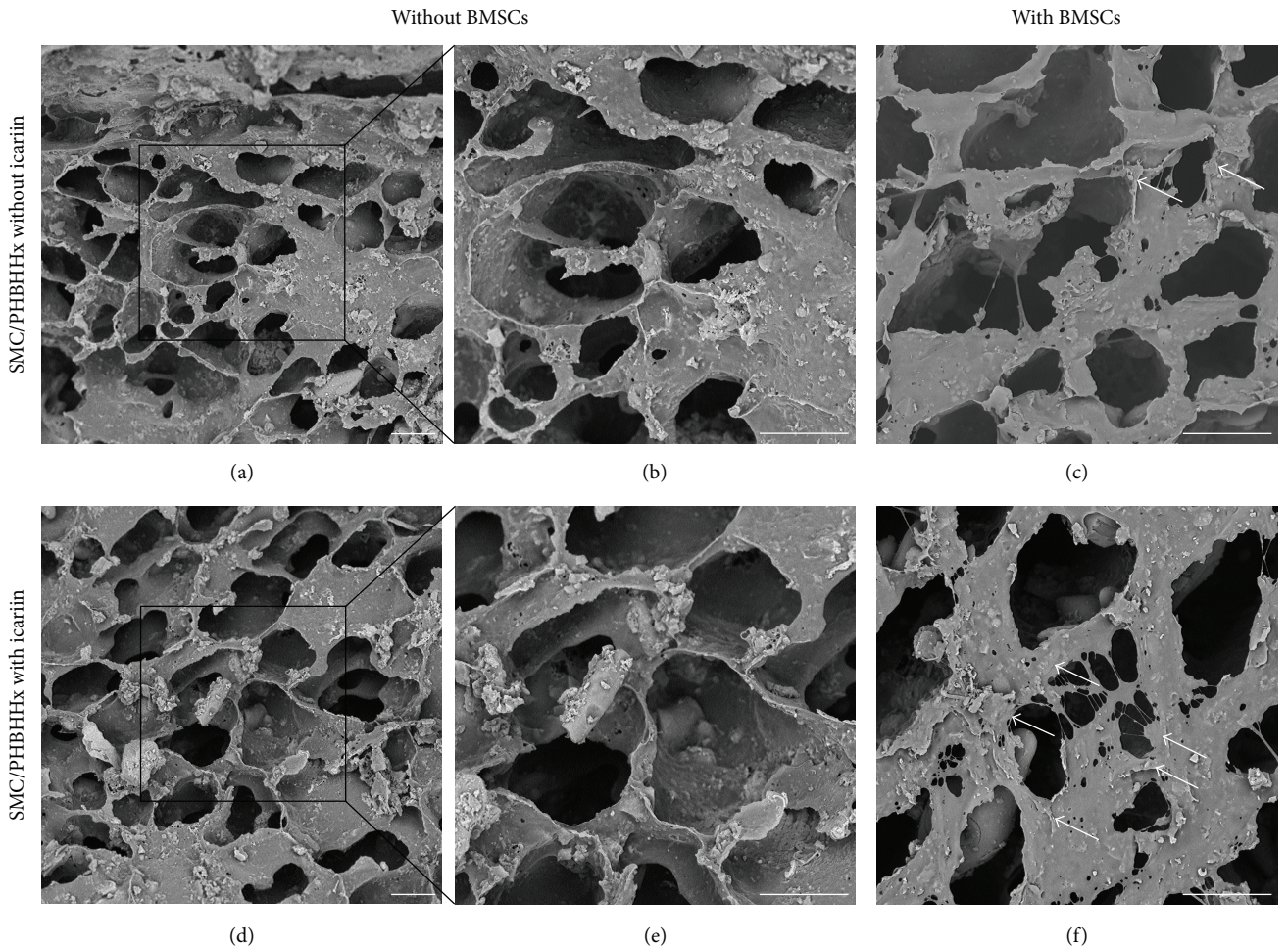

Figure 6: Scanning electron microscopy graphs depicting the morphology and topography of SMC-PHBHHx scaffolds without (a, b, d, e) or with (c, f) BMSCs in the absence (a, b, c) or presence (c, d, e) of 10^{-6} mol/L icariin. Bar = 30 μm.

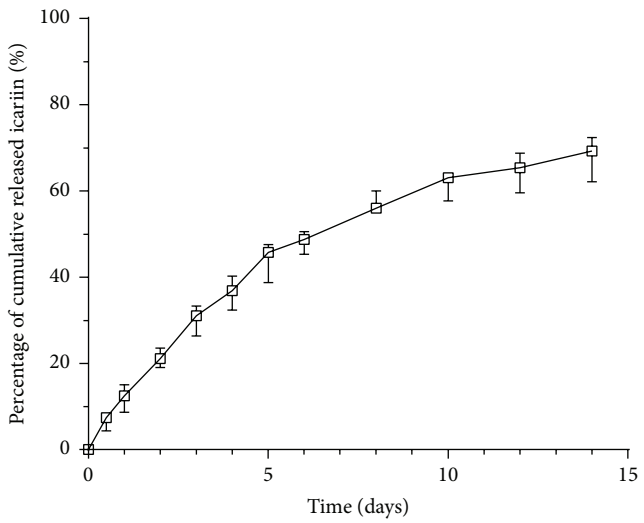

Figure 7: The in vitro release profile of icariin from a SMC-PHBHHx scaffold. All data are presented as mean values together with the standard deviation (SD).

expression of endogenous BMPs and subsequent osteogenic signaling pathways, such as Smad4, Runx2, and OPG [18, 29]. The induction of endogenous BMP-2 by icariin was, at least partially, mediated by the Wnt/β-Catenin-BMP signaling pathway [30]. Ohba et al. suggested two possible mechanisms for the involvement of BMP signaling in the effects of icariin [31]: (1) icariin indirectly activated BMP signaling through extracellular BMPs; (2) icariin directly activated BMP signaling by interacting with Smads via unknown mechanisms. The indispensability of endogenous BMPs for the effect of icariin was proved by the fact that noggin, an extracellular BMP antagonist, could diminish the icariin-induced enhancement of osteogenic differentiation (such as ALP, OCN, and mineralization) in osteogenic cells [18]. Consistently, the specific inhibitor for the Smad-independent ERK, JNK, and p38 MAPK signaling pathways could dramatically attenuate the promoting effect of icariin on the osteogenesis of BMSCs [32]. In addition to the BMP-associated signaling pathways, icariin could also stimulate the osteogenic differentiation of rat bone marrow stromal cells via activating the PI3K-AKT-eNOS-NO-cGMP-PKG [33]. More importantly, icariin

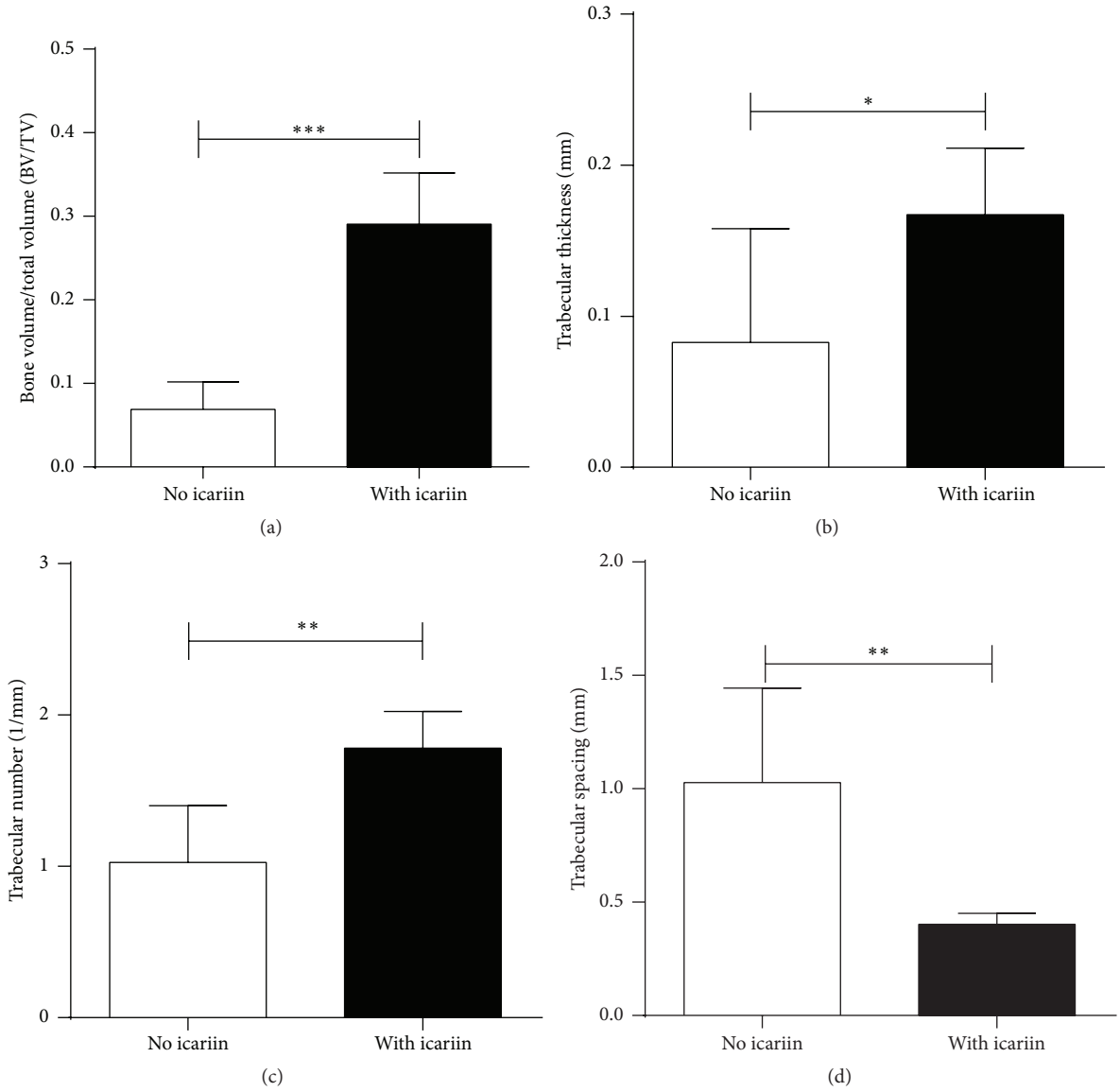

Figure 8: Graph depicting the micro-CT analysis of the BV/TV (a), Tb.N (b), Tb.Th (c), and Tb.Sp (d) of the newly formed bone within the calvarial critical-size bone defects that were treated with SMC-PHBHHx scaffolds/allogeneic BMSCs either without or with adsorbed icariin. All data are presented as mean values together with the standard deviation (SD). $^{*}p < 0.05$; $^{**}p < 0.01$; $^{***}p < 0.001$.

could induce the osteogenic differentiation of BMSCs in many pathological conditions, such as osteoporosis [34, 35] and osteonecrosis [36]. Interestingly, icariin could activate different molecular cascades on BMSCs in corticosterone and ovariectomy induced osteoporotic rats [35]. Estrogen and epigenetic modulation were the newly found targets of icariin for its beneficial effect on osteogenesis in pathological conditions [34, 36]. In addition to the promoting effect on osteoblastic differentiation, icariin could also suppress osteoclastic activity, which was different from BMPs. Icariin inhibited osteoclastic differentiation in both its coculture with osteoblasts and single culture [21]. This effect was, at least partially, mediated by icariin-induced increase of OPG/RANKL expression ratios [37]. Consequently, although the potency of icariin in inducing bone formation is less than that of BMP-2, icariin is advantageous in balancing the osteoblastic and osteoclastic activity. This is especially important for the patients with osteoporosis. All these properties confer a very promising clinical application potential on icariin.

Although most of the previous reports indicated the promoting effect of icariin on osteogenesis of BMSCs, whether icariin can promote the repairing efficacy of allogeneic BMSCs in vivo is, hitherto, not known. In this study, we hypothesized that the slowly released icariin could significantly promote the efficacy of SMC-PHBHHx composite and allogeneic BMSCs for repairing critical-size bone defects. We tried to answer this question in a step-forward way. Firstly, we

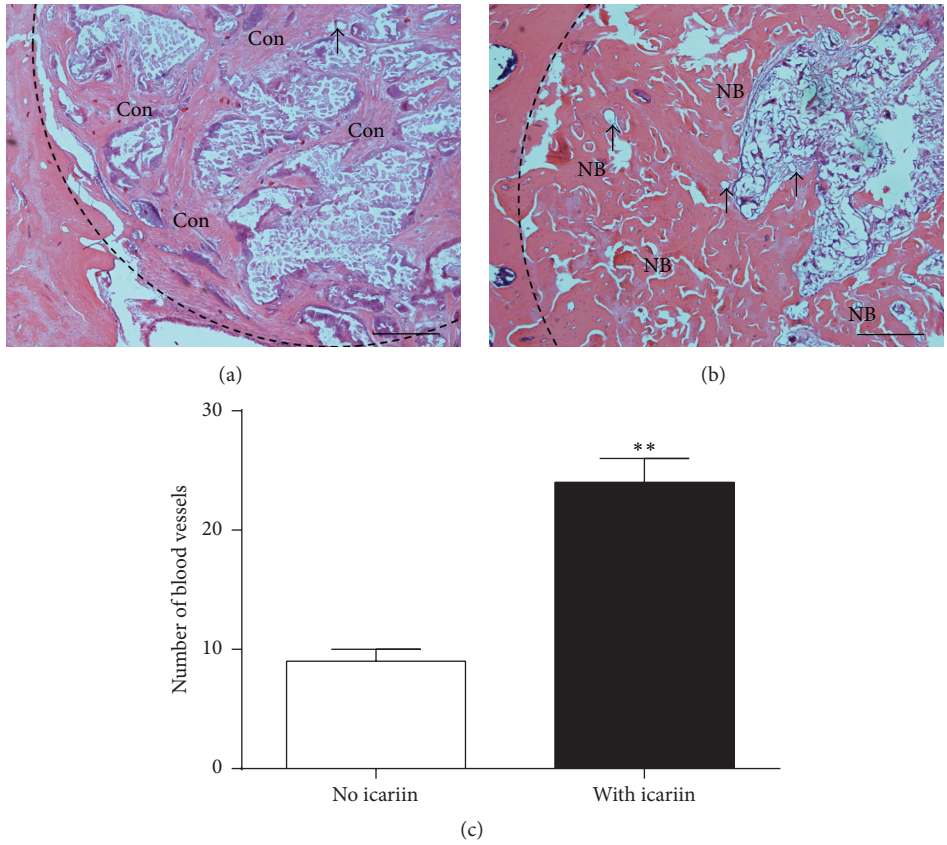

FIGURE 9: Light micrographs depicting the new bone formation within the calvarial critical-size bone defects that were treated with SMC-PHBHHx/allogeneic BMSCs either (a) without or (b) with icariin. Bar = 200 μm. Then all data are presented as mean values together with the standard deviation (SD). NB: new bone; Con: connective tissue; black arrow: blood vessels. (c) Graph depicting the number of vessels per section. All data are presented as mean values together with the standard deviation (SD). $^{**}p < 0.01$.

showed the multipotency (Figure 1) of the purchased BMSCs using well-established assays. Thereafter, we determined the optimal concentration of icariin at 10^{-6} mol/L in the time-course and dose-dependent proliferation assays (Figure 2(a)) and ALP assays (Figure 2(b)). The following RT-PCR and western blot analyses corroborated that icariin was associated with either equivalent or significantly higher level of osteogenesis-related genes and proteins, such as Runx2, ALP, and OCN (Figures 3 and 4) during the monitoring span (3–14 days). Interestingly, the icariin-induced upregulation magnitude of Runx2 and OCN proteins was much more significant than their genes on the 3rd, 5th, and 7th day, while the upregulation fold of OCN protein was much lower than OCN gene. These phenomena suggested a posttranscriptional modulation might also be involved in icariin-related effects. In the mineralization assay, we showed that 10^{-6} mol/L icariin could significantly promote the calcium nodule formation on both 14th day and 21st day (Figure 5).

A suitable scaffold is indispensable for the application of allogeneic BMSCs. In previous studies, SMC-PHBHHx composite materials showed good biocompatibility, proper stiffness, and, more importantly, the ability to carry and control release of bioactive agents [24]. Moreover, the radiolucency of this material is highly suitable for radiographic examination of new bone formation in clinic. In this study, we tried to functionalize SMC-PHBHHx with icariin in order to achieve enhanced efficacy in bone regeneration. Our data showed that the adsorbed icariin did not significantly influence the morphology of SMC-PHBHHx scaffold (Figures 6(a), 6(b), 6(d), and 6(e)). The adsorbed icariin showed a controlled slow release profile with 30% left by the end of 14 days in the in vitro condition (Figure 7). Moreover, qualitative scanning electron microscope observation showed that more BMSCs could be found on icariin-containing SMC-PHBHHx composite scaffolds than on non-icariin-containing ones (Figures 6(c) and 6(f)). These results indicated the feasibility to construct icariin/SMC-PHBHHx/allogeneic BMSCs constructs for bone tissue engineering.

Subsequently, we tested the effect of icariin on the efficacy of SMC-PHBHHx/allogeneic BMSCs in a calvarial critical-size bone defect. Eight weeks after implantation, micro-CT evaluation showed that the BV/TV, Tb.Th, and Tb.N of the new bone regenerated in the SMC-PHBHHx/allogeneic BMSCs with icariin were 4.2 times, 1.8 times, and 2.0 times higher than those in the SMC-PHBHHx/allogeneic BMSCs without icariin, respectively (Figures 8(a), 8(b), and 8(c)). The

presence of icariin was also associated with a significantly lower Tb.Sp (Figure 8(d)). Consistent with the radiographic analysis, histological observation also indicated the significantly promoting effect of icariin on bone regeneration (Figures 9(a) and 9(b)). These results clearly indicated that the slowly delivered icariin could promote bone regeneration of SMC-PHBHHx/allogeneic BMSCs in critical-size bone defects.

In addition to the direct promoting effect, icariin may also benefit bone regeneration through enhancing angiogenesis. Vascularization is a crucial step in bone regeneration, which brings mesenchymal stem cells and nutrition to wounds [38]. Icariin could promote not only in vitro endothelial tubulogenesis assay but also in vivo angiogenesis [39], possibly through activating EGF-EGFR pathway and thereafter endothelial NO synthase [40]. Moreover, icariin could directly stimulate angiogenesis through activating a series of angiogenic signals, such as ERK, PI3K, and Akt [41]. In our in vitro cellular experiments, icariin could significantly promote the angiogenesis-related genes and proteins, such as VEGF and FGF (Figures 3 and 4). Accordingly, our histomorphometric analysis indicated that the slowly released icariin resulted in significantly higher number of blood vessels (Figure 9(c)).

This study bears also some limitations, such as the limited group setup in the animal studies and no in vivo tracking of allogeneic BMSCs. Consequently, the contribution of allogeneic and autologous BMSCs could not be precisely determined. However, our findings clearly showed that the slowly delivered icariin could promote the efficacy of SMC-PHBHHx/allogeneic BMSCs for healing the critical-bone defects in rats. Such an effect may be mediated by icariin-induced upregulation of osteogenesis and angiogenesis. With the indication of the current study, we are trying to further explore these factors.

Competing Interests

The authors declare that there is no conflict of interests regarding the publication of this paper.

Acknowledgments

This work was supported by the grants from Shanghai Science and Technology Committee (14411963500), Shanghai East Hospital (DFZY-9), and National Natural Science Foundation of China (Grants nos. 81400475 and 81470724). The authors sincerely thank Professor Hailiang Ge for providing the lab facility. They also thank Professor Changsheng Liu and Professor Jing Wang for providing the SMC-PHBHHx material.

References

[1] J. S. Carson and M. P. G. Bostrom, "Synthetic bone scaffolds and fracture repair," *Injury*, vol. 38, no. 1, pp. S33–S37, 2007.

[2] J. D. Haman, R. N. Scripa, J. M. Rigsbee, and L. C. Lucas, "Production of thin calcium phosphate coatings from glass source materials," *Journal of Materials Science: Materials in Medicine*, vol. 13, no. 2, pp. 175–184, 2002.

[3] N. Saito and K. Takaoka, "New synthetic biodegradable polymers as BMP carriers for bone tissue engineering," *Biomaterials*, vol. 24, no. 13, pp. 2287–2293, 2003.

[4] S. S. Tseng, M. A. Lee, and A. H. Reddi, "Nonunions and the potential of stem cells in fracture-healing," *The Journal of Bone & Joint Surgery—American Volume*, vol. 90, supplement 1, pp. 92–98, 2008.

[5] A. H. Undale, J. J. Westendorf, M. J. Yaszemski, and S. Khosla, "Mesenchymal stem cells for bone repair and metabolic bone diseases," *Mayo Clinic Proceedings*, vol. 84, no. 10, pp. 893–902, 2009.

[6] S. Huang, L. Xu, Y. Zhang, Y. Sun, and G. Li, "Systemic and local administration of allogeneic bone marrow-derived mesenchymal stem cells promotes fracture healing in rats," *Cell Transplantation*, vol. 24, no. 12, pp. 2643–2655, 2015.

[7] A. Berner, J. C. Reichert, M. A. Woodruff et al., "Autologous vs. allogenic mesenchymal progenitor cells for the reconstruction of critical sized segmental tibial bone defects in aged sheep," *Acta Biomaterialia*, vol. 9, no. 8, pp. 7874–7884, 2013.

[8] L. Watson, S. J. Elliman, and C. M. Coleman, "From isolation to implantation: a concise review of mesenchymal stem cell therapy in bone fracture repair," *Stem Cell Research & Therapy*, vol. 5, article 51, 2014.

[9] M. R. Urist and B. S. Strates, "Bone morphogenetic protein," *Journal of Dental Research*, vol. 50, no. 6, pp. 1392–1406, 1971.

[10] D. Chen, M. Zhao, and G. R. Mundy, "Bone morphogenetic proteins," *Growth Factors*, vol. 22, no. 4, pp. 233–241, 2004.

[11] H. Cheng, W. Jiang, F. M. Phillips et al., "Osteogenic activity of the fourteen types of human bone morphogenetic proteins (BMPs)," *The Journal of Bone & Joint Surgery*, vol. 85-A, no. 8, pp. 1544–1552, 2003.

[12] S. D. Boden, J. Kang, H. Sandhu, and J. G. Heller, "Use of recombinant human bone morphogenetic protein-2 to achieve posterolateral lumbar spine fusion in humans: a prospective, randomized clinical pilot trial 2002 volvo award in clinical studies," *Spine*, vol. 27, no. 23, pp. 2662–2673, 2002.

[13] S. Govender, C. Csimma, H. K. Genant et al., "Recombinant human bone morphogenetic protein-2 for treatment of open tibial fractures a prospective, controlled, randomized study of four hundred and fifty patients," *The Journal of Bone & Joint Surgery—American Volume*, vol. 84, no. 12, pp. 2123–2134, 2002.

[14] J. M. Toth, S. D. Boden, J. K. Burkus, J. M. Badura, S. M. Peckham, and W. F. McKay, "Short-term osteoclastic activity induced by locally high concentrations of recombinant human bone morphogenetic protein-2 in a cancellous bone environment," *Spine*, vol. 34, no. 6, pp. 539–550, 2009.

[15] X. Zhang, T. Liu, Y. Huang, D. Wismeijer, and Y. Liu, "Icariin: does it have an osteoinductive potential for bone tissue engineering?" *Phytotherapy Research*, vol. 28, no. 4, pp. 498–509, 2014.

[16] H.-P. Ma, L.-G. Ming, B.-F. Ge et al., "Icariin is more potent than genistein in promoting osteoblast differentiation and mineralization in vitro," *Journal of Cellular Biochemistry*, vol. 112, no. 3, pp. 916–923, 2011.

[17] H. Cao, Y. Ke, Y. Zhang, C.-J. Zhang, W. Qian, and G.-L. Zhang, "Icariin stimulates MC3T3-E1 cell proliferation and differentiation through up-regulation of bone morphogenetic protein-2," *International Journal of Molecular Medicine*, vol. 29, no. 3, pp. 435–439, 2012.

[18] T.-P. Hsieh, S.-Y. Sheu, J.-S. Sun, M.-H. Chen, and M.-H. Liu, "Icariin isolated from *Epimedium pubescens* regulates osteoblasts anabolism through BMP-2, SMAD4, and Cbfa1 expression," *Phytomedicine*, vol. 17, no. 6, pp. 414–423, 2010.

[19] H. J. Seeherman, K. Azari, S. Bidic et al., "rhBMP-2 delivered in a calcium phosphate cement accelerates bridging of critical-sized defects in rabbit radii," *The Journal of Bone & Joint Surgery—American Volume*, vol. 88, no. 7, pp. 1553–1565, 2006.

[20] T.-P. Hsieh, S.-Y. Sheu, J.-S. Sun, and M.-H. Chen, "Icariin inhibits osteoclast differentiation and bone resorption by suppression of MAPKs/NF-κB regulated HIF-1α and PGE_2 synthesis," *Phytomedicine*, vol. 18, no. 2-3, pp. 176–185, 2011.

[21] J. Huang, L. Yuan, X. Wang, T.-L. Zhang, and K. Wang, "Icaritin and its glycosides enhance osteoblastic, but suppress osteoclastic, differentiation and activity in vitro," *Life Sciences*, vol. 81, no. 10, pp. 832–840, 2007.

[22] D. Arcos and M. Vallet-Regí, "Sol-gel silica-based biomaterials and bone tissue regeneration," *Acta Biomaterialia*, vol. 6, no. 8, pp. 2874–2888, 2010.

[23] H. Wang, Y. Li, Y. Zuo, J. Li, S. Ma, and L. Cheng, "Biocompatibility and osteogenesis of biomimetic nano-hydroxyapatite/polyamide composite scaffolds for bone tissue engineering," *Biomaterials*, vol. 28, no. 22, pp. 3338–3348, 2007.

[24] S. Yang, S. Xu, P. Zhou et al., "Siliceous mesostructured cellular foams/poly(3-hydroxybutyrate-co-3-hydroxyhexanoate) composite biomaterials for bone regeneration," *International Journal of Nanomedicine*, vol. 9, pp. 4795–4807, 2014.

[25] N. Mardas, A. Stavropoulos, and T. Karring, "Calvarial bone regeneration by a combination of natural anorganic bovine-derived hydroxyapatite matrix coupled with a synthetic cell-binding peptide (PepGen): an experimental study in rats," *Clinical Oral Implants Research*, vol. 19, no. 10, pp. 1010–1015, 2008.

[26] J. Guo and G. Wu, "The signaling and functions of heterodimeric bone morphogenetic proteins," *Cytokine and Growth Factor Reviews*, vol. 23, no. 1-2, pp. 61–67, 2012.

[27] R. Derynck and Y. E. Zhang, "Smad-dependent and Smad-independent pathways in TGF-β family signalling," *Nature*, vol. 425, no. 6958, pp. 577–584, 2003.

[28] J. Wang, J. Guo, J. Liu, L. Wei, and G. Wu, "BMP-functionalised coatings to promote osteogenesis for orthopaedic implants," *International Journal of Molecular Sciences*, vol. 15, no. 6, pp. 10150–10168, 2014.

[29] W. N. Liang, M. N. Lin, X. H. Li et al., "Icariin promotes bone formation via the BMP-2/Smad4 signal transduction pathway in the hFOB 1.19 human osteoblastic cell line," *International Journal of Molecular Medicine*, vol. 30, no. 4, pp. 889–895, 2012.

[30] X.-F. Li, H. Xu, Y.-J. Zhao et al., "Icariin augments bone formation and reverses the phenotypes of osteoprotegerin-deficient mice through the activation of WNT/ β-Catenin-BMP Signaling," *Evidence-Based Complementary and Alternative Medicine*, vol. 2013, Article ID 652317, 13 pages, 2013.

[31] S. Ohba, K. Nakajima, Y. Komiyama et al., "A novel osteogenic helioxanthin-derivative acts in a BMP-dependent manner," *Biochemical and Biophysical Research Communications*, vol. 357, no. 4, pp. 854–860, 2007.

[32] Y. Wu, L. Xia, Y. Zhou, Y. Xu, and X. Jiang, "Icariin induces osteogenic differentiation of bone mesenchymal stem cells in a MAPK-dependent manner," *Cell Proliferation*, vol. 48, no. 3, pp. 375–384, 2015.

[33] Y.-K. Zhai, X.-Y. Guo, B.-F. Ge et al., "Icariin stimulates the osteogenic differentiation of rat bone marrow stromal cells via activating the PI3K-AKT-eNOS-NO-cGMP-PKG," *Bone*, vol. 66, pp. 189–198, 2014.

[34] Z. Luo, M. Liu, L. Sun, and F. Rui, "Icariin recovers the osteogenic differentiation and bone formation of bone marrow stromal cells from a rat model of estrogen deficiency-induced osteoporosis," *Molecular Medicine Reports*, vol. 12, no. 1, pp. 382–388, 2015.

[35] Q. Bian, J. H. Huang, S. F. Liu et al., "Different molecular targets of Icariin on bMSCs in CORT and OVX-rats," *Frontiers in Bioscience*, vol. 4, pp. 1224–1236, 2012.

[36] Z.-B. Sun, J.-W. Wang, H. Xiao et al., "Icariin may benefit the mesenchymal stem cells of patients with steroid-associated osteonecrosis by ABCB1-promoter demethylation: a preliminary study," *Osteoporosis International*, vol. 26, no. 1, pp. 187–197, 2015.

[37] F. Wang, Z. Liu, S. Lin, H. Lu, and J. Xu, "Icariin enhances the healing of rapid palatal expansion induced root resorption in rats," *Phytomedicine*, vol. 19, no. 11, pp. 1035–1041, 2012.

[38] E. Wernike, M.-O. Montjovent, Y. Liu et al., "Vegf incorporated into calcium phosphate ceramics promotes vascularisation and bone formation in vivo," *European Cells and Materials*, vol. 19, pp. 30–40, 2010.

[39] B. H. Chung, J. D. Kim, C. K. Kim et al., "Icariin stimulates angiogenesis by activating the MEK/ERK- and PI3K/Akt/eNOS-dependent signal pathways in human endothelial cells," *Biochemical and Biophysical Research Communications*, vol. 376, no. 2, pp. 404–408, 2008.

[40] T. Liu, X.-C. Qin, W.-R. Li et al., "Effects of icariin and icariside II on eNOS expression and NOS activity in porcine aorta endothelial cells," *Beijing Da Xue Xue Bao*, vol. 43, no. 4, pp. 500–504, 2011.

[41] H.-B. Xu and Z.-Q. Huang, "Icariin enhances endothelial nitric-oxide synthase expression on human endothelial cells in vitro," *Vascular Pharmacology*, vol. 47, no. 1, pp. 18–24, 2007.

Hindawi Publishing Corporation
Stem Cells International
Volume 2016, Article ID 1318256, 9 pages
http://dx.doi.org/10.1155/2016/1318256

Research Article

Cytokines TNF-α, IL-6, IL-17F, and IL-4 Differentially Affect Osteogenic Differentiation of Human Adipose Stem Cells

Angela P. Bastidas-Coral,[1] Astrid D. Bakker,[1] Behrouz Zandieh-Doulabi,[1] Cornelis J. Kleverlaan,[2] Nathalie Bravenboer,[3] Tim Forouzanfar,[4] and Jenneke Klein-Nulend[1]

[1]*Department of Oral Cell Biology, Academic Centre for Dentistry Amsterdam (ACTA), University of Amsterdam and Vrije Universiteit Amsterdam, MOVE Research Institute Amsterdam, Amsterdam, Netherlands*
[2]*Department of Dental Materials Science, Academic Centre for Dentistry Amsterdam (ACTA), University of Amsterdam and Vrije Universiteit Amsterdam, MOVE Research Institute Amsterdam, Amsterdam, Netherlands*
[3]*Department of Clinical Chemistry, VU University Medical Center, MOVE Research Institute Amsterdam, Amsterdam, Netherlands*
[4]*Department of Oral and Maxillofacial Surgery, VU University Medical Center, MOVE Research Institute Amsterdam, Amsterdam, Netherlands*

Correspondence should be addressed to Jenneke Klein-Nulend; j.kleinnulend@acta.nl

Received 29 April 2016; Revised 9 August 2016; Accepted 16 August 2016

Academic Editor: Yang D. Teng

During the initial stages of bone repair, proinflammatory cytokines are released within the injury site, quickly followed by a shift to anti-inflammatory cytokines. The effect of pro- and anti-inflammatory cytokines on osteogenic differentiation of mesenchymal stem cells is controversial. Here, we investigated the effect of the proinflammatory cytokines TNF-α, IL-6, IL-8, and IL-17F and the anti-inflammatory cytokine IL-4 on proliferation and osteogenic differentiation of human adipose stem cells (hASCs). hASCs were treated with TNF-α, IL-6, IL-8, IL-17F, or IL-4 (10 ng/mL) for 72 h mimicking bone repair. TNF-α reduced collagen type I gene expression but increased hASC proliferation and ALP activity. IL-6 also strongly enhanced ALP activity (18-fold), as well as bone nodule formation by hASCs. IL-8 did not affect proliferation or osteogenic gene expression but reduced bone nodule formation. IL-17F decreased hASC proliferation but enhanced ALP activity. IL-4 enhanced osteocalcin gene expression and ALP activity but reduced RUNX2 gene expression and bone nodule formation. In conclusion, all cytokines studied have both enhancing and reducing effects on osteogenic differentiation of hASCs, even when applied for 72 h only. Some cytokines, specifically IL-6, may be suitable to induce osteogenic differentiation of mesenchymal stem cells as a strategy for enhancing bone repair.

1. Introduction

The treatment of critical-size cranial defects is still a significant challenge. These defects can result from craniectomy due to trauma and tumors. Despite complications related to the harvesting procedure, such as haemorrhage, nerve and vascular lesions, and prolonged or chronic postoperative pain, bone grafts are still considered the gold standard in the reconstruction of craniomaxillofacial skeletal defects [1, 2]. Yet, bone tissue engineering techniques, including the use of mesenchymal stem cells (MSCs), scaffolds, and inductive factors such as cytokines, can also be used as a strategy to repair critical-size cranial defects [3].

The physiological process of bone repair implicates the formation of a haematoma followed by an inflammatory response, which has been demonstrated to play a crucial role in early fracture repair [4, 5]. During the inflammatory phase, different cytokines are released at the injury site to aid the recruitment of mesenchymal progenitor cells, followed by replacement of the haematoma with granulation tissue [6]. Known proinflammatory cytokines, such as tumor necrosis factor-α (TNF-α), interleukin-6 (IL-6), and interleukin-8 (IL-8), can be detected in an early stage of fracture healing. High levels of TNF-α have been detected within the first 24 hours after bone injury in a mouse tibia fracture model [7]. In patients with hip fractures, expression of IL-6 and

IL-8 has been shown to be elevated within the first 24 to 72 hours after bone injury [8, 9]. TNF-α and IL-6 are secreted by macrophages and T-cells, and IL-6 is also secreted by osteoblasts [10]. TNF-α is known to promote the recruitment of MSCs and osteoblasts [7]. IL-6 has been shown to stimulate osteoblast differentiation [10]. In addition, IL-6 positively influences the mitogen-activated protein kinase signaling cascade, which is essential for bone formation in human bone marrow MSCs (BMSCs) [11]. The hypoxia-regulated cytokine IL-8 is upregulated during haematoma formation [9]. Interleukin-17F (IL-17F), a cytokine secreted by T-helper cell 17 (Th17) subset, has been shown to be expressed during the early phase of fracture healing, that is, 72 hours after fracture in mice, using immunohistochemistry [12]. Moreover, IL-17F stimulates osteoblast maturation *in vitro* [12, 13]. Recently, IL-17F has been shown to strongly induce osteogenic differentiation of MSCs [14].

Following the initial inflammatory response, a shift from proinflammatory to anti-inflammatory cytokines occurs, which is crucial for the repair process [15]. The T-helper 2 (Th2) cytokines IL-4, IL-10, and IL-13 belong to the family of anti-inflammatory cytokines that play an important role in inflammatory and immune responses [16, 17]. In particular, IL-4 inhibits bone resorption [18, 19], and its depletion can lead to a reduction in cortical bone mass in adult male mice [20]. In addition, IL-4 enhances osteogenesis by cocultures of proinflammatory M1 macrophages with preosteoblastic MC3T3 cells by modulating the M1 macrophage phenotype towards M2 [21].

Cytokines may affect the osteogenic differentiation of MSCs, besides their role in the immune response initiated upon injury. Both positive and negative effects of cytokines on osteogenic differentiation of MSCs have been reported, which might be related to the kinetics of their application [22, 23]. Whether IL-4, TNF-α, IL-6, IL-8, and/or IL-17F application for a duration of 72 hours, mimicking the *in vivo* situation, affects proliferation and osteogenic differentiation of MSCs is still unclear. A better understanding of the inflammatory phase during bone repair is crucial to exploit the regenerative potential of MSCs. Therefore, the aim of this study was to investigate whether a short exposure to proinflammatory and anti-inflammatory cytokines, known to be released during bone fracture, modulates proliferation and/or osteogenic differentiation of MSCs. We stimulated human adipose stem cells (hASCs) with the proinflammatory cytokines TNF-α, IL-6, IL-8, and IL-17F and the anti-inflammatory cytokine IL-4 for 72 hours. Proliferation was assessed by KI67 gene expression and DNA quantification. Osteogenic differentiation of hASCs was studied by analysis of gene expression of RUNX2, collagen type 1 (COL1), and osteocalcin (OC), as well as alkaline phosphatase (ALP) activity and bone nodule formation.

2. Materials and Methods

2.1. Adipose Tissue Donors. Subcutaneous adipose tissue samples were harvested from abdominal wall resections of five healthy female donors (age range: 33–54 years, mean: 47 years), who underwent elective plastic surgery at the Tergooi Hospital Hilversum and a clinic in Bilthoven, The Netherlands. The Ethical Review Board of the VU Medical Center, Amsterdam, The Netherlands, approved the protocol (number 2016/105) and informed consent was obtained from all patients.

2.2. Isolation and Culture of hASCs. Isolation, characterization, and osteogenic differentiation capacity of hASCs have been reported previously by our group [24]. For the isolation of hASCs, adipose tissue was cut into small pieces and enzymatically digested with 0.1% collagenase A (Roche Diagnostics GmbH, Mannheim, Germany) in phosphate-buffered saline (PBS) containing 1% bovine serum albumin (Roche Diagnostics GmbH) under continuous shaking conditions for 45 min at 37°C. Next a Ficoll® density-centrifugation step (Lymphoprep™; 1,000 g, 20 min, ρ = 1.077 g/mL Ficoll, osmolarity 280 ± 15 mOsm; Axis-Shield, Oslo, Norway) was performed, and the cell-containing interface was harvested and resuspended in Dulbecco's modified Eagle's medium (Life Technologies™ Europe BV, Bleiswijk, The Netherlands). hASCs were counted and stored in liquid nitrogen. Cryopreserved hASCs from the different donors were pooled and cultured in α-Minimum Essential Medium (α-MEM; Gibco, Life Technologies, Waltham, MA, USA) with 1% penicillin, streptomycin, and fungizone (PSF; Sigma, St. Louis, MO, USA), 10 IU/mL heparin (LEO Pharma A/S, Ballerup, Denmark), and 2% human platelet lysate, at 37°C in 5% CO_2 in air. The medium was refreshed every 3 days. When near confluent (90%), hASCs were harvested by adding 0.25% trypsin (Gibco, Invitrogen, Waltham, MA, USA) and 0.1% ethylenediaminetetraacetic acid (Merck, Darmstadt, Germany) in PBS at 37°C. ASCs were stored in liquid nitrogen until further use. For experiments, hASCs were thawed and seeded at 0.5×10^6 cells in T-175 cm^2 culture flasks (Greiner Bio-One, Kremsmünster, Austria) in α-MEM containing 1% PSF, 10 IU/mL heparin, and 2% human platelet lysate, at 37°C in 5% CO_2 in air. In all experiments, hASCs at passage 2 (P2) were used. Medium was changed every 3 days.

2.3. Platelet Lysate. Pooled platelet products from five donors were obtained from the Bloodbank Sanquin (Sanquin, Amsterdam, The Netherlands) and contained approximately 1×10^9 platelets per mL [25]. Platelet lysate was obtained by lysing the platelets through temperature shock at −80°C. For usage, platelet lysate was thawed and centrifuged at 600 g for 10 min to eliminate remaining platelet fragments. The supernatant was added at 2% (v/v) to the medium or stored at 4°C until usage within 1 week.

2.4. Stimulation of hASCs with Proinflammatory and Anti-Inflammatory Cytokines. hASCs (1×10^4 cells/cm^2) were seeded in 24-well plates and cultured in α-MEM containing 1% PSF, 10 IU/mL heparin, and 2% human platelet lysate, at 37°C in 5% CO_2 in air. hASCs were allowed to attach for 24 h before stimulation with cytokines. After cytokine stimulation, the medium was replaced with osteogenic medium (OM), consisting of α-MEM containing 1% PSF, 10 IU/mL heparin, 2% human platelet lysate, 50 μM ascorbic acid-2-phosphate (vitamin C; Sigma, St. Louis, MO, USA), 5 mM

Table 1: Primer sequences for determination of proliferation and osteogenic differentiation of hASCs through PCR. *YWHAZ*: tyrosine 3-monooxygenase/tryptophan 5-monooxygenase activation protein, zeta; *UBC*: ubiquitin C; *KI67*: proliferation marker; *RUNX2*: runt-related transcription factor-2; *COL1*: collagen type 1; *Osteocalcin*.

Target gene (human)	Oligonucleotide sequences	
	Forward	Reverse
YWHAZ	5′ GATGAAGCCATTGCTGAACTTG 3′	5′ CTATTTGTGGGACAGCATGGA 3′
UBC	5′ GCGGTGAACGCCGATGATTAT 3′	5′ TTTGCCTTGACATTCTCGATGG 3′
KI67	5′ CCCTCAGCAAGCCTGAGAA 3′	5′ AGAGGCGTATTAGGAGGCAAG 3′
RUNX2	5′ ATGCTTCATTCGCCTCAC 3′	5′ ACTGCTTGCAGCCTTAAAT 3′
COL1	5′ TCCGGCTCCTGCTCCTCTTA 3′	5′ GGCCAGTGTCTCCCTTG 3′
Osteocalcin	5′AGCCACCGAGACACCATGAGA 3′	5′ CTCCTGAAAGCCGATGTGGTC 3′

β-glycerophosphate (βGP; Sigma), and 10 nM 1,25-$(OH)_2$ vitamin D_3 (Sigma). Recombinant human TNF-α (R&D Systems, Minneapolis, MN, USA), recombinant human IL-4 (R&D Systems), recombinant human IL-6 (R&D Systems), recombinant human IL-6Rα (R&D Systems), recombinant human IL-8 (R&D Systems), and recombinant human IL-17F (R&D Systems) were added to the OM at 10 ng/mL and incubated for 72 h at 37°C in 5% CO_2 in air. Then, the medium was changed to OM without cytokines and was replaced every 3 days. hASCs were harvested at 6 and 48 h (early time points) and at 4, 7, and 14 days (late time points) to assess proliferation and osteogenic differentiation of hASCs.

2.5. Cell Proliferation. hASCs cultured for 48 h, 4 days, and 7 days with proinflammatory and anti-inflammatory cytokines were washed with PBS, and CyQuant lysis buffer was added. DNA content, as a measure for cell number, was determined using the CyQuant Cell Proliferation Assay Kit (Molecular Probes, Leiden, The Netherlands). Absorption was read at 485 nm excitation and 528 nm emission in a microplate reader (Synergy HT® spectrophotometer; BioTek Instruments Inc., Highland Park, Winooski, VT, USA).

2.6. RNA Isolation and Real-Time RT-PCR. Total RNA was isolated from hASCs using TRIzol® reagent (Invitrogen, Carlsbad, CA, USA), according to the manufacturer's instructions. Total RNA concentration and quality were determined using a Synergy HT spectrophotometer. RNA was reverse-transcribed to cDNA using a RevertAid™ First Strand cDNA Synthesis Kit (Fermentas, St. Leon-Rot, Germany) according to the manufacturer's instructions. Real-time PCR was performed using SYBR® Green I Mastermix (Roche Diagnostics, Mannheim, Germany) in a LightCycler® 480 (Roche Diagnostics, Basel, Switzerland). Every PCR reaction was prepared with 3 μL PCR-H2O, 0.5 μL forward primer (1 μM), 0.5 μL reverse primer (1 μM), 5 μL LightCycler 480 SYBR Green I Mastermix (Roche Diagnostics, Mannheim, Germany), and 1 μL cDNA in a final volume of 10 μL. Based on BestKeeper [26], the values obtained were normalized to YWHAZ and UBC housekeeping genes. Real-time PCR was used to assess expression of the following genes: KI67, RUNX2, COL1, and osteocalcin. All primers used were from Life Technologies. The primer sequences are listed in Table 1. mRNA preparations from human bone were used as a reference and internal control in each assay.

2.7. Alkaline Phosphatase Activity. hASCs cultured for 48 h, 4 days, and 7 days with proinflammatory and anti-inflammatory cytokines were lysed with CyQuant lysis buffer. ALP activity was measured in the cell lysate using 4-nitrophenyl phosphate disodium salt (Merck, Darmstadt, Germany) at pH 10.3 as a substrate for ALP, according to the method described by Lowry [27]. The absorbance was read at 405 nm with a Synergy HT spectrophotometer. ALP activity was expressed as μM per ng DNA.

2.8. Mineralization. Matrix mineralization was analyzed by alizarin red staining after incubation of hASCs with proinflammatory and anti-inflammatory cytokines at day 14 by using 1% Alizarin Red S (pH 4.1; Sigma-Aldrich, St. Louis, MO, USA) in water as described earlier [28]. Briefly, hASCs were fixed with 10% formaldehyde for 15 min and rinsed with deionized water before adding 350 mL of 1% Alizarin Red S solution per well. After incubation for 15 min at room temperature, the cells were washed with deionized water. Cells differentiating into osteoblasts show mineralized matrix deposition, producing bright red nodules.

2.9. Statistical Analysis. Values are provided as mean ± SD. Differences between two groups were tested for statistical significance using paired t-test. Analysis of variance (ANOVA) was used to compare data between three or more groups, with application of Dunnett's multiple comparison test to compare with untreated controls. A p value < 0.05 was considered significant. Statistical analysis was performed using GraphPad Prism 5.4 (GraphPad Software, San Diego, CA, USA).

3. Results

3.1. TNF-α, but Not IL-6, IL-8, IL-17F, or IL-4, Stimulates hASCs DNA Content. DNA content and gene expression of the proliferation marker KI67 were analyzed to assess whether proinflammatory and anti-inflammatory cytokines affect hASCs proliferation. All cytokines did not affect KI67 gene expression compared with untreated cultures at 48 h, day 4, or day 7 (Figure 1(a)). TNF-α significantly decreased DNA content by 1.1-fold at 48 h, but it increased DNA content by 1.1-fold at days 4 and 7 compared to untreated controls (Figure 1(b)). IL-17F decreased DNA content by 1.2-fold at day 4 (Figure 1(b)). All other cytokines did not affect DNA

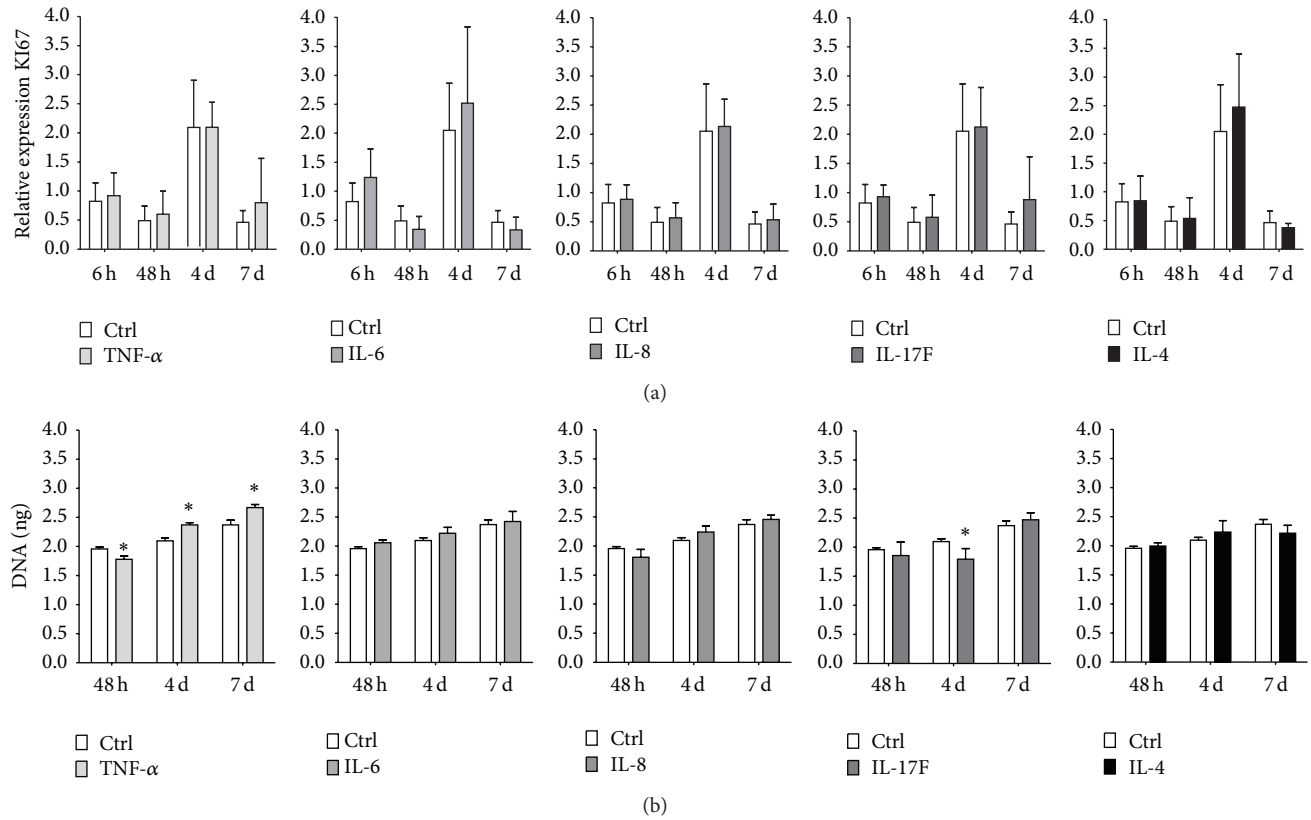

Figure 1: Comparative analysis of the effect of pro- and anti-inflammatory cytokines on hASC proliferation. ASCs were stimulated for 72 h with proinflammatory cytokines TNF-α, IL-6, IL-8, and IL-17F and the anti-inflammatory cytokine IL-4 (10 ng/mL). (a) Gene expression of proliferation marker KI67 at 6 h, 48 h, and days 4 and 7. No significant effects of cytokines on KI67 expression were found, $n = 7$. (b) DNA content at 48 h, day 4, and day 7. TNF-α decreased DNA content at 48 h but increased DNA content at days 4 and 7. IL-17F decreased DNA content at day 4. $n = 3$, results are mean ± SD. *Significant effect of cytokine treatment, $p < 0.05$.

content compared with untreated cultures at 48 h, day 4, or day 7 (Figure 1(b)).

3.2. Cytokines Exerted Various Effects on Gene Expression of Osteogenic Markers in hASCs. The effect of treatment with the proinflammatory cytokines TNF-α, IL-6, IL-8, and IL-17F and the anti-inflammatory cytokine IL-4 (concentration of all cytokines tested 10 ng/mL) on osteogenic differentiation of hASCs was assessed. IL-4 significantly decreased RUNX2 gene expression by 4.7–5.0-fold at days 4 and 7 compared to untreated hASCs (Figure 2(a)).

COL1 gene expression was decreased by the proinflammatory cytokines TNF-α (4-fold decrease, day 4) and IL-6 (2.2-fold decrease, 48 h; Figure 2(b)). The other cytokines tested did not affect COL1 expression. IL-4 significantly increased the expression of the mature bone marker osteocalcin by 7.4-fold at day 4 and by 7.2-fold at day 7, compared to untreated controls (Figure 2(c)). The other cytokines tested did not significantly affect osteocalcin expression.

3.3. Pro- and Anti-Inflammatory Cytokines Enhanced ALP Activity and Mineralization of hASCs. The proinflammatory cytokines significantly increased ALP activity. TNF-α increased ALP activity by 9-fold and IL-6 by 18-fold at day 7. IL-17F increased ALP activity by 2.3–2.6-fold at 48 h and at day 4 (Figure 3(a)). IL-8 did not affect ALP activity at any of the time points measured. The proinflammatory cytokine IL-4 enhanced ALP activity by 1.5-fold at day 4 (Figure 3(a)).

IL-6 enhanced mineralization of hASCs at day 14 compared to the untreated controls. In contrast, TNF-α and IL-17F decreased mineralization of hASCs at day 14 compared to the untreated controls. Treatment with IL-8 and IL-4 resulted in low mineralization compared to untreated controls as well as compared to the other cytokines (Figure 3(b)).

4. Discussion

Understanding the mechanism of fracture repair, especially the inflammatory response, is relevant in the search for new strategies or treatments to optimize bone repair, which may have implications for the treatment of critical-size cranial defects. We added pro- and anti-inflammatory cytokines for 72 hours, which simulates the kinetics of their expression during early stages of fracture repair *in vivo*, and investigated their effects on the proliferation and osteogenic differentiation of hASCs.

The proliferative capacity of mesenchymal precursors is highly relevant for tissue repair [29]. Cytokines are known to affect proliferation of different cell types [22, 30]. Therefore, we first analyzed the effect of the different cytokines on

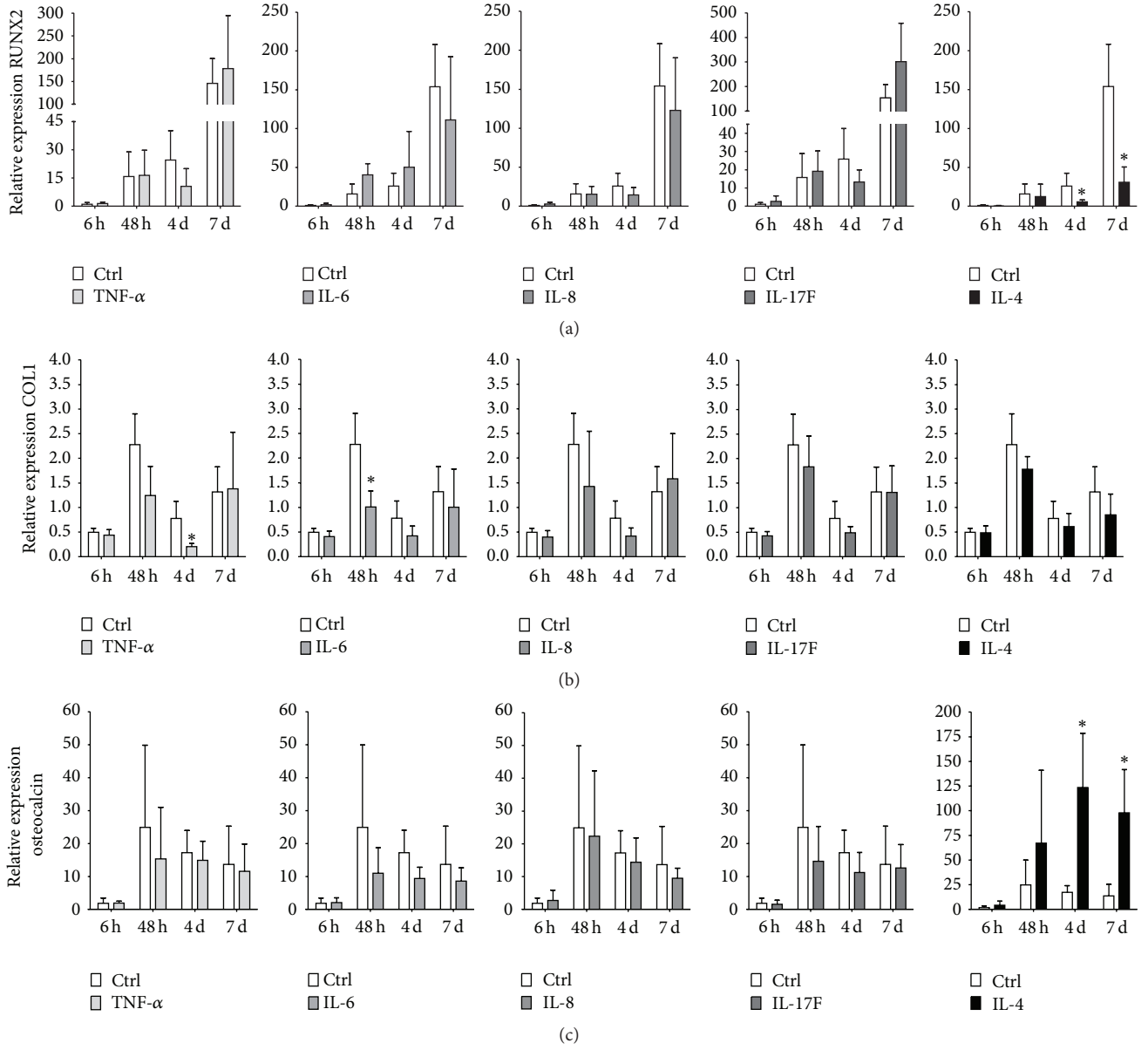

Figure 2: Comparative analysis of the effect of pro- and anti-inflammatory cytokines on osteogenic differentiation of hASCs. ASCs were stimulated for 72 h with proinflammatory cytokines TNF-α, IL-6, IL-8, and IL-17F and the anti-inflammatory cytokine IL-4 (10 ng/mL). (a) IL-4 decreased RUNX2 gene expression at days 4 and 7, $n = 7$. (b) TNF-α and IL-6 decreased gene expression of COL1 at day 4 and 48 h, $n = 7$. (c) Only IL-4, but not the other cytokines tested, increased osteocalcin gene expression at days 4 and 7. Results are mean ± SD, $n = 7$. *Significant effect of cytokine treatment, $p < 0.05$.

the proliferation of hASCs. This study demonstrated that 10 ng/mL TNF-α increased DNA content of hASCs at 7 days. However, IL-4, IL-6, IL-8, and IL-17F (10 ng/mL) did not affect DNA content or expression of KI67. Thus, TNF-α may be more important than the other cytokines to induce MSCs proliferation during bone tissue repair. Interestingly, it has been reported that TNF-α at 50 ng/mL for 7 days does not affect MSC proliferation, while TNF-α at only 5 ng/mL significantly stimulates MSC proliferation by 2-fold [31]. We also showed that TNF-α at a relatively low concentration of 10 ng/mL increases hASC proliferation after 7 days of culture. It is thus possible that the observed effect of cytokines on indicators of stem cell proliferation, or lack thereof, is strongly dose-dependent.

Proinflammatory and anti-inflammatory cytokines differentially affected osteogenic differentiation of hASCs. TNF-α and IL-6 affected osteogenic differentiation of hASCs by decreasing COL1 gene expression, followed at a later stage by enhancing ALP activity. IL-6 also induced mineralization as shown by alizarin red staining of the cultures. Our findings confirm findings by others showing that IL-6 enhances osteogenic differentiation of MSCs [10, 32, 33]. Moreover, IL-6 at 100 ng/mL accelerates mineralization as well as RUNX2 gene expression in hASCs [28]. In our study, we used only

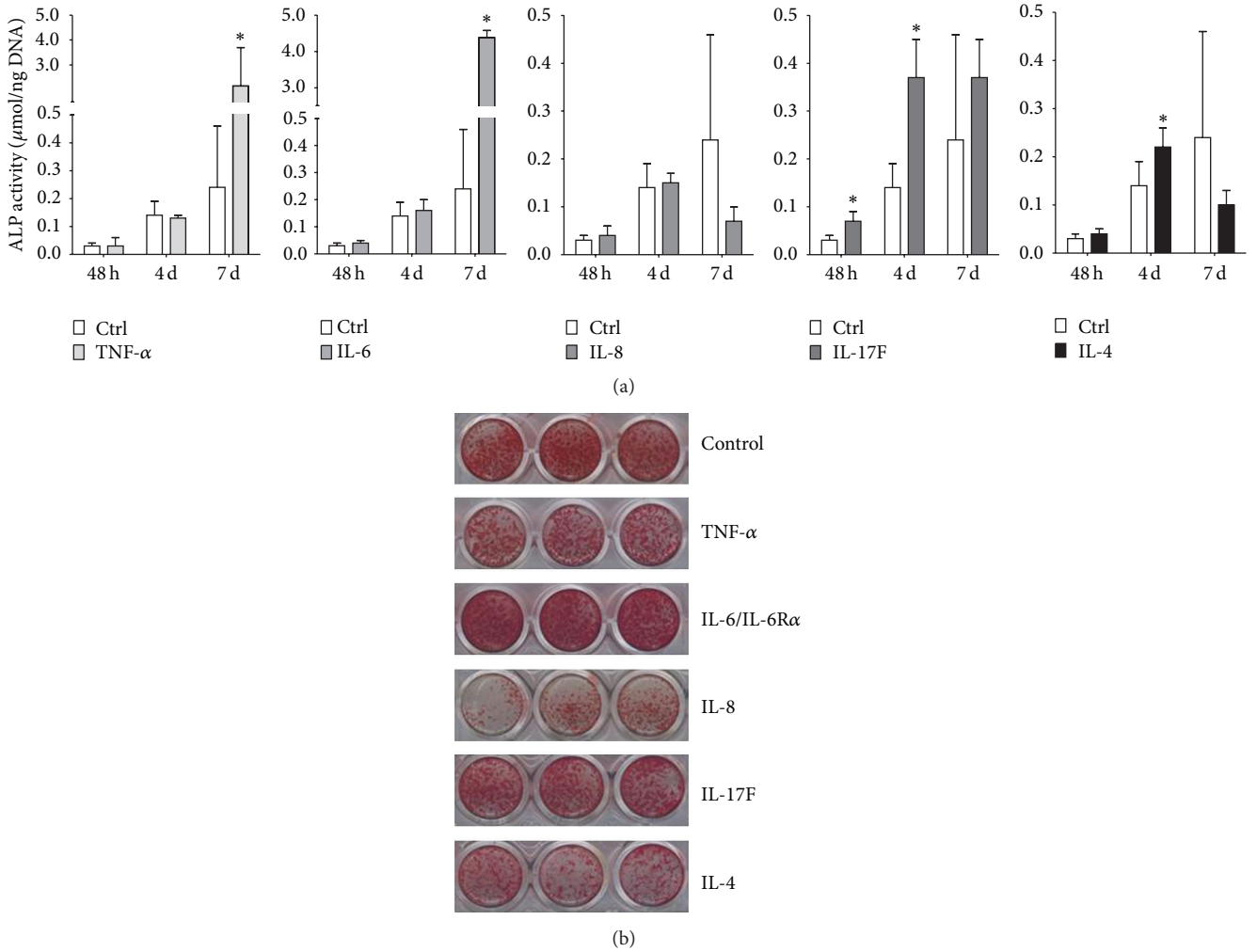

Figure 3: Comparative analysis of the effect of pro- and anti-inflammatory cytokines on osteogenic differentiation of hASCs. ASCs were stimulated for 72 h with proinflammatory cytokines TNF-α, IL-6, IL-8, and IL-17F and the anti-inflammatory cytokine IL-4 (10 ng/mL). (a) TNF-α and IL-6 increased ALP activity at 7 days and IL-17F at 48 h and day 7. IL-4 increased ALP activity at day 4. Results are mean ± SD, $n = 3$. *Significant effect of cytokine treatment, $p < 0.05$. (b) ASCs showed enhanced mineralization using alizarin red staining after IL-6 treatment at day 14 compared to untreated controls. TNF-α, IL-8, IL-17F, and IL-4 decreased mineralization of hASCs at day 14 compared to untreated controls.

10 ng/mL IL-6 to treat hASCs, which might explain the lack of effect of IL-6 on RUNX2 expression. IL-6 has been shown to stimulate osteoblast differentiation [10]. A femoral fracture model in IL-6 knockout mice showed delayed callus remodeling and mineralization [32]. Therefore, IL-6 may play a crucial role in osteogenic differentiation of MSCs and might be used to enhance mineralization during fracture healing.

In the present study, 10 ng/mL IL-17F enhanced ALP activity by hASCs. In addition, the proinflammatory cytokine IL-17F stimulates osteoblast maturation and activation allowing bone synthesis [12, 14]. Four days of stimulation with IL-17F increases gene expression of COL1 and osteocalcin in MC3T3-E1 preosteoblasts and mouse primary mesenchymal stromal cells [12]. The difference between these data and our data might be related to differences in cell type and cytokine concentration, since we added IL-17F at 10 ng/mL to hASCs, while others added 20 ng/mL IL-17F to MC3T3-E1 preosteoblasts and mouse primary mesenchymal stromal cells [12].

Since our data showed that proinflammatory cytokines TNF-α, IL-6, and IL-17F affected the expression of proliferation and osteogenic differentiation markers by hASCs, we expected to also see an effect by IL-8 treatment. However, 10 ng/mL IL-8 did not affect proliferation or osteogenic differentiation of hASCs, suggesting that IL-8 does not likely play an important role in these processes during early stages of fracture repair. IL-8 is mostly known as an enhancer of cell migration, more than differentiation, and might thus still play a positive role in bone repair *in vivo*. *In vivo* studies are needed to unravel the role of IL-8 and the implications of its effects during the early stages of bone healing.

During fracture repair, the proinflammatory response switches to an anti-inflammatory response, where IL-4 may play an important role. Expression of the genes for T-cell

effector cytokines such as IL-4 is significantly elevated in the fracture callus [34]. To our knowledge, this is the first study reporting on the effect of IL-4 on osteogenic differentiation of hASCs, although other cell types have been investigated [35–37]. A recent study has reported that bone marrow mesenchymal stem cells (BMMSCs) from FBN1-deficient ($Fbn1^{+/-}$) mice exhibit decreased osteogenic differentiation and that this lineage alteration is regulated by IL4/IL4Rα-mediated activation of mTOR signaling to downregulate RUNX2 [38]. So, this study provides relevant information that IL-4 is involved during osteogenic differentiation. In our study, we demonstrated that IL-4 at 10 ng/mL decreased gene expression of the early osteogenic marker RUNX2 but increased expression of the marker of later osteogenic differentiation osteocalcin in hASCs at days 4 and 7. IL-4 also increased ALP activity in hASCs. This is in agreement with findings by others showing that IL-4 stimulates ALP activity in a dose-dependent manner in cultured human osteoblasts and in the human osteosarcoma cell line MG63 [35–37]. On the other hand, we observed decreased mineralization in hASCs treated with 10 ng/mL IL-4, while others showed that M1 macrophages cocultured with preosteoblastic MC3T3 cells treated with IL-4 for 72 hours enhance osteogenic differentiation and mineralization [21]. MC3T3 monocultures treated with IL-4 for 72 hours did not reveal significant differences in mineralization compared with untreated MC3T3 cells [21]. This indicates that specific conditions within the inflammatory environment such as the presence of inflammatory cells, that is, macrophages, may influence the effects of IL-4 during fracture repair and then enhance the osteogenic differentiation of MSCs.

To obtain an optimal effect of cytokines in an *in vivo* critical-size cranial defect model is a significant challenge, since different concentrations of cytokines are produced, or different cytokine expression occurs by MSCs during their differentiation to osteoblasts [39]. The synergistic and antagonistic effects of different cytokines combined, as this occurs within the fracture site *in vivo*, are important, since the effect of combined cytokines might be different from the observed effect of individual cytokines on bone formation. We have focused on whether each cytokine will enhance or decrease the osteogenic potential of hASCs and on the time point that markers of bone formation are significantly expressed. A previous study from our group has also shown that the combination of cytokines present in the circulation of patients with active rheumatoid arthritis might contribute to generalized bone loss by directly inhibiting osteoblast proliferation and differentiation [40].

Exposure duration is also a critical element in determining cytokine effects on bone regeneration [41]. We showed that cytokines present during the inflammatory response may play an important role in the osteogenic differentiation of progenitor cells. Moreover, the coordinated interactions with cytokines, cells, and extracellular matrix have been documented to define a local biochemical and mechanical niche [42]. So, additional studies assessing the effect of proinflammatory and anti-inflammatory cytokines under conditions that better simulate the environment of the inflammatory response, such as hypoxia and the presence of inflammatory cells in a 3D environment, may provide additional information that might be useful when using MSCs and cytokines for bone tissue engineering purposes.

In summary, our data show that hASCs respond to the different cytokines by changes in osteogenic differentiation. Each cytokine analyzed had a specific effect in a specific time frame, which in combination with each other may enable successful bone repair. The stimulatory effects of IL-6 on ALP activity and mineralization in hASCs suggest that this cytokine may enhance osteogenic differentiation of MSCs and therefore could be used to optimize strategies focused on the treatment of critical-size cranial defects *in vivo*. In conclusion, all cytokines investigated seemed to exert both enhancing and reducing effects on osteogenic differentiation of hASCs. Specifically IL-6 may be suitable to induce osteogenic differentiation of MSCs as a strategy for enhancing bone repair.

Competing Interests

Angela P. Bastidas-Coral, Astrid D. Bakker, Behrouz Zandieh-Doulabi, Cornelis J. Kleverlaan, Nathalie Bravenboer, Tim Forouzanfar, and Jenneke Klein-Nulend declare that there are no competing interests regarding the publication of this paper.

Acknowledgments

The authors thank Henk-Jan Prins, Benno Naaijkens, and Jolanda Hogervorst for adipose stem cell isolation and excellent technical assistance. This research was funded by ACTA Dental Research Institute, University of Amsterdam and Vrije Universiteit Amsterdam, The Netherlands.

References

[1] P. Sieg, C. Taner, S. G. Hakim, and H.-C. Jacobsen, "Long-term evaluation of donor site morbidity after free fibula transfer," *British Journal of Oral and Maxillofacial Surgery*, vol. 48, no. 4, pp. 267–270, 2010.

[2] A. Ridwan-Pramana, P. Marcián, L. Borák, N. Narra, T. Forouzanfar, and J. Wolff, "Structural and mechanical implications of PMMA implant shape and interface geometry in cranioplasty—a finite element study," *Journal of Cranio-Maxillofacial Surgery*, vol. 44, no. 1, pp. 34–44, 2016.

[3] T. Albrektsson and C. Johansson, "Osteoinduction, osteoconduction and osseointegration," *European Spine Journal*, vol. 10, no. 2, pp. S96–S101, 2001.

[4] R. Dimitriou, E. Tsiridis, and P. V. Giannoudis, "Current concepts of molecular aspects of bone healing," *Injury*, vol. 36, no. 12, pp. 1392–1404, 2005.

[5] P. M. Mountziaris and A. G. Mikos, "Modulation of the inflammatory response for enhanced bone tissue regeneration," *Tissue Engineering Part B: Reviews*, vol. 14, no. 2, pp. 179–186, 2008.

[6] A. C. Wu, L. J. Raggatt, K. A. Alexander, and A. R. Pettit, "Unraveling macrophage contributions to bone repair," *BoneKEy Reports*, vol. 2, article 373, 2013.

[7] T. Kon, T.-J. Cho, T. Aizawa et al., "Expression of osteoprotegerin, receptor activator of NF-κB ligand (osteoprotegerin ligand) and related proinflammatory cytokines during fracture healing," *Journal of Bone and Mineral Research*, vol. 16, no. 6, pp. 1004–1014, 2001.

[8] T.-J. Cho, L. C. Gerstenfeld, and T. A. Einhorn, "Differential temporal expression of members of the transforming growth factor β superfamily during murine fracture healing," *Journal of Bone and Mineral Research*, vol. 17, no. 3, pp. 513–520, 2002.

[9] P. Kolar, T. Gaber, C. Perka, G. N. Duda, and F. Buttgereit, "Human early fracture hematoma is characterized by inflammation and hypoxia," *Clinical Orthopaedics and Related Research*, vol. 469, no. 11, pp. 3118–3126, 2011.

[10] D. Heymann and A.-V. Rousselle, "gp130 Cytokine family and bone cells," *Cytokine*, vol. 12, no. 10, pp. 1455–1468, 2000.

[11] F. Rezaee, S. L. Rellick, G. Piedimonte et al., "Neurotrophins regulate bone marrow stromal cell IL-6 expression through the MAPK pathway," *PLoS ONE*, vol. 5, no. 3, Article ID e9690, 2010.

[12] D. Nam, E. Mau, Y. Wang et al., "T-lymphocytes enable osteoblast maturation via IL-17F during the early phase of fracture repair," *PLoS ONE*, vol. 7, no. 6, Article ID e40044, 2012.

[13] Y. Shi, S. J. Ullrich, J. Zhang et al., "A novel cytokine receptor-ligand pair: identification, molecular characterization, and in vivo immunomodutory activity," *Journal of Biological Chemistry*, vol. 275, no. 25, pp. 19167–19176, 2000.

[14] M. Croes, F. C. Öner, D. van Neerven et al., "Proinflammatory T cells and IL-17 stimulate osteoblast differentiation," *Bone*, vol. 84, pp. 262–270, 2016.

[15] D. Toben, I. Schroeder, T. El Khassawna et al., "Fracture healing is accelerated in the absence of the adaptive immune system," *Journal of Bone and Mineral Research*, vol. 26, no. 1, pp. 113–124, 2011.

[16] E. V. Marietta, Y. Chen, and J. H. Weis, "Modulation of expression of the anti-inflammatory cytokines interleukin-13 and interleukin-10 by interleukin-3," *European Journal of Immunology*, vol. 26, no. 1, pp. 49–56, 1996.

[17] M. Wills-Karp, "Immunologic basis of antigen-induced airway hyperresponsiveness," *Annual Review of Immunology*, vol. 17, pp. 255–281, 1999.

[18] K. Watanabe, Y. Tanaka, I. Morimoto et al., "Interleukin-4 as a potent inhibitor of bone resorption," *Biochemical and Biophysical Research Communications*, vol. 172, no. 3, pp. 1035–1041, 1990.

[19] Y. Onoe, C. Miyaura, T. Kaminakayashiki et al., "IL-13 and IL-4 inhibit bone resorption by suppressing cyclooxygenase-2-dependent prostaglandin synthesis in osteoblasts," *The Journal of Immunology*, vol. 156, no. 2, pp. 758–764, 1996.

[20] C.-J. Silfverswärd, S. Larsson, C. Ohlsson, A. Frost, and O. Nilsson, "Reduced cortical bone mass in mice with inactivation of interleukin-4 and interleukin-13," *Journal of Orthopaedic Research*, vol. 25, no. 6, pp. 725–731, 2007.

[21] F. Loi, L. A. Córdova, R. Zhang et al., "The effects of immunomodulation by macrophage subsets on osteogenesis in vitro," *Stem Cell Research & Therapy*, vol. 7, no. 1, pp. 1–15, 2016.

[22] D. C. Lacey, P. J. Simmons, S. E. Graves, and J. A. Hamilton, "Proinflammatory cytokines inhibit osteogenic differentiation from stem cells: implications for bone repair during inflammation," *Osteoarthritis and Cartilage*, vol. 17, no. 6, pp. 735–742, 2009.

[23] S. Deshpande, A. W. James, J. Blough et al., "Reconciling the effects of inflammatory cytokines on mesenchymal cell osteogenic differentiation," *Journal of Surgical Research*, vol. 185, no. 1, pp. 278–285, 2013.

[24] M. J. O. Varma, R. G. M. Breuls, T. E. Schouten et al., "Phenotypical and functional characterization of freshly isolated adipose tissue-derived stem cells," *Stem Cells and Development*, vol. 16, no. 1, pp. 91–104, 2007.

[25] H.-J. Prins, H. Rozemuller, S. Vonk-Griffioen et al., "Bone-forming capacity of mesenchymal stromal cells when cultured in the presence of human platelet lysate as substitute for fetal bovine serum," *Tissue Engineering A*, vol. 15, no. 12, pp. 3741–3751, 2009.

[26] M. W. Pfaffl, A. Tichopad, C. Prgomet, and T. P. Neuvians, "Determination of stable housekeeping genes, differentially regulated target genes and sample integrity: BestKeeper—excel-based tool using pair-wise correlations," *Biotechnology Letters*, vol. 26, no. 6, pp. 509–515, 2004.

[27] O. H. Lowry, "Micromethods for the assay of enzymes," *Methods in Enzymology*, vol. 4, pp. 366–381, 1957.

[28] S. Fukuyo, K. Yamaoka, K. Sonomoto et al., "IL-6-accelerated calcification by induction of ROR2 in human adipose tissue-derived mesenchymal stem cells is STAT3 dependent," *Rheumatology*, vol. 53, no. 7, Article ID ket496, pp. 1282–1290, 2014.

[29] V. Feisst, S. Meidinger, and M. B. Locke, "From bench to bedside: Use of human adipose-derived stem cells," *Stem Cells and Cloning: Advances and Applications*, vol. 8, pp. 149–162, 2015.

[30] D. M. Butler, D. S. Piccoli, P. H. Hart, and J. A. Hamilton, "Stimulation of human synovial fibroblast DNA synthesis by recombinant human cytokines," *Journal of Rheumatology*, vol. 15, no. 10, pp. 1463–1470, 1988.

[31] V. Egea, L. von Baumgarten, C. Schichor et al., "TNF-α respecifies human mesenchymal stem cells to a neural fate and promotes migration toward experimental glioma," *Cell Death & Differentiation*, vol. 18, no. 5, pp. 853–863, 2011.

[32] X. Yang, B. F. Ricciardi, A. Hernandez-Soria, Y. Shi, N. Pleshko Camacho, and M. P. G. Bostrom, "Callus mineralization and maturation are delayed during fracture healing in interleukin-6 knockout mice," *Bone*, vol. 41, no. 6, pp. 928–936, 2007.

[33] K. Hess, A. Ushmorov, J. Fiedler, R. E. Brenner, and T. Wirth, "TNFα promotes osteogenic differentiation of human mesenchymal stem cells by triggering the NF-κB signaling pathway," *Bone*, vol. 45, no. 2, pp. 367–376, 2009.

[34] T. A. Einhorn, R. J. Majeska, E. B. Rush, P. M. Levine, and M. C. Horowitz, "The expression of cytokine activity by fracture callus," *Journal of Bone and Mineral Research*, vol. 10, no. 8, pp. 1272–1281, 1995.

[35] C.-J. Silfverswärd, H. Penno, A. Frost, O. Nilsson, and Ö. Ljunggren, "Expression of markers of activity in cultured human osteoblasts: effects of interleukin-4 and interleukin-13," *Scandinavian Journal of Clinical and Laboratory Investigation*, vol. 70, no. 5, pp. 338–342, 2010.

[36] J. A. Riancho, M. T. Zarrabeitia, J. M. Olmos, J. A. Amado, and J. Gonzalez-Macias, "Effects of interleukin-4 on human osteoblast-like cells," *Bone and Mineral*, vol. 21, no. 1, pp. 53–61, 1993.

[37] K. Nohtomi, K. Sato, K. Shizume et al., "Stimulation of interleukin-4 of cell proliferation and mRNA expression of alkaline phosphatase and collagen type I in human osteoblast-like cells of trabecular bone," *Bone and Mineral*, vol. 27, no. 1, pp. 69–79, 1994.

[38] C. Chen, K. Akiyama, D. Wang et al., "mTOR inhibition rescues osteopenia in mice with systemic sclerosis," *The Journal of Experimental Medicine*, vol. 212, no. 1, pp. 73–91, 2015.

[39] A. L. Strong, J. M. Gimble, and B. A. Bunnell, "Analysis of the pro- and anti-inflammatory cytokines secreted by adult stem cells during differentiation," *Stem Cells International*, vol. 2015, Article ID 412467, 12 pages, 2015.

[40] J. L. Pathak, N. Bravenboer, P. Verschueren et al., "Inflammatory factors in the circulation of patients with active rheumatoid arthritis stimulate osteoclastogenesis via endogenous cytokine production by osteoblasts," *Osteoporosis International*, vol. 25, no. 10, pp. 2453–2463, 2014.

[41] Z. Lu, G. Wang, C. R. Dunstan, and H. Zreiqat, "Short-term exposure to tumor necrosis factor-alpha enables human osteoblasts to direct adipose tissue-derived mesenchymal stem cells into osteogenic differentiation," *Stem Cells and Development*, vol. 21, no. 13, pp. 2420–2429, 2012.

[42] D. E. Discher, D. J. Mooney, and P. W. Zandstra, "Growth factors, matrices, and forces combine and control stem cells," *Science*, vol. 324, no. 5935, pp. 1673–1677, 2009.

Hindawi Publishing Corporation
Stem Cells International
Volume 2016, Article ID 1934270, 12 pages
http://dx.doi.org/10.1155/2016/1934270

Research Article

Enhanced Osteogenic and Vasculogenic Differentiation Potential of Human Adipose Stem Cells on Biphasic Calcium Phosphate Scaffolds in Fibrin Gels

Fransisca A. S. van Esterik,[1,2] Behrouz Zandieh-Doulabi,[1] Cornelis J. Kleverlaan,[2] and Jenneke Klein-Nulend[1]

[1]*Department of Oral Cell Biology, Academic Centre for Dentistry Amsterdam (ACTA), University of Amsterdam and Vrije Universiteit Amsterdam, MOVE Research Institute Amsterdam, Amsterdam, Netherlands*
[2]*Department of Dental Materials Science, Academic Centre for Dentistry Amsterdam (ACTA), University of Amsterdam and Vrije Universiteit Amsterdam, MOVE Research Institute Amsterdam, Amsterdam, Netherlands*

Correspondence should be addressed to Jenneke Klein-Nulend; j.kleinnulend@acta.nl

Received 1 March 2016; Revised 6 June 2016; Accepted 27 June 2016

Academic Editor: Susan Liao

For bone tissue engineering synthetic biphasic calcium phosphate (BCP) with a hydroxyapatite/β-tricalcium phosphate (HA/β-TCP) ratio of 60/40 (BCP60/40) is successfully clinically applied, but the high percentage of HA may hamper efficient scaffold remodelling. Whether BCP with a lower HA/β-TCP ratio (BCP20/80) is more desirable is still unclear. Vascular development is needed before osteogenesis can occur. We aimed to test the osteogenic and/or vasculogenic differentiation potential as well as degradation of composites consisting of human adipose stem cells (ASCs) seeded on BCP60/40 or BCP20/80 incorporated in fibrin gels that trigger neovascularization for bone regeneration. ASC attachment to BCP60/40 and BCP20/80 within 30 min was similar (>93%). After 11 days of culture BCP20/80-based composites showed increased alkaline phosphatase activity and *DMP1* gene expression, but not *RUNX2* and osteonectin expression, compared to BCP60/40-based composites. BCP20/80-based composites also showed enhanced expression of the vasculogenic markers *CD31* and *VEGF189*, but not *VEGF165* and endothelin-1. Collagen-1 and collagen-3 expression was similar in both composites. Fibrin degradation was increased in BCP20/80-based composites at day 7. In conclusion, BCP20/80-based composites showed enhanced osteogenic and vasculogenic differentiation potential compared to BCP60/40-based composites *in vitro*, suggesting that BCP20/80-based composites might be more promising for *in vivo* bone augmentation than BCP60/40-based composites.

1. Introduction

Bone tissue engineering has become a promising alternative for bone reconstruction. It is based on combinations of scaffolds, (stem) cells, and mechanical and/or chemical stimuli [1]. Autologous bone is the golden standard for clinical bone augmentation, for example, maxillary sinus floor elevation (MSFE) [2]. An alternative to the golden standard is biphasic calcium phosphate (BCP). BCPs are used as bone substitute materials for dental and orthopaedic applications. Ellinger et al. (1986) were the first to use the term BCP to describe bioceramics composed of hydroxyapatite (HA) and β-tricalcium phosphate (β-TCP) [3]. The chemical composition of BCP resembles the inorganic part of the natural bone matrix [4]. LeGeros and Daculsi reported in 1986 the first basic studies on the preparation of BCP and its *in vitro* properties [5, 6]. Thereafter, there was a significant increase in manufacture and use of commercial BCP as bone substitute. HA is rigid, brittle, and hardly resorbed after application in, for example, MSFE, while β-TCP degrades faster and has a different resorption pattern [7]. For efficient scaffold remodelling, a BCP with an optimum ratio of HA and β-TCP is desired. BCP with a HA/β-TCP ratio of 60/40 (BCP60/40) is successfully applied clinically [4, 8, 9], but

the high percentage of HA may hamper efficient scaffold remodelling. Whether BCP with a HA/β-TCP ratio of 20/80 (BCP20/80) is more desirable compared to BCP60/40 is still unclear.

BCP supports attachment, proliferation, and osteogenic differentiation of progenitor cells, and can be combined with regeneration-competent stem cells, such as adipose stem cells (ASCs), to introduce osteogenic bioactivity [10, 11]. Clinically relevant stem cell numbers with a high proliferative capacity can be easily extracted from human adipose tissue [12, 13]. ASCs have multilineage potential including the osteogenic lineage [14], and probably the endothelial lineage [15]. In the field of bone tissue engineering, ASCs have been successfully used for bone augmentation in MSFE [16].

Adequate vascularization is pivotal for cell survival of transplanted regeneration-competent stem cells in cell-based bone constructs. Osteogenesis and vasculogenesis are tightly coupled processes, and vascular development needs to be induced before osteogenesis can take place. This complexity has been a major challenge for engineering viable and functional bone grafts [17, 18]. Bioscaffolds, like natural human-derived extracellular matrix scaffolds, enhance vascular development [19]. Another bioscaffold is fibrin, an insoluble, elastic protein playing a crucial role in blood clotting and wound healing. Cell-based bone constructs might be combined with bioscaffolds to induce vascular development.

BCP combined with bioscaffolds, like fibrin, has demonstrated its ability to fill bone defects and promote bone healing in animal and clinical studies [20–23]. Fibrin gel provides a biocompatible carrier for cellular function, survival, proliferation, and differentiation [24]. Enhanced bone formation has been shown after injection of mesenchymal stem cell-(MSC-) seeded β-TCP in fibrin glue admixtures into the subcutaneous space on rat dorsa [24]. MSCs in fibrin gel used as a cell delivery system *in vivo* migrate out of the gel and invade ceramic scaffold [25].

A comparative study of BCP with different HA/TCP ratios in mandibular bone defects in minipigs showed that BCP20/80 results in similar bone formation as autologous bone after 52 weeks [26]. BCP scaffolds with a HA/β-TCP ratio of 60/40, a total porosity of 70% of which 50% were macropores (diameter 300–600 μm) and 30% were micropores (diameter < 10 μm) combined with fibrin sealant stimulated bone formation in animals and humans [20–23]. A pore size of 300–400 μm enhances bone formation and promotes neovascularization which is crucial before osteogenesis can take place in rats [27]. Therefore, in this study BCP biomaterials were used with a porosity of 90%, and a pore size of 500–1000 μm. Human MSCs seeded on BCP60/40 or BCP20/80 incorporated subcutaneously in the back of immunodeficient mice showed the highest amount of bone filling in the pore space and even distribution throughout the entire porous structure of the implant in BCP20/80-loaded composites [28].

Since both osteogenic and vasculogenic differentiation potential of regeneration-competent ASCs seeded on BCP60/40 or BCP20/80 incorporated in fibrin gels is crucial for bone formation in cell-based bone constructs, we aimed to test the osteogenic and/or vasculogenic differentiation potential as well as degradation of composites consisting of human ASCs seeded on BCP60/40 or BCP20/80 incorporated in fibrin gels for bone regeneration. We hypothesized that BCP60/40- and BCP20/80-based composites would enhance osteogenic and vasculogenic differentiation potential of ASCs. We expected that ASCs in BCP20/80-based composites would result in earlier osteogenic differentiation compared to ASCs in BCP60/40-based composites since degradation rate of BCP20/80-based composites is expected to be higher. ASCs were seeded on BCP60/40 or BCP20/80, with similar pore size and porosity, and then incorporated in fibrin gels or directly incorporated in fibrin gels, and cultured for 11 days. Cell attachment to both BCPs was assessed 30 min after cell seeding, and cell proliferation, osteogenic and vasculogenic differentiation potential, and fibrin degradation were assessed up to 11 days of culture.

2. Materials and Methods

2.1. Biphasic Calcium Phosphate Scaffolds. Two different calcium phosphate scaffolds were used: (1) Straumann® BoneCeramic 60/40 (Institut Straumann AG, Basel, Switzerland), a porous BCP scaffold composed of 60% HA and 40% β-TCP (BCP60/40), and (2) Straumann BoneCeramic 20/80 (Institut Straumann AG, Basel, Switzerland), a porous BCP scaffold composed of 20% HA and 80% β-TCP (BCP20/80). To avoid differences in osteogenic and vasculogenic differentiation potential of ASCs seeded on BCP60/40 or BCP20/80 incorporated in fibrin gels caused by the BCP fabrication process, the two different BCPs were produced by the same company, and had similar pore size and porosity (Table 1).

2.2. Donors. Subcutaneous adipose tissue was harvested from residues of abdominal wall resections of five healthy female donors (aged 33, 40, 47, 50, and 54), who underwent elective abdominal wall correction at the Tergooi Hospital Hilversum and a clinic in Bilthoven, Netherlands. The Ethical Review Board of the VU Medical Center, Amsterdam, Netherlands, approved the protocol. Informed consent was obtained from all patients.

2.3. Isolation and Culture of Human ASCs. ASCs were isolated from the resection material as described with minor modifications [12]. In brief, adipose tissue was cut into small pieces and enzymatically digested with 0.1% collagenase A (Roche Diagnostics GmbH, Mannheim, Germany) for 45 min at 37°C in phosphate-buffered saline (PBS) containing 1% bovine serum albumin (Roche Diagnostics GmbH) under continuous stirring. Ficoll® density-centrifugation step (Lymphoprep™; Axis-Shield, Oslo, Norway; 1000 ×g for 20 min, ρ = 1.077 g/mL Ficoll, osmolarity 280 ± 15 mOsm) was performed to remove remaining erythrocytes from the stromal vascular fraction. After centrifugation, the resulting stromal vascular fraction pellet containing ASCs was resuspended in Dulbecco's modified Eagle's medium (Life Technologies™ Europe BV, Bleiswijk, Netherlands), counted, frozen, and stored in liquid nitrogen until further use. Heterogeneity studies including cell characterization and

Table 1: Characteristics of the different BCPs used. Composition, particle size, porosity, and pore width of Straumann BoneCeramic 60/40 and Straumann BoneCeramic 20/80. HA: hydroxyapatite; β-TCP: β-tricalcium phosphate; BCP: biphasic calcium phosphate; SSA: specific surface area. Magnification 50x and 5000x.

Scaffold	Composition	Particle size (μm)	Crystal size (μm)	Porosity (%)	Interconnected pores (μm)	SSA (10^{-3} m^2/g)	Microporosity (%)
Straumann BoneCeramic BCP60/40	60% HA 40% β-TCP	500–1000	0.6–6.0	90	100–500	6.9	2.0
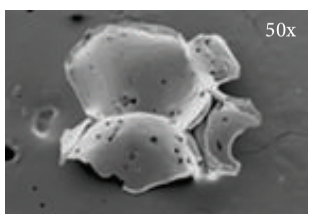	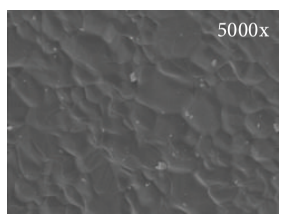						
Straumann BoneCeramic BCP20/80	20% HA 80% β-TCP	500–1000	1.0–6.0	90	100–500	9.5	2.0
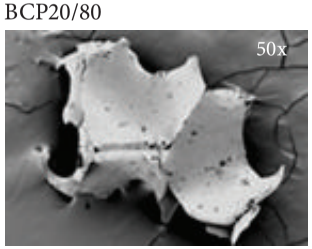	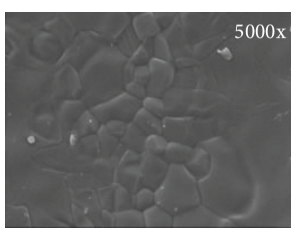						

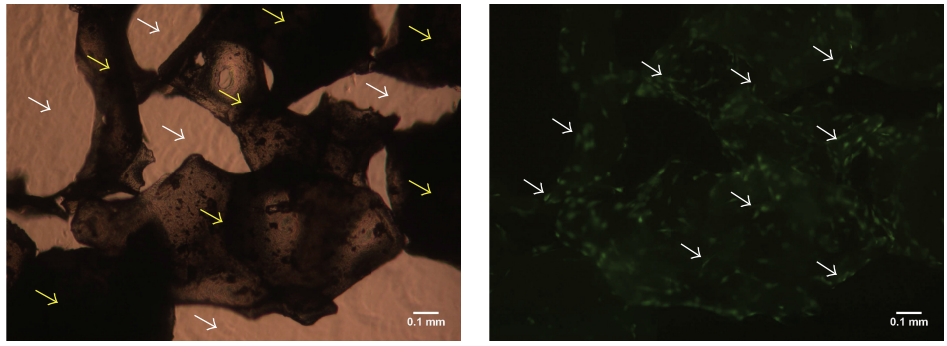

(a) (b)

Figure 1: BCP-based composite consisting of ASCs seeded on BCP scaffold incorporated in fibrin gel immediately after preparation. (a) BCP60/40 particles in fibrin gel visualized by light microcopy. Yellow arrows, BCP; white arrows, fibrin gel. (b) ASCs visualized by fluorescence (green) on the same BCP60/40 particles in fibrin gel. White arrows: ASCs. Magnification 40x.

multipotent differentiation potential of these cells have been reported previously by our group [12].

Cryopreserved stromal vascular fraction-containing cell suspensions of the abovementioned donors were pooled and cultured in α-Minimum Essential medium (α-MEM; Gibco, Life Technologies, Waltham, MA, USA) with 5% platelet lysate (see below), 100 U/mL penicillin (Sigma-Aldrich, Hamburg, Germany), 100 μg/mL streptomycin sulfate (Sigma-Aldrich), and 10 IU/mL heparin (LEO Pharma A/S, Ballerup, Denmark) to prevent coagulation at 37°C in a humidified atmosphere with 5% CO_2. The medium was refreshed three times a week. After reaching confluency, cells were harvested by incubation with 0.25% trypsin (Gibco, Invitrogen, Waltham, MA, USA) and 0.1% ethylenediaminetetraacetic acid (Merck, Darmstadt, Germany) in PBS at 37°C, replated, cultured until passage 2 (P2), and stored in liquid nitrogen until further use. Cryopreserved pooled ASCs-containing cell suspensions were thawed and seeded at 0.5×10^5 cells per T-225 culture flask (Greiner Bio-One, Kremsmuenster, Austria) in α-MEM with 2% platelet lysate, antibiotics, and 10 IU/mL heparin. Cells were cultured until P3-P4, and used for preparation of composites (see below).

2.4. Platelet Lysate. Pooled platelet products from five donors were obtained from the Bloodbank Sanquin (Sanquin, Amsterdam, The Netherlands). Platelet lysate was obtained by lysing the platelets through temperature-shock by freezing at −80°C, thawing, and centrifugation at 600 ×g for 10 min to eliminate remaining platelet fragments. The supernatant was added at 2% (v/v) to the medium.

2.5. Fibrin Gel. Human fibrinogen plasminogen-depleted protein (Enzyme Research Laboratories, South Bend, IN, USA) was dissolved in Medium 199 (M199; Gibco, Life Technologies) with antibiotics at 37°C for 1 h. Solubilized fibrinogen was filtered through a 0.2 μm filter (Millipore, Amsterdam, Netherlands), and the concentration measured with a Synergy HT® spectrophotometer (BioTek Instruments Inc., Winooski, VT, USA). To prepare fibrin gel, 2 mg/mL fibrinogen solution was polymerized with 1.0 IU/mL bovine α-thrombin (Enzyme Research Laboratories, South Bend, IA, USA) in a buffer containing 50 mM sodium citrate, 0.2 M sodium chloride, and 0.1% polyethylene glycol-8000, for 1 h at room temperature followed by 1 h at 37°C, and used for fibrin coating of polystyrene 48-well culture plates (Cellstar, Greiner Bio-One International GmbH, Frickenhausen, Germany), as well as for preparation of BCP60/40- and BCP20/80-based composites, and ASCs in gels (see below).

2.6. Preparation and Culture of Composites. Cultured ASCs were washed three times with PBS to remove platelet lysate, and seeded on either BCP60/40 or BCP20/80 and then incorporated in fibrin gels to prepare BCP60/40- and BCP20/80-based composites, or directly incorporated in fibrin gels. Twenty-five to 30 mg BCP60/40 or BCP20/80 was hydrated in PBS for 30 min. After PBS removal, 1×10^5 ASCs in 100 μL α-MEM were allowed to attach for 30 min at room temperature. Unattached cells were counted using a counting chamber (Optik Labor, Lancing, UK). Cell-seeded BCP scaffolds were embedded in fibrin gel and placed on fibrin-coated plates. Immediately after preparation, some composites were used for light microscopy to show the BCP particles in fibrin gel (Figure 1(a)), and to visualize ASCs on these particles in gel by cytotracker green (Invitrogen) according to the manufacturer's instructions (Figure 1(b)). As a control, 1×10^5 ASCs were embedded in fibrin and placed on fibrin-coated plates.

BCP60/40- and BCP20/80-based composites, and ASCs in gels were cultured in α-MEM without phenol red (Gibco, Life Technologies, Waltham, MA, USA) with 2% platelet lysate, antibiotics, 50 μg/mL 2-phospho-L-ascorbic acid trisodium salt (Sigma-Aldrich, Steinheim, Germany), and 10 IU/mL heparin for 11 days at 37°C in a humidified atmosphere with 5% CO_2. Medium was refreshed after 7 days.

2.7. Human ASC Proliferation in Composites and Fibrin Gels. Proliferation was assessed by determining cell number in BCP60/40- and BCP20/80-based composites and fibrin gels

at days 1 and 11 by using alamarBlue® fluorescent assay (Invitrogen, Frederick, MD, USA), according to the manufacturer's instructions. We found a linear relationship between alamarBlue fluorescence and cell number (data not shown). Fluorescence was read in medium samples at 530 nm with a Synergy HT spectrophotometer.

2.8. Alkaline Phosphatase Activity. Alkaline phosphatase (ALP) activity was measured to assess the osteoblastic phenotype of ASCs in BCP60/40- and BCP20/80-based composites and fibrin gels after 1 and 11 days of culture. Both composites and fibrin gels were transferred to 24-well culture plates (Cellstar), washed with PBS, crushed in 300 μL Milli-Q water, and stored at −20°C prior to further use. ALP activity was measured in the cell lysate using 4-nitrophenyl phosphate disodium salt (Merck, Darmstadt, Germany) as a substrate at pH 10.3, according to the method described by Lowry [29]. The absorbance was read at 405 nm with a Synergy HT spectrophotometer. ALP activity was expressed as μM per ng DNA.

2.9. Analysis of Gene Expression. At days 1, 7, and 11 of culture, BCP60/40- and BCP20/80-based composites and fibrin gels were transferred to 24-well culture plates, washed with PBS, crushed in 750 μL TRIzol® reagent (Life Technologies, Waltham, MA, USA), and stored at −20°C until further use. Total RNA was isolated using RNeasy® Mini Spin Columns (Qiagen Sciences, Gaithersburg, MD, USA) according to the manufacturer's instructions, and stored at −20°C until further use. Complementary DNA (cDNA) synthesis was performed using SuperScript® VILO™ cDNA Synthesis kit (Invitrogen, Life Technologies, Carlsbad, CA, USA), with 10.5 μL total RNA in a 15 μL reaction mix containing 3 μL VILO Reaction Mix and 1.5 μL SuperScript Enzyme Mix in a thermocycler GeneAmp® PCR System 9700 PE (Applied Biosystems, Foster City, CA, USA). cDNA was stored at −20°C prior to quantitative real-time PCR (qPCR) analysis, and diluted 5x for gene expression analysis. qPCR reactions were performed using 2 μL cDNA per reaction (10 μL total reaction volume containing 10 pmol of each primer) and LightCycler® 480 SYBR® Green I Mastermix (Roche Diagnostics, Mannheim, Germany) in a LightCycler 480 (Roche Diagnostics). qPCR conditions for all genes were as follows: 10 min preincubation at 95°C, followed by 35 cycles of amplification at 95°C for 2 s, 56°C for 8 s, 72°C for 10 s, and 82°C for 5 s, after which melting curve analysis was performed. With Light Cycler® software (version 1.2), crossing points were assessed and plotted versus the serial dilution of known concentrations of the standard (human primary bone: 2.5–0.004 ng/μL). A human trabecular bone sample (surgical waste) was taken from the femoral head, immediately (within 1 h) after hip surgery for cox-arthrosis, and used as positive control. The protocol was approved by the Ethical Review Board of the VU University Medical Center. PCR efficiency (E) was obtained by using the formula $E = 10^{-1/\text{slope}}$. Data were used only if E = 1.85–2.0. For gene expression analysis, the values of target gene expression were normalized to *YWHAZ* housekeeping gene expression to obtain relative gene expression. qPCR was used to assess expression of the following genes: *KI67*, runt-related transcription factor-2 (*RUNX2*), osteonectin (*ON*), dentin matrix acidic phosphoprotein-1 (*DMP1*), collagen-1 (*COL1*), collagen-3 (*COL3*), cluster of differentiation-31 (*CD31*), vascular endothelial growth factor-165 (*VEGFI65*), vascular endothelial growth factor-189 (*VEGFI89*), and endothlin-1 (*EDN1*). Primer sequences used for qPCR are listed in Table 2.

2.10. Fibrin Degradation. Fibrin degradation products were quantified using an enzyme-linked immunosorbent assay as described [30]. Briefly, the antibody fibrin degradation products-14 (FDP-14; TNO, Quality of Life, Leiden, Netherlands) recognizing different epitopes of fibrin degradation products was used as catching antibody. Fibrin degradation product concentrations in the medium of BCP60/40- and BCP20/80-based composites and fibrin gels were investigated after 1, 4, 7, and 11 days of culture, and Biopool standard (Trinity Biotech, Wicklow, Ireland) was used as a reference. Finally, monoclonal antibody D-dimer-13 (DD-13; TNO) labeled with horseradish peroxidase was used as tagging antibody. The coloring reaction was performed using 3,3′,5,5′-tetramethybenzidine (Sigma-Aldrich, St. Louis, MO, USA) and stopped with 1 M H_2SO_4. The optical density was read at 450 nm with Synergy HT spectrophotometer.

2.11. Statistical Analysis. Data were obtained from quadruple cultures of three independent experiments for BCP60/40-based composites and fibrin gels, and two independent experiments for BCP20/80-based composites. Data are presented as mean ± SEM. Two-tailed unpaired t-test was used to compare cell attachment to BCP60/40 and BCP20/80. Differences in alamarBlue fluorescence, ALP activity, and gene expression between BCP60/40- and BCP20/80-based composites and fibrin gels were tested with one-way variance of analysis (ANOVA). To compare fibrin degradation, one-way repeated measures ANOVA was performed. Differences were considered significant if $p < 0.05$. Statistical analysis was performed using IBM® SPSS® Statistics version 21 software package (SPSS Inc., Chicago, IL, USA) and GraphPad Prism® 5.0 (GraphPad Software Inc., La Jolla, CA, USA).

3. Results

3.1. Cell Attachment to BCP60/40 and BCP20/80. Cell attachment to BCP60/40 and BCP20/80 was similar (BCP60/40: 92730 ± 640, mean cell number ± SEM, n = 60 samples; BCP20/80: 98100 ± 350, n = 30 samples). After incorporation of cell-seeded BCP in fibrin gel, microscopic observations showed migration of cells towards the fibrin gel in both composites at day 1 (data not shown). The exact number of migrated cells could not be determined with the currently available assays. Future studies have to reveal the precise contribution of cells on BCP and migrated cells to the osteogenic and vasculogenic differentiation potential of both composites.

3.2. Increased Cell Proliferation and ALP Activity in BCP60/40- and BCP20/80-Based Composites. Cell proliferation in BCP60/40- and BCP20/80-based composites was similar, and 1.4–1.5-fold higher compared to fibrin gels (Figure 2(a)).

Table 2: Primer sequences for determination of osteogenic and vasculogenic differentiation potential through PCR. *YWHAZ*: tyrosine 3-monooxygenase/tryptophan 5-monooxygenase activation protein, zeta; *KI67*: proliferation marker; *RUNX2*: runt-related transcription factor-2; *ON*: osteonectin; *DMP1*: dentin matrix acidic phosphoprotein-1; *COL1*: collagen-1; *COL3*: collagen-3; *CD31*: cluster of differentiation-31; *VEGF165*: vascular endothelial growth factor-165; *VEGF189*: vascular endothelial growth factor-189; *EDN1*: endothlin-1; bp: base pairs.

Target gene		Oligonucleotide sequence	Product size (bp)	Annealing temperature (°C)
YWHAZ	Forward	5′ gATgAAgCCATTgCTGAACTTg 3′	229	56
	Reverse	5′ CTATTTgTgggACAgCATggA 3′		
KI67	Forward	5′ CCCTCAgCAAgCCTgAgAA 3′	202	56
	Reverse	5′ AgAggCgTATTAggAggCAAg 3′		
RUNX2	Forward	5′ ATgCTTCATTCgCCTCAC 3′	156	56
	Reverse	5′ ACTgCTTgCAgCCTTAAAT 3′		
ON	Forward	5′ CTgTCCAggTggAAgTAgg 3′	233	56
	Reverse	5′ gTggCAggAAgAgTCgAAg 3′		
DMP1	Forward	5′ TAggCTAgCTggTggCTTCT 3′	375	56
	Reverse	5′ AACTCggAgCCgTCTCCAT 3′		
COL1	Forward	5′ TCCggCTCCTgCTCCTCTTA 3′	336	56
	Reverse	5′ ggCCAgTgTCTCCCTTg 3′		
COL3	Forward	5′ gATCCgTTCTCTgCgATgAC 3′	279	56
	Reverse	5′ AgTTCTgAggACCAgTAggg 3′		
CD31	Forward	5′ AACAggAgggAgAgTATTACTg 3′	236	56
	Reverse	5′ TggTACTgCTggCCTggA 3′		
VEGF165	Forward	5′ ATCTTCAAgCCATCCTgTgTgC 3′	224	56
	Reverse	5′ CAAggCCCACAgggATTTTC 3′		
VEGF189	Forward	5′ ATCTTCAAgCCATCCTgTgTgC 3′	289	56
	Reverse	5′ CACAgggAACgCTCCAggAC 3′		
EDN1	Forward	5′ gTTTgTggCTTgCCAAggA 3′	207	56
	Reverse	5′ ACgTgCTCgggAgTgTTgA 3′		

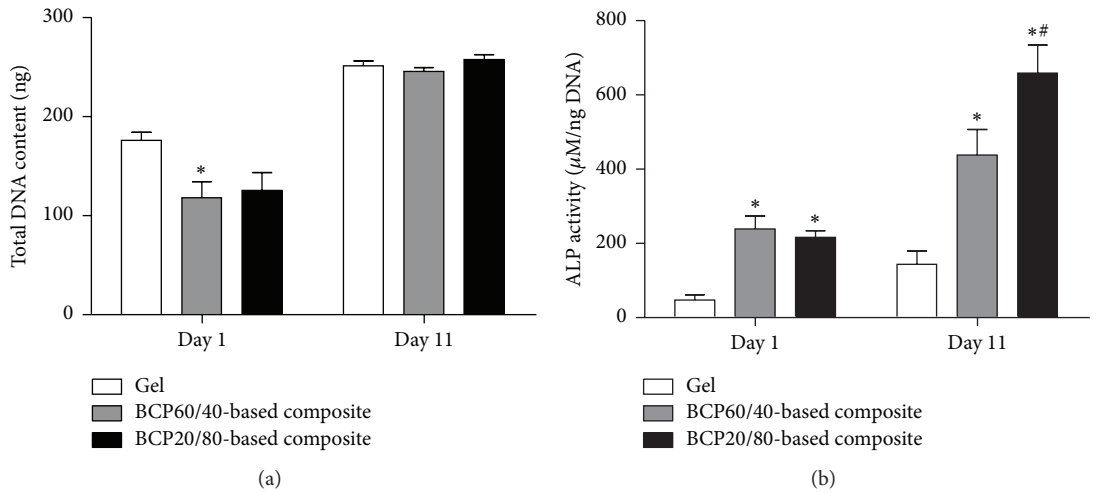

Figure 2: ASC proliferation and osteogenic differentiation in BCP60/40- and BCP20/80-based composites and fibrin gels at day 1 and 11 of culture. (a) Total DNA content in BCP60/40- and BCP20/80-based composites and fibrin gels. The increase in total DNA content from day 1 to day 11 was significantly higher in BCP60/40- and BCP20/80-based composites compared to fibrin gels, indicating similar proliferation in both composites, but increased proliferation in both composites compared to fibrin gels. (b) ALP activity in BCP60/40- and BCP20/80-based composites and fibrin gels. BCP20/80-based composites showed higher ALP activity compared to BCP60/40-based composites at day 11. ALP activity of both BCP60/40- and BCP20/80-based composites was higher compared to fibrin gels at days 1 and 11. Values are mean ± SEM (n = 8–12). *Significant effect of BCP60/40- or BCP20/80-based composites compared to fibrin gels, $p < 0.05$. #Significantly different from BCP60/40-based composites, $p < 0.05$. BCP, biphasic calcium phosphate; ALP, alkaline phosphatase.

BCP20/80-based composites showed a 1.5-fold increased ALP activity compared to BCP60/40-based composites at day 11 (Figure 2(b)). ALP activity in both composites was higher compared to fibrin gels at days 1 (4.6–5.0-fold) and 11 (3.1–4.6-fold; Figure 2(b)).

3.3. Enhanced Osteogenic Differentiation Potential of BCP20/80-Based Composites. No differences were observed in gene expression of the proliferation marker *KI67* in both composites at all time points. *KI67* gene expression was increased in BCP60/40- (3.0-fold) as well as BCP20/80-based composites (4.0-fold) compared to fibrin gels at day 11 (Figure 3(a)). Gene expression of the early osteogenic differentiation marker *RUNX2* in both composites was similar as well as compared to fibrin gels at all time points (Figure 3(b)). Expression of the early-to-late osteogenic differentiation marker *ON* in both composites was also similar at all time points (Figure 3(c)). BCP60/40-based composites resulted in decreased *ON* gene expression compared to fibrin gels at days 1 (0.2-fold) and 7 (0.1-fold). *ON* expression in BCP20/80-based composites was also decreased compared to fibrin gels at day 7 (0.2-fold; Figure 3(c)). Gene expression of the late osteogenic differentiation marker *DMP1* in BCP20/80-based composites was increased compared to BCP60/40-based composites at days 1 (2.1-fold) and 11 (9.2-fold). *DMP1* expression in BCP20/80-based was also increased compared to fibrin gels at days 1 (6.8-fold) and 11 (10.4-fold; Figure 3(d)). The extracellular matrix proteins *COL1* and *COL3* are expressed in osteogenesis and vasculogenesis. *COL1* gene expression was similar in both composites as well as compared to fibrin gels at all time points (Figure 3(e)). BCP60/40- and BCP20/80-based composites showed no significant differences in *COL3* gene expression at all time points (Figure 3(f)). *COL3* gene expression in BCP60/40-based composites was decreased compared to fibrin gels at day 7 (0.2-fold; Figure 3(f)).

3.4. Enhanced Vasculogenic Differentiation Potential of BCP20/80-Based Composites. BCP20/80-based composites showed increased *CD31* gene expression compared to BCP60/40-based composites at day 11 (2.8-fold), as well as compared to fibrin gels (6.2-fold; Figure 4(a)). *CD31* gene expression in both composites was decreased (2.3–2.8-fold) compared to fibrin gels at day 1 (Figure 4(a)). Gene expression of *VEGF165* in both composites was similar, as well as compared to fibrin gels at all time points (Figure 4(b)). BCP20/80-based composites showed increased *VEGF189* gene expression at days 1 (3.6-fold) and 7 (2.6-fold) compared to BCP60/40-based composites, as well as compared to fibrin gels at day 11 (5.5-fold; Figure 4(c)). Gene expression of *EDN1* in both composites showed no significant differences at all time points (Figure 4(d)). BCP60/40-based composites resulted in decreased *EDN1* gene expression compared to fibrin gels at day 7 (0.2-fold; Figure 4(d)).

3.5. Differences in Fibrin Degradation between Composites. A decreased concentration of fibrin degradation products in the medium of BCP20/80-based composites compared to fibrin gels was observed at day 1 (0.02-fold; Figure 5). The degradation products concentration was increased in BCP20/80-based composites compared to BCP60/40-based composites (1.7-fold) and fibrin gels at day 7 (1.8-fold), but reached similar levels at day 11.

4. Discussion

This study aimed to test the osteogenic and/or vasculogenic differentiation potential as well as degradation of composites consisting of human ASCs seeded on BCP60/40 or BCP20/80 incorporated in fibrin gels for bone regeneration. We found that (i) ASC attachment to both BCPs was similar; (ii) proliferation in BCP60/40- and BCP20/80-based composites was similar, but higher compared to fibrin gels; (iii) BCP20/80-based composites showed higher ALP activity compared to BCP60/40-based composites; (iv) gene expression of the late osteogenic marker *DMP1* in BCP20/80-based composites was increased compared to BCP60/40-based composites as well as to fibrin gels; (v) higher gene expression of the vasculogenic markers *CD31* and *VEGF189* was seen in BCP20/80-based composites compared to both BCP60/40-based composites and fibrin gels. Therefore, our results showed enhanced osteogenic and vasculogenic differentiation potential in BCP20/80-based composites compared to BCP60/40-based composites *in vitro*, suggesting that BCP20/80-based composites might be more promising for *in vivo* bone augmentation than BCP60/40-based composites.

We found that ASC attachment to both BCPs was similar, as shown earlier [31], indicating that different HA/β-TCP ratios of BCP did not affect ASC attachment. To ensure cell survival, proliferation, and differentiation of transplanted cell-seeded scaffolds after implantation, adequate nutrient and oxygen supply is crucial. A composite will easily become hypoxic after implantation in the body. ASCs cultured on fibrin gel-coated plates show enhanced proliferation under severe hypoxic conditions (1% oxygen) compared to conventional oxygen conditions (20% oxygen) [32]. Therefore, enhanced proliferation in both composites might be explained by a stimulatory effect of the BCP scaffold [33], and/or a hypoxic microenvironment, which likely also occurs after *in vivo* implantation.

The concept that degradation by-products can influence stem cell function, including cell fate decisions, is emerging [34]. TCP supports cell ingrowth and promotes osteogenic differentiation of osteoprogenitor cells [35]. The extent of dissolution of BCP depends on the HA/β-TCP ratio; the lower the ratio, the more the dissolution [36]. We found higher ALP activity, indicating enhanced osteogenic differentiation in BCP20/80-based composites compared to BCP60/40-based composites. This can be explained by the low HA/β-TCP ratio in BCP20/80 compared to BCP60/40, indicating higher Ca^{2+} ion release in BCP20/80-based composites which is crucial for bone formation. Degradation of surrounding material, that is, fibrin gel, can lead to cell-traction forces, which are crucial for osteogenic differentiation of human MSCs in a three-dimensional context and might explain the acceleration in osteogenic differentiation in both composites and fibrin gels [37]. This speculation is

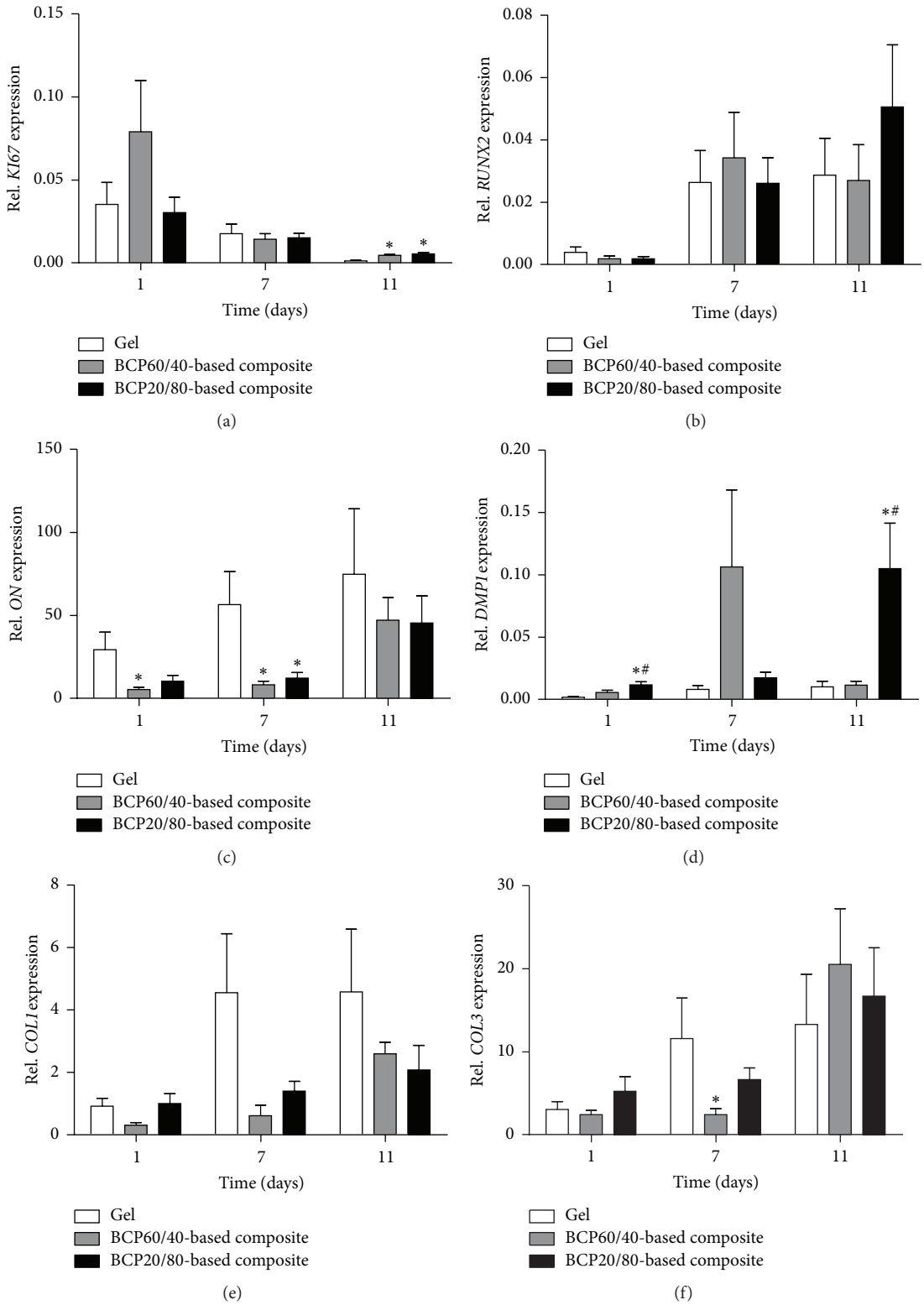

Figure 3: Gene expression of the proliferation marker *KI67* and osteogenic differentiation markers *RUNX2*, *ON*, *DMP1*, *COL1*, and *COL3* in BCP60/40- and BCP20/80-based composites and fibrin gels at days 1, 7, and 11 of culture. (a) BCP60/40- and BCP20/80-based composites showed increased *KI67* gene expression compared to fibrin gels at day 11. (b) *RUNX2* gene expression was similar for BCP60/40- and BCP20/80-based composites and fibrin gels at all time points. (c) BCP60/40- and BCP20/80-based composites showed similar *ON* gene expression at all time points. (d) BCP20/80-based composites showed increased *DMP1* gene expression compared to BCP60/40-based composites, as well as to fibrin gels at days 1 and 11. (e, f) Gene expression of *COL1* and *COL3* in BCP60/40- and BCP20/80-based composites was similar at all time points. Values are mean ± SEM (n = 7–12). *Significant effect of BCP60/40- or BCP20/80-based composites compared to fibrin gels, $p < 0.05$. #Significantly different from BCP60/40-based composites, $p < 0.05$. BCP, biphasic calcium phosphate; *KI67*, proliferation marker; *RUNX2*, runt-related transcription factor-2; *ON*, osteonectin; *DMP1*, dentin matrix acidic phosphoprotein-1; *COL1*, collagen-1; *COL3*, collagen-3.

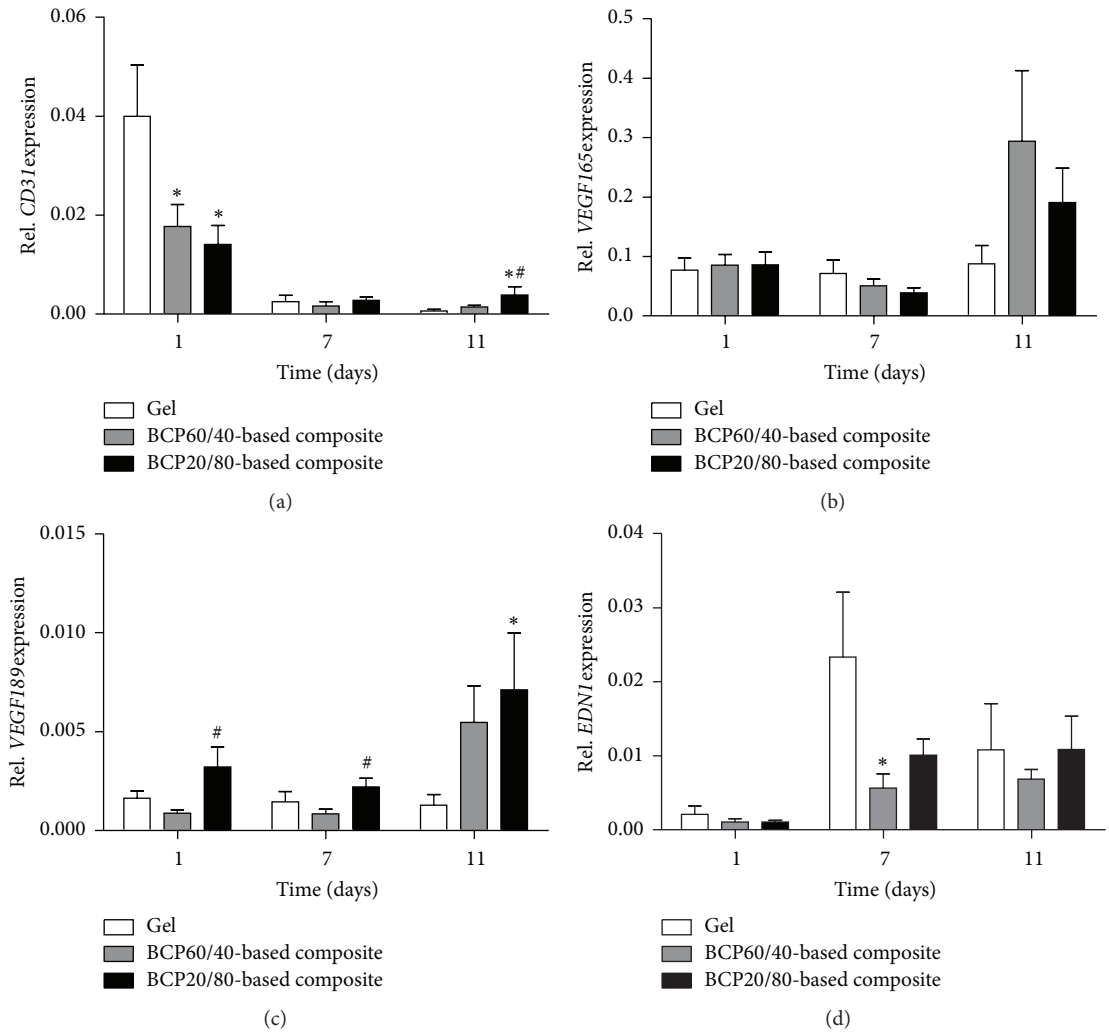

Figure 4: Gene expression of the vasculogenic differentiation markers *CD31*, *VEGF165* and *VEGF189*, and *EDN1* in BCP60/40- and BCP20/80-based composites, and fibrin gels at days 1, 7, and 11 of culture. (a) BCP20/80-based composites showed increased *CD31* gene expression compared to BCP60/40-based composites at day 11, as well as to fibrin gels. (b) BCP60/40- and BCP20/80-based composites demonstrated similar *VEGF165* gene expression at all time points. (c) BCP20/80-based composites showed increased *VEGF189* gene expression compared to BCP60/40-based composites at days 1 and 7. (d) BCP60/40- and BCP20/80-based composites showed similar *EDN1* gene expression at all time points. Values are mean ± SEM (n = 5–12). *Significant effect of BCP60/40- or BCP20/80-based composites compared to fibrin gels, $p < 0.05$. #Significantly different from BCP60/40-based composites, $p < 0.05$. BCP, biphasic calcium phosphate; *CD31*, cluster of differentiation-31; *VEGF165*, vascular endothelial growth factor-165; *VEGF189*, vascular endothelial growth factor-189; *EDN1*, endothelin-1.

consistent with our fibrin degradation products data showing increased fibrin degradation in BCP20/80-based composites compared to BCP60/40-based composites at day 7. We found higher expression of the late stage osteogenic differentiation marker *DMP1*, but similar expression of early and early-to-late osteogenic differentiation markers in BCP20/80-based composites compared to BCP60/40-based composites, suggesting that BCP20/80-based composites were in a later stage of osteogenic commitment compared to BCP60/40-based composites as well as to fibrin gels. Therefore, BCP20/80-based composites seem promising for implantation *in vivo* for enhanced bone formation.

Vascular development needs to be induced prior to osteogenesis. CD31 is expressed on the cell surface of endothelial and hematopoietic cells. BCP20/80-based composites showed increased *CD31* expression compared to BCP60/40-based composites indicating higher vessel-forming potency. During culture, *CD31* expression decreased, while *VEGF165*, *VEGF189*, and *EDN1* expression increased over time in both composites. The high expression of these vasculogenic genes indicates increased vasculogenic differentiation potential of both composites, although *CD31* expression decreased, which suggests that the number of endothelial progenitor cells had decreased over time. VEGF probably functions as a hypoxia-inducible angiogenic factor [38]. We found increased expression of the vasculogenic marker *VEGF189* in BCP20/80-based composites compared to fibrin gels. Therefore, BCP20/80-based composites might offer a hypoxic microenvironment for the ASCs, resulting in increased VEGF expression. Endothelin-1 is a potent vasoconstrictor and

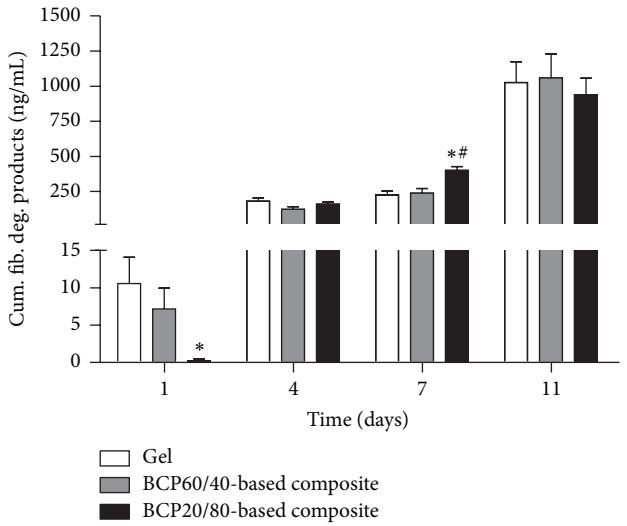

Figure 5: Differences in fibrin degradation of BCP60/40- and BCP20/80-based composites and fibrin gels. BCP60/40- and BCP20/80-based composites degradation was similar at day 11. BCP20/80-based composites resulted in increased concentration of fibrin degradation products compared to BCP60/40-based composites at day 7 of culture, as well as to fibrin gels. Values are mean ± SEM (n = 8–12). *Significant effect of BCP60/40- or BCP20/80-based composites compared to fibrin gels, $p < 0.05$. #Significantly different from BCP60/40-based composites, $p < 0.05$. BCP, biphasic calcium phosphate; cum, cumulative; fib, fibrin; deg, degradation.

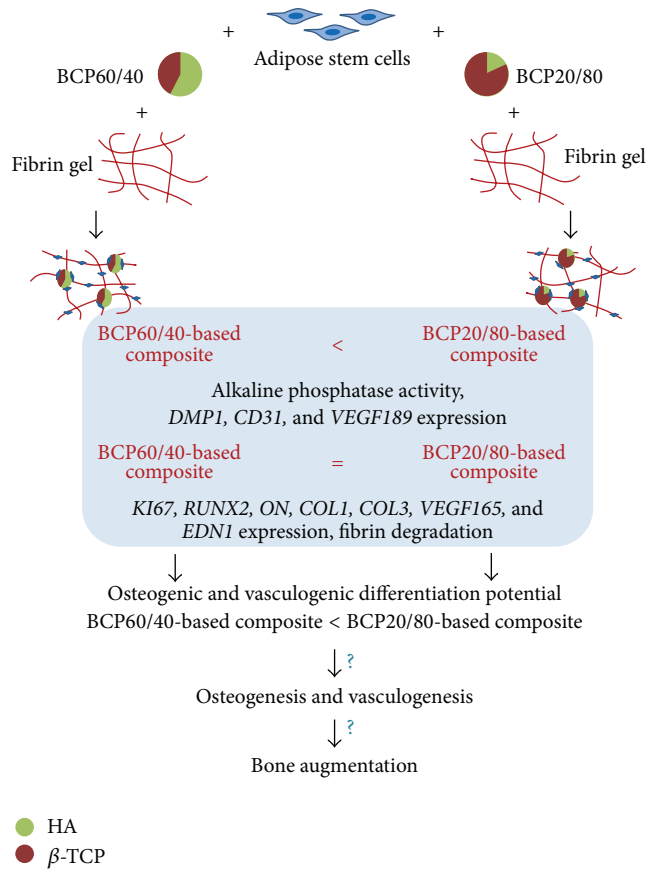

Figure 6: Development of BCP60/40-based composites and BCP20/80-based composites. Human adipose stem cells were seeded on BCP60/40 or BCP20/80 and incorporated in fibrin gels. BCP20/80-based composites showed enhanced osteogenic differentiation and vasculogenic potential compared to BCP60/40-based composites *in vitro*. =, similar in both composites; <, higher in BCP20/80-based composites compared to BCP60/40-based composites; HA, hydroxyapatite; β-TCP, β-tricalcium phosphate; *KI67*, proliferation marker; *RUNX2*, runt-related transcription factor-2; *ON*, osteonectin; *DMP1*, dentin matrix acidic phosphoprotein-1; *COL1*, collagen-1; *COL3*, collagen-3; *CD31*, cluster of differentiation-31; *VEGF165*, vascular endothelial growth factor-165; *VEGF189*, vascular endothelial growth factor-189; *EDN1*, endothelin-1.

has been identified originally in vascular endothelial cells. In osteoblasts, it stimulates inorganic phosphate transport, which is important for bone matrix calcification [39]. *EDN1* expression was increased during culture in both BCP60/40- and BCP20/80-based composites, which indicates enhanced vasculogenic and osteogenic differentiation potential. Future studies are needed to verify possible differences in blood vessel and bone formation using composites with ASCs, BCPs with different HA/β-TCP ratios, and fibrin gels *in vivo*.

The stem cell-matrix interface is a complex, dynamic microenvironment in which the cell and the material cooperatively dictate one another's fate and regulate stem cell differentiation [37]. Changes in fibrin composition will create different matrix stiffness and architectural properties, which will have impact on cellular response. Stem cells are extremely sensitive to elasticity of their surrounding matrix, through mechanosensitive ion channels, focal adhesions, cell surface receptors, actin cytoskeleton, and cell-cell adhesions, and they respond dramatically in lineage to the matrix presented [40]. Understanding the mechanisms of cellular sensory capabilities of ASCs will be relevant for application of our composites in tissue engineering. Fibrin remodelling was increased in BCP20/80-based composites compared to BCP60/40-based composites, but reached a similar level at the end of culture. The difference in fibrin remodelling possibly results in differences in cellular behaviour. The increase in fibrin degradation products during culture suggests dissolution of fibrin. After implantation of BCP60/40- and BCP20/80-based composites in the body, dissolution of the three-dimensional biological matrix fibrin will occur. As in fracture healing, cells migrate through the three-dimensional biological matrix and might be directly or indirectly directed through cytokines or growth factors released [41]. We observed migration of ASCs from BCP into the fibrin gel, which likely also occurs after implantation of composites *in vivo*. Later, fibrous tissue will be formed replacing fibrin, thereby holding cell-seeded BCP in place. Thus, our composites seem promising candidates for bone augmentation *in vivo*.

BCP-based composites might fit in a one-step surgical procedure. We used an expanded stem cell pool consisting of a homogeneous mixture of cells. However, only a freshly isolated stromal vascular fraction will fit in a one-step surgical procedure [42]. Stromal vascular fraction consists of a

heterogeneous mixture of cells including endothelial cells and lineage-committed progenitor cells and is not characterized while our stem cell pool was characterized [14, 43]. To determine whether freshly isolated stromal vascular fraction gives similar results in BCP-fibrin composites, it is necessary to test the osteogenic and/or vasculogenic differentiation potential of composites with freshly isolated stromal vascular fraction seeded on BCPs with different HA/β-TCP ratios incorporated in fibrin gels.

In summary, BCP20/80-based composites showed increased ALP activity as well as *DMP1*, *CD31*, and *VEGF189* gene expression compared to BCP60/40-based composites (Figure 6). In addition, BCP20/80-based composites showed increased fibrin degradation. Therefore, we conclude that BCP20/80-based composites showed enhanced osteogenic and vasculogenic differentiation potential compared to BCP60/40-based composites *in vitro*, suggesting that BCP20/80-based composites might be more promising for *in vivo* bone augmentation than BCP60/40-based composites.

Competing Interests

The authors declare that there is no conflict of interests regarding the publication of this paper.

Acknowledgments

The work of Fransisca A. S. van Esterik was supported by a grant from the University of Amsterdam for the stimulation of a research priority area Oral Regenerative Medicine. The authors thank Henk-Jan Prins, Benno Naaijkens, and Jolanda Hogervorst for adipose stem cell isolation, Ester Weijers and Pieter Koolwijk for providing fibrinogen, thrombin, and advice, Leo van Ruijven for microcomputed tomography evaluation, and Institut Straumann AG for providing Straumann BoneCeramic 20/80.

References

[1] M. N. Helder, M. Knippenberg, J. Klein-Nulend, and P. I. J. M. Wuisman, "Stem cells from adipose tissue allow challenging new concepts for regenerative medicine," *Tissue Engineering*, vol. 13, no. 8, pp. 1799–1808, 2007.

[2] S. A. Zijderveld, I. R. Zerbo, J. P. A. van den Bergh, E. A. J. M. Schulten, and C. M. ten Bruggenkate, "Maxillary sinus floor augmentation using a β-tricalcium phosphate (Cerasorb) alone compared to autogenous bone grafts," *The International Journal of Oral & Maxillofacial Implants*, vol. 20, no. 3, pp. 432–440, 2005.

[3] R. F. Ellinger, E. B. Nery, and K. L. Lynch, "Histological assessment of periodontal osseous defects following implantation of hydroxyapatite and biphasic calcium phosphate ceramics: a case report," *The International Journal of Periodontics and Restorative Dentistry*, vol. 6, no. 3, pp. 22–33, 1986.

[4] J. W. F. H. Frenken, W. F. Bouwman, N. Bravenboer, S. A. Zijderveld, E. A. J. M. Schulten, and C. M. ten Bruggenkate, "The use of Straumann® Bone Ceramic in a maxillary sinus floor elevation procedure: a clinical, radiological, histological and histomorphometric evaluation with a 6-month healing period," *Clinical Oral Implants Research*, vol. 21, no. 2, pp. 201–208, 2010.

[5] R. Z. LeGeros, "Variability of HAP/β-TCP ratios in sintered apatites," *Journal of Dental Research*, vol. 65, no. 110, p. 292, 1986.

[6] G. Daculsi, R. Z. LeGeros, E. Nery, K. Lynch, and B. Kerebel, "Transformation of biphasic calcium phosphate ceramics in vivo: ultrastructural and physicochemical characterization," *Journal of Biomedical Materials Research*, vol. 23, no. 8, pp. 883–894, 1989.

[7] R. Fujita, A. Yokoyama, T. Kawasaki, and T. Kohgo, "Bone augmentation osteogenesis using hydroxyapatite and β-tricalcium phosphate blocks," *Journal of Oral and Maxillofacial Surgery*, vol. 61, no. 9, pp. 1045–1053, 2003.

[8] C. M. Schmitt, H. Doering, T. Schmidt, R. Lutz, F. W. Neukam, and K. A. Schlegel, "Histological results after maxillary sinus augmentation with Straumann® BoneCeramic, Bio-Oss®, Puros®, and autologous bone. A randomized controlled clinical trial," *Clinical Oral Implants Research*, vol. 24, no. 5, pp. 576–585, 2013.

[9] C. Lindgren, A. Mordenfeld, and M. Hallman, "A prospective 1-year clinical and radiographic study of implants placed after maxillary sinus floor augmentation with synthetic biphasic calcium phosphate or deproteinized bovine bone," *Clinical Implant Dentistry and Related Research*, vol. 14, no. 1, pp. 41–50, 2012.

[10] A. K. Guha, S. Singh, R. Kumaresan, S. Nayar, and A. Sinha, "Mesenchymal cell response to nanosized biphasic calcium phosphate composites," *Colloids and Surfaces B: Biointerfaces*, vol. 73, no. 1, pp. 146–151, 2009.

[11] A. Vats, R. C. Bielby, N. S. Tolley, R. Nerem, and J. M. Polak, "Stem cells," *The Lancet*, vol. 366, no. 9485, pp. 592–602, 2005.

[12] M. J. Oedayrajsingh Varma, R. G. M. Breuls, T. E. Schouten et al., "Phenotypical and functional characterization of freshly isolated adipose tissue-derived stem cells," *Stem Cells and Development*, vol. 16, no. 1, pp. 91–104, 2007.

[13] C. M. Cowan, Y.-Y. Shi, O. O. Aalami et al., "Adipose-derived adult stromal cells heal critical-size mouse calvarial defects," *Nature Biotechnology*, vol. 22, no. 5, pp. 560–567, 2004.

[14] P. A. Zuk, M. Zhu, P. Ashjian et al., "Human adipose tissue is a source of multipotent stem cells," *Molecular Biology of the Cell*, vol. 13, no. 12, pp. 4279–4295, 2002.

[15] V. Planat-Benard, J.-S. Silvestre, B. Cousin et al., "Plasticity of human adipose lineage cells toward endothelial cells: physiological and therapeutic perspectives," *Circulation*, vol. 109, no. 5, pp. 656–663, 2004.

[16] H. J. Prins, M. N. Helder, J. R. Overman, C. M. ten Bruggenkate, E. A. J. M. Schulten, and J. Klein-Nulend, "Bone augmentation with adipose stem cells and calcium phosphate carriers for human maxillary sinus floor elevation: an ongoing phase I clinical trial," in *Proceedings of the 9th Annual Symposium on Adipose Stem Cells and Clinical Applications of Adipose Tissue*, p. 54, Miami, Fla, USA, 2011.

[17] D. L. Hutton, E. M. Moore, J. M. Gimble, and W. L. Grayson, "Platelet-derived growth factor and spatiotemporal cues induce development of vascularized bone tissue by adipose-derived stem cells," *Tissue Engineering Part A*, vol. 19, no. 17-18, pp. 2076–2086, 2013.

[18] C. Correia, W. Grayson, R. Eton et al., "Human adipose-derived cells can serve as a single-cell source for the *in vitro* cultivation of vascularized bone grafts," *Journal of Tissue Engineering and Regenerative Medicine*, vol. 8, no. 8, pp. 629–639, 2014.

[19] M. C. Moore, V. Pandolfi, and P. S. McFetridge, "Novel human-derived extracellular matrix induces *in vitro* and *in vivo* vascularization and inhibits fibrosis," *Biomaterials*, vol. 49, pp. 37–46, 2015.

[20] L. Le Guehennec, E. Goyenvalle, E. Aguado et al., "MBCP® biphasic calcium phosphate granules and tissucol® fibrin sealant in rabbit femoral defects: the effect of fibrin on bone ingrowth," *Journal of Materials Science: Materials in Medicine*, vol. 16, no. 1, pp. 29–35, 2005.

[21] D. Le Nihouannen, A. Saffarzadeh, O. Gauthier et al., "Bone tissue formation in sheep muscles induced by a biphasic calcium phosphate ceramic and fibrin glue composite," *Journal of Materials Science: Materials in Medicine*, vol. 19, no. 2, pp. 667–675, 2008.

[22] M. Bagot D'Arc and G. Daculsi, "Micro macroporous biphasic ceramics and fibrin sealant as a moldable material for bone reconstruction in chronic otitis media surgery. A 15 years experience," *Journal of Materials Science: Materials in Medicine*, vol. 14, no. 3, pp. 229–233, 2003.

[23] M. Bagot d'Arc, G. Daculsi, and N. Emam, "Biphasic ceramics and fibrin sealant for bone reconstruction in ear surgery," *Annals of Otology, Rhinology and Laryngology*, vol. 113, no. 9, pp. 711–720, 2004.

[24] Y. Yamada, J. S. Boo, R. Ozawa et al., "Bone regeneration following injection of mesenchymal stem cells and fibrin glue with a biodegradable scaffold," *Journal of Cranio-Maxillofacial Surgery*, vol. 31, no. 1, pp. 27–33, 2003.

[25] W. Bensaïd, J. T. Triffitt, C. Blanchat, K. Oudina, L. Sedel, and H. Petite, "A biodegradable fibrin scaffold for mesenchymal stem cell transplantation," *Biomaterials*, vol. 24, no. 14, pp. 2497–2502, 2003.

[26] S. S. Jensen, M. M. Bornstein, M. Dard, D. D. Bosshardt, and D. Buser, "Comparative study of biphasic calcium phosphates with different HA/TCP ratios in mandibular bone defects. A long-term histomorphometric study in minipigs," *Journal of Biomedical Materials Research Part B: Applied Biomaterials*, vol. 90, no. 1, pp. 171–181, 2009.

[27] Y. Kuboki, Q. Jin, and H. Takita, "Geometry of carriers controlling phenotypic expression in BMP-induced osteogenesis and chondrogenesis," *The Journal of Bone & Joint Surgery—American Volume*, vol. 83, supplement 1, part 2, pp. S105–S115, 2001.

[28] T. L. Arinzeh, T. Tran, J. Mcalary, and G. Daculsi, "A comparative study of biphasic calcium phosphate ceramics for human mesenchymal stem-cell-induced bone formation," *Biomaterials*, vol. 26, no. 17, pp. 3631–3638, 2005.

[29] O. H. Lowry, "Micromethods for the assay of enzyme II specific procedure. Alkaline phosphatase," *Methods in Enzymology*, vol. 4, p. 371, 1995.

[30] E. M. Weijers, M. H. van Wijhe, L. Joosten et al., "Molecular weight fibrinogen variants alter gene expression and functional characteristics of human endothelial cells," *Journal of Thrombosis and Haemostasis*, vol. 8, no. 12, pp. 2800–2809, 2010.

[31] J. R. Overman, E. Farré-Guasch, M. N. Helder, C. M. ten Bruggenkate, E. A. J. M. Schulten, and J. Klein-Nulend, "Short (15 minutes) bone morphogenetic protein-2 treatment stimulates osteogenic differentiation of human adipose stem cells seeded on calcium phosphate scaffolds *in vitro*," *Tissue Engineering Part A*, vol. 19, no. 3-4, pp. 571–581, 2013.

[32] E. M. Weijers, L. J. van den Broek, T. Waaijman, V. W. M. van Hinsbergh, S. Gibbs, and P. Koolwijk, "The influence of hypoxia and fibrinogen variants on the expansion and differentiation of adipose tissue-derived mesenchymal stem cells," *Tissue Engineering Part A*, vol. 17, no. 21-22, pp. 2675–2685, 2011.

[33] L. Saldaña, S. Sánchez-Salcedo, I. Izquierdo-Barba et al., "Calcium phosphate-based particles influence osteogenic maturation of human mesenchymal stem cells," *Acta Biomaterialia*, vol. 5, no. 4, pp. 1294–1305, 2009.

[34] A. M. C. Barradas, H. A. M. Fernandes, N. Groen et al., "A calcium-induced signaling cascade leading to osteogenic differentiation of human bone marrow-derived mesenchymal stromal cells," *Biomaterials*, vol. 33, no. 11, pp. 3205–3215, 2012.

[35] I. R. Zerbo, A. L. J. J. Bronckers, G. de Lange, and E. H. Burger, "Localisation of osteogenic and osteoclastic cells in porous β-tricalcium phosphate particles used for human maxillary sinus floor elevation," *Biomaterials*, vol. 26, no. 12, pp. 1445–1451, 2005.

[36] R. Z. LeGeros, "Biodegradation and bioresorption of calcium phosphate ceramics," *Clinical Materials*, vol. 14, no. 1, pp. 65–88, 1993.

[37] S. Khetan, M. Guvendiren, W. R. Legant, D. M. Cohen, C. S. Chen, and J. A. Burdick, "Degradation-mediated cellular traction directs stem cell fate in covalently crosslinked three-dimensional hydrogels," *Nature Materials*, vol. 12, no. 5, pp. 458–465, 2013.

[38] D. Shweiki, A. Itin, D. Soffer, and E. Keshet, "Vascular endothelial growth factor induced by hypoxia may mediate hypoxia-initiated angiogenesis," *Nature*, vol. 359, no. 6398, pp. 843–845, 1992.

[39] H. Masukawa, Y. Miura, I. Sato, Y. Oiso, and A. Suzuki, "Stimulatory effect of endothelin-1 on Na-dependent phosphate transport and its signaling mechanism in osteoblast-like cells," *Journal of Cellular Biochemistry*, vol. 83, no. 1, pp. 47–55, 2001.

[40] A. J. Engler, S. Sen, H. L. Sweeney, and D. E. Discher, "Matrix elasticity directs stem cell lineage specification," *Cell*, vol. 126, no. 4, pp. 677–689, 2006.

[41] B. A. Bromberek, P. A. J. Enever, D. I. Shreiber, M. D. Caldwell, and R. T. Tranquillo, "Macrophages influence a competition of contact guidance and chemotaxis for fibroblast alignment in a fibrin gel coculture assay," *Experimental Cell Research*, vol. 275, no. 2, pp. 230–242, 2002.

[42] E. Farré-Guasch, H.-J. Prins, J. R. Overman et al., "Human maxillary sinus floor elevation as a model for bone regeneration enabling the application of one-step surgical procedures," *Tissue Engineering Part B: Reviews*, vol. 19, no. 1, pp. 69–82, 2013.

[43] P. A. Zuk, M. Zhu, H. Mizuno et al., "Multilineage cells from human adipose tissue: implications for cell-based therapies," *Tissue Engineering*, vol. 7, no. 2, pp. 211–228, 2001.

Hindawi Publishing Corporation
Stem Cells International
Volume 2016, Article ID 8792191, 16 pages
http://dx.doi.org/10.1155/2016/8792191

Research Article

Bone Formation from Porcine Dental Germ Stem Cells on Surface Modified Polybutylene Succinate Scaffolds

Nergis Abay,[1] Gorke Gurel Pekozer,[1,2,3] Mustafa Ramazanoglu,[4] and Gamze Torun Kose[1,3]

[1]*Genetics and Bioengineering Department, Yeditepe University, 34755 Istanbul, Turkey*
[2]*Molecular Biology, Genetics and Biotechnology Department, Istanbul Technical University, 34469 Istanbul, Turkey*
[3]*Center of Excellence in Biomaterials and Tissue Engineering, BIOMATEN, METU, 06800 Ankara, Turkey*
[4]*Department of Oral Surgery, Faculty of Dentistry, Istanbul University, 34093 Istanbul, Turkey*

Correspondence should be addressed to Gamze Torun Kose; gamzekose@yeditepe.edu.tr

Received 24 March 2016; Revised 5 May 2016; Accepted 16 May 2016

Academic Editor: Bin Li

Designing and providing a scaffold are very important for the cells in tissue engineering. Polybutylene succinate (PBS) has high potential as a scaffold for bone regeneration due to its capacity in cell proliferation and differentiation. Also, stem cells from 3rd molar tooth germs were favoured in this study due to their developmentally and replicatively immature nature. In this study, porcine dental germ stem cells (pDGSCs) seeded PBS scaffolds were used to investigate the effects of surface modification with fibronectin or laminin on these scaffolds to improve cell attachment, proliferation, and osteogenic differentiation for tissue engineering applications. The osteogenic potentials of pDGSCs on these modified and unmodified foams were examined to heal bone defects and the effects of fibronectin or laminin modified PBS scaffolds on pDGSC differentiation into bone were compared for the first time. For this study, MTS assay was used to assess the cytotoxic effects of modified and unmodified surfaces. For the characterization of pDGSCs, flow cytometry analysis was carried out. Besides, alkaline phosphatase (ALP) assay, von Kossa staining, real-time PCR, CM-Dil, and immunostaining were applied to analyze osteogenic potentials of pDGSCs. The results of these studies demonstrated that pDGSCs were differentiated into osteogenic cells on fibronectin modified PBS foams better than those on unmodified and laminin modified PBS foams.

1. Introduction

Bone tissue engineering research focuses on differentiation of different sources of stem cells into bone cells on novel biocompatible biomaterials [1]. Also cell, scaffold, and biosignaling molecules with biomaterials have been used to form suitable cellular environments for tissue regeneration [2].

Scaffolds are the nonliving component of tissue engineering. Polybutylene succinate (PBS) is a novel biodegradable aliphatic polyester and can be used in bone tissue engineering applications because of its good mechanical properties, adjustable degradation rate, and nontoxic degradation products for the healing of bone defects. In addition to that, the use of PBS as a scaffolding material for bone repair is advantageous due to its processability. However, the surface modification is still required for the improvement of the biocompatibility and bioactivity of PBS scaffolds [3].

Surface modification by surface coating provides a way to conserve the mechanical properties of materials and to improve the surface biocompatibility of scaffolds. Most of the extracellular matrix (ECM) proteins, such as fibronectin, laminin, vitronectin, and collagen, have a sequence of amino acids like arginine–glycine–aspartic acid (RGD) which can be recognized by cells. Integrin-mediated binding of cells to those bioactive surfaces supports cell attachment, proliferation, and differentiation. Integrin-binding mechanism supplies communication of cells with noncellular surroundings. Besides, prolonged proliferation and survival can be observed by the coating of the surface of the scaffold with protein molecule. Particularly, either fibronectin or collagen type I treated surfaces exhibit both mineralization and the presence of bone formation better than laminin treated surfaces [4, 5].

In the bone tissue engineering field, bone marrow is the most widely used source of mesenchymal stem cells (MSCs)

[6]. However, bone marrow collection from a patient is an invasive procedure. Thus, scientists focused on finding new sources of mesenchymal stem cells which require minimally invasive collection procedures. Since the first isolation and characterization of stem cells from dental pulp in 2000 [7], dental tissues gained attention as rich mesenchymal stem cell sources due to accessibility and multilineage differentiation capacity [8].

Dental stem cells (DSCs) that are an attractive alternative source of MSCs easily differentiated into osteo-, adipo-, and neurogenic cells [9] are comprised of dental pulp stem cells (DPSCs), dental follicle stem cells (DFSCs), stem cells from exfoliated deciduous teeth (SHED), periodontal ligament stem cells (PDLSCs), stem cells from immature dental tissues such as apical papilla (SCAP), and dental germs which contain follicle and surrounding tissues (DGSCs) [10]. They are derived from neural crest and contain both ectodermal and mesenchymal components. Isolation of dental germ stem cells (DGSCs) from immature teeth such as third molars (wisdom teeth) has a definite advantage because of their ability to come from an organ. They are known as a source of more developmentally immature stem cells that have increased proliferation and differentiation potentials [9].

Domestic pig is preferred as an experimental model to isolate DGSCs due to its anatomical, physiological, and metabolic similarities with humans. Also, the diphyodont and heterodont dentition of the pig resemble that of humans which makes it a good candidate to study tooth morphogenesis and dental stem cell-mediated tissue engineering. In this study, bone regeneration potential of DGSCs on unmodified and fibronectin and laminin modified PBS scaffolds was investigated for the first time in the literature to treat the critical size bone defects.

2. Materials and Methods

2.1. Preparation of Poly(1,4-butylene succinate) Scaffolds. Poly(1,4-butylene succinate), extended with 1,6-diisocyanatohexane ($M_n = 5.0 \times 10^5$, $M_w/M_n = 2.7$) (Sigma-Aldrich Corporation, Germany) solution (4%), was prepared by using chloroform (Sigma-Aldrich Corporation, Germany) as a solvent. This solution was sonicated on ice for 2 h and then transferred into an Erlenmeyer flask. PBS scaffolds were prepared by solvent casting/particulate leaching technique using 300–500 μm salt particles for the leaching. In order to obtain a porous scaffold, salt was removed by leaving the scaffold overnight in distilled water and changing the distilled water 3 times until all the salt was removed. Porous polymers were then frozen at 80°C and freeze-dried for 48 h. Scaffolds were prepared by cutting into circular pieces of $1 \times 1\,cm^2$.

2.2. Characterization of PBS Scaffolds by Scanning Electron Microscopy. PBS scaffolds were coated with gold by Sputter Coater (BAL-TEC SCD 005, Germany) and samples were analyzed with Scanning Electron Microscope (Carl Zeiss EVO, Germany).

2.3. Degradation of PBS Scaffolds. For this study, PBS scaffolds that were weighed were put into 20 mL of 0.09% sodium azide in physiological isotonic saline solution (0.0095 M PO_4, pH: 7.32) in the sterile centrifuge tubes and they were placed into the shaking water bath at 37∘C. After 7th, 15th, 30th, 60th, and 120th days, pH of physiological isotonic saline solution was measured to observe the decrease of pH values due to the degradation of PBS scaffolds. After that, PBS scaffolds were lyophilized and their weights were measured. According to that, the rate of degradation of PBS scaffolds was analyzed.

2.4. Surface Modification of PBS Scaffolds with Adhesion Proteins. PBS foams were placed into the 24-well cell culture plates and sterilized in 70% ethanol for 2 h at 4°C. After they were washed with physiological saline solution, the foams were dried under the laminar flow cabinet (Telstar, Bio-II-A, Spain). PBS foams were coated with either fibronectin or laminin solution (50 μg/mL, 500 μL) (Roche, USA) by incubating them in CO_2 incubator (37°C, 5% CO_2) (Thermo Scientific, USA) for 2 h. When the incubation was completed, foams were washed with physiological saline solution to remove excess protein. Unmodified foams were used as control.

2.5. In Vitro Cell Culture Studies

2.5.1. Isolation and Culturing of pDGSCs. The cells were isolated by explant culture of tooth germs excised from 6-month-old domestic pigs under anesthesia and aseptic conditions approved by Yeditepe University Animal Research Local Ethics Committee (YÜDHEK). Tooth germ tissues were minced with a sterile scalpel and allowed cells to migrate from the tissue and adhere to tissue culture plate. When the cells reached confluency after 1 week, they were frozen for further use. For this study, cells that were previously frozen and kept in liquid nitrogen were thawed and expanded in an incubator at 37°C, in 5% CO_2 and 90% humidity. The medium was changed every other day until confluency was reached.

2.5.2. Characterization of pDGSCs by Flow Cytometry. pDGSCs (P1) were trypsinized and counted with hemacytometer (Hausser Bright-Line, USA). Cells (5×10^5) for each antibody and negative control were taken into FACS tubes. They were incubated with the antibodies for CD34 (BD Pharmingen, Philippines), CD45 (BD Pharmingen, Philippines), CD105 (Abcam, USA), CD90 (BD Pharmingen, Philippines), and CD44 (Abcam, USA) cell surface markers at room temperature for 1 h. Cells were washed with physiological saline solution and centrifuged at 2,200 rpm for 5 min to remove excess antibodies. After centrifugation, they were resuspended in 400 μL physiological saline solution and samples were analyzed in flow cytometer (FACSCalibur, Becton Dickinson, USA).

2.5.3. Cell Seeding. Cells (30,000/foam) were seeded onto the sterilized unmodified, fibronectin modified, and laminin modified PBS foams. Cell seeded foams were incubated in a CO_2 incubator at 37°C, in 5% CO_2 and 90%

humidity throughout 20 days. At day 3, osteogenic medium (Dulbecco's Modified Eagle Medium (DMEM: 4.5 g/liter glucose)) (Gibco Invitrogen, USA) supplemented with 10% fetal bovine serum (FBS) (Gibco-Invitrogen, USA), 100 units/mL Penicillin-Streptomycin-Amphotericin (PSA) (Lonza, Switzerland), 50 μM ascorbic acid (AppliChem, Germany), 100 nM dexamethasone (AppliChem, Germany), and 10 mM β-glycerophosphate (AppliChem, Germany) was added into the wells and it was changed twice a week. All tests were carried out in triplicate throughout the whole study.

2.5.4. Determination of Cell Viability on Modified and Unmodified PBS Scaffolds by MTS Assay. The CellTiter 96® Aqueous One Solution Cell Proliferation Assay (MTS) (Promega, USA) was applied to the cell seeded modified and unmodified foams at 3, 4, and 10 days of incubation.

For this assay, first of all, cell seeded PBS foams were transferred to new 24-well plate and washed with physiological saline solution to remove media which were left overnight before. MTS working solution (MTS: media mixture (1 : 5), 500 μL) was added onto each cell seeded foam in 24-well plate and incubated for 2 h at 37°C in a CO_2 incubator. After the incubation, 200 μL of solution from each well was transferred into a 96-well plate. Absorbances were measured at 490 nm by using Elisa Plate Reader (Bio-Tek, Elx800, USA). Absorbance values were then converted to cell numbers according to a calibration curve that was constructed by using known cell numbers.

2.5.5. Alkaline Phosphatase Assay. Alkaline phosphatase (ALP) (Randox, UK) assay was applied to pDGSCs on modified and unmodified PBS scaffolds at 4, 10, and 20 days of incubation. In this assay, the absorbance was measured at 405 nm for time points of 0, 2, 4, 6, 8, 10, 12, and 14 min by Elisa Plate Reader. After the measurement of absorbance values, the slope of the absorbance versus time plot was used to calculate the alkaline phosphatase activity per min.

After the measurement of absorbance values, DNA was isolated from each sample and their DNA concentrations were measured using NanoDrop (Implen NanoPhotometer® P-Class, USA). To get normalized values, absorbance values were divided into DNA concentrations of each sample and the normalized ALP graph was constructed.

2.5.6. Determination of Mineralization by von Kossa Staining. von Kossa staining (Sigma-Aldrich Corporation, Germany) procedure was used to determine the extent of minerals deposited on PBS scaffolds. Mineralization of pDGSCs seeded on unmodified and fibronectin and laminin modified PBS scaffolds and TCP at the end of 10 and 20 days of incubation was evaluated. In this method, silver nitrate solution (500 μL) (Sigma-Aldrich Corporation, Germany) was added onto PBS scaffolds and the plate was exposed to ultraviolet light for 30 min. Positively charged silver ions reacted with negatively charged phosphates and carbonates in calcium deposits and were then reduced to black metallic silver by UV light. After that, the scaffolds were washed with physiological saline solution and the reaction was stopped with the addition of 500 μL of 5% sodium thiosulfate (Sigma-Aldrich Corporation, Germany). After scaffolds were washed with physiological saline solution, their images were obtained by inverted microscope (Nikon Eclipse TC 100, USA). Ultimately, cells were stained with nuclear fast red to label the nucleus and cytoplasm of cells to make cells apparently visible for brightfield microscopy.

2.5.7. Immunostaining of PBS Scaffolds. Cells on the scaffolds were fixed using 3.7% formalin containing 0.001% Tween® 20 (AppliChem, Germany) for 30 min at room temperature after 10 and 20 days of incubation. After fixation, samples were incubated with 3% FBS in physiological saline solution at room temperature for 10 min to prevent unspecific binding of the dyes used for confocal microscopy study.

Alexa Fluor 546 Phalloidin (Molecular Probes, Invitrogen, USA) dye was mixed with 1.5% FBS in physiological saline solution with a ratio of 2 : 100, and this mixture was added onto each sample. Scaffolds were incubated with Phalloidin solution for 1 h at 37°C and washed with physiological saline solution to remove excess Phalloidin.

For collagen type I staining (Millipore, USA), the primary antibody of collagen type I was mixed with 1.5% FBS in physiological saline solution with a ratio of 1 : 100. Solution of collagen type I primary antibody was added onto the foams and the samples were incubated at 37°C for 1 h. Then, samples were washed with physiological saline solution. Secondary antibody of collagen type I was mixed with physiological saline solution with a ratio of 1 : 100 and added onto the samples. Samples were incubated at 37°C for 1 h. After the incubation, samples were washed with physiological saline solution.

After the staining of the samples with Phalloidin or collagen type I, all samples were double stained with TO-PRO solution. For that purpose, TO-PRO-3 Iodide (Molecular Probes, Invitrogen, USA) dye was diluted with a ratio of 2 : 100 using 1.5% FBS in PBS solution. TO-PRO dye was added to the wells and samples were incubated at 37°C for 15 min. After the incubation, TO-PRO dye was removed, and samples were washed with physiological saline solution. Finally, all samples were cured with Prolong Gold antifade reagent (Invitrogen, USA) at 4°C overnight. The foams were observed using confocal microscope (Leica, Germany).

2.5.8. CellTracker CM-Dil Staining of PBS Scaffolds. CM-Dil stock solution (1 mg/mL) (Invitrogen, USA) was prepared from 50 μg CM-Dil powder. CM-Dil solution was used at 2 μM concentration to stain the cells at 37°C for 10 min. Cells were washed and then seeded onto the unmodified, fibronectin modified, and laminin modified PBS scaffolds. As a control, cells were also seeded onto the surface of tissue culture plates.

2.5.9. Real-Time PCR Analysis. Expressions of bone-specific genes such as osteopontin, osteocalcin, ALP, Runx2, and type I collagen were determined by real-time PCR analysis. Briefly, after 10 and 20 days of incubation period, total RNA was extracted from the cells on the scaffolds using RNA extraction kit (Thermo Scientific, USA). Total mRNA was

Table 1: Sequences of the primers used for the real-time PCR.

ALP	F: CGACAACTACCAGGCACAGT R: GCCCTCAGAACAAGATGCCT	Tm: 57°C	Product length: 248
Runx2	F: ACTGAACCCCACGCTTGTTC R: AGTCACCTCCGCTTTCAAGG	Tm: 59°C	Product length: 253
Osteopontin	F: AGTCCAACGAAAGCCCTGAG R: GCTTCGGATCTGCGGAACTT	Tm: 57°C	Product length: 292
Osteocalcin	F: CCTAGTGGTGCGGATTCTGG R: GCTGCGAGGTCTAGGCTATG	Tm: 55°C	Product length: 241
Collagen type I	F: GACATCCCACCAGTCACCTG R: CTCCCGTGGTTTCCTGGTC	Tm: 58°C	Product length: 229
Beta-actin	F: GACTTCGAGCAGGAGATGG R: GCACCGTGTTGGCGTAGAG	Tm: 56°C	Product length: 233

reverse-transcribed into cDNA using the Sensiscript RT Kit (Qiagen, Germany). Real-time PCR analysis was performed using Maxima SYBR Green Master Mix (Thermo Scientific, USA) and the reaction was carried out in Bio-Rad CFX96 Touch™ Real-Time PCR Detection System for cDNAs of osteogenic genes and beta-actin (β-actin) as housekeeping gene. β-Actin mRNA was used as an internal control for normalization. Sequences of primers for both osteogenic and housekeeping mRNAs are listed in Table 1.

3. Statistical Analysis

Statistical significance was assessed using two-tailed t-test on Excel. Differences were considered as statistically significant when $p \leq 0.05$ and $p \leq 0.1$.

4. Results

4.1. Characterization of Scaffolds by Scanning Electron Microscopy. PBS scaffolds were prepared by salt leaching technique and observed by SEM to investigate the surface characteristics and porosity. In Figure 1, the structural details were observed and the pore sizes were measured by Scion Image Analyzer. The average pore size was found around 100 μm. Appropriate pore size provides an advantage for cells to penetrate inside the scaffolds to support cell growth and development homogeneously throughout the scaffold. Also, porosity and pore size are important for nutrient and oxygen diffusion to the deep inside the scaffolds. According to the SEM images, the surfaces of PBS scaffolds were rough and provided cell attachment (Figure 1).

4.2. Degradation of PBS Scaffolds. In the first part of the experiment, the changes of pH values of PBS scaffolds were obtained on 7th, 15th, 30th, 60th, and 120th days of incubation (Figure 2). The pH level increased slightly during the first 30 days. After 30 days, decrease in pH level was observed. The changes in the pH were statistically not significant. It was observed that throughout 120 days of incubation there was no drastic change in the pH of the environment which might harm the cells.

In the second part of degradation experiment, % weight loss of PBS scaffolds throughout 120 days of incubation was investigated. It was observed that after 15 days % weight loss was approximately 11.2, and then it reached 69.93 after 30 days of incubation. At the end of 120 days of incubation, PBS scaffolds completely degraded (Figure 3).

Table 2: Cell surface antigen expression of pDGSCs.

Surface antigen	Percentage of positively marked pDGSCs
pDGSCs (only cells)	1.27
CD105	88.71
CD90	99.04
CD44	98.23
CD45	3.44
CD34	1.18

4.3. Characterization of pDGSCs by Flow Cytometry Analysis. The mesenchymal stem cell properties of pDGSCs were investigated by tagging mesenchymal stem cell related (CD105, CD90, and CD44) and hematopoietic stem cell (CD45 and CD34) related cell surface markers. Cells were negative for CD45 and CD34 hematopoietic stem cell markers and positive for CD105, CD90, and CD44 mesenchymal stem cell markers (Figure 4). Percentage of positively marked cells for each antibody is listed in Table 2. Cell surface marker expression shows that isolated cells were mesenchymal stem cells.

4.4. Cell Viability on PBS Scaffolds. The effect of fibronectin and laminin modification of PBS scaffolds on the proliferation of pDGSCs was investigated by MTS cell proliferation assay after 3, 4, and 10 days of incubation. Figure 5 showed that cell numbers increased in both modified and unmodified scaffolds through 10 days of incubation.

The highest cell number at all time points was found on TCP. However, at the end of 10-day incubation period, decrease in cell number was observed on TCP due to the cell death related to lack of available space. At the end of 3 days of incubation period, cell numbers were found as 1.5×10^4 on fibronectin modified scaffold, 1.3×10^4 on laminin modified scaffold, and 1.2×10^4 on unmodified scaffold. After 10 days of

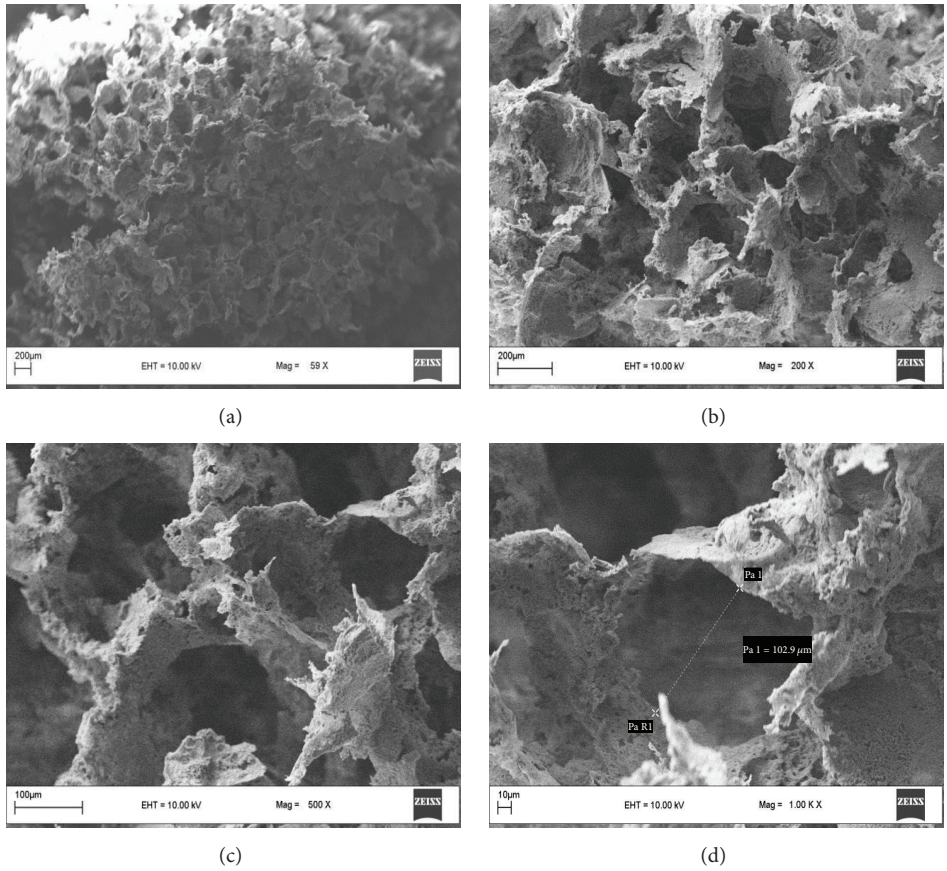

Figure 1: SEM images of PBS scaffolds: (a) 59x, (b) 200x, (c) 500x, and (d) 1,000x objectives.

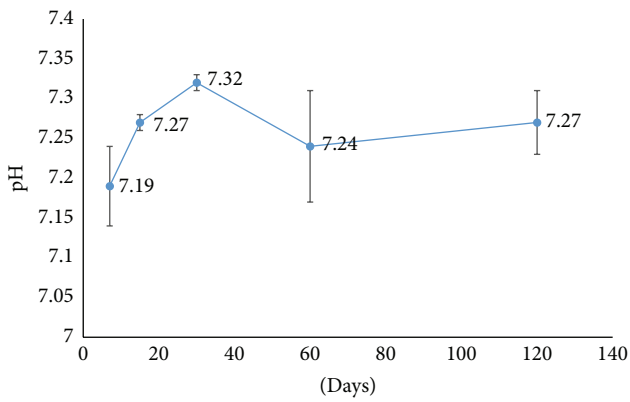

Figure 2: Degradation of PBS scaffolds with respect to pH throughout 120 days of incubation.

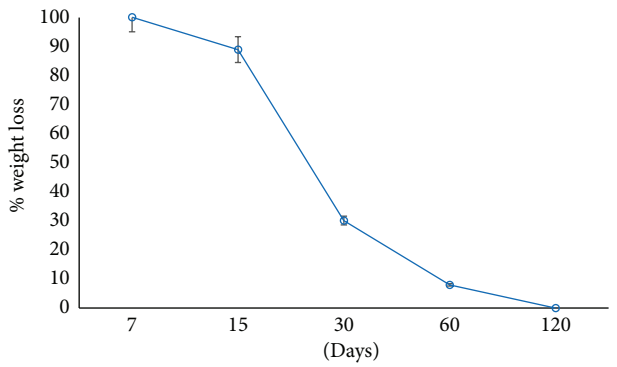

Figure 3: Degradation of PBS scaffolds with respect to weight during 120 days of incubation.

incubation, cell number on fibronectin modified scaffold (3.5×10^4 cells/foam) was significantly ($p \leq 0.05$) higher than the cell numbers on both laminin modified (1.4×10^4 cells/foam) and unmodified scaffolds (2.1×10^4 cells/foam).

4.5. Alkaline Phosphatase Assay. Alkaline phosphatase activity of pDGSCs on PBS foams was investigated at 4, 10, and 20 days. Alkaline phosphatase assay was used to measure the conversion of p-nitrophenyl phosphate to p-nitrophenol in the presence of alkaline phosphatase at 405 nm.

It was observed from Figure 6 that in all samples ALP expression was similar during early stage (day 4) of differentiation. At 10 days of incubation, approximately 1.3-fold difference in the ALP activity was observed when unmodified and fibronectin modified scaffolds were compared. ALP level was significantly ($p \leq 0.1$) higher in fibronectin modified samples than that in unmodified and laminin modified ones. It was

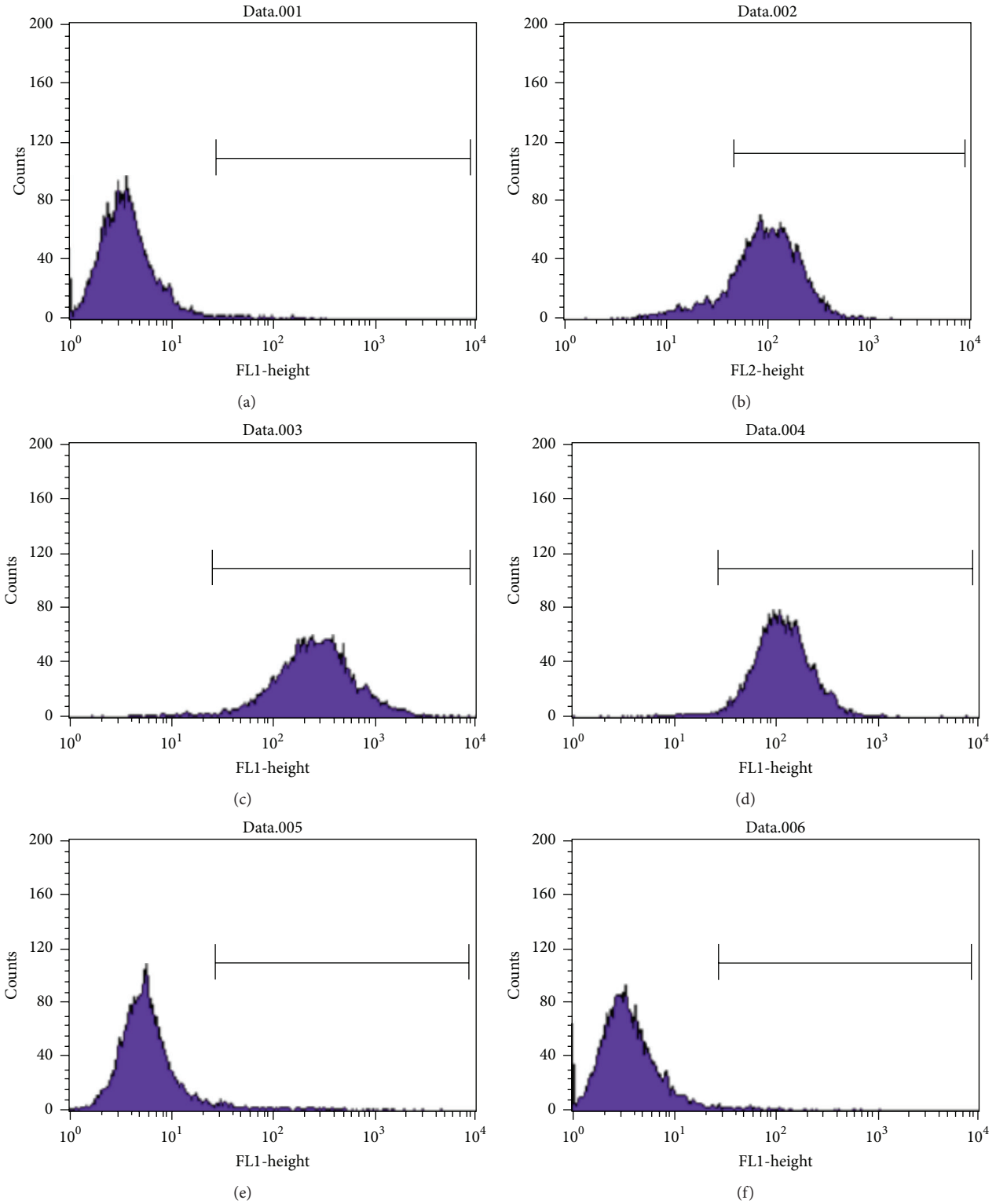

Figure 4: Flow cytometry histogram of pDGSCs with a label by FACSCalibur: (a) only cells without antibody, (b) CD105, (c) CD90, (d) CD44, (e) CD45, and (f) CD34.

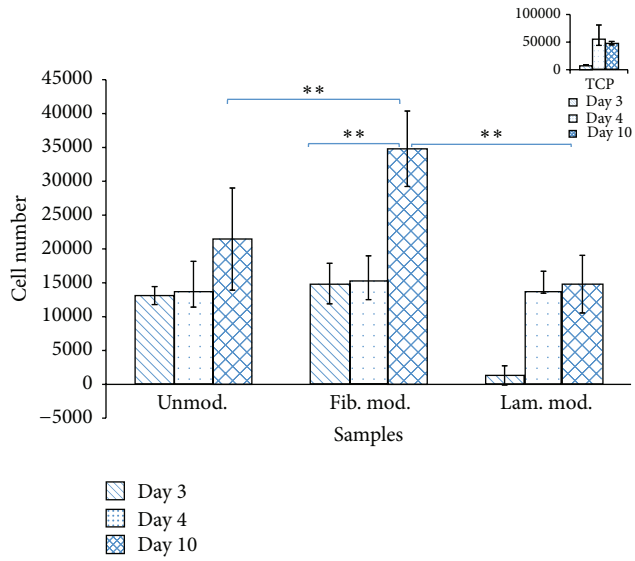

Figure 5: Cell proliferation on surface modified and unmodified foams after 3, 4, and 10 days of incubation. Initial cell seeding was 3×10^4 cells/sample ($^{**}p \leq 0.05$). Indent on the top right corner shows the cell proliferation on tissue culture plate.

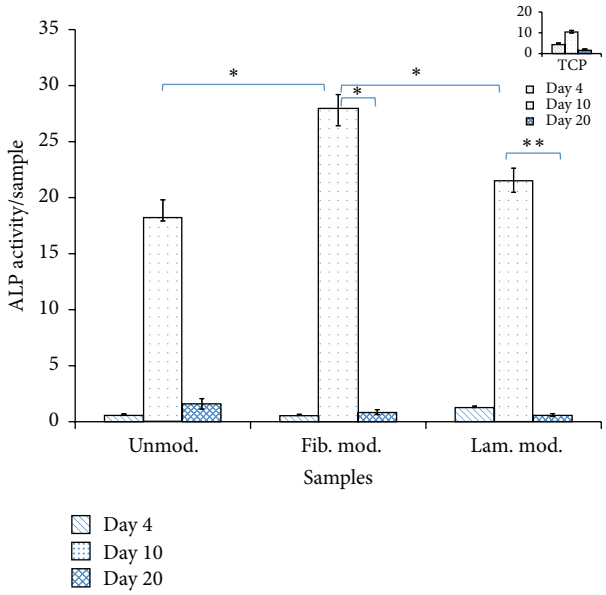

Figure 6: Normalized ALP activity of pDGSCs on modified and unmodified scaffolds throughout 20 days of incubation ($^{*}p \leq 0.1$ and $^{**}p \leq 0.05$). Indent on the top right corner shows ALP activity of cells seeded on tissue culture plate.

demonstrated that the differentiation of pDGSCs was higher on fibronectin modified samples than the others. Then, 12-fold significant decrease of alkaline phosphatase activity was seen from 10 to 20 days of incubation in unmodified scaffolds. Also, significant (35-fold) decrease from day 10 to day 20 was seen in modified scaffolds ($p \leq 0.1$ and $p \leq 0.05$).

4.6. von Kossa Staining. von Kossa staining was used for the observation of mineralization on unmodified, fibronectin modified, and laminin modified PBS scaffolds after 10 and 20 days of incubation. Mineralization of pDGSCs seeded on TCP was observed at the end of 10 and 20 days of incubation (Figures 7(c) and 7(d)). The brown regions demonstrated the presence of mineralized nodules on TCP. After 10 days of incubation, red regions that were the indication of the presence of cells appeared more than brown regions. However, red areas reduced at the end of 20 days of incubation.

Mineralization is known as a late marker of osteoblast differentiation. In this study, mineralization was observed at high levels on unmodified foams at the end of 10 days of incubation period compared to either laminin or fibronectin modified PBS scaffolds (Figure 7(a)). At this time point, the extent of mineralization was not too much on fibronectin modified scaffold whereas more mineralization was observed on the laminin modified scaffold. However, after 20 days of incubation, mineralization on the fibronectin modified scaffold was found to be higher than the others (Figure 7(b)).

4.7. Immunostaining with Confocal Microscopy. Immunostaining with confocal microscopy studies was conducted for the investigation of the cell-to-cell and cell-to-scaffold relation after 10 and 20 days of incubation periods. Alexa Fluor 546 Phalloidin and TO-PRO-3 Iodide were used to stain the cells.

When the microscope images of cells stained with Phalloidin were analyzed, the attachment of cells onto the surface of scaffolds was observed (Figure 8). At 10 days of incubation, cell-to-cell interaction on the unmodified and fibronectin and laminin modified PBS scaffolds was observed (Figures 8(a), 8(c), and 8(e)). It was also observed that cells mostly attached and proliferated around the pores of the foam where nutrient and oxygen diffusion is easier. Cell morphology and organization of actin filaments were investigated more clearly on TCP (Figures 8(g) and 8(h)). The amount of cell proliferation decreased from day 10 to day 20 on both TCP (Figure 8(h)) and PBS scaffolds (Figures 8(b), 8(d), and 8(f)).

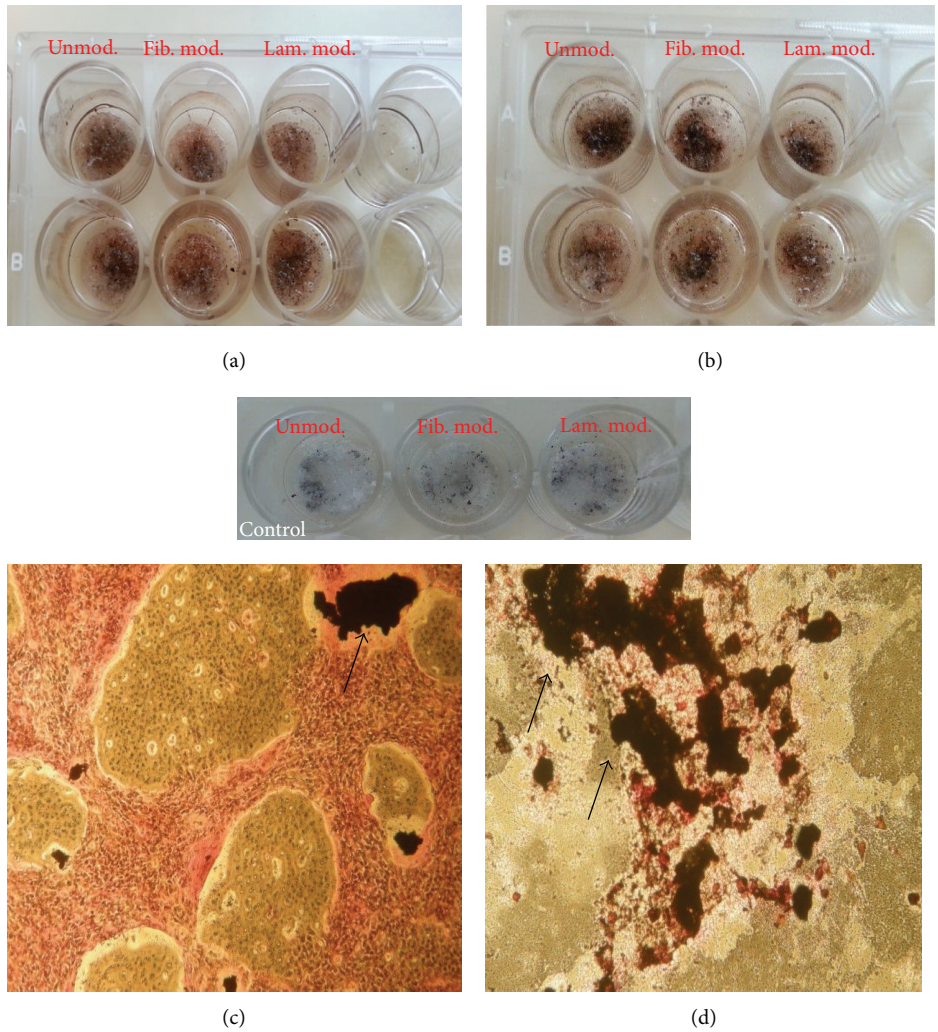

Figure 7: Mineralization of pDGSCs seeded on (a, b) unmodified and fibronectin and laminin modified PBS scaffolds; (c, d) TCP (10x) at the end of (a, c) 10 and (b, d) 20 days of incubation. Arrows indicate mineralized nodules.

In order to observe ECM synthesis by the cells seeded on modified and unmodified foams and on glass slides, type I collagen fibers were tagged with primary and secondary antibodies. Collagen type I fibers are the most important component of the organic matrix, as well as an important determinant of bone differentiation. When the images of cell seeded unmodified, fibronectin modified, and laminin modified scaffolds that were stained with collagen type I were observed (Figures 9(a) and 9(e)), the increase in the intensity of the green staining showing the synthesis of collagen could be seen from 10 to 20 days of incubation period, especially in fibronectin modified PBS scaffolds (Figures 9(c) and 9(d)). These images show induced bone differentiation, especially on fibronectin modified samples at 20 days of incubation. Also, throughout 20 days of incubation on TCP, the increase in collagen type I was observed around the cells (Figures 9(g) and 9(h)).

4.8. CellTracker CM-Dil Staining. CM-Dil is a fluorescent dye that has a thiol-reactive chloromethyl moiety which can bind to cellular thiols. By using this technique, viable cells can be stained without any fixation step, unlike other fluorescent dyes. In this way, the migration of viable cells and the increase of their cell number can be observed easily under the fluorescent microscope. The images showed that cells seeded on TCP, modified, and unmodified scaffolds still maintained their viability (Figure 10).

When the images were investigated, high amount of viable cells was seen on the unmodified PBS scaffolds at the end of 1 day of incubation (Figure 10(a)). Throughout 7 days of incubation, the increase in cell number was observed on the same unmodified PBS scaffold (Figure 10(b)). However, on either fibronectin or laminin modified scaffold, once cells were attached onto the surfaces, they migrate inside the pores and proliferate there from 1 to 7 days of incubation, especially on fibronectin modified scaffold (Figures 10(c) and 10(d)). Also, the cells were found around the pores, especially on fibronectin modified scaffolds. On TCP flasks, the highest cell number was observed throughout 7 days of incubation (Figures 10(g) and 10(h)). However, after 7 days of incubation period (data not shown), decrease in cell number was observed on TCP as it was expected due to the lack of

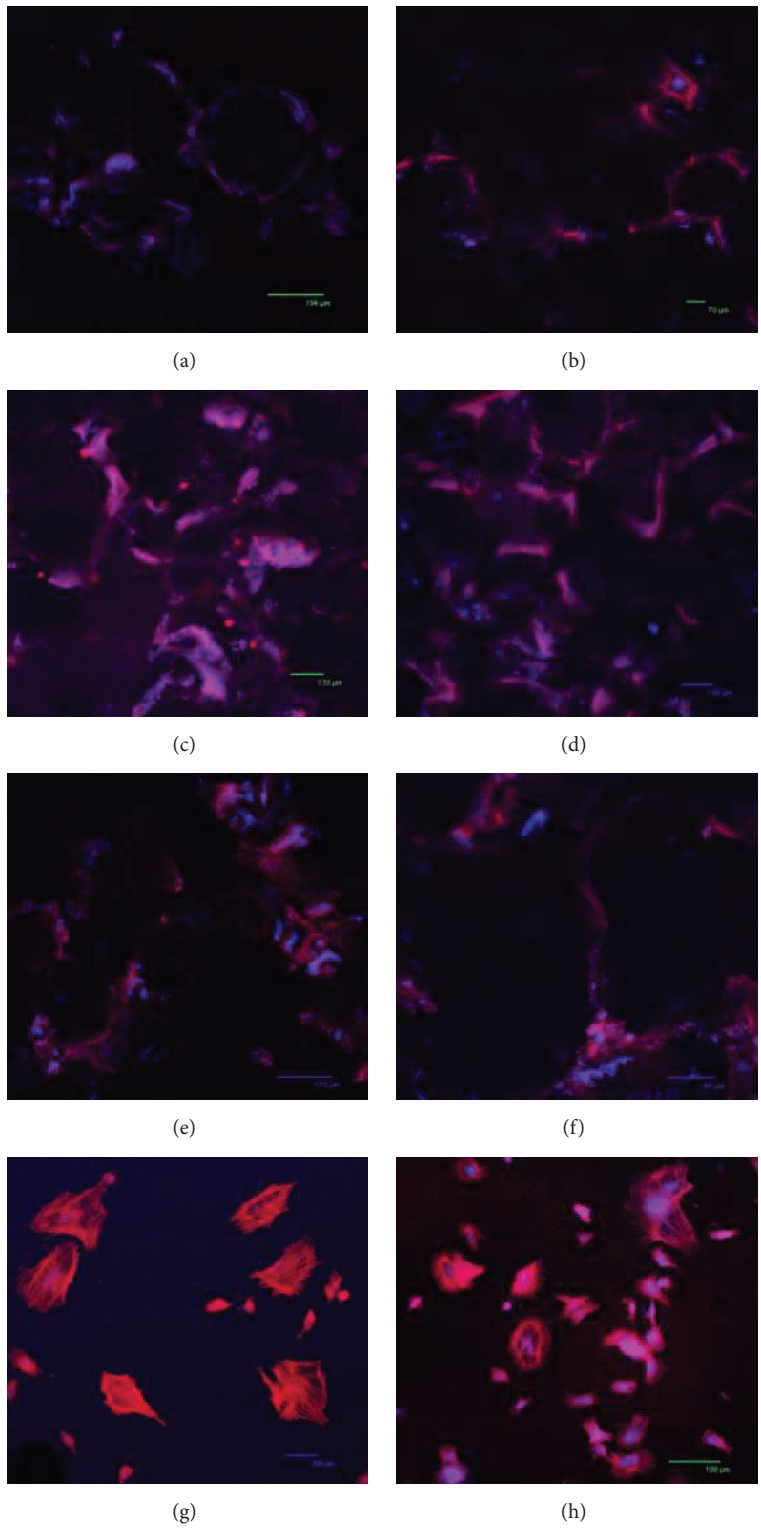

Figure 8: Confocal microscopy images of cells seeded on (a, b) unmodified; (c, d) fibronectin modified; and (e, f) laminin modified PBS scaffolds; (g, h) TCP after (a, c, e, g) 10 days and (b, d, f, h) 20 days of incubation. Red stains show actin filaments in the cytoskeleton of the cells stained with Alexa Fluor® 546 Phalloidin and blue stains show the nucleus of the cells stained with TO-PRO-3® Iodide. Scale bars (a) 194 μm, (b) 70 μm, (c) 133 μm, (d) 106 μm, (e) 170 μm, (f) 97 μm, (g) 69 μm, and (h) 186 μm.

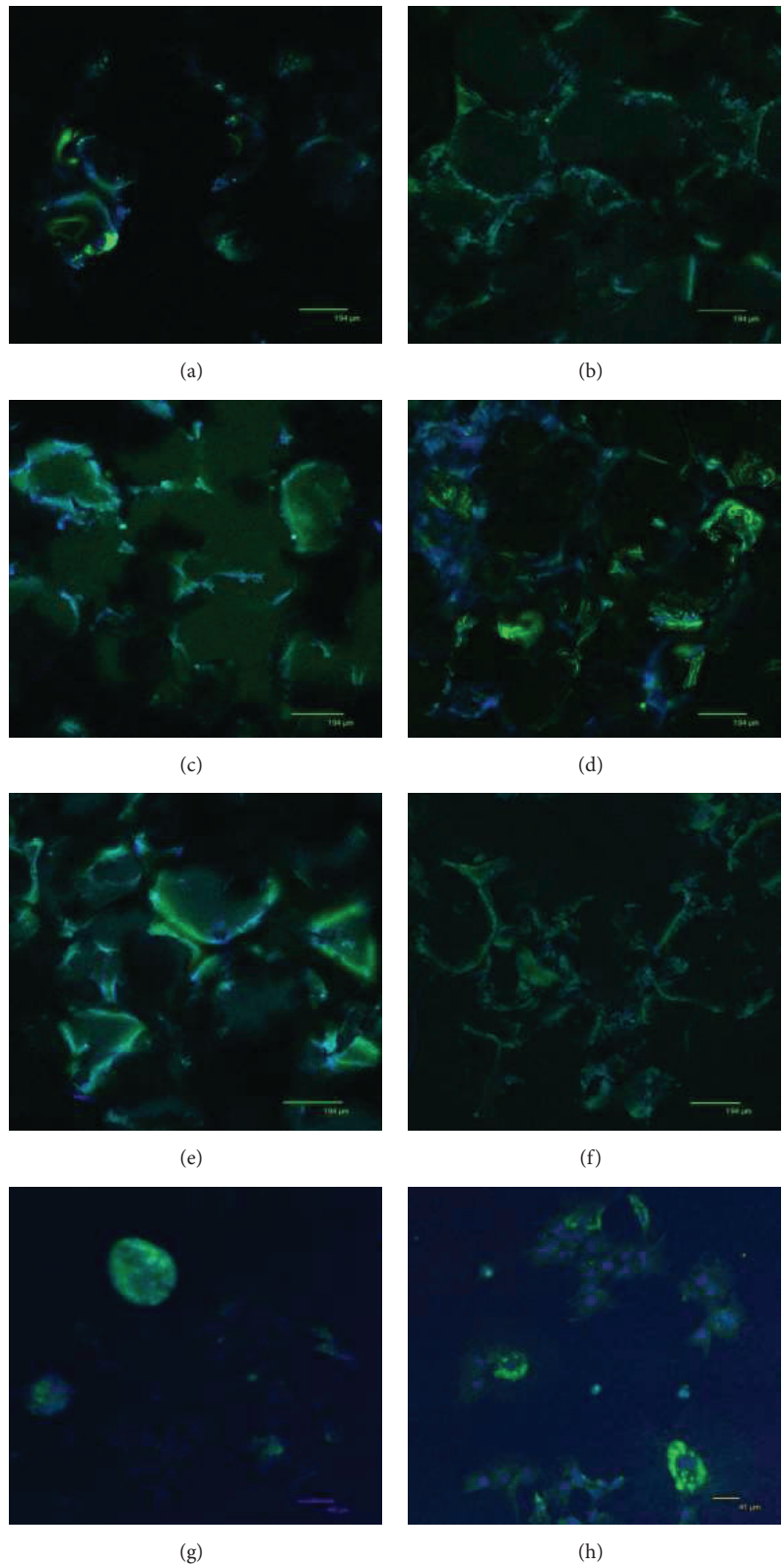

Figure 9: Confocal microscopy images of cells seeded on (a, b) unmodified; (c, d) fibronectin modified; and (e, f) laminin modified PBS scaffolds; (g, h) TCP after (a, c, e, g) 10 days and (b, d, f, h) 20 days of incubation. Green stains show the synthesis of collagen in the cytoskeleton of the cells stained with collagen type I and blue stains show the nucleus of the cells stained with TO-PRO-3 Iodide. Scale bars (a, b, c, d, e, f) 194 μm, (g) 85 μm, and (h) 41 μm.

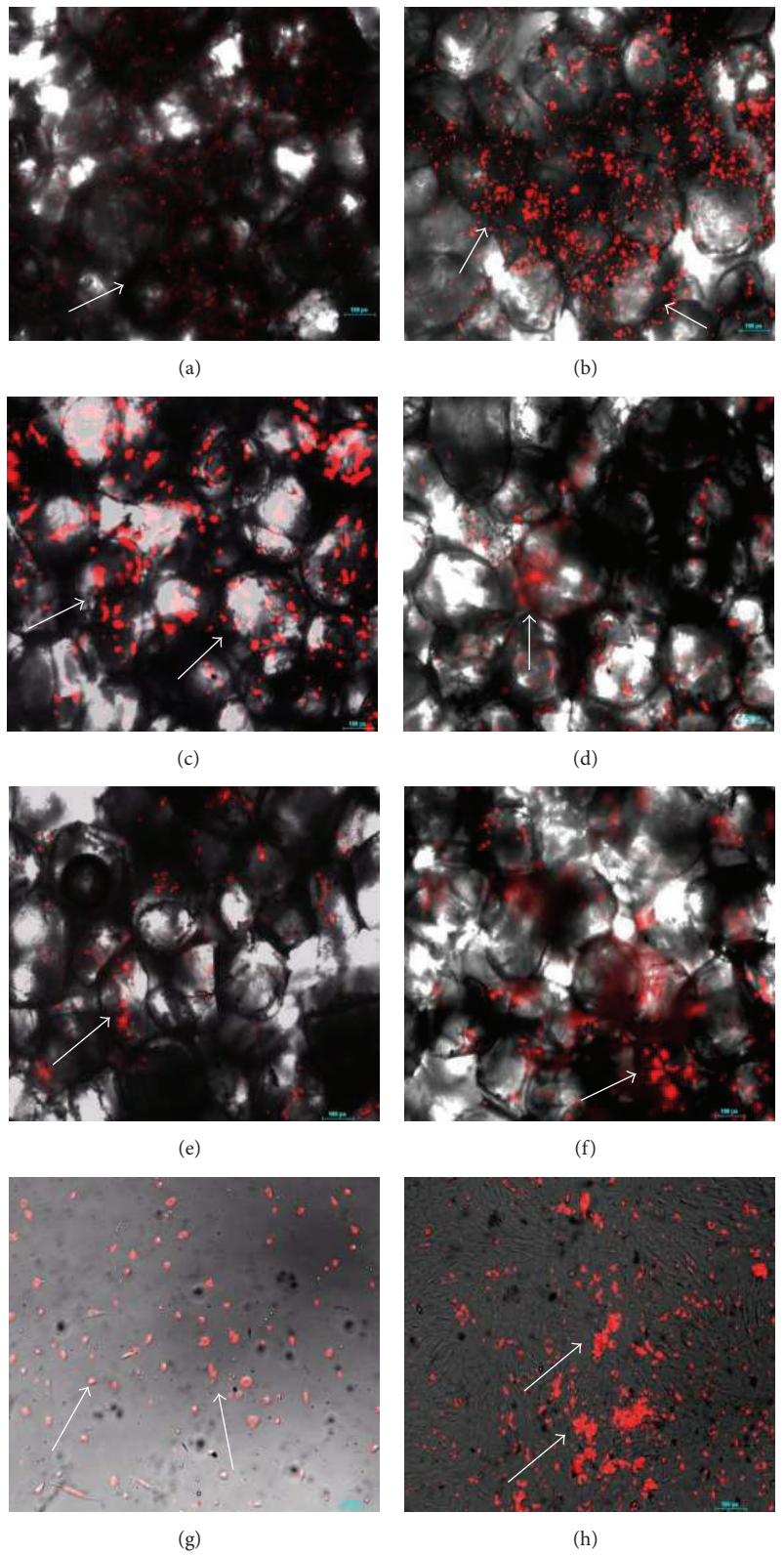

Figure 10: The images of viable cells stained with CellTracker™ CM-Dil on (a, b) unmodified; (c, d) fibronectin modified; and (e, f) laminin modified PBS scaffolds; (g, h) TCP after 1 day (a, c, e, g) and 7 days (b, d, f, h) of incubation. Scale bars show 100 μm. Arrows indicate viable cells.

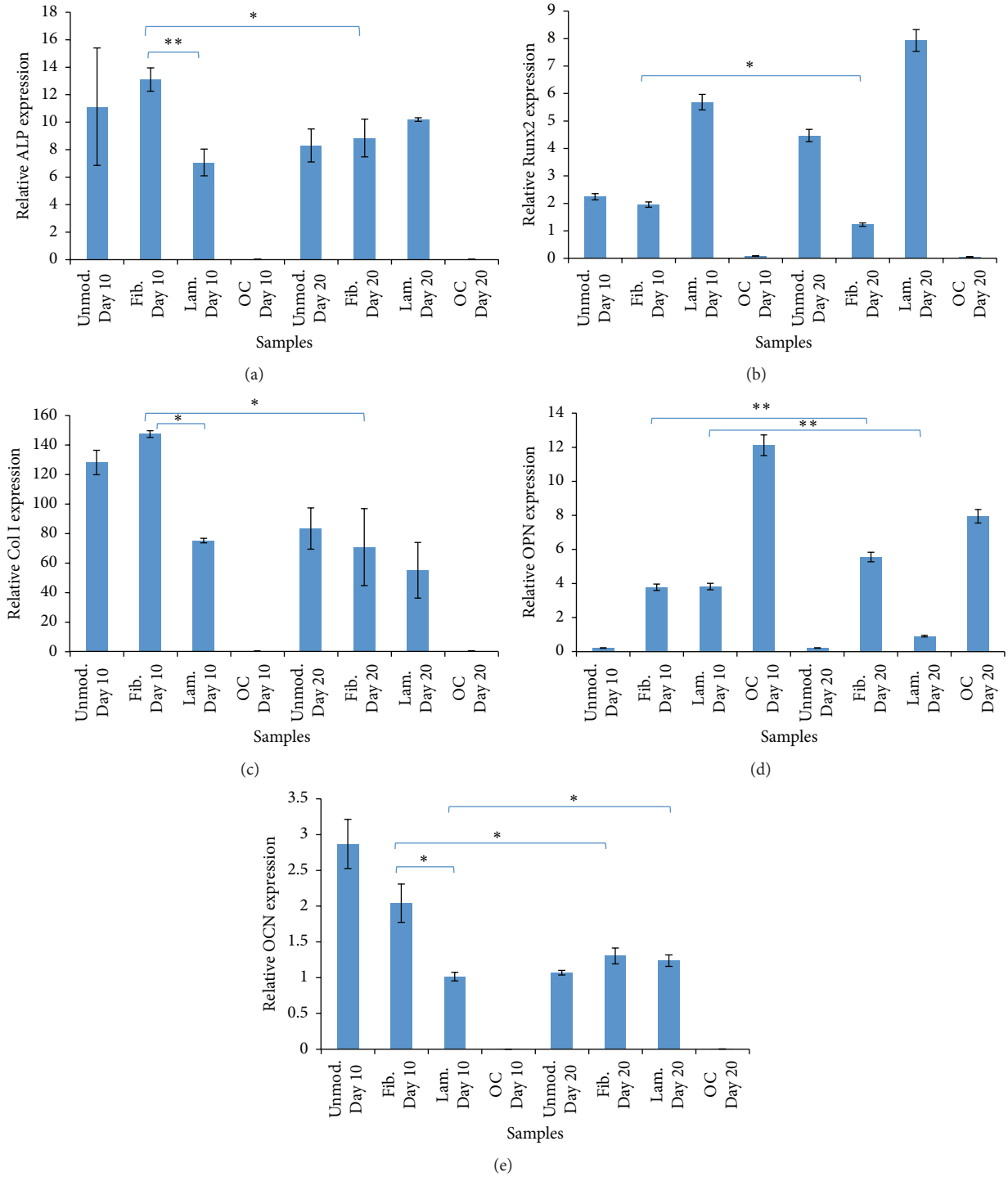

Figure 11: Expression levels of (a) alkaline phosphatase (ALP), (b) Runx2, (c) collagen type I (Col I), (d) osteopontin (OPN), and (e) osteocalcin (OCN) on fibronectin (fib.) or laminin (lam.) modified scaffolds, unmodified (unmod.) scaffolds, and TCP (OC refers to "only cell," i.e., cells seeded on TCP) throughout 20 days of incubation ($^{*}p \leq 0.1$ and $^{**}p \leq 0.05$).

available space for cells to grow more and the detachment of cells from the surface of TCP was seen.

4.9. Real-Time PCR. Real-time PCR was performed to determine the expression levels of bone-specific genes: alkaline phosphatase (ALP), Runx2, collagen type I (Col I), osteopontin (OPN), and osteocalcin (OCN) (Figure 11). The PCR results were normalized using the housekeeping gene, beta-actin.

According to the results, the highest ALP production was significantly observed on the fibronectin modified scaffold at day 10 whereas laminin modified scaffold showed lower

expression level of ALP ($^{**}p \leq 0.05$). As expected, significant decrease of the level of ALP expression on fibronectin modified scaffold was observed at day 20 ($^{*}p \leq 0.1$). Moreover, expression of Runx2 was significantly decreased from day 10 to day 20 on fibronectin modified scaffold ($^{*}p \leq 0.1$). However, on laminin modified scaffold, increase of the expression of Runx2 was observed throughout 20 days of incubation. Besides, collagen type I expression was significantly the highest on fibronectin and the lowest on laminin modified scaffolds at day 10. In fibronectin modified samples, at day 20, significant decrease in collagen type I level was observed ($^{*}p \leq 0.1$). Furthermore, although the expression level of osteopontin was similar on fibronectin and laminin modified scaffolds at day 10, it was significantly increased on fibronectin modified scaffold from day 10 to day 20 ($^{**}p \leq 0.05$) whereas decrease of osteopontin level was seen on laminin modified scaffold ($^{**}p \leq 0.05$). Finally, osteocalcin expression was observed to be significantly higher on fibronectin modified scaffold than on laminin modified scaffold at day 10. Throughout 20 days of incubation, the expression of osteocalcin decreased on fibronectin modified scaffold ($^{*}p \leq 0.1$).

5. Discussion

Designing a scaffold is an important part of tissue engineering and it requires a good knowledge of biomaterials and cell-surface interactions. A scaffold that is used in tissue engineering must be compatible with the selected cell type. Cell adherence to the substrate should be strong and maintained until the healthy tissue formation is observed.

In this study, polybutylene succinate (PBS) was used for the production of scaffolds by salt leaching technique due to good scaffolding properties of PBS, such as biocompatibility, biodegradability, nontoxicity, and porosity [2].

Pore size is a very important issue since pores are required for efficient flow of O_2 and nutrients, cellular penetration, production of extracellular matrix, and neovascularization of the scaffold to achieve bone formation. It is well accepted that for bone tissue engineering purposes pore size should be within a range of 100–900 μm [6]. In the present study, pore sizes of PBS scaffolds were measured as approximately 100 μm which is within the accepted range.

In one of the studies, biodegradable textile-based structures were used for tissue engineering applications. For that purpose, silk fibroin (SF) filaments and polybutylene succinate (PBS) scaffolds were chosen. Although SF is a preferable scaffold for bone tissue engineering, SF matrices have low porosity because of their compact structures. To get the SF matrices with higher porosity and 100% interconnectivity, it can be used with PBS. PBS/SF construction can help us to observe porosity in desired ranges and get the minimal pore size (~75–100 μm) required for bone tissue engineering studies. This study also proved that PBS scaffolds are suitable and usable to get desirable porosity of constructs [11].

The degradation behaviour of PBS scaffolds was also investigated in this study since it affects cell behaviour and tissue regeneration. The degradation rate is a balance between scaffold degradation and tissue regeneration [12]. For that reason, pH was measured at the end of 7, 15, 30, 60, and 120 days of incubation since the degradation products of PBS are butyric acid and succinic acid which could make the environment acidic enough to disturb the cells seeded on the scaffolds. During 120 days of incubation, pH was generally stable and its decrease was not in a level that would disturb the cells since the cells were not exposed to too much acidic environment by the degradation products of PBS and increase of cell proliferation was observed throughout 10 days of incubation in MTS assay. Wuertz et al. also studied the effect of pH on MSC proliferation. They showed that cell viability decreased with acidity [13]. The degradation of PBS scaffolds was also studied with respect to weight loss during 120 days of incubation. According to the results, weight loss started after 7 days of incubation and polymer was completely degraded after 120 days of incubation.

Although PBS is biocompatible enough, either surface modification of scaffolds with extracellular matrix proteins or blending of scaffolds with some biomaterials can also be applied in order to improve bioactivity of scaffolds. Both of them are recommended to observe increase in bioactivity. In one study, bioactivity of PBS scaffolds was improved by blending PBS with chitosan to obtain better cell attachment and viability [14]. Similarly in our study, we also aimed to increase the bioactivity of the scaffolds by the surface modification with fibronectin or laminin.

Fibronectin and laminin that have a sequence of amino acid, arginine–glycine–aspartic acid (RGD), are some of the ECM proteins. Cells can bind easily to RGD sequence of fibronectin due to their surface receptors called integrin. The surface of scaffolds can be modified with these materials to support cell attachment, growth, and differentiation onto the surface of the scaffolds [15, 16].

In addition, laminin modified surfaces are generally preferred to be used for neuron cell attachment and neuronal differentiation [17, 18]. In our study, the usage of laminin modified surfaces was preferred to seed pDGSCs since these cells are known as cells of neural crest origin. Thus, it was thought that pDGSCs might preferably attach onto the laminin modified surface.

Dental germs are preferable cell source since they contain MSCs which have the ability to be isolated, expanded, and cryopreserved easily. These cells maintain their properties after long-term cryopreservation. Also, dental germ stem cells (DGSCs) have the ability to differentiate into osteo-, adipo-, and neurogenic cells, easily [9]. Domestic pigs were used as an experimental model in the present study. Thus, DGSCs were isolated from the domestic pigs instead of human because they have the anatomical, physiological, and metabolic similarities with humans.

In this study, after cell seeding of unmodified and fibronectin and laminin modified scaffolds, cell proliferation was investigated throughout 10 days of incubation. Cell proliferation rate was the highest on fibronectin modified scaffolds and the lowest on laminin modified scaffolds. It was found out that increase in cell number on fibronectin modified scaffolds was much better than the others. In one of the studies, cell attachment on fibronectin modified PVDF surface and the application of PVDF as biomaterial in bone

contact were studied. This study showed improvement in osteoblast adhesion on fibronectin modified PVDF surfaces [4]. This study supports our findings and showed the increase in cell proliferation due to fibronectin coating. It was also reported that cells proliferate readily on surfaces coated with fibronectin but poorly on surfaces coated with laminin [19]. Our MTS result also supported this finding. In another study it was demonstrated that human osteoblasts prefer to adhere to fibronectin compared to collagen types I and IV and vitronectin. In contrast, they adhere weakly to laminin and collagen type V and do not adhere to collagen type III at all [20].

In order to observe cell differentiation onto modified and unmodified scaffolds, some experiments such as ALP, immunocytochemistry, von Kossa staining, CM-Dil staining, and real-time PCR were carried out. Alkaline phosphatase is an early marker that shows beginning of the osteoblastic activity of the cell during the bone formation. Besides, it is an enzyme that plays an important role in mineralization. In the alkaline phosphatase activity assay, intracellular ALP was exposed by bursting pDGSCs seeded on PBS scaffolds. It was found from this assay that the expression of ALP was increased in all samples throughout 10 days of incubation. Then, it was decreased from mid stage (day 10) to late stage (day 20) in all scaffolds. This trend was expected since ALP is an early marker of osteoblast differentiation. It was shown before that ALP activity decreases when mineralization starts [21]. One of the studies showed that either collagen type I or fibronectin treated surfaces demonstrated early onset of mineralization and the enhancement of bone matrix secretion. Unlike fibronectin treated surfaces, laminin treated surfaces exhibited the failure of both mineralization and the presence of bone formation [21]. Mathews et al.'s study also supported our findings.

In von Kossa study, when unmodified and modified scaffolds were compared, mineralization was found to be the highest on the fibronectin modified scaffolds throughout 20 days of incubation. This and previous experiments showed that pDGSCs adhered and proliferated on fibronectin modified scaffolds more than the others and then they committed differentiation into bone tissue through 20 days of incubation and bone minerals were observed on the surface. According to one of the studies, the von Kossa staining revealed high calcium deposits on fibronectin treated surfaces [21]. Laminin modified surfaces showed the lowest staining on day 21 of osteogenic induction. These findings also support our results.

When the cell seeded unmodified and modified samples were observed under the confocal microscope, it was observed that the cells that were attached and dispersed onto the surface of the unmodified and fibronectin and laminin modified foams showed decrease in their proliferation rate throughout 20 days of incubation due to differentiation, especially in fibronectin modified scaffolds. After the cells stained with Phalloidin and TO-PRO on PBS scaffolds, it was observed that the cell attachment and proliferation occurred especially around the pores of the foam. This might be due to the accessibility of oxygen and nutrients. Cell seeded modified and unmodified foams were also stained with collagen type I. It was observed that cells on all scaffolds synthesized collagen type I. This indicates the differentiation of cells to bone and the secretion of extracellular matrix demonstrated the initialization of tissue formation. Throughout 20 days of incubation, the amount of synthesized collagen was increased and found to be the highest, especially on the fibronectin modified scaffolds. It also proved that cell differentiation was better on fibronectin modified scaffolds compared to the others.

In one of the experiments, it was showed that the usage of fibronectin generally supplies benefits for cell attachment and spreading even if different techniques are applied for the attachment of fibronectin onto the surfaces [22]. According to the study, fibronectin was conjugated onto highly porous 3D poly(carbonate) urethane scaffolds to distribute cells rapidly throughout the scaffold. In another study, MSCs were seeded on modified poly(HEMA/MA) hydrogel surfaces and cultivated for 4 days. They were stained with Phalloidin and their fluorescence microscopy images were taken. According to the results of this experiment, cells adhered poorly and did not proliferate on unmodified poly(HEMA/MA) hydrogel. Cell growth increased after collagen I coating of hydrogel surface. However, cell growth significantly increased by the attachment of fibronectin and laminin on the collagen layer, especially with fibronectin attachment [23].

Cell-to-cell and cell-to-matrix interaction were also determined by CM-Dil staining in our study. Cellular spreading could be observed because of the binding of a thiol-reactive chloromethyl moiety in the structure of CM-Dil dye to cellular thiols. According to results, increase in cell number was observed on unmodified PBS scaffold throughout 7 days of incubation. On the other hand, cell number was decreased on fibronectin or laminin modified scaffolds after 7 days of incubation. It might be due to cell differentiation on modified PBS scaffolds. This data also supports confocal microscopy results.

Finally, the expression of bone-specific genes which were ALP, Runx2, collagen type I, osteopontin, and osteocalcin was analyzed by real-time PCR. According to the results, the highest ALP expression was observed on fibronectin modified scaffolds at day 10. Then, there was a decrease in ALP expression at day 20. However, ALP expression on laminin modified scaffold was increased throughout 20 days of incubation period. This result was expected due to the increase of ALP enzyme activity in the early stages of the cell culture and this elevated ALP activity was assumed to show the number of osteogenic committed progenitor cells in the culture [24].

During bone formation, lots of transcription factors are needed for the activation of osteoblast differentiation. One of them is Runx2 that is expressed at early stages of differentiation [25]. In our results, decrease of the expression of Runx2 was observed throughout 20 days of incubation on fibronectin modified scaffold since it was induced at early stages whereas Runx2 expression on laminin modified scaffold was increased throughout 20 days of incubation period. Additionally, the direction of preosteoblast cells into immature osteoblasts can be provided by Runx2 which then binds to promoter regions of bone-specific genes such

as collagen type I (Col I), alkaline phosphatase (ALP), osteocalcin (OCN), and osteopontin (OPN) and activates their expression. However, expression levels of these genes can differ according to the osteoblast maturation stages. The expression of Col I and OPN proteins is provided by immature osteoblasts, while OCN protein is strongly expressed by early and late mature osteoblasts. Although bone matrix proteins are expressed by immature osteoblasts, the cells are unable to induce bone mineralization [26].

According to the results, the expression of collagen type I that was the major part of the organic extracellular matrix was supplied by immature osteoblasts as the highest one at day 10 on fibronectin modified scaffold. It showed that rapid bone formation was more on fibronectin modified scaffold than on laminin modified and unmodified scaffold since the organic matrix of bone was comprised of collagen which was synthesized by osteoblasts. At day 20, decrease in expression level of collagen was observed due to the bone remodeling cycle where the osteoblast recruitment potential of the collagen is demineralized by the osteoclast. After that, it triggers bone matrix formation through the osteoblasts that subsequently become mineralized [27, 28].

At the initial stage of bone formation, the production of ALP and Col I is observed by osteoblasts [29]. These proteins supply extracellular matrices suitable enough for mineral deposition. After that, the expressions of osteopontin and osteocalcin proteins are seen. These are also related to bone-mineral deposition.

Additionally, expressions of osteopontin and osteocalcin were analyzed. Osteopontin was a multifunctional phosphorylated glycoprotein secreted by osteoblasts [30]. The increase of the osteopontin expression was seen from day 10 to day 20 on fibronectin modified scaffold since through the mineralization phase osteopontin expression could be seen at maximum level [29]. It showed that bone formation occurred during 20 days of incubation. However, decrease of the osteopontin expression was observed through the mineralization phase on laminin modified scaffold. Also, osteocalcin was highly expressed on fibronectin modified scaffold at day 10 compared to laminin modified scaffold whereas decrease of their expression was observed on fibronectin modified scaffold at day 20. Osteocalcin could be expressed by early and late mature osteoblasts [26] and the secretion of bone matrix protein "osteocalcin" could be seen at maximum level through the mineralization phase, like osteopontin [29]. Therefore, our results could be due to the presence of mineralized bone matrix that was obtained on fibronectin modified scaffold at day 10. It also showed that the mesenchymal stem cells differentiated into mature osteoblasts on fibronectin modified scaffold more than the others.

6. Conclusion

This study aimed to observe the effect of fibronectin or laminin modified polybutylene succinate (PBS) scaffolds on porcine dental germ stem cell (pDGSC) differentiation into bone for the treatment of injuries of the critical size bone defects.

PBS scaffolds were preferred due to their appropriate properties for cell attachment, alignment, and differentiation. Surface modification of PBS scaffolds was made by using either fibronectin or laminin to provide better cell proliferation and to develop surface biocompatibility. According to the results, the surface modification of PBS scaffolds with fibronectin modification can be preferable for pDGSCs, compared to the surface modification with laminin.

In conclusion, all tests showed the positive effects of fibronectin and laminin modifications on PBS scaffolds for proliferation and differentiation of pDGSC into bone. PBS scaffold has a good potential for the healing of critical size bone defect. Besides, pDGSCs have a great potential for bone tissue engineering studies. *In vivo* experimentation should be carried out to show the success of this material for bone tissue engineering studies.

Competing Interests

The authors declare that there is no conflict of interests regarding the publication of this paper.

Acknowledgments

This work has been financially supported by FABED (Feyzi Akkaya Scientific Research Grant).

References

[1] R. Langer and J. P. Vacanti, "Tissue engineering," *Science*, vol. 260, no. 5110, pp. 920–926, 1993.

[2] Y. Tabata, "Biomaterial technology for tissue engineering applications," *Journal of the Royal Society Interface*, vol. 6, no. 3, pp. S311–S324, 2009.

[3] J. Ji, H. Wang, and W. Zhang, "Surface modification of biodegradable poly (butylene succinate) by gas PIII," in *Proceedings of the 3rd International Nanoelectronics Conference (INEC '10)*, pp. 832–833, IEEE, Hong Kong, January 2010.

[4] D. Klee, Z. Ademovic, A. Bosserhoff, H. Hoecker, G. Maziolis, and H.-J. Erli, "Surface modification of poly(vinylidenefluoride) to improve the osteoblast adhesion," *Biomaterials*, vol. 24, no. 21, pp. 3663–3670, 2003.

[5] X. Li, J. Yao, X. Yang, W. Tian, and L. Liu, "Surface modification with fibronectin or collagen to improve the cell adhesion," *Applied Surface Science*, vol. 255, no. 2, pp. 459–461, 2008.

[6] A. J. Salgado, O. P. Coutinho, and R. L. Reis, "Bone tissue engineering: state of the art and future trends," *Macromolecular Bioscience*, vol. 4, no. 8, pp. 743–765, 2004.

[7] S. Gronthos, M. Mankani, J. Brahim, P. G. Robey, and S. Shi, "Postnatal human dental pulp stem cells (DPSCs) in vitro and in vivo," *Proceedings of the National Academy of Sciences of the United States of America*, vol. 97, no. 25, pp. 13625–13630, 2000.

[8] M. Lei, K. Li, B. Li, L.-N. Gao, F.-M. Chen, and Y. Jin, "Mesenchymal stem cell characteristics of dental pulp and periodontal ligament stem cells after *in vivo* transplantation," *Biomaterials*, vol. 35, no. 24, pp. 6332–6343, 2014.

[9] M. E. Yalvaç, M. Ramazanoglu, M. Tekguc et al., "Human tooth germ stem cells preserve neuro-protective effects after long-term cryo-preservation," *Current Neurovascular Research*, vol. 7, no. 1, pp. 49–58, 2010.

[10] M. Ramazanoglu, K. A. Schlegel, and G. T. Kose, "Stem cells potential use of dental stem cells for craniofacial tissue regeneration," in *Stem Cells: Current Challenges and New Directions*, K. Turksen, Ed., Stem Cell Biology and Regenerative Medicine Series, pp. 105–124, Humana Press, New York, NY, USA, 2013.

[11] L. R. Almeida, A. R. Martins, E. M. Fernandes et al., "New biotextiles for tissue engineering: development, characterization and in vitro cellular viability," *Acta Biomaterialia*, vol. 9, no. 9, pp. 8167–8181, 2013.

[12] Y. S. Liu, Q. L. Huang, A. Kienzle, W. E. G. Müller, and Q. L. Feng, "In vitro degradation of porous PLLA/pearl powder composite scaffolds," *Materials Science and Engineering C*, vol. 38, no. 1, pp. 227–234, 2014.

[13] K. Wuertz, K. Godburn, and J. C. Iatridis, "MSC response to pH levels found in degenerating intervertebral discs," *Biochemical and Biophysical Research Communications*, vol. 379, no. 4, pp. 824–829, 2009.

[14] A. R. Costa-Pinto, V. M. Correlo, P. C. Sol et al., "Chitosan-poly(butylene succinate) scaffolds and human bone marrow stromal cells induce bone repair in a mouse calvaria model," *Journal of Tissue Engineering and Regenerative Medicine*, vol. 6, no. 1, pp. 21–28, 2012.

[15] K. Rezwan, Q. Z. Chen, J. J. Blaker, and A. R. Boccaccini, "Biodegradable and bioactive porous polymer/inorganic composite scaffolds for bone tissue engineering," *Biomaterials*, vol. 27, no. 18, pp. 3413–3431, 2006.

[16] V. Karageorgiou and D. Kaplan, "Porosity of 3D biomaterial scaffolds and osteogenesis," *Biomaterials*, vol. 26, no. 27, pp. 5474–5491, 2005.

[17] C. Martínez-Ramos, S. Lainez, F. Sancho et al., "Differentiation of postnatal neural stem cells into glia and functional neurons on laminin-coated polymeric substrates," *Tissue Engineering Part A*, vol. 14, no. 8, pp. 1365–1375, 2008.

[18] Y.-C. Huang, C.-C. Huang, Y.-Y. Huang, and K.-S. Chen, "Surface modification and characterization of chitosan or PLGA membrane with laminin by chemical and oxygen plasma treatment for neural regeneration," *Journal of Biomedical Materials Research A*, vol. 82, no. 4, pp. 842–851, 2007.

[19] R. Carlsson, E. Engvall, A. Freeman, and E. Ruoslahti, "Laminin and fibronectin in cell adhesion: enhanced adhesion of cells from regenerating liver to laminin," *Proceedings of the National Academy of Sciences of the United States of America*, vol. 78, no. 4, pp. 2403–2406, 1981.

[20] K. Anselme, "Osteoblast adhesion on biomaterials," *Biomaterials*, vol. 21, no. 7, pp. 667–681, 2000.

[21] S. Mathews, R. Bhonde, P. K. Gupta, and S. Totey, "Extracellular matrix protein mediated regulation of the osteoblast differentiation of bone marrow derived human mesenchymal stem cells," *Differentiation*, vol. 84, no. 2, pp. 185–192, 2012.

[22] G. Dubey and K. Mequanint, "Conjugation of fibronectin onto three-dimensional porous scaffolds for vascular tissue engineering applications," *Acta Biomaterialia*, vol. 7, no. 3, pp. 1114–1125, 2011.

[23] E. Brynda, M. Houska, J. Kysilka et al., "Surface modification of hydrogels based on poly(2-hydroxyethyl methacrylate) with extracellular matrix proteins," *Journal of Materials Science: Materials in Medicine*, vol. 20, no. 4, pp. 909–915, 2009.

[24] H.-J. Prins, A. K. Braat, D. Gawlitta et al., "*In vitro* induction of alkaline phosphatase levels predicts *in vivo* bone forming capacity of human bone marrow stromal cells," *Stem Cell Research*, vol. 12, no. 2, pp. 428–440, 2014.

[25] R. T. Franceschi, C. Ge, G. Xiao, H. Roca, and D. Jiang, "Transcriptional regulation of osteoblasts," *Annals of the New York Academy of Sciences*, vol. 1116, pp. 196–207, 2007.

[26] M. D. Aisha, M. N. K. Nor-Ashikin, A. B. Shaaniza, H. M. Nawawi, M. Y. Kapitonova, and G. R. A. Froemming, "Short-term moderate hypothermia stimulates alkaline phosphatase activity and osteocalcin expression in osteoblasts by upregulating Runx2 and osterix in vitro," *Experimental Cell Research*, vol. 326, no. 1, pp. 46–56, 2014.

[27] D. J. Hadjidakis and I. I. Androulakis, "Bone remodeling," *Annals of the New York Academy of Sciences*, vol. 1092, pp. 385–396, 2006.

[28] M. E. Abdelgawad, K. Søe, T. L. Andersen et al., "Does collagen trigger the recruitment of osteoblasts into vacated bone resorption lacunae during bone remodeling?" *Bone*, vol. 67, pp. 181–188, 2014.

[29] P. Tripuwabhrut, M. Mustafa, C. G. Gjerde, P. Brudvik, and K. Mustafa, "Effect of compressive force on human osteoblast-like cells and bone remodelling: an in vitro study," *Archives of Oral Biology*, vol. 58, no. 7, pp. 826–836, 2013.

[30] I. Jankovska, M. Pilmane, and I. Urtane, "Osteopontin and osteocalcin in maxilla tissue of skeletal Class III patients," *Stomatologija, Baltic Dental and Maxillofacial Journal*, vol. 11, no. 4, pp. 125–128, 2009.

Hindawi Publishing Corporation
Stem Cells International
Volume 2016, Article ID 8741641, 13 pages
http://dx.doi.org/10.1155/2016/8741641

Research Article

Restoration of a Critical Mandibular Bone Defect Using Human Alveolar Bone-Derived Stem Cells and Porous Nano-HA/Collagen/PLA Scaffold

Xing Wang,[1,2] Helin Xing,[1] Guilan Zhang,[1] Xia Wu,[1] Xuan Zou,[1] Lin Feng,[1] Dongsheng Wang,[1] Meng Li,[1] Jing Zhao,[2] Jianwei Du,[3] Yan Lv,[1] Lingling E,[1] and Hongchen Liu[1]

[1]*Institute of Stomatology, Chinese PLA General Hospital, Beijing 100853, China*
[2]*Hospital of Stomatology, Shanxi Medical University, Taiyuan 030001, China*
[3]*Department of Orthopedics, Chinese PLA General Hospital, Beijing 100853, China*

Correspondence should be addressed to Lingling E; elingling2004@sina.com and Hongchen Liu; chinese621@163.com

Received 22 November 2015; Accepted 8 March 2016

Academic Editor: Armand Keating

Periodontal bone defects occur in a wide variety of clinical situations. Adult stem cell- and biomaterial-based bone tissue regeneration are a promising alternative to natural bone grafts. Recent evidence has demonstrated that two populations of adult bone marrow mesenchymal stromal cells (BMSCs) can be distinguished based on their embryonic origins. These BMSCs are not interchangeable, as bones preferentially heal using cells that share the same embryonic origin. However, the feasibility of tissue engineering using human craniofacial BMSCs was unclear. The goal of this study was to explore human craniofacial BMSC-based therapy for the treatment of localized mandibular defects using a standardized, minimally invasive procedure. The BMSCs' identity was confirmed. Scanning electron microscopy, a cell proliferation assay, and supernatant detection indicated that the nHAC/PLA provided a suitable environment for aBMSCs. Real-time PCR and electrochemiluminescence immunoassays demonstrated that osteogenic markers were upregulated by osteogenic preinduction. Moreover, in a rabbit critical-size mandibular bone defect model, total bone formation in the nHAC/PLA + aBMSCs group was significantly higher than in the nHAC/PLA group but significantly lower than in the nHAC/PLA + preinduced aBMSCs. These findings demonstrate that this engineered bone is a valid alternative for the correction of mandibular bone defects.

1. Introduction

Periodontal bone defects caused by periodontal disease, trauma, surgery, or tumor resection are very common and thus consume a large amount of medical resources annually. Autogenous bone (AB) grafting is the gold standard to reconstruct these defects, but sources of donor tissue are limited. Allografts have not been extensively applied in clinical practice due to the associated risks of antigenicity and cross-infection [1]. Synthetic materials have been studied extensively as potential bone substitutes, but, due to a lack of inherent osteogenic cells and osteoinductivity, limited formation of new bone occurs after osteoconduction is achieved [2].

As one approach to overcome these problems, biomaterial- and autologous stem cell-based tissue engineering has attracted much attention as a promising alternative to natural bone grafts. Among adult stem cells, mesenchymal stromal cells (MSCs) are favorite candidate seed cells for bone tissue regeneration because of their multipotency, immunomodulatory properties, and ability to release trophic factors [3, 4]. Although various adult tissue sources of MSCs, such as bone marrow, fat, muscle, dermis, and dental tissues, have been discovered, iliac bone marrow aspirates remain the principal source for bone regeneration [5, 6].

In preclinical and clinical studies, iliac-derived bone marrow mesenchymal stromal cells (BMSCs) have demonstrated promise for restoring bone defects and healing nonunion

fractures [7, 8]. However, in clinical treatment, fear of pain and postoperative iliac complications has precluded the routine therapeutic use of BMSCs, particularly in dental patients who require alveolar bone augmentation. This issue suggests the need for the development of a more usable and minimally invasive procedure to isolate BMSCs [9, 10].

Recent evidence has suggested that at least two populations of adult skeletal progenitor cells can be distinguished based on their embryonic origins. Craniofacial bone arises from neural crest cells and ossifies via intramembranous ossification, whereas the appendicular skeleton arises from mesenchymal condensations of the mesoderm, which then undergoes perichondral ossification [11, 12]. Bridging craniofacial defects with grafts obtained from a craniofacial donor site is usually more successful than doing so with grafts from appendicular sites, indicating that skeletal site-specific differences affect graft integration [13, 14]. Furthermore, a selective recruitment mechanism through which adult skeletal defects heal, involving recruitment of progenitor cells of the same origin, has been demonstrated, indicating that BMSCs from the craniofacial and appendicular skeletons are not interchangeable [15]. The presence of two distinct populations of BMSCs in the adult might have clinical implications because if bones preferentially heal using cells that share the same embryonic origin, then reparative strategies may have to take this variable into account to be maximally effective. However, before the present investigation, the feasibility and effectiveness of tissue engineering using human craniofacial BMSCs to restore mandibular bone defects were unclear.

The goal of this study was to explore human craniofacial BMSC-based tissue engineering for the treatment of localized mandibular defects using a standardized, minimally invasive procedure. For this purpose, human alveolar BMSCs (aBMSCs) were isolated painlessly during conventional dental implant surgery, and the characteristics of the aBMSCs were analyzed in 2-dimensional cultures and on a porous nanohydroxyapatite/collagen/poly(L-lactide) (nHAC/PLA) scaffold. The osteogenic capability, biocompatibility, and biological safety of the constructs were also evaluated both *in vitro* and *in vivo*.

2. Materials and Methods

2.1. Isolation and Culture of aBMSCs. Human alveolar bone marrow specimens were obtained from 52 patients during dental implant surgery following Chinese PLA General Hospital Review Board approval. In particular, after informed consent was obtained, we administered local anesthesia and removed the gingival flap and bone cortex at the implant sites using a flapless surgical procedure. Next, we gradually drilled into the cancellous bone at 50 rpm without irrigation until the desired diameter and length for the implant were obtained. Bone marrow scraped from the bone core that was harvested from the pilot drill was immediately placed in sterile tubes containing minimum essential alpha medium (αMEM; Gibco, Carlsbad, CA, USA) (Figure 1). Before dental implant placement, a 22.5-gauge needle connected to a heparinized syringe was inserted into the drill holes to obtain the marrow aspirate [16]. Both the collected debris and the aspirate were immediately transported to the laboratory for aBMSC isolation. The samples in αMEM medium were then centrifuged at 500 g for 5 minutes. The supernatant was removed, and the cell pellets were transferred to 25 cm^2 culture flasks and resuspended in 5 mL of basic medium, consisting of αMEM supplemented with 15% fetal bovine serum (FBS; Gibco). The culture flasks were then incubated undisturbed, without medium changes, for 5 days in a 37°C humidified tissue culture incubator at 5% CO_2. Once the cell density reached approximately 80% confluence, the cells were detached using trypsin/ethylenediaminetetraacetic acid (EDTA; Sigma, St. Louis, MO, USA) treatment and were passaged or used for subsequent analysis. Not all specimens could be included in every experiment because of the surgical schedule and the number of cells needed for each assay. In each experiment, cells obtained from different subjects were stored for analysis at the same time to avoid technical differences between assays.

2.2. Flow Cytometric Analysis. aBMSCs at passage 3 were trypsinized, washed, and resuspended in phosphate-buffered saline (PBS; Gibco) at a concentration of 1×10^5 cells/mL. The cells were subsequently immunolabeled with mouse monoclonal anti-human antibodies specific for the following: CD14, CD34, CD44, CD90, CD106, and HLA-DR (Abcam, Cambridge, MA, USA). Mouse isotype antibodies served as controls. The cells were then washed again with PBS and fixed in 2% paraformaldehyde, after which the immunolabeled cells were detected by flow cytometry (BD Biosciences, NJ, USA).

2.3. Immunofluorescence. aBMSCs at passage 3 were detached using solution of versene (EDTA/PBS) and were subcultured on 12-chamber slides for 24 hours. The samples were then fixed in 2% paraformaldehyde for 15 minutes, followed by incubation with anti-STRO-1 antibody (1 : 200; R&D Systems Inc., Minneapolis, MN, USA) for 3 hours. The cells were subsequently incubated with anti-mouse IgG TRITC (1 : 50; Santa Cruz Biotechnology, Inc., USA) for 1 hour and stained with 4′,6-diamidino-2-phenylindole (DAPI; 2 μg/mL; Sigma).

2.4. Multilineage Differentiation. aBMSCs at passage 3 were cultured on six-well culture plates at a density of 2×10^5 cells/cm^2 in induction medium. For osteogenic differentiation, the osteogenic induction medium consisted of αMEM, 15% FBS, 10 nM dexamethasone, 100 mM glycerophosphate, and 50 μg/mL ascorbic acid [17]. The medium was renewed two times each week. At day 21, the cells were stained with Alizarin red.

For adipogenic differentiation, the induction medium consisted of 200 μM indomethacin, 1 μM dexamethasone, 0.5 mM 3-isobutyl-1-methylxanthine, and 100 nM insulin. The medium was renewed two times each week. At day 21, the cells were fixed and stained with fresh Oil red O solution. As a control, the same batch of aBMSCs was cultured in αMEM containing 15% FBS and stained at day 21.

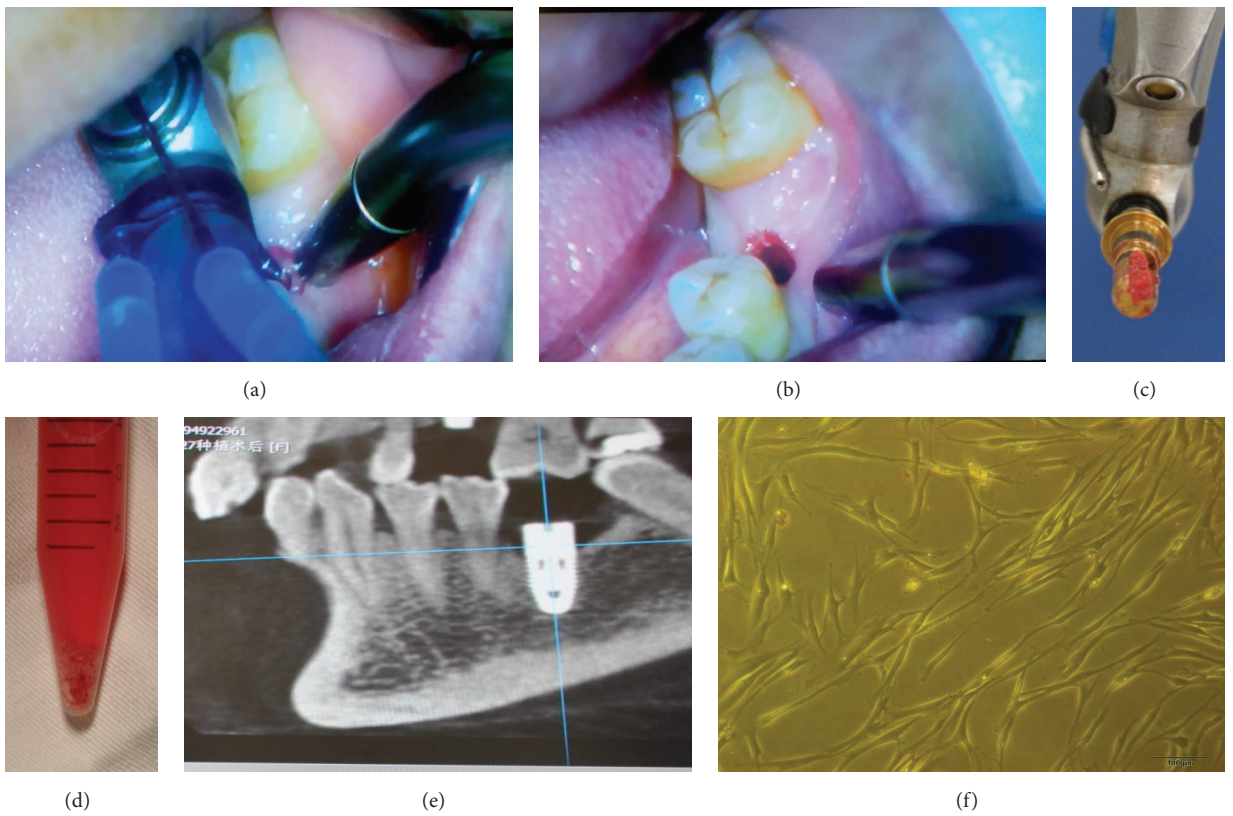

Figure 1: Clinical techniques for harvesting alveolar bone marrow. (a) The cancellous bone was drilled at 50 rpm until achieving the desired diameter and length for the implant site. (b) Before dental implant placement, bone marrow was harvested using a flapless, minimally invasive surgical procedure. (c, d) Bone marrow scraped from the pilot drill was immediately placed in sterile tubes and transported to the laboratory. (e) Confirmation of the initial stability of the dental implant by cone-beam CT. (f) Photomicrograph of aBMSCs 7–10 days following initial plating, revealing a fibroblastic, spindle shaped morphology similar to that of stem cells from other cell sources. Magnification: ×400.

2.5. Biometric Preparation and Seeding of nHAC/PLA Scaffolds. The features of the nHAC/PLA porous scaffold (Allgens, Beijing, China) were similar to that of natural bone: a porosity of 70–90% and a pore size of 300–400 ± 150 μm [18]. aBMSCs at passage 3 were seeded into nHAC/PLA materials that had been cut into 10 × 5 × 3 mm blocks. The nHAC/PLA + aBMSCs constructs were then incubated in basic medium in a 24-well plate for 24 hours at 37°C. After the aBMSCs had adhered to the nHAC/PLA, the constructs were cultured in basic medium or osteogenic induction medium for *in vitro* characterization and *in vivo* implantation.

2.6. MTS Assay. 3-(4,5-Dimethylthiazol-2-yl)-5-(3-carboxymethoxyphenyl)-2-(4-sulfophenyl)-2H-tetrazolium, inner salt (MTS; Promega), was used as an indicator of cell viability. In preparation, aBMSCs at passage 3 were seeded onto nHAC/PLA discs in 96-well culture plates at density of 1.5×10^4 cells/cm^2. After culture for 24 hours, the cells were serum starved overnight in αMEM with 1% FBS and then cultured in basic medium (nHAC/PLA + aBMSCs group) or osteogenic induction medium (nHAC/PLA + preinduced aBMSCs group) for another 7 days. On days 1, 3, 5, and 7 during this period, 20 μL of MTS was added, and the samples were incubated for 2 hours at 37°C. Subsequently, the absorbance of each well was measured at 490 nm using an ELx800 UV reader (Bio-Tek Instruments, Winooski, VT, USA).

2.7. Scanning Electron Microscopy (SEM). aBMSCs were cultured on nHAC/PLA scaffolds in basic medium or osteogenic induction medium at 1×10^5 cells/cm^2 for 7 days, after which the samples were washed with PBS and fixed in 2.5% glutaraldehyde. The samples were then coated with several nanometer-thick layers of gold. The adhesion and morphology of the aBMSCs on the surface of the nHAC/PLA composite were observed using a variable-pressure scanning electron microscope (S-3400N, Hitachi, Japan) with beam energies of 6–25 kV.

2.8. Osteogenic Gene. aBMSCs on nHAC/PLA scaffolds were cultured in osteogenic induction medium or basic medium for 7 days. Total RNA was subsequently extracted using TRIzol (Invitrogen, Grand Island, NY, USA), and first-strand complementary DNA (cDNA) was synthesized using a cDNA synthesis kit (Promega, Madison, WI, USA). Quantitative real-time PCR was then performed using human osteocalcin (OCN), Runx2, Osterix, and β-actin primers and Fast SYBR Green MasterMix in a StepOnePlus™ Real-Time

PCR System (Applied Biosystems, Carlsbad, CA, USA). The following primer sets were used: Runx2, GenBank Accession number 860, F5′-CGGAATGCCTCTGCTGTTATGAA-3′, R5′-AGGATTTGTGAAGACGGTTATGG-3′; Osterix, number 121340, F5′-CTCCTCCTGCGACTGCCCTAAT-3′, R5′-AGGTG CGAAGCCTTG CCATACA-3′; OCN, number 632, F5′-GGAGGGCAGCGAGGTAGTGAAG-3′, R5′-GATGTGGTCA GCCAACTCGTCA-3′; actin, number 60, F5′-TGCCCATCTA CGAGGGGTATG-3′, R5′-TCCTTAAT GTCACGCACGATTTC-3′. The expressions of the genes were normalized to the internal control b-actin mRNA levels. Data were analyzed using the comparison Ct ($2^{-\Delta\Delta Ct}$) method. The specificity of single-target amplification by each primer pair was confirmed by melting curve analysis.

2.9. Alkaline Phosphatase (ALP), OCN, Calcium, and Phosphonium Content Assays. aBMSCs on nHAC/PLA scaffolds were cultured for 21 days in basic medium or osteogenic induction medium at $1.5 \times 10^4/cm^2$ cells per graft. The supernatants were collected at 3 time points: days 7, 14, and 21. The ALP activity in the medium was assayed using Roche Diagnostics ALP kits on the cobas e602 platform (Roche Diagnostics, Mannheim, Germany), and calcium content and phosphonium content were assayed using Roche Diagnostics Ca/P kits. OCN activity was assayed using N-MID osteocalcin kits, based on electrochemiluminescence immunoassay techniques. All data were measured and analyzed on the cobas 8000 platform (Roche Diagnostics).

2.10. Genetic Stability Assay. Reverse transcription PCR was performed to examine the gene expression of tumor suppressors and protooncogenes. For this purpose, RNA was isolated from aBMSCs cultured on flasks at passages 1 and 2 and from aBMSCs cultured on nHAC/PLA scaffolds in basic medium or osteogenic induction medium at passage 3. The primer sequences were as follows: p53, F5′-CCTCACCATCATCACA CTGG-3′, R5′-TTATGGCGGGAGGTAGACTG-3′; c-myc, F5′-CTCCTGGCAAAAGGTCAG AG-3′, R5′-GGCCTTTTCATTGTTTTCCA-3′; ARF, F5′-TGGGTCCCAGTCTGCA GTTA-3′, R5′-CTGCCCATCATCATGACCT-3′; GAPDH, F5′-ACAGTCAGCC GCATCTTCTT-3′, R5′-ACGACCAAAT CCGTTGACTC-3′.

At the end of culture, aBMSCs from three different patient samples at passage 4 were subjected to karyotyping analysis. These aBMSCs were cultured on nHAC/PLA scaffolds in osteogenic induction medium, followed by treatment with 60 ng/mL colcemid (Sigma) and harvesting with 0.25% trypsin/EDTA. The cells were then collected by centrifugation, and karyotyping analysis was performed using G-banding techniques in a clinical laboratory at the Chinese PLA General Hospital.

2.11. Bone Regeneration in the Mandibular Defect Model. The bone-forming capacity of 20 different aBMSCs populations was evaluated qualitatively in a New Zealand white rabbit segmental critical-size mandibular defect model [18, 19]. For this purpose, 30 female rabbits were housed in the laboratory animal center at the Chinese PLA General Hospital. The rabbits had weights of 2.50–3.00 kg. All surgical procedures and care followed Chinese PLA General Hospital Review Board approval. The rabbits were first intravenously anesthetized with 2% pentobarbital sodium (30 mg/kg). The hair on the right of the rabbit mandible was then depilated. Under aseptic conditions, a 10 mm incision was made along the upper edge of the rabbit mandible, and the right buccal was exposed. A segmental defect ($10 \times 5 \times 3$ mm) was prepared in the alveolar bone of all rabbits using a surgical oscillating saw and sterile saline irrigation. nHAC/PLA blocks with/without 5×10^6 aBMSCs were implanted in the segmental defect, and the rabbits were assigned to five groups: mandibular defects were treated with nHAC/PLA, nHAC/PLA + aBMSCs, or nHAC/PLA + preinduced aBMSCs (preinduced in osteogenic induction medium for 7 days) or with AB from the iliac bone as a positive control or untreated defect as a negative control.

After eight weeks, the samples were surgically removed and fixed. Goldner's trichrome staining was used to examine bone regeneration at the defects. All samples were analyzed by morphometric analysis using the Leica-Q Win 3.2 image analysis system. Five sequential sections per implant were selected, and the type of tissue (mature bone-like or osteoid-like) was identified by an independent observer. The extent of newly formed bone was indicated by the percentage of the newly formed bone areas within a section. An average value was then calculated for each implant, and data were averaged across all implants within each group.

2.12. Assessment of Bone Regeneration by Micro-CT. The bone volume and trabecular microarchitecture were monitored using a Quantum FX micro-CT Imaging System (Caliper, USA) at 70 kV and 114 mA. A total of 512 binary images were obtained with a wide field of view (FOV), with scanning at 36 mm and a 4.5 μm voxel size resolution. The thresholds were set at 1300, which was adequate to separate bone and nHAC using discrimination analysis. The calculated bone volume density (bone volume/total volume) in this area is presented as the percentage regeneration of the defect.

2.13. Statistical Analysis. All data are presented as the mean ± standard deviation. Statistical analyses of the results were performed using SPSS 16.0 software. Student's t-test was used to study significant differences in the MTS, PCR, SEM, ALP, OCN, and calcium and phosphonium content results. One-way ANOVA and an unpaired t-test were used to study significant differences in the bone volume density and the percentage of bone formation area between study groups. The significance threshold was set at $p < 0.05$.

3. Results

3.1. Isolation and Characterization of aBMSCs. We collected alveolar bone marrow samples from 52 patients undergoing dental implant surgery. Every dental implant was initially stable (final torque > 35 Ncm), and no complications after bone marrow collection were reported. Postoperative 1- to 3-month cone-beam CT results revealed closely aligned dental implants and bone (Figure 1(e)).

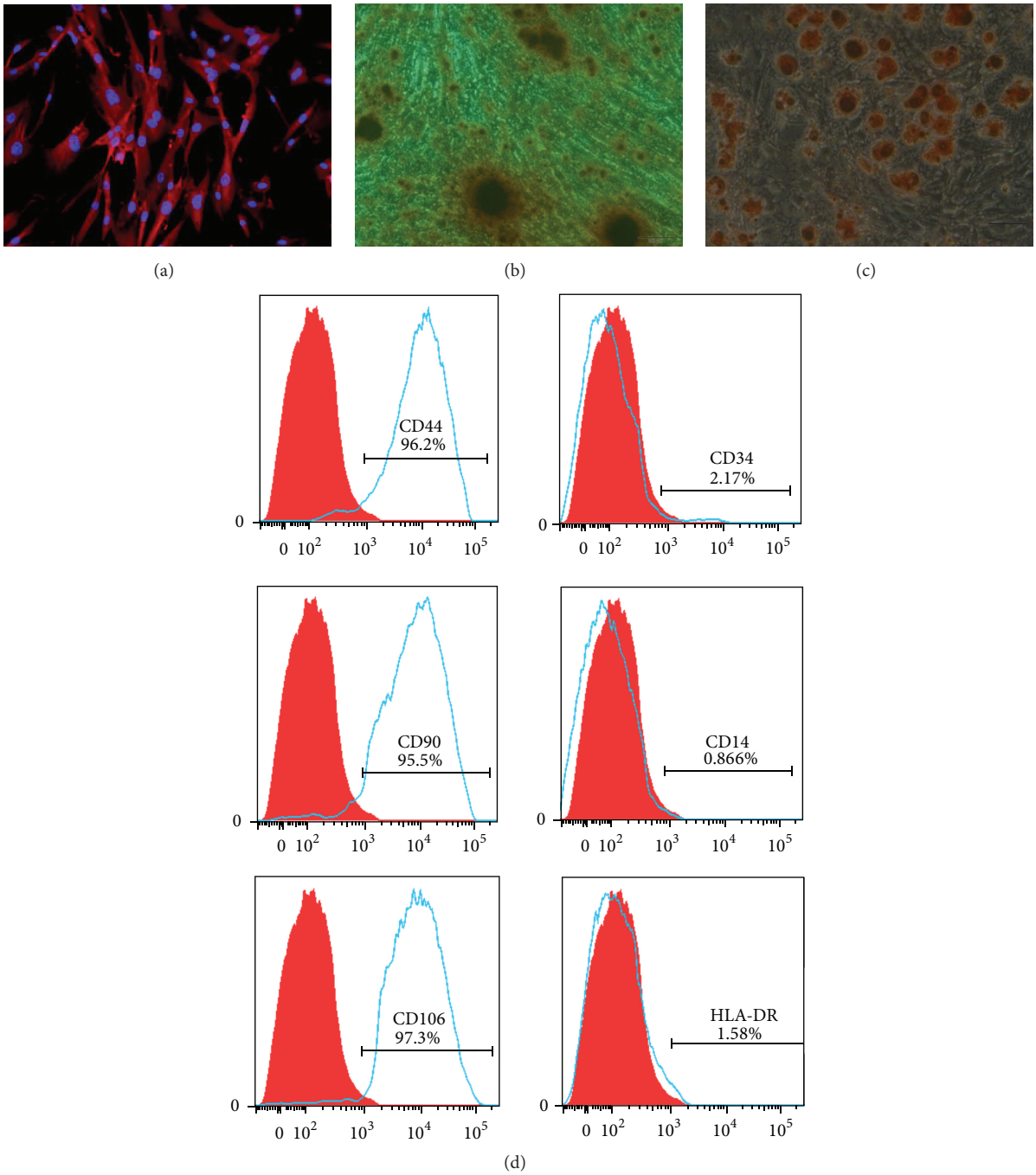

Figure 2: Characterization of human aBMSCs. (a) The aBMSCs expressed STRO-1, a mesenchymal stromal cell marker. Positive staining of the cells with Alizarin red (b) or Oil red O (c) demonstrated the osteogenic and adipogenic differentiation potential of the aBMSCs. Magnification: ×400. (d) The aBMSCs were positive for MSC markers, including CD44, CD90, and CD106, and negative for hematopoietic and endothelial markers, including CD14, CD34, and HLA-DR.

The aBMSCs in 37 samples adhered to the culture surface and proliferated *in vitro*. The isolated aBMSCs formed single-cell-derived colonies, and most of the cells retained their fibroblastic spindle shape (Figure 1(f)). The aBMSCs were expanded in culture, followed by characterization of cell surface markers by flow cytometry and immunofluorescence. Immunofluorescence analysis demonstrated that the cells were STRO-1 positive (Figure 2(a)). To evaluate the *in vitro* differentiation potential of the aBMSCs, the cells were induced to differentiate along osteogenic and adipogenic lineages under specific culture conditions, as revealed by Alizarin red (Figure 2(b)) and Oil red O (Figure 2(c)) staining. Flow cytometry revealed that the cultured cells were homogenously positive for CD44, CD90, and CD106

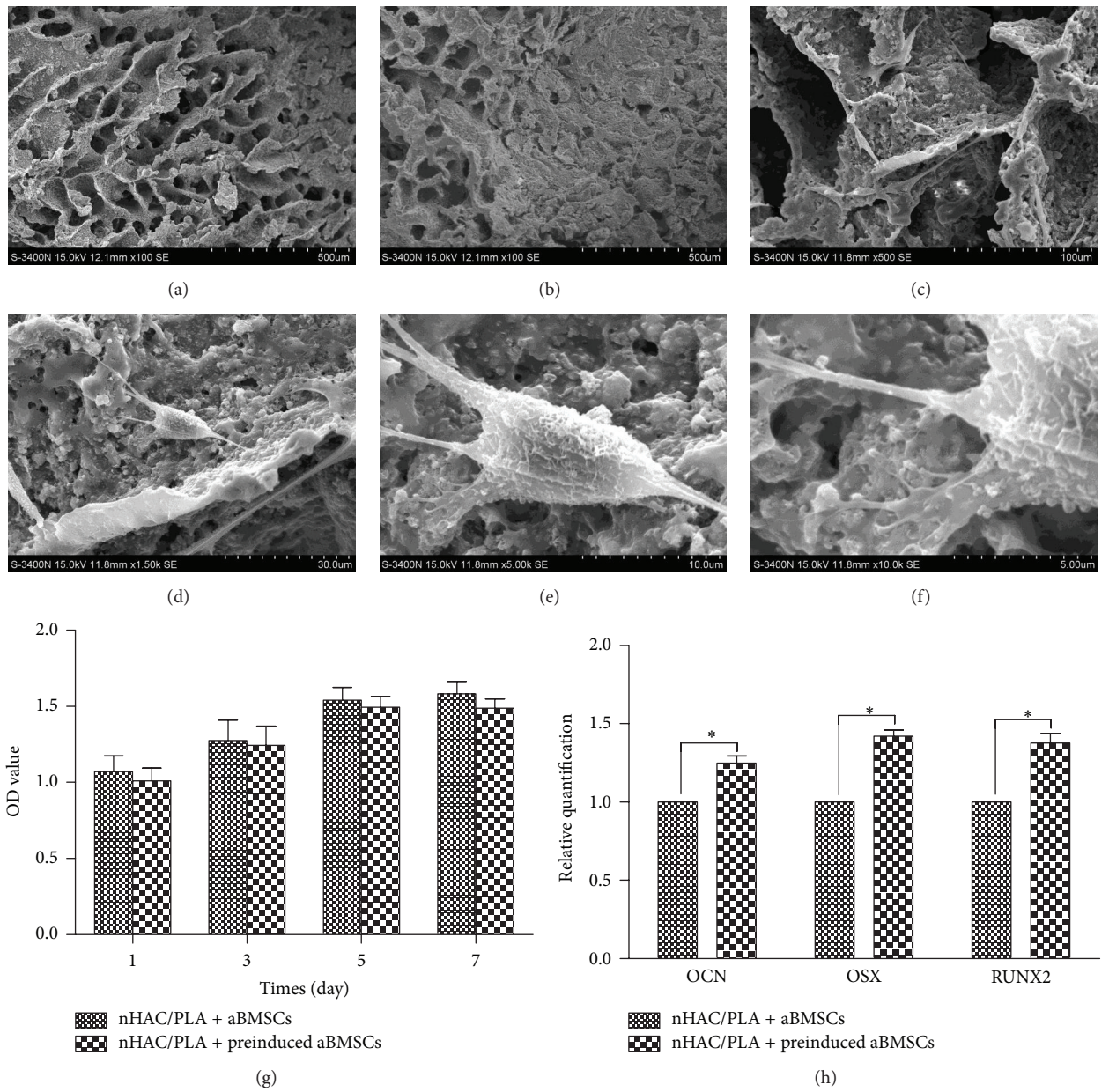

Figure 3: Proliferation and osteogenic differentiation potential of aBMSCs on nHAC/PLA. (a) SEM analysis showed that nHAC/PLA was similar to natural bone in terms of microstructure. (b) After 3 days of culture, the aBMSCs adhered to, extended, and connected with each other and produced ECM on the nHAC/PLA surface. The aBMSCs (c–f) were spindle, triangle, or cube shaped, with developed cytoplasmic extensions attached to the scaffold. (g) The MTS results demonstrated that the aBMSCs were proliferative on days 1, 3, 5, and 7 after seeding onto nHAC/PLA ($n = 6$, mean ± SD). (h) Real-time PCR revealed that osteogenic induction for 7 days promoted aBMSC expression of OCN, Runx2, and Osterix ($n = 6$, mean ± SD). *Compared with nHAC/PLA + aBMSCs. Differences are significant at $p < 0.05$. Magnification: (a, b) ×100 SE; (c) ×500 SE; (d) ×1.50 k SE; (e) ×5.00 k SE; (f) ×10.0 k SE.

and negative for hematopoietic and endothelial cell surface markers, including CD14, CD34, and HLA-DR (Figure 2(d)).

3.2. Biocompatibility between aBMSCs and nHAC/PLA. The adherence and morphology of aBMSCs on nHAC/PLA were observed by SEM, which revealed that the nHAC/PLA blocks without cells exhibited a hierarchical microstructure (Figure 3(a)). After 3 days of culture, the aBMSCs adhered to, extended, and connected with each other and produced extracellular matrix (ECM) on the nHAC/PLA surface (Figure 3(b)). The aBMSCs were spindle, triangle, or cube shaped, with developed cytoplasmic extensions attached to the scaffold (Figures 3(c)–3(f)).

The proliferation of aBMSCs on nHAC/PLA was evaluated using the MTS method on days 1, 3, 5, and 7 (Figure 3(g)). Throughout the 7 days of culture, the cell numbers increased, indicating that the nHAC/PLA had no negative effect on proliferation. Compared with cells cultured in basic medium

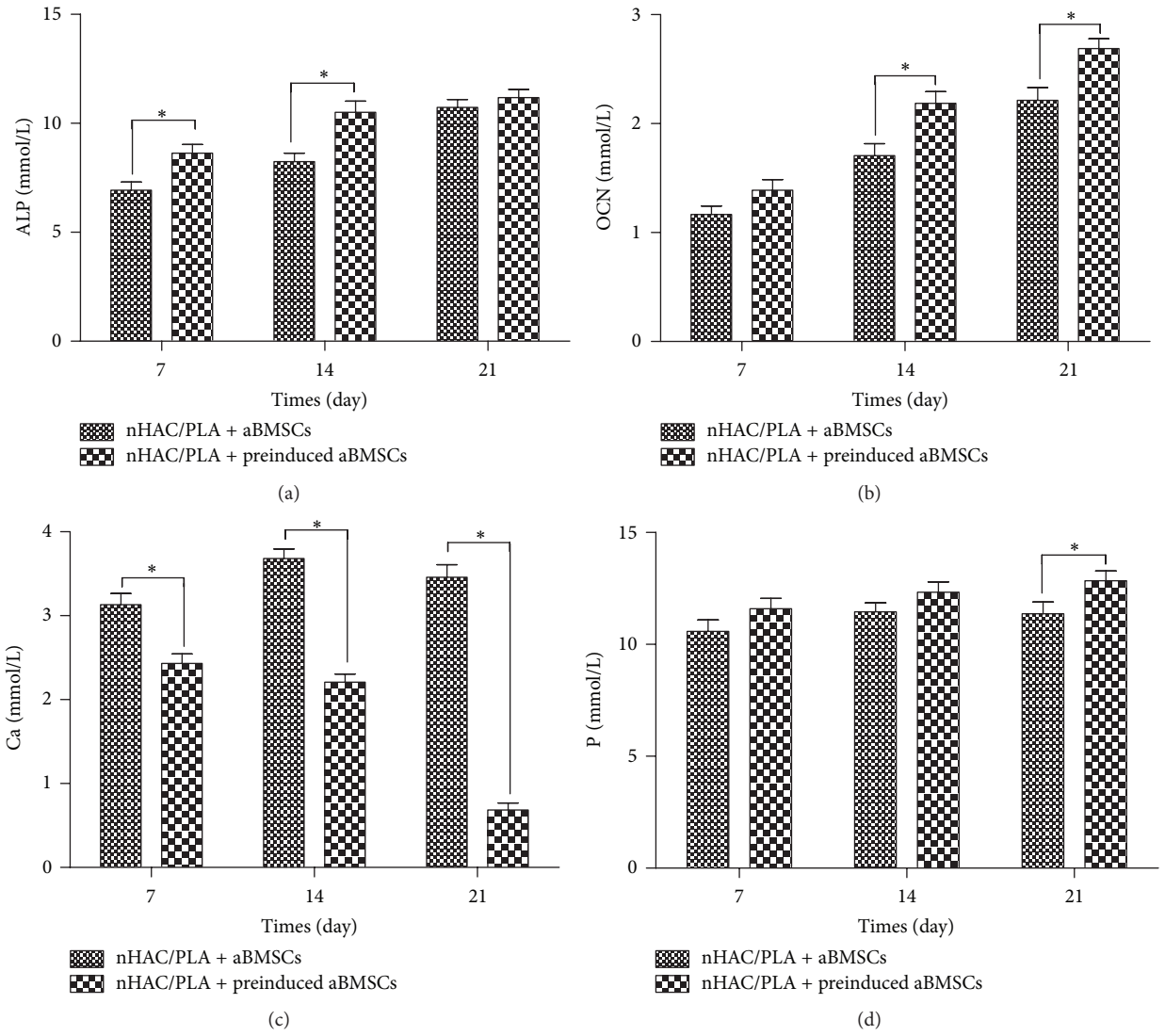

Figure 4: Effect of osteogenic induction on the ALP activity (a), OCN content (b), calcium content (c), and phosphonium content (d) of aBMSCs cultured on nHAC/PLA ($n = 6$, mean ± SD). *Compared with nHAC/PLA + aBMSCs. Differences are significant at $p < 0.05$.

(nHAC/PLA + aBMSCs group), the number of aBMSCs on nHAC/PLA decreased in the nHAC/PLA + preinduced aBMSCs group, but the difference was not significant ($p > 0.05$).

3.3. Osteogenic Capability of aBMSCs on nHAC/PLA. To confirm their osteogenic potential, aBMSCs on nHAC/PLA were cultured in basic medium or osteogenic induction medium for 7 days, followed by the evaluation of osteogenesis-related genes by quantitative real-time PCR. The PCR results demonstrated that osteogenic inductive treatment promoted expression of the osteogenesis-related genes OCN, Runx2, and Osterix in the BMSCs (Figure 3(h)).

To investigate the osteogenic capability of aBMSCs on nHAC/PLA, the ALP activity, calcium and phosphonium content, and OCN content in the culture supernatant were assayed at days 7, 14, and 21. The aBMSCs and nHAC/PLA constructs were cultured in basic medium or osteogenic induction medium for this purpose. During the 28 days of culture, the ALP activity and OCN and phosphonium content in both groups increased with culture time, but the calcium content decreased. However, the ALP activity and OCN and phosphonium content were significantly higher in the nHAC/PLA + preinduced aBMSCs group than in nHAC/PLA + aBMSCs group at day 21 (Figure 4). Although the calcium content in both groups declined, the content in the nHAC/PLA + preinduced aBMSCs group was always significantly lower.

3.4. Genetic Stability Assessment. To evaluate transformational alterations in gene expression, the levels of the tumor suppressor genes p53 and ARF and the protooncogene c-myc were measured ($n = 6$). However, no significant changes were observed over time or upon osteogenic induction (Figure 5(a)).

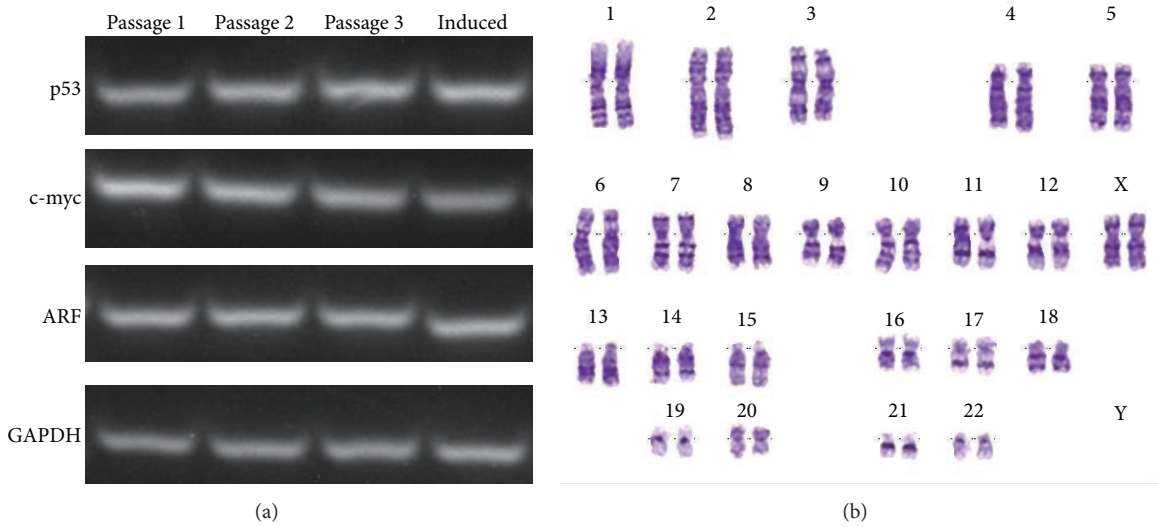

Figure 5: Genetic stability evaluation. (a) The expression levels of p53, ARF, and c-myc in aBMSCs were unchanged over time and under osteogenic induction. (The term "induced" denotes aBMSCs at passage 3 that were cultured on nHAC/PLA scaffolds in osteogenic induction medium.) (b) aBMSCs at passage 4 that were cultured on nHAC/PLA in osteogenic induction medium exhibited a normal karyotype.

After culture on nHAC/PLA scaffolds in osteogenic induction medium for 21 days, aBMSCs at passage 4 exhibited a normal diploid karyotype ($n = 6$). Chromosome structural abnormalities such as inversion, deletion, translocation, and rings were not observed by karyotyping analysis of G-banding (Figure 5(b)).

3.5. Bone Regeneration in a Mandibular Defect Model. In the critical-size mandibular defect rabbit model, the mandible was harvested for histological analyses at 8 weeks. In the nHAC/PLA and the nHAC/PLA + aBMSCs groups, the mandibular defects were filled with abundant red-stained osteoid tissue and some green-stained newly formed bone (Figures 6(a) and 6(b)), and many osteoclasts were observed in the newly formed osteoid tissue. Meanwhile, the defects in the nHAC/PLA + preinduced aBMSCs group were filled with a large amount of mature thickened bone (Figure 6(c)), and osteoblasts lined the surface of the newly formed bone. In the AB group, there were areas of autogenous grafted bone as well as areas of new bone regeneration (Figure 6(d)). In different maturation stages, the autologous bone and newly formed bone exhibited different trabecular arrangements. Little bone regeneration was observed in the untreated defect group, which served as the negative control.

A total of 68 slides from the different groups were quantified by morphological analysis. The extent of newly formed mature bone and osteoid tissue was indicated by the percentage of total bone formation area within the section; this percentage was averaged across all slides within each group. The percentages of the osteoid tissue formation area in the nHAC/PLA, nHAC/PLA + aBMSCs, nHAC/PLA + preinduced aBMSCs, and AB groups were 23.5 ± 3.3, 15.6 ± 1.2, 7.9 ± 1.9, and 9.2 ± 1.1, respectively. The percentages of mature bone formation area in the nHAC/PLA, nHAC/PLA + aBMSCs, nHAC/PLA + preinduced aBMSCs, and AB groups were 3.2 ± 1.2, 19.2 ± 1.3, 41.2 ± 2.4, and 43.2 ± 2.7, respectively. The percentages of total bone formation area in the nHAC/PLA, nHAC/PLA + aBMSCs, nHAC/PLA + preinduced aBMSCs, and AB groups were 26.7±4.5, 34.8±2.5, 49.1 ± 4.3, and 52.2 ± 3.8, respectively.

Histomorphometric measurements revealed significant differences in bone formation (Figure 7(F)). The nHAC/PLA group had the lowest percentage of total bone formation area of the five implanted groups and differed significantly from the other groups ($p < 0.05$). Total bone formation in the nHAC/PLA + aBMSCs group was significantly higher than in the nHAC/PLA group ($p < 0.05$) but significantly lower than in the nHAC/PLA + preinduced aBMSCs and the AB groups ($p < 0.05$). The maximal percentage of total bone formation area was observed in the AB group. However, there were no significant differences between the nHAC/PLA + preinduced aBMSCs and the AB groups ($p > 0.05$).

Regeneration of the mandibular defects was evaluated using micro-CT. In the 3-dimensional volume reconstruction of the images, the bone defect in the untreated defect group was unfilled (Figure 7(A)). For defects filled with an nHAC/PLA scaffold, new bone formation in the open scaffold pores, with incomplete healing of the defect, was observed (Figure 7(B)). For defects filled with nHAC/PLA + aBMSCs, the defect surface was healed with a thin cortical shell bridge (Figure 7(C)). For defects filled with nHAC/PLA + preinduced aBMSCs, the defect surface was also completely healed with a thick cortical shell bridge (Figure 7(D)). In the AB group, the defects healed well, and the iliac graft block and mandibular bone could not be distinguished (Figure 7(E)).

To quantify new bone formation, the bone volume density in the defect is presented as the percentage regeneration of the defect. The bone volume densities in the nHAC/PLA, nHAC/PLA + aBMSCs, nHAC/PLA + preinduced aBMSCs, and AB groups and the untreated defect group were 25.1 ±

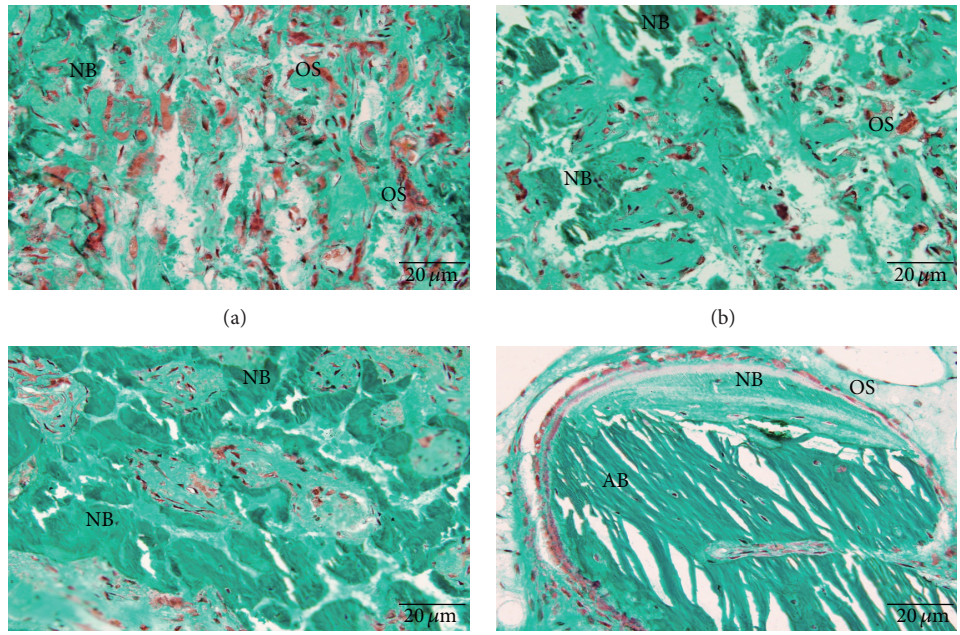

Figure 6: Bone regeneration in a rabbit critical-size mandibular defect model stained with Goldner's trichrome. (a) The defects in the nHAC/PLA group were filled with abundant red-stained osteoid tissue and some green-stained newly formed bone. (b) The defects in the nHAC/PLA + aBMSCs group were filled with more newly formed trabeculae. (c) The defects in the nHAC/PLA + preinduced aBMSCs group were filled with a large amount of mature thickened bone. (d) The AB group exhibited areas of newly formed bone, osteoid tissue, osteoblastic seams, and residual bone graft. Magnification: ×400. NB: new mature bone; AB: autogenous bone; OS: osteoid tissue.

4.5, 33.2 ± 3.4, 47.8 ± 4.2, 55.4 ± 3.9, and 58.5 ± 3.8, respectively (Figure 7(G)). The bone volume density in the nHAC/PLA + aBMSCs group was significantly higher than in the nHAC/PLA group ($p < 0.05$) but significantly lower than in the nHAC/PLA + preinduced aBMSCs and the AB groups ($p < 0.05$). There were no significant differences between the nHAC/PLA + preinduced aBMSCs and the AB groups ($p > 0.05$), indicating that new bone formation was significantly improved by the nHAC/PLA + preinduced aBMSCs.

4. Discussion

As a promising alternative approach for the treatment of bone defects, bone tissue engineering creates a bone grafting material with osteogenic, osteoinductive, and osteoconductive properties. These events are also essential for optimal bone healing when a combination of BMSCs and biomaterials is to be used to treat periodontal bone defects. *In vitro* studies of BMSCs often involve cells derived from the tibia of animals, including mice and rats. When human skeletal progenitor cells are studied, most bone grafting procedures performed for craniofacial applications use cells derived from the mesodermal lineage (e.g., the fibula, iliac crest, and ribs). Recently, several scholars have described the isolation of BMSCs from the marrow of maxillofacial bones and demonstrated that these cells share the basic characteristics of MSCs [10, 16]. In the same individuals, maxillofacial-derived BMSCs were found to have greater osteogenic potentials than iliac crest-derived BMSCs [20]. In previous studies, we also found that osteogenic differentiation capacity of alveolar BMSCs was higher than that of femoral BMSCs in the middle-aged and old group [21]. These reports indicate the BMSCs from maxillofacial bones with some characteristics that may be beneficial for treating maxillofacial bone defects. Nevertheless, in most published studies, alveolar BMSCs have not been used in critical-size mandibular bone defect model.

In this study, we describe a convenient and minimally invasive process for craniofacial BMSC isolation and further demonstrate that a combination of aBMSCs after osteogenic induction and nHAC/PLA could effectively restore mandibular defects. It would be an advantage to use aBMSCs via this process, thereby reducing donor-site morbidity and residual pain related to bone harvesting from, for example, the iliac crest.

At the histological level, defect repair in the craniofacial skeleton is indistinguishable from appendicular bone repair: both defect sites are vascularized following trauma, both become populated by osteoblast progenitor cells, and both undergo bony matrix remodeling within a similar time frame. However, cellular and molecular analyses belie this histological equivalency. In particular, Hox expression status as well as embryonic origin has an influence on the fate of skeletal progenitor cells in the regenerative context. Leucht et al. found that, initially, mandibular skeletal progenitor cells are Hox negative but that they adopt a Hoxa11-positive profile when transplanted into a tibial defect. Conversely, tibial skeletal progenitor cells are Hox positive and maintain this Hox status even when transplanted into a Hox-negative

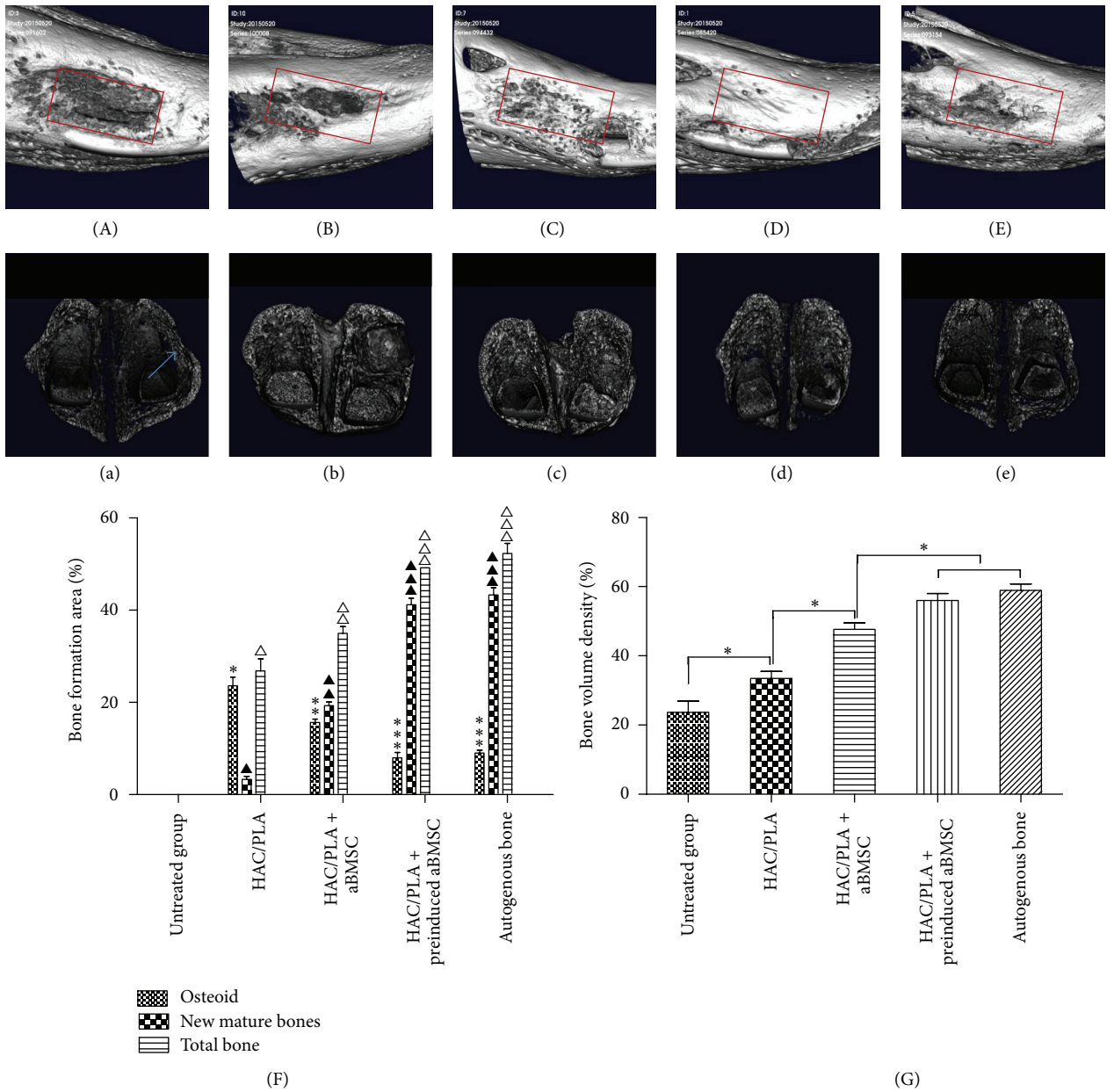

Figure 7: Micro-CT images of the mandibular defects at 8 weeks after implantation. (A, a) The critical-size bone defect in the untreated group was unfilled. (B, b) For defects filled with an nHAC/PLA scaffold, new bone formation in the open scaffold pores, with incomplete healing on the surface of the defect, was observed. (C, c) The defect surface was healed with a thin cortical shell bridge in the nHAC/PLA + aBMSCs group. (D, d) The defect surface was completely healed with a thick cortical shell bridge in the nHAC/PLA + preinduced aBMSCs group. (E, e) In the AB group, the defect healed well, and the iliac graft block and mandibular bone could not be distinguished. (The red boxes represent the defect area in the mandible, and the blue arrow indicates an incomplete cortical shell.) (F) The percentages of osteoid tissue formation, mature bone formation, and total bone formation were determined by histomorphometric measurements. Differences are significant at $p < 0.05$. Groups with the same symbol (∗, ▲, △) were not significantly different. (G) The bone volume density in micro-CT is presented as the percentage regeneration of the defect. Differences are significant at $p < 0.05$.

mandibular defect [15]. This mismatch between the Hox gene expression statuses of host and donor cells is correlated with a disruption in bone regeneration, such that the grafted cells fail to differentiate into osteoblasts [22]. When iliac crest-derived BMSCs are placed in a mandibular defect, these mesoderm-derived progenitor cells differentiate into chondrocytes [23]. Conversely, craniofacial bone-derived BMSCs can integrate into and contribute to bony regeneration in a mandibular defect.

In the present study, we isolated and characterized aBMSCs, which fulfill the criteria of the International Society for Cellular Therapy, including fibroblast-like morphology,

expression of surface markers, and a capacity for multilineage differentiation [24]. Although the maintenance of stemness is difficult to achieve in *ex vivo* culture, this profile suggests that cells collected from alveolar bone resemble immature mesenchymal cells. We also determined that the aBMSCs were STRO-1 positive. STRO-1, which recognizes only clonogenic and highly osteogenic progenitors, is expressed by stromal elements in the bone marrow [25]. Additionally, we evaluated the osteogenic potential of the aBMSCs. Runx2 and Osterix are essential transcription factors for osteoblastic differentiation and skeletal morphogenesis, and OCN is a major noncollagenous protein specific to bone and the most recently identified osteogenic expression marker.

The cellular state under 2D and 3D cell culture conditions may vary considerably [26]. Accordingly, the proliferation and osteogenic capabilities of the aBMSCs on the 3D porous nHAC/PLA scaffold were further evaluated. The nHAC/PLA scaffold was formed from new mineralized collagen consisting of a combination of collagen fibrils and PLA attached to nanohydroxyapatite by a self-assembly method. The microstructure of this composite was a mineralized collagen fiber bundle, similar to the hierarchical structure of natural bone [27]. We have previously demonstrated that this composite has good biocompatibility and osteoconductivity, suggesting its potential for hard tissue repair [18]. The results of the current study further confirmed that nHAC/PLA provides a suitable environment for aBMSC adhesion, proliferation, and differentiation. The upregulation of both osteogenic gene expression and protein expression suggests that the osteogenic potential of aBMSCs on nHAC/PLA was activated by the osteogenic induction medium.

In this study, a localized mandibular defect model was used to characterize the osteogenic differentiation of the nHAC/PLA + aBMSCs construct *in vivo*. Micro-CT and histomorphometric analyses further confirmed the capability of this method to repair bone defects. In the rabbit mandible, a defect diameter greater than 5 mm has been reported to be a critical size that prevents spontaneous healing [19]. In the present study, after 8 weeks of implantation, histological analysis demonstrated that the untreated group exhibited no bone formation and that the nHAC/PLA group had abundant engineered osteoid tissue and some newly formed bone. These results indicated that a critical-size defect was successfully established and that nHAC/PLA can be used as a potential scaffold for mandibular bone regeneration. Furthermore, the nHAC/PLA + aBMSCs group had significantly greater bone formation than the nHAC/PLA group did. These results once again confirmed that the structure and composition of the nHAC/PLA had good biocompatibility and promoted cell proliferation and osteogenic differentiation. The ECM and other factors in the bone defect environment played a key role in this osteogenic differentiation of the aBMSCs. Specifically, for defects filled with nHAC/PLA + preinduced aBMSCs, a large amount of mature thickened bone was observed in the morphometric analysis, and the defect surface exhibited complete healing, with a thick cortical shell bridge in CT images. These results demonstrated that the nHAC/PLA + aBMSCs preinduced in osteogenic induction medium did indeed exhibit enhanced initial bone formation *in vivo*. These results also indicated that factors from defects are insufficient to stimulate aBMSCs to undergo osteogenic differentiation. To achieve improved therapeutic effects, regulating the degree of aBMSCs' osteogenic differentiation is desirable. The selected inducer may include osteoblasts that have undergone osteogenic preinduction *in vitro*. Osteoblast-secreted factors can promote the proliferation and osteogenic differentiation of BMSCs via the VEGF/heme-oxygenase-1 pathway [28]. To verify that the tissue-engineered bone generated from nHAC/PLA + preinduced aBMSCs is a valid alternative for the reconstruction of mandibular bone defects, a positive-control, gold-standard fresh autogenous iliac bone graft was also tested in this study. Quantitative histomorphometric and micro-CT analyses demonstrated that the tissue-engineered bone was similar to that derived from the gold-standard method.

The effects of the nHAC/PLA + preinduced aBMSCs method on bone defect repair are similar to those of the autologous bone method, but with less trauma. Therefore, the method presented here needs to be considered carefully for clinical applications. Cone-beam CT also confirmed that the method does not affect the osseointegration of dental implants. From a purely technical perspective, aBMSC collection offers advantages over collection from other sites because the cells are passed through the mucous membrane, without damaging the skin, which avoids the need for general anesthesia and effectively reduces patient discomfort. Moreover, the cells can be easily obtained during routine dental surgery, such as dental implant surgery, wisdom tooth extraction, and tooth crown-lengthening measures. The selection of surgical methods depends on the surgeon's familiarity with the anatomic region, but most maxillofacial surgeons and dentists feel confident about extracting bone marrow from alveolar bones.

It is noteworthy that although complete absence of teratoma formation was observed in this study, it is only a speculation whether some aBMSCs still survive *in vivo* or are killed in xenogeneic hosts. Several studies have suggested that the stem cells could suppress immune responses through immune-privileged, immunosuppressive, or tolerance-inducing methods [29, 30]. Others have suggested that the functional improvements after implantation of xenogeneic stem cells are only caused by paracrine effects rather than by engraftment [31]. Thus, further studies about immune mechanisms will be necessary to correctly interpret the results of animal models and for future translation into clinical practice.

Another safety consideration for tissue engineering strategies is genetic stability in *ex vivo* cell culture. In the present study, aBMSCs were expanded, passaged, and osteogenically induced. Following long-term cell culture, the results of karyotyping, tumor suppressor, and protooncogene analyses were unchanged. These results are in agreement with those of Poloni et al., who observed that human adipocytes dedifferentiated into endothelial cells and did not undergo transformational changes [32]. Our results thus demonstrated that genetic instability does not occur among aBMSCs cultured on nHAC/PLA in osteogenic induction medium.

5. Conclusion

The key parameter of bone reconstruction in bone tissue engineering is the selection of favorable seed cells, biomaterials, and an osteogenic inducer; changes in any of these three factors will affect osteogenesis. The present study overcame the difficulties of isolating human craniofacial BMSCs and demonstrated the bone regeneration potential of an innovative seed cell type, namely, aBMSCs, without viral gene delivery. These findings also demonstrated that this method of applying nHAC/PLA + aBMSCs with osteogenic preinduction is a valid alternative for the correction of mandibular bone defects. This study is an important step in the clinical application of human craniofacial BMSCs, although additional studies will be necessary to determine the effects of immunity on human autologous aBMSCs after preinduction *in vitro*.

Competing Interests

No competing financial interests exist.

Authors' Contributions

Xing Wang and Helin Xing contributed equally to this paper.

Acknowledgments

This study was supported by National Natural Science Foundation of China (81271180), the National Natural Science Director Foundation of China (81150019), Beijing Natural Science Foundation (7164297), and the Open Research Fund Program of the State Key Laboratory of Low-Dimensional Quantum Physics (20120908). The authors are also grateful to the staff and faculty of Institute of Stomatology, Chinese People Liberation Army General Hospital.

References

[1] S. Marthy and M. Richter, "Human immunodeficiency virus activity in rib allografts," *Journal of Oral and Maxillofacial Surgery*, vol. 56, no. 4, pp. 474–476, 1998.

[2] J.-W. Jang, J.-H. Yun, K.-I. Lee et al., "Osteoinductive activity of biphasic calcium phosphate with different rhBMP-2 doses in rats," *Oral Surgery, Oral Medicine, Oral Pathology and Oral Radiology*, vol. 113, no. 4, pp. 480–487, 2012.

[3] M. F. Pittenger, A. M. Mackay, S. C. Beck et al., "Multilineage potential of adult human mesenchymal stem cells," *Science*, vol. 284, no. 5411, pp. 143–147, 1999.

[4] G. Ren, L. Zhang, X. Zhao et al., "Mesenchymal stem cell-mediated immunosuppression occurs via concerted action of chemokines and nitric oxide," *Cell Stem Cell*, vol. 2, no. 2, pp. 141–150, 2008.

[5] G. Ciapetti, L. Ambrosio, G. Marletta, N. Baldini, and A. Giunti, "Human bone marrow stromal cells: in vitro expansion and differentiation for bone engineering," *Biomaterials*, vol. 27, no. 36, pp. 6150–6160, 2006.

[6] W.-K. Min, J.-S. Bae, B.-C. Park et al., "Proliferation and osteoblastic differentiation of bone marrow stem cells: comparison of vertebral body and iliac crest," *European Spine Journal*, vol. 19, no. 10, pp. 1753–1760, 2010.

[7] D. Kaigler, G. Pagni, C. H. Park et al., "Stem cell therapy for craniofacial bone regeneration: a randomized, controlled feasibility trial," *Cell Transplantation*, vol. 22, no. 5, pp. 767–777, 2013.

[8] G. J. Meijer, J. D. de Bruijn, R. Koole, and C. A. van Blitterswijk, "Cell based bone tissue engineering in jaw defects," *Biomaterials*, vol. 29, no. 21, pp. 3053–3061, 2008.

[9] D. R. Reissmann, B. Dietze, M. Vogeler, R. Schmelzeisen, and G. Heydecke, "Impact of donor site for bone graft harvesting for dental implants on health-related and oral health-related quality of life," *Clinical Oral Implants Research*, vol. 24, no. 6, pp. 698–705, 2013.

[10] S. Mason, S. A. Tarle, W. Osibin, Y. Kinfu, and D. Kaigler, "Standardization and safety of alveolar bone-derived stem cell isolation," *Journal of Dental Research*, vol. 93, no. 1, pp. 55–61, 2014.

[11] E. J. Mackie, Y. A. Ahmed, L. Tatarczuch, K.-S. Chen, and M. Mirams, "Endochondral ossification: how cartilage is converted into bone in the developing skeleton," *International Journal of Biochemistry and Cell Biology*, vol. 40, no. 1, pp. 46–62, 2008.

[12] Y. Chai, X. Jiang, Y. Ito et al., "Fate of the mammalian cranial neural crest during tooth and mandibular morphogenesis," *Development*, vol. 127, no. 8, pp. 1671–1679, 2000.

[13] I. T. Jackson, G. Helden, and R. Marx, "Skull bone grafts in maxillofacial and craniofacial surgery," *Journal of Oral and Maxillofacial Surgery*, vol. 44, no. 12, pp. 949–955, 1986.

[14] P. D. Sawin, V. C. Traynelis, and A. H. Menezes, "A comparative analysis of fusion rates and donor-site morbidity for autogeneic rib and iliac crest bone grafts in posterior cervical fusions," *Journal of Neurosurgery*, vol. 88, no. 2, pp. 255–265, 1998.

[15] P. Leucht, J.-B. Kim, R. Amasha, A. W. James, S. Girod, and J. A. Helms, "Embryonic origin and Hox status determine progenitor cell fate during adult bone regeneration," *Development*, vol. 135, no. 17, pp. 2845–2854, 2008.

[16] T. Matsubara, K. Suardita, M. Ishii et al., "Alveolar bone marrow as a cell source for regenerative medicine: differences between alveolar and iliac bone marrow stromal cells," *Journal of Bone and Mineral Research*, vol. 20, no. 3, pp. 399–409, 2005.

[17] L. L. E, L. L. Xu, X. Wu et al., "The interactions between rat-adipose-derived stromal cells, recombinant human bone morphogenetic protein-2, and beta-tricalcium phosphate play an important role in bone tissue engineering," *Tissue Engineering Part A*, vol. 16, no. 9, pp. 2927–2940, 2010.

[18] H.-C. Liu, D.-S. Wang, F. Su et al., "Reconstruction of alveolar bone defects using bone morphogenetic protein 2 mediated rabbit dental pulp stem cells seeded on nano-hydroxyapatite/collagen/ poly(l-lactide)," *Tissue Engineering A*, vol. 17, no. 19-20, pp. 2417–2433, 2011.

[19] V. Thomaidis, K. Kazakos, D. N. Lyras et al., "Comparative study of 5 different membranes for guided bone regeneration of rabbit mandibular defects beyond critical size," *Medical Science Monitor*, vol. 14, no. 4, pp. BR67–BR73, 2008.

[20] S. O. Akintoye, T. Lam, S. Shi, J. Brahim, M. T. Collins, and P. G. Robey, "Skeletal site-specific characterization of orofacial and iliac crest human bone marrow stromal cells in same individuals," *Bone*, vol. 38, no. 6, pp. 758–768, 2006.

[21] X. Wang, X. Zou, J. Zhao et al., "Site-specific characteristics of bone marrow mesenchymal stromal cells modify the effect of aging on the skeleton," *Rejuvenation Research*, 2016.

[22] S. Creuzet, G. Couly, C. Vincent, and N. M. Le Douarin, "Negative effect of Hox gene expression on the development of the neural crest-derived facial skeleton," *Development*, vol. 129, no. 18, pp. 4301–4313, 2002.

[23] A. D'Addona and H. Nowzari, "Intramembranous autogenous osseous transplants in aesthetic treatment of alveolar atrophy," *Periodontology 2000*, vol. 27, no. 1, pp. 148–161, 2001.

[24] M. Dominici, K. Le Blanc, I. Mueller et al., "Minimal criteria for defining multipotent mesenchymal stromal cells. The International Society for Cellular Therapy position statement," *Cytotherapy*, vol. 8, no. 4, pp. 315–317, 2006.

[25] P. J. Simmons and B. Torok-Storb, "Identification of stromal cell precursors in human bone marrow by a novel monoclonal antibody, STRO-1," *Blood*, vol. 78, no. 1, pp. 55–62, 1991.

[26] P.-C. Tseng, T.-H. Young, T.-M. Wang, H.-W. Peng, S.-M. Hou, and M.-L. Yen, "Spontaneous osteogenesis of MSCs cultured on 3D microcarriers through alteration of cytoskeletal tension," *Biomaterials*, vol. 33, no. 2, pp. 556–564, 2012.

[27] S. Liao, K. Tamura, Y. Zhu et al., "Human neutrophils reaction to the biodegraded nano-hydroxyapatite/collagen and nano-hydroxyapatite/collagen/poly(L-lactic acid) composites," *Journal of Biomedical Materials Research A*, vol. 76, no. 4, pp. 820–825, 2006.

[28] L.-F. Zhang, J. Qi, G. Zuo et al., "Osteoblast-secreted factors promote proliferation and osteogenic differentiation of bone marrow stromal cells via VEGF/heme-oxygenase-1 pathway," *PLoS ONE*, vol. 9, no. 6, Article ID e99946, 2014.

[29] L. Li, M. L. Baroja, A. Majumdar et al., "Human embryonic stem cells possess immune-privileged properties," *STEM CELLS*, vol. 22, no. 4, pp. 448–456, 2004.

[30] C. A. Koch, P. Geraldes, and J. L. Platt, "Immunosuppression by embryonic stem cells," *Stem Cells*, vol. 26, no. 1, pp. 89–98, 2008.

[31] R. Dressel, "Effects of histocompatibility and host immune responses on the tumorigenicity of pluripotent stem cells," *Seminars in Immunopathology*, vol. 33, no. 6, pp. 573–591, 2011.

[32] A. Poloni, G. Maurizi, S. Anastasi et al., "Plasticity of human dedifferentiated adipocytes toward endothelial cells," *Experimental Hematology*, vol. 43, no. 2, pp. 137–146, 2015.

Hindawi Publishing Corporation
Stem Cells International
Volume 2016, Article ID 7130653, 8 pages
http://dx.doi.org/10.1155/2016/7130653

Research Article

Naringin Stimulates Osteogenic Differentiation of Rat Bone Marrow Stromal Cells via Activation of the Notch Signaling Pathway

Guo-yong Yu,[1] Gui-zhou Zheng,[1] Bo Chang,[1] Qin-xiao Hu,[1] Fei-xiang Lin,[1] De-zhong Liu,[1] Chu-cheng Wu,[1] Shi-xin Du,[1,2] and Xue-dong Li[1,2]

[1]*Department of Orthopedics, The First Affiliated Hospital, Shantou University Medical College, 57 Changping Road, Shantou, Guangdong Province 515041, China*
[2]*Department of Orthopedics, The Affiliated Luohu Hospital of Shenzhen University, Shenzhen, Guangdong Province 518000, China*

Correspondence should be addressed to Shi-xin Du; dsx1232013@sina.com and Xue-dong Li; xdl622@sina.com

Received 25 November 2015; Revised 23 January 2016; Accepted 3 February 2016

Academic Editor: Zufu Lu

Naringin is a major flavonoid found in grapefruit and is an active compound extracted from the Chinese herbal medicine Rhizoma Drynariae. Naringin is a potent stimulator of osteogenic differentiation and has potential application in preventing bone loss. However, the signaling pathway underlying its osteogenic effect remains unclear. We hypothesized that the osteogenic activity of naringin involves the Notch signaling pathway. Rat bone marrow stromal cells (BMSCs) were cultured in osteogenic medium containing-naringin, with or without DAPT (an inhibitor of Notch signaling), the effects on ALP activity, calcium deposits, osteogenic genes (ALP, BSP, and cbfa1), adipogenic maker gene PPARγ2 levels, and Notch expression were examined. We found that naringin dose-dependently increased ALP activity and Alizarin red S staining, and treatment at the optimal concentration (50 μg/mL) increased mRNA levels of osteogenic genes and Notch1 expression, while decreasing PPARγ2 mRNA levels. Furthermore, treatment with DAPT partly reversed effects of naringin on BMSCs, as judged by decreases in naringin-induced ALP activity, calcium deposits, and osteogenic genes expression, as well as upregulation of PPARγ2 mRNA levels. These results suggest that the osteogenic effect of naringin partly involves the Notch signaling pathway.

1. Introduction

Osteoporosis is becoming increasingly prevalent due to demographic changes and longer life expectancies. In particular, postmenopausal osteoporosis is the most widespread form of osteoporosis, affecting one in two women over the age of sixty. Although hormone replacement therapy has been the most commonly used therapeutic for the prevention and treatment of postmenopausal osteoporosis, the Women's Health Initiative reported that the health risks of hormone replacement therapy exceed its benefits [1]. The use of bisphosphonates has also been used to treat osteoporosis [2]. However, the potential bone-forming agents in bisphosphonates can have serious side-effects and may not yield the expected improvements in the bone quality and bone union ratio [3], and the cost effectiveness of their widespread or long-term use has been questioned. In addition, despite the availability of an armamentarium of agents, finding the optimal agent remains a challenge [4]. Therefore, more and more people have turned to, or are searching for, alternative or natural therapies for osteoporosis [5].

Naringin is a major flavonoid found in grapefruit and an active compound extracted from the Chinese herbal medicine Rhizoma Drynariae [6]. Studies have shown that naringin possesses many beneficial pharmacological properties, such as anti-inflammatory, antioxidant, antiapoptotic, and anticancer activities in various animal disease models [7], estrogen-like activities in rat UMR-106 osteoblast-like cells [8], and in particular improves the bone mass of retinoic acid-induced [9] or ovariectomy-induced osteoporosisin rats

[10, 11]. In addition, naringin increases proliferation and osteogenic differentiation of the MC3T3-E1 osteogenic precursor cell line [12] and inhibits osteoclast formation and bone resorption, suggesting that naringin offers a beneficial alternative for the prevention and treatment of osteoporosis [13, 14]. Furthermore, a number of studies have shown naringin plays a significant role in proliferation and differentiation of BMSCs [11, 15], which can differentiate into osteoblasts. In human mesenchymal stem cells, naringin promotes osteogenic differentiation through miR-20a and PPARγ [16]. However, the mechanism of naringin on the proliferation and osteogenic differentiation of BMSCs remains unknown.

Notch receptors, a family of transmembrane proteins, control various cell functions, including proliferation, differentiation, and cell-fate decisions [17]. The activation of Notch receptors, following cognate interaction with jagged, delta-like family ligands, are cleaved by membrane-bound γ-secretase, followed by nuclear entry of the Notch intracellular domain. This in turn activates transcription of target genes, such as hairy enhancer of split (HES) and Hes family-related genes [18]. Although Notch signaling was first identified in fly neurogenesis [17], additional evidence highlights the importance of Notch signaling in other systems, including tumor formation, glucose metabolism, and bone formation [19]. The Notch signaling pathway is activated during osteogenic differentiation of dental follicle cells and regulates BMP2/DLX3-directed differentiation of dental follicle cells via a negative feedback loop [20]. Here, we hypothesize that the osteogenic effects of naringin are related to the Notch signaling pathway. In the current study, we found that naringin stimulates osteogenic differentiation of rat BMSCs via activation of the Notch signaling pathway.

2. Materials and Methods

2.1. Animals. Four-week-old female Sprague-Dawley rats were purchased from the Experimental Animal Center of Shantou University Medical College, Shantou, China, and were housed under environmentally controlled conditions (22°C, a 12-h light/dark cycle with a light cycle from 6:00 to 18:00 hours and a dark cycle from 18:00 to 6:00 hours) with ad libitum access to standard laboratory chow. The local Institution Review Board approved the study protocol, and all animal experiments were performed according to the guidelines of the Institutional Animal Care and Use Committee of Shantou University Medical College.

2.2. Chemicals and Reagents. Naringin (from citrus fruit, chemical purity ≥ 98.0%) was purchased from Sigma-Aldrich (St. Louis, MO) and was dissolved in dimethyl sulfoxide (DMSO). Culture media (DMEM/F12) and fetal bovine serum (FBS) were purchased from Invitrogen (Grand Island, NY, USA). Penicillin and streptomycin were obtained from Gibco BRL (Gaithersburg, MD, USA). A majority of the drugs were purchased from Sigma (Steinheim, Germany), including cetylpyridinium chloride (CPC), Alizarin red S, dexamethasone, β-glycerophosphate, and ascorbic acid phosphate. Kits for measurement of alkaline phosphatase were purchased from Nanjing Jiancheng Company (Nanjing, China). The CCK-8 cell counting kit was purchased from Xingzhi Biotechnology Co., Ltd. (Guangdong, China).

2.3. Cell Culture and Treatments. Primary culture of BMSCs, obtained from three random four-week-old female Sprague-Dawley rats, was established as described previously [21]. Briefly, tibias and femurs were immediately removed from euthanized rats, and the attached muscles and tissues were removed using aseptic technique. The ends of the bones were removed, and marrow plugs were flushed out by injecting basal medium (as control: DMEM/F12 medium containing 10% heat-inactivated FBS, 1% penicillin, and streptomycin). A suspension of single bone marrow cells from the tibias and femurs was obtained by gentle pipetting in a 10 cm petri dish. Cells were then counted with a hemacytometer and 15 mL, of a 1×10^6 cells/mL cell suspension, was inoculated into a culture flask. Cells were maintained in a humidified incubator with 5% CO_2 and 95% air at 37°C. Cells were detached using 1 mM EDTA and 0.25% trypsin at 80% confluence and then subcultured. Cells (passages 3–6) were subcultured or plated for subsequent experiments.

2.4. Osteogenic Differentiation Protocol and Differentiation Assays. For osteogenic differentiation, BMSCs were inoculated at approximately 1×10^4 cells/cm^2 on culture dishes and induced in osteogenic induction medium (OIM: DMEM/F12, 0.1 μM dexamethasone, 50 μM ascorbic acid, and 10 mM sodium β-glycerophosphate) with or without naringin (final concentration at 1, 10, and 50 μg/mL). To examine the involvement of the Notch signaling pathway in naringin action, BMSCs under OIM were stimulated to differentiate by addition of 50 μg/mL naringin in the presence or absence of 10 μM DAPT, a Notch inhibitor. DAPT was dissolved in DMSO and was freshly diluted to the desired concentration with culture medium. The final concentration of DMSO was 0.05% (v/v). Differentiation was evaluated by measuring ALP activity and mineralization.

2.5. Assessment of Proliferation by CCK-8 Assay. Cells (1×10^4 per well) were plated in a 96-well plate and cultured in basal medium for 24 h. Then cells were treated with basal medium or basal medium containing-naringin at a concentration of 1, 10, 50, or 100 μg/mL, and cell proliferation was determined after 12–96 hours using the Cell Counting Kit-8 (CCK-8) assay as instructed by the manufacturer. Absorbance was measured at 450 nm using a microplate reader (Thermo Scientific, Beijing, China). Cell proliferation was expressed as the optical density (OD) value.

2.6. Alkaline Phosphatase (ALP) Assay. ALP activity is an early phase marker of bone formation. BMSCs were cultured in basal medium or osteogenesis was induced by culture in OIM, with or without naringin for 1, 3, 5, 7, and 9 days; then ALP activity was determined as previously described [22]. Cells were lysed by sonication in 0.5 mL of 10 nM Tris-HCl (pH 7.5) containing 0.1% Triton X-100. Absorbance was measured at 520 nm using a microtiter plate reader (KHB Labsystems Wellscan K3, Finland). Total protein

Table 1: PCR primer sequences and cycling conditions.

Gene and GenBank accession number	Primer sequence (forward/reverse)	Temperature (°C)	Product size (bp)
ALP (J03572)	5′-TCCGTGGGTCGGATTCCT-3′ 5′-GCCGGCCCAAGAGAGAA-3′	58.0	280
BSP (NM_012587)	5′-GCTATGAAGGCTACGAGGGTCAGGATTAT-3′ 5′-GGGTATGTTAGGGTGGTTAGCAATGGTGT-3′	59.1	386
Cbfa1 (AF053950)	5′-CCTCACAAACAACCACAGAAC CA-3′ 5′-AACTGA AAATACAAA CCATACCC-3′	60	325
PPARγ2 (NM_013124)	5′-ATCCCGTTCACAAGAGCTGA-3′ 5′-GCAGGCTCTACTTTGATCGC-3′	54.8	177
β-actin (NM_031144)	5′-ATCGTGGGCCGCCCTAGGCA-3′ 5′-TGGCCTTAGGGTTCAGAGGGG-3′	61.0	260

Note: ALP, alkaline phosphatase; BSP, bone sialoprotein; Cbfa1, core-binding factor a1; PPARγ2, peroxisome proliferator-activated receptor gamma 2; β-actin.

concentrations were determined by the Bradford protein assay method and ALP activity was normalized to total protein.

2.7. Calcium Deposit Analysis. On day 21, medium was removed and the cells were fixed with 70% ice-cold ethanol (v/v) for 10 min and rinsed thoroughly with distilled water. Cultures were then stained with 40 mM Alizarin red S in deionized water (pH 4.2) for 10 min at room temperature. After removing Alizarin red S solution by aspiration, cells were rinsed with fresh PBS and dried at room temperature. Calcium deposits were evaluated using the cetylpyridinium chloride (CPC) method. Alizarin red S concentrations were calculated by comparison with an Alizarin red S dye standard curve and expressed as nmol/mL [22].

2.8. Real-Time Quantitative PCR. BMSCs were cultured for 14 days and then washed with PBS. Total RNA was extracted using Trizol reagent (Dongsheng Biotechnology Co., Ltd., Guangdong, China) according to the protocol from the supplier. First-strand cDNA synthesis was carried out using a High Capacity cDNA Reverse Transcription Kit (TaKaRa). Real-time quantitative PCR was then performed using SYBR PreMix Ex TaqTM (TaKaRa) and a CFX96TM Real-time PCR Detection System (Applied Biosystems). PCR conditions and the sequences of primers are listed in Table 1 for the genes encoding the following proteins: alkaline phosphatase (ALP), bone sialoprotein (BSP), core-binding factor a1 (cbfa1), peroxisome proliferator-activated receptor gamma 2 (PPARγ2), and β-actin. Gene expression was calculated using $2^{-\Delta\Delta Ct}$ method and normalized against β-actin. PCR was performed at 95°C for 30 s, followed by 40 cycles of 5 s at 95°C and 30 s at 56°C. PCR was run in triplicate, and at least three times independently.

2.9. Western Blotting Assays. Total cellular lysates were prepared using RIPA lysis buffer (Boster, Wuhan, China) following the manufacturer's instructions. Immunoblotting was carried out as previously described [23], and anti-Notch1 antibodies were used for the procedure (Abcam, UK). Protein bands were visualized using a SuperSignal Western Blotting Kit (Pierce, Rockford, IL). Densitometric analysis was performed using Quantity One Software v4.62 (Bio-Rad, Hercules, CA). β-actin was used as a loading control.

2.10. Statistical Analyses. All experiments were performed at least in triplicate, and one representative set was chosen to be shown. All data are presented as mean ± standard deviation (SD) and analyzed using SPSS 17.0 software (SPSS Inc., Chicago, IL). One-way analysis of variance (ANOVA) followed by the Student-Newman-Keuls's test was performed to reveal differences among groups. A probability (P) value less than 0.05 was considered to be statistically significant.

3. Results

3.1. Naringin Enhances BMSCs Proliferation. CCK-8 assays were performed on BMSCs, cultured under basal medium or basal medium with or without naringin at a series of concentrations, to determine whether naringin can affect proliferation. Naringin at 1, 10, and 50 μg/mL caused a dose and time-dependent increase in the proliferation of BMSCs. Naringin at 50 μg/mL caused a statistically significant increase in the growth of BMSCs at hours 24 to 72, as compared to controls ($P < 0.01$ or 0.05). Naringin at a higher dose (100 μg/mL), by contrast, markedly depressed the proliferation of BMSCs (Figure 1(a)). The proliferation of the cells treated with 100 μg/mL naringin was decreased compared with control. Thus, naringin concentrations did not exceed 50 μg/mL for the remaining experiments.

3.2. Naringin Enhances Osteogenic Differentiation in a Dose-Dependent Manner. Prior to investigating the signaling pathways involved in naringin-mediated enhancement of osteogenic differentiation, the optimal concentration of naringin on osteogenic activity was determined. ALP activity and Alizarin red S staining were increased by being treated with naringin in a dose-dependent manner, with significant enhancement at 1 μg/mL, and maximal enhancement at 50 μg/mL. (Figures 1(b), 1(c), and 1(d)).

We further investigated the expression of genes involved in osteogenesis in BMSCs under OIM with or without

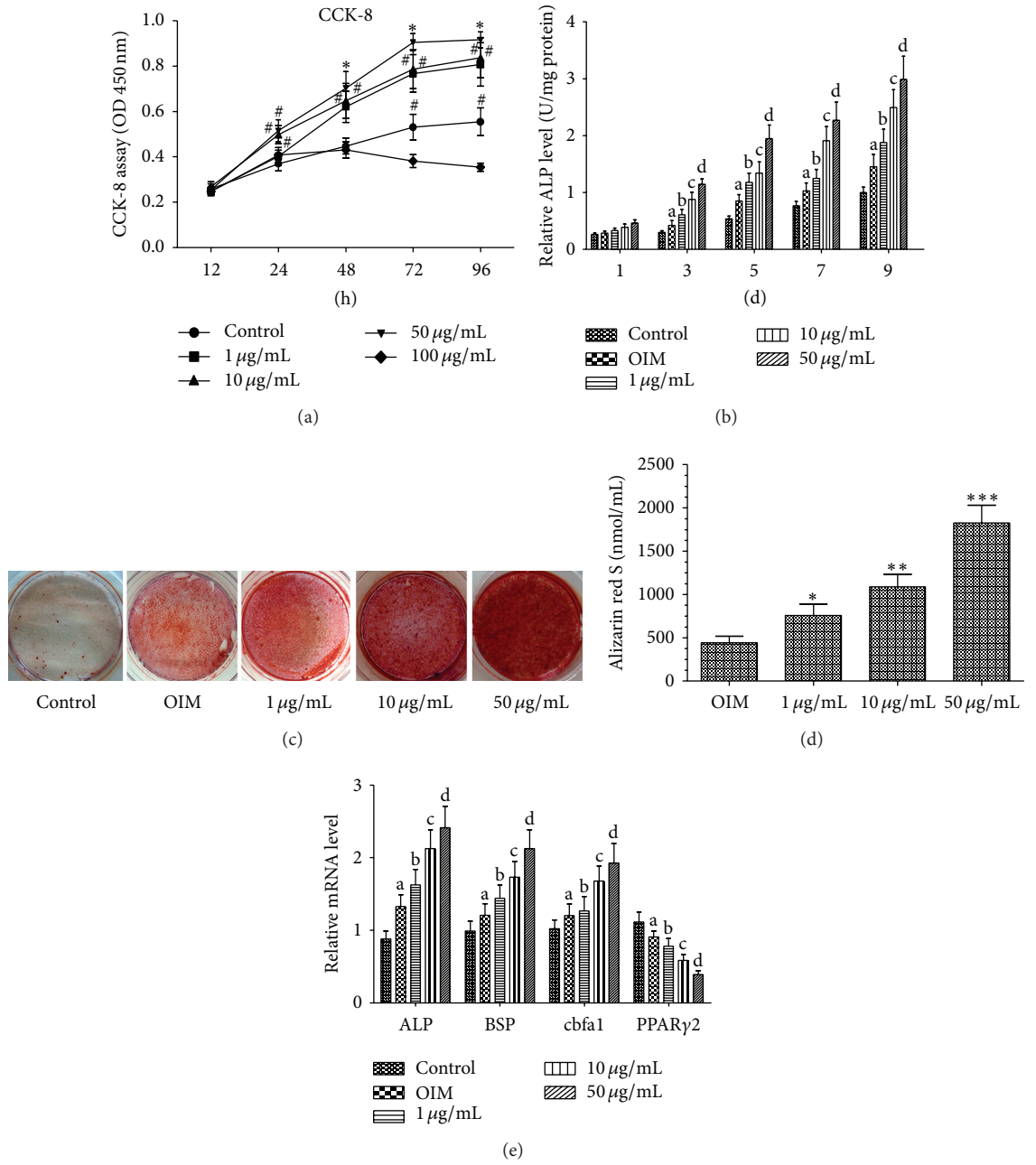

Figure 1: Naringin potentiates proliferation and osteogenic differentiation of BMSCs. (a) BMSCs were cultured in basal medium with or without various doses of naringin (1, 10, 50, and 100 μg/mL) for 12–96 hours, and the proliferation rate was assessed by CCK-8 assay. Cell proliferation of BMSCs was enhanced by naringin treatment. Naringin showed the most prominent stimulatory effect on proliferation at 50 μg/mL. Data is expressed as mean ± SD. Experiments were done in quadruplicate ($n = 4$). $^{*}P < 0.01$ versus the control group; $^{\#}P < 0.05$ versus the control group at same time point. (b) BMSCs were cultured in basal medium with or without various doses of naringin (1, 10, 50, and 100 μg/mL) for 1, 3, 5, 7, and 9 days. Data represent the mean ± SD ($n = 4$). ALP activity was measured by the manufacturer's instructions. $^{a}P < 0.05$ versus the control group at the same time point; $^{b}P < 0.01$ versus the OIM group at the same time point; $^{c}P < 0.05$ versus the 1 μg/mL group at the same time point; $^{d}P < 0.01$ versus the 10 μg/mL group at the same time point. (c) BMSCs were cultured in basal medium and OIM with or without various doses of naringin (1, 10, and 50 μg/mL) for 21 days; then calcium deposits were stained with Alizarin red S solution. For quantitative analysis, the stained samples underwent cetylpyridinium chloride (CPC) extraction (10% CPC) and extracts were measured by spectrophotometry. Data represent the mean ± SD ($n = 5$). $^{*}P < 0.01$ versus the OIM group; $^{**}P < 0.05$ versus the 1 μg/mL group; $^{***}P < 0.01$ versus the 10 μg/mL group. (e) BMSCs were cultured in basal medium, OIM, or OIM with 1 μg/mL, 10 μg/mL, or 50 μg/mL naringin for 14 days, and then ALP, BSP, Cbfa1, and PPARγ2 mRNA levels were measured by RT-PCR. Data represent the mean ± SD ($n = 5$). $^{a}P < 0.05$ versus the control group; $^{b}P < 0.05$ versus the OIM group; $^{c}P < 0.01$ versus the 1 μg/mL group; $^{d}P < 0.01$ versus the 10 μg/mL group.

naringin for 14 days. Real-time PCR assays showed that osteogenic genes (ALP, BSP, and core-binding factor a1) in BMSCs were significantly upregulated ($P < 0.01$) by naringin treatment. On the other hand, naringin caused a reduction in the PPARγ2 mRNA transcript levels (Figure 1(e)).

3.3. Naringin Enhances Osteogenesis of BMSCs by Activating the Notch Pathway. To further examine the mechanisms whereby naringin potentiated the osteogenesis of BMSCs, we treated cells with the Notch inhibitor, DAPT, to investigate if the Notch pathway is associated with the enhancement of osteogenesis by naringin. We found that, compared with OIM alone, 50 μg/mL naringin in OIM markedly increases ALP activity, calcium deposits, and osteogenesis-related gene transcript levels and conversely inhibited PPARγ2 gene expression. On the other hand, DAPT treatment markedly attenuated the biological effects of naringin on BMSCs (Figures 2(a), 2(b), 2(c), and 2(d)). These findings suggest that the Notch signaling pathway could play a critical role in naringin-enhanced osteogenic differentiation of BMSCs by modulating the expression of multiple genes involved in osteogenesis. To further investigate whether naringin potentiated osteogenesis of BMSCs via the Notch signaling pathway, we examined Notch1 protein levels by western blot analysis using antibodies against Notch1. Notch1 became activated in BMSCs under osteogenic induction, which was further enhanced by naringin, as evidenced by increased levels of Notch1. DAPT could markedly attenuate naringin-enhanced Notch1 expression (Figures 2(e) and 2(f)). Taken together, these results suggest that naringin-potentiated osteogenesis involves enhancing the expressing of Notch signaling pathways.

4. Discussion

Osteoporosis is a common disease characterized by reduced bone formation due to impaired osteoblastic differentiation and increased in bone resorption by elevated osteoclast function [23]. It is well established that BMSCs differentiate into a variety of cell types, including osteoblasts, adipocytes, chondrocytes, neurons, and myoblasts [24, 25]. BMSCs from osteoporotic women have a low growth rate and exhibit reduced differentiation into the osteogenic linage, as evidenced by the ALP activity and calcium phosphate deposition [26]. Therefore, enhancement of BMSC osteogenesis is an excellent strategy for osteoporosis [27].

Previous studies have demonstrated naringin administration is able to reduce bone resorption [13, 28, 29], can prevent bone loss, and promotes osteoclast apoptosis in rat osteoporosis models [11, 15, 28]. Naringin exerting needless estrogenic effects, since the uterine weight in ovariectomized rats is not obviously changed by naringin treatment [11, 13]. Recent studies have shown that naringin, as a phytoestrogen, shows estrogenic activities, at low concentrations, and antiestrogenic activities at high concentrations [30]. Naringin exerts estrogen-like activities to strengthen bone mass of ovariectomized mice [8, 31] and has lower toxicity and fewer negative side effects than other drugs used to treat osteoporosis [10]. Naringin also has been shown to be a potent stimulator of osteogenic differentiation of BMSCs in vitro [11, 15]. In the present study, we show that naringin dose-dependently promotes proliferation and potentiates the osteogenesis of BMSCs. Thus naringin is a promising candidate for osteoporosis treatment.

The mechanisms whereby naringin promotes osteogenesis of BMSCs have remained undefined. BMSCs are considered as the most suitable cell source for osteoblasts due to their superior osteogenic potential [32]. In this study, naringin increases both ALP activity and the expression of osteoblast-related gene markers in a dose-dependent manner. Furthermore, the formation of calcified nodules, another specific characteristic of osteoblastic differentiation, is also increased by naringin treatment. Our results are consistent with a prior report, by Fan et al., who reported that naringin decreases protein expression levels of PPARγ and promotes differentiation of BMSCs [16]. PPARγ is a member of the nuclear receptor superfamily known for its anti-inflammatory and macrophage-differentiating effects, as well as an ability to promote fat cell differentiation, reduce insulin resistance, and contribute to glucose homeostasis [33, 34]. High glucose levels induce osteoblast apoptosis, by activating the p38MAPK/AP-1 signaling pathway, and inhibit osteogenic differentiation of BMSCs [35, 36]. Although our study does not investigate glucose metabolism, our study indicates that suppression of PPARγ2 activity, in response to enhanced osteogenesis, can be associated with lowered glucose levels.

Our demonstration that naringin promotes osteogenic differentiation of BMSCs via enhancing Notch signal pathway activation is consistent with a previous study showing that Notch family members positively regulate the differentiation of osteoblasts, and that Notch could be an interesting target molecule for the treatment of osteoporosis [37]. However, others have shown contradictory observations regarding Notch signaling and osteogenic differentiation [28, 38–40]. The effect of Notch signaling on osteogenic gene induction appears to be dependent upon the cell line studied and the cell culture conditions used [19]. DAPT, as a γ-secretase inhibitor, prevents the cleavage of the Notch receptor and blocks the Notch signaling pathway [41, 42]. In the present study, we show that naringin also enhances the expression level of Notch1. Conversely, treatment with the Notch inhibitor, DAPT, caused partial reduction of naringin-induced expression level of Notch1. Similarly, the naringin-mediated upregulation of ALP activity, calcium deposits, and osteogenesis gene mRNA transcript levels, as well as downregulation of PPARγ2 mRNA, was blocked by DAPT. Our results together suggest that naringin promotes osteogenic differentiation of BMSCs through activation of the Notch signaling pathway.

5. Conclusions

In summary, our study shows that naringin potentiates the osteogenic differentiation of rat BMSCs, as reflected by increased ALP activity, enhanced mineralization, upregulated osteogenesis gene mRNAs, and downregulated PPARγ2 gene mRNA transcript levels. We further demonstrate that naringin enhanced Notch1 in BMSCs under osteogenic induction. Our findings shed light on the mechanisms of how naringin potentiates the osteogenesis of rat BMSCs.

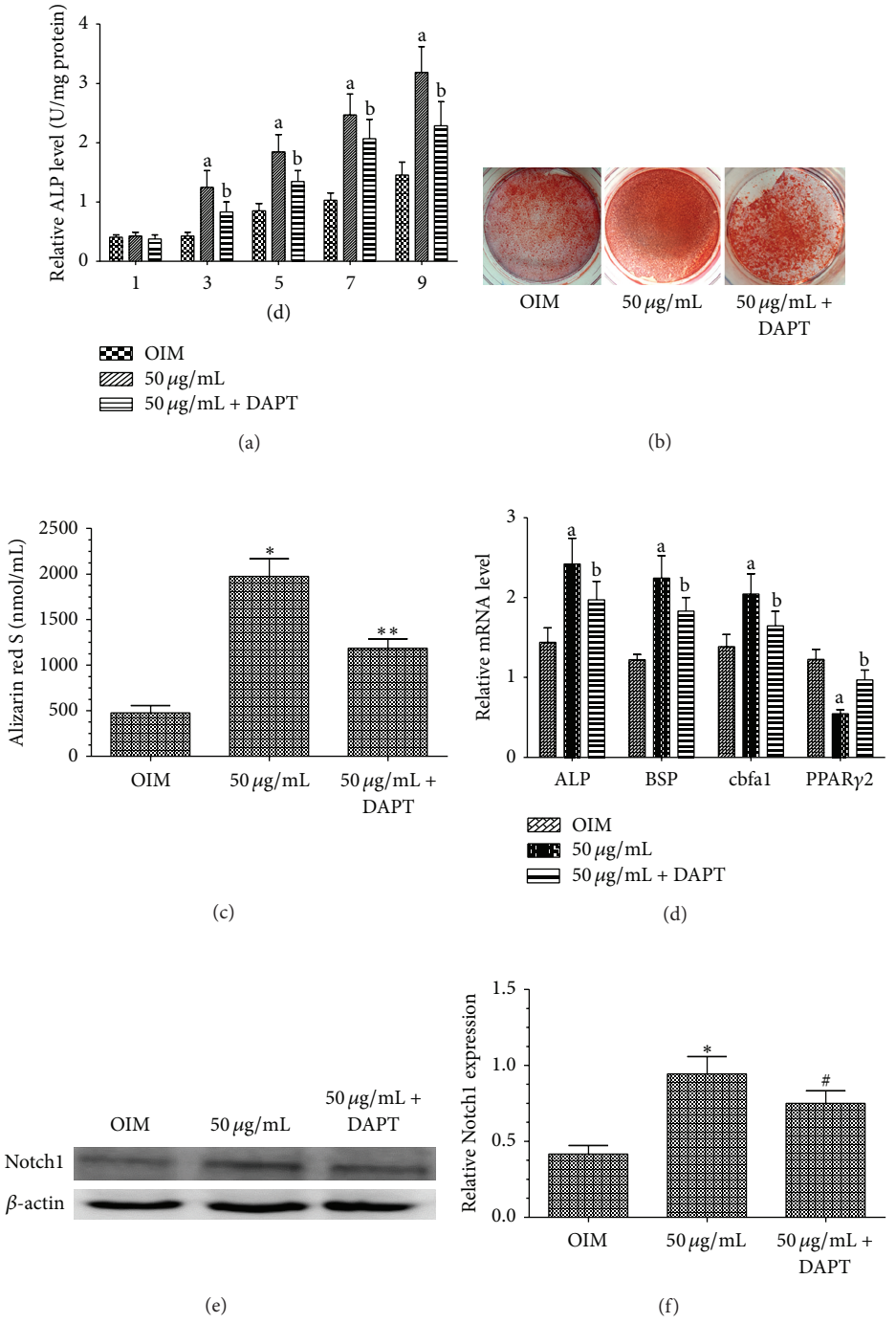

Figure 2: Involvement of Notch signaling in naringin-enhanced osteogenesis of BMSCs. (a) Effects of naringin on ALP activity of BMSCs cultured in OIM or OIM containing 50 μg/mL naringin with or without 10 μM DAPT, for 1–9 days. Data represent the mean ± SD ($n = 4$). $^{a}P < 0.01$ versus the OIM group; $^{b}P < 0.01$ versus the 50 μg/mL naringin group at the same time point. (b) Alizarin red S staining shows that DAPT inhibited naringin-enhanced mineralization of BMSCs. (c) Quantification and statistical analysis of calcium deposits. Data represent the mean ± SD ($n = 5$). $^{*}P < 0.01$ versus the OIM group; $^{**}P < 0.01$ versus the 50 μg/mL group. (d) BMSCs were cultured in OIM or OIM containing 50 μg/mL naringin with or without 10 μM DAPT, for 14 days. Expression levels of osteogenesis-related genes and PPARγ2 were measured by RT-PCR. Data represent the mean ± SD ($n = 5$). $^{a}P < 0.01$ versus the OIM group; $^{b}P < 0.05$ versus the 50 μg/mL group. (e) Western blot analysis of Notch1. BMSCs were cultured in OIM or OIM containing 50 μg/mL naringin with or without 10 μM DAPT for 14 days. (f) Band density in the western blots was quantified by densitometry. Data represent the mean ± SD ($n = 4$). $^{*}P < 0.01$ versus the OIM group; $^{\#}P < 0.05$ versus the 50 μg/mL naringin group.

Disclaimer

The authors alone are responsible for the content and writing of the paper.

Conflict of Interests

The authors declare no conflict of interests.

Authors' Contribution

Guo-yong Yu, Gui-zhou Zheng, and Bo Chang contributed equally.

Acknowledgments

The study is supported by National Natural Science Foundation of China (81341103, 81271947), Administration of Traditional Chinese Medicine of Guangdong Province, China (20131248, 20142084), The Department of Education, Guangdong Government, under the Top-Tier University Development Scheme for Research and Control of Infectious Diseases (2015092), and Natural Science Foundation of Guangdong Province, China (2014A030313467). All research was completed in the Laboratory of Molecular Cardiology, First Affiliated Hospital of Shantou University Medical College. The authors gratefully acknowledge the support of Xin Zhang, Li-biao Wu, and Bo-zhi Cai for their helpful advice and collaboration. Guo-yong Yu works at Hanzhong Central Hospital, Hanzhong, Shanxi Province, China, now.

References

[1] J. E. Rossouw, G. L. Anderson, R. L. Prentice et al., "Risks and benefits of estrogen plus progestin in healthy postmenopausal women: principal results from the women's health initiative randomized controlled trial," *The Journal of the American Medical Association*, vol. 288, no. 3, pp. 321–333, 2002.

[2] R. G. Russell, "Bisphosphonates: mode of action and pharmacology," *Pediatrics*, vol. 119, supplement 2, pp. S150–S162, 2007.

[3] A. Lühe, K.-P. Künkele, M. Haiker et al., "Preclinical evidence for nitrogen-containing bisphosphonate inhibition of farnesyl diphosphate (FPP) synthase in the kidney: implications for renal safety," *Toxicology in Vitro*, vol. 22, no. 4, pp. 899–909, 2008.

[4] O. Demontiero, C. Vidal, and G. Duque, "Aging and bone loss: new insights for the clinician," *Therapeutic Advances in Musculoskeletal Disease*, vol. 4, no. 2, pp. 61–76, 2012.

[5] F. Borrelli and E. Ernst, "Alternative and complementary therapies for the menopause," *Maturitas*, vol. 66, no. 4, pp. 333–343, 2010.

[6] N. Ramesh, M. B. Viswanathan, A. Saraswathy, K. Balakrishna, P. Brindha, and P. Lakshmanaperumalsamy, "Phytochemical and antimicrobial studies on *Drynaria quercifolia*," *Fitoterapia*, vol. 72, no. 8, pp. 934–936, 2001.

[7] S. Bharti, N. Rani, B. Krishnamurthy, and D. S. Arya, "Preclinical evidence for the pharmacological actions of naringin: a review," *Planta Medica*, vol. 80, no. 6, pp. 437–451, 2014.

[8] W.-Y. Pang, X.-L. Wang, S.-K. Mok et al., "Naringin improves bone properties in ovariectomized mice and exerts oestrogen-like activities in rat osteoblast-like (UMR-106) cells," *British Journal of Pharmacology*, vol. 159, no. 8, pp. 1693–1703, 2010.

[9] M. Wei, Z. Yang, P. Li, Y. Zhang, and W. C. Sse, "Anti-osteoporosis activity of naringin in the retinoic acid-induced osteoporosis model," *The American Journal of Chinese Medicine*, vol. 35, no. 4, pp. 663–667, 2007.

[10] J.-B. Wu, Y.-C. Fong, H.-Y. Tsai, Y.-F. Chen, M. Tsuzuki, and C.-H. Tang, "Naringin-induced bone morphogenetic protein-2 expression via PI3K, Akt, c-Fos/c-Jun and AP-1 pathway in osteoblasts," *European Journal of Pharmacology*, vol. 588, no. 2-3, pp. 333–341, 2008.

[11] N. Li, Y. Jiang, P. H. Wooley, Z. Xu, and S.-Y. Yang, "Naringin promotes osteoblast differentiation and effectively reverses ovariectomy-associated osteoporosis," *Journal of Orthopaedic Science*, vol. 18, no. 3, pp. 478–485, 2013.

[12] L. N. Li, Z. Zeng, and G. P. Cai, "Comparison of neoeriocitrin and naringin on proliferation and osteogenic differentiation in MC3T3-E1," *Phytomedicine*, vol. 18, no. 11, pp. 985–989, 2011.

[13] M. Hirata, C. Matsumoto, M. Takita, C. Miyaura, and M. Inada, "Naringin suppresses osteoclast formation and enhances bone mass in mice," *Journal of Health Science*, vol. 55, no. 3, pp. 463–467, 2009.

[14] S. H. Kim, K.-W. Cho, H. S. Choi et al., "The forkhead transcription factor Foxc2 stimulates osteoblast differentiation," *Biochemical and Biophysical Research Communications*, vol. 386, no. 3, pp. 532–536, 2009.

[15] P. Zhang, K.-R. Dai, S.-G. Yan et al., "Effects of naringin on the proliferation and osteogenic differentiation of human bone mesenchymal stem cell," *European Journal of Pharmacology*, vol. 607, no. 1–3, pp. 1–5, 2009.

[16] J. Fan, J. Li, and Q. Fan, "Naringin promotes differentiation of bone marrow stem cells into osteoblasts by upregulating the expression levels of microRNA-20a and downregulating the expression levels of PPARγ," *Molecular Medicine Reports*, vol. 12, no. 3, pp. 4759–4765, 2015.

[17] K. A. Wharton, B. Yedvobnick, V. G. Finnerty, and S. Artavanis-Tsakonas, "*opa*: a novel family of transcribed repeats shared by the *Notch* locus and other developmentally regulated loci in D. melanogaster," *Cell*, vol. 40, no. 1, pp. 55–62, 1985.

[18] M. A. Simpson, M. D. Irving, E. Asilmaz et al., "Mutations in NOTCH2 cause Hajdu-Cheney syndrome, a disorder of severe and progressive bone loss," *Nature Genetics*, vol. 43, no. 4, pp. 303–305, 2011.

[19] M. P. Yavropoulou and J. G. Yovos, "The role of notch signaling in bone development and disease," *Hormones*, vol. 13, no. 1, pp. 24–37, 2014.

[20] S. Viale-Bouroncle, M. Gosau, and C. Morsczeck, "NOTCH1 signaling regulates the BMP2/DLX-3 directed osteogenic differentiation of dental follicle cells," *Biochemical and Biophysical Research Communications*, vol. 443, no. 2, pp. 500–504, 2014.

[21] L. G. Ming, B. F. Ge, M. G. Wang, and K. M. Chen, "Comparison between 8-prenylnarigenin and narigenin concerning their activities on promotion of rat bone marrow stromal cells' osteogenic differentiation in vitro," *Cell Proliferation*, vol. 45, no. 6, pp. 508–515, 2012.

[22] X.-D. Li, J.-S. Wang, B. Chang et al., "*Panax notoginseng* saponins promotes proliferation and osteogenic differentiation of rat bone marrow stromal cells," *Journal of Ethnopharmacology*, vol. 134, no. 2, pp. 268–274, 2011.

[23] S. C. Manolagas and R. L. Jilka, "Mechanisms of disease: bone marrow, cytokines, and bone remodeling—emerging insights into the pathophysiology of osteoporosis," *The New England Journal of Medicine*, vol. 332, no. 5, pp. 305–311, 1995.

[24] Y. Jiang, B. N. Jahagirdar, R. L. Reinhardt et al., "Pluripotency of mesenchymal stem cells derived from adult marrow," *Nature*, vol. 418, no. 6893, pp. 41–49, 2002.

[25] K. Taguchi, R. Ogawa, M. Migita, H. Hanawa, H. Ito, and H. Orimo, "The role of bone marrow-derived cells in bone fracture repair in a green fluorescent protein chimeric mouse model," *Biochemical and Biophysical Research Communications*, vol. 331, no. 1, pp. 31–36, 2005.

[26] J. P. Rodríguez, S. Garat, H. Gajardo, A. M. Pino, and G. Seitz, "Abnormal osteogenesis in osteoporotic patients is reflected by altered mesenchymal stem cells dynamics," *Journal of Cellular Biochemistry*, vol. 75, no. 3, pp. 414–423, 1999.

[27] J.-F. Zhang, G. Li, C.-Y. Chan et al., "Flavonoids of Herba Epimedii regulate osteogenesis of human mesenchymal stem cells through BMP and Wnt/β-catenin signaling pathway," *Molecular and Cellular Endocrinology*, vol. 314, no. 1, pp. 70–74, 2010.

[28] F. Li, X. Sun, J. Ma et al., "Naringin prevents ovariectomy-induced osteoporosis and promotes osteoclasts apoptosis through the mitochondria-mediated apoptosis pathway," *Biochemical and Biophysical Research Communications*, vol. 452, no. 3, pp. 629–635, 2014.

[29] E. S. M. Ang, X. Yang, H. Chen, Q. Liu, M. H. Zheng, and J. Xu, "Naringin abrogates osteoclastogenesis and bone resorption via the inhibition of RANKL-induced NF-κB and ERK activation," *FEBS Letters*, vol. 585, no. 17, pp. 2755–2762, 2011.

[30] D. Guo, J. Wang, X. Wang et al., "Double directional adjusting estrogenic effect of naringin from *Rhizoma drynariae* (Gusuibu)," *Journal of Ethnopharmacology*, vol. 138, no. 2, pp. 451–457, 2011.

[31] K.-C. Wong, W.-Y. Pang, X.-L. Wang et al., "Drynaria fortunei-derived total flavonoid fraction and isolated compounds exert oestrogen-like protective effects in bone," *The British Journal of Nutrition*, vol. 110, no. 3, pp. 475–485, 2013.

[32] Q. Chen, P. Shou, L. Zhang et al., "An osteopontin-integrin interaction plays a critical role in directing adipogenesis and osteogenesis by mesenchymal stem cells," *STEM CELLS*, vol. 32, no. 2, pp. 327–337, 2014.

[33] M. Lehrke and M. Lazar, "The many faces of PPARγ," *Cell*, vol. 123, no. 6, pp. 993–999, 2005.

[34] M. Armoni, C. Harel, and E. Karnieli, "PPARγ gene expression is autoregulated in primary adipocytes: ligand, sumoylation, and isoform specificity," *Hormone and Metabolic Research*, vol. 47, no. 2, pp. 89–96, 2015.

[35] Z. P. Feng, H. C. Deng, R. Jiang, J. Du, and D. Y. Cheng, "Involvement of AP-1 in p38MAPK signaling pathway in osteoblast apoptosis induced by high glucose," *Genetics and Molecular Research*, vol. 14, no. 2, pp. 3149–3159, 2015.

[36] B. Zhang, N. Liu, H. Shi et al., "High glucose microenvironments inhibit the proliferation and migration of bone mesenchymal stem cells by activating GSK3β," *Journal of Bone and Mineral Metabolism*, 2015.

[37] K.-I. Tezuka, M. Yasuda, N. Watanabe et al., "Stimulation of osteoblastic cell differentiation by Notch," *Journal of Bone and Mineral Research*, vol. 17, no. 2, pp. 231–239, 2002.

[38] Q. Xing, Q. Ye, M. Fan, Y. Zhou, Q. Xu, and A. Sandham, "*Porphyromonas gingivalis* lipopolysaccharide inhibits the osteoblastic differentiation of preosteoblasts by activating Notch1 signaling," *Journal of Cellular Physiology*, vol. 225, no. 1, pp. 106–114, 2010.

[39] N. Zamurovic, D. Cappellen, D. Rohner, and M. Susa, "Coordinated activation of notch, Wnt, and transforming growth factor-beta signaling pathways in bone morphogenic protein 2-induced osteogenesis. Notch target gene Hey1 inhibits mineralization and Runx2 transcriptional activity," *The Journal of Biological Chemistry*, vol. 279, no. 36, pp. 37704–37715, 2004.

[40] C. Zhang, J. Chang, W. Sonoyama, S. Shi, and C.-Y. Wang, "Inhibition of human dental pulp stem cell differentiation by Notch signaling," *Journal of Dental Research*, vol. 87, no. 3, pp. 250–255, 2008.

[41] H. Li, B. Yu, Y. Zhang, Z. Pan, W. Xu, and H. Li, "Jagged1 protein enhances the differentiation of mesenchymal stem cells into cardiomyocytes," *Biochemical and Biophysical Research Communications*, vol. 341, no. 2, pp. 320–325, 2006.

[42] B. Q. Song, Y. Chi, X. Li et al., "Inhibition of notch signaling promotes the adipogenic differentiation of mesenchymal stem cells through autophagy activation and PTEN-PI3K/AKT/mTOR pathway," *Cellular Physiology and Biochemistry*, vol. 36, no. 5, pp. 1991–2002, 2015.